ISSN: 2408-2384 (Online)

Environment and Natural Resources Journal

Volume 21, Number 4, July - August 2023

Environment and Natural Resources Journal (EnNRJ)
Volume 21, Number 4, July - August 2023 ISSN: 2408-2384 (Online)

AIMS AND SCOPE

The Environment and Natural Resources Journal is a peer-reviewed journal, which provides insight scientific knowledge into the diverse dimensions of integrated environmental and natural resource management. The journal aims to provide a platform for exchange and distribution of the knowledge and cutting-edge research in the fields of environmental science and natural resource management to academicians, scientists and researchers. The journal accepts a varied array of manuscripts on all aspects of environmental science and natural resource management. The journal scope covers the integration of multidisciplinary sciences for prevention, control, treatment, environmental clean-up and restoration. The study of the existing or emerging problems of environment and natural resources in the region of Southeast Asia and the creation of novel knowledge and/or recommendations of mitigation measures for sustainable development policies are emphasized.

The subject areas are diverse, but specific topics of interest include:

- Biodiversity
- Climate change
- Detection and monitoring of polluted sources e.g., industry, mining
- Disaster e.g., forest fire, flooding, earthquake, tsunami, or tidal wave
- Ecological/Environmental modelling
- Emerging contaminants/hazardous wastes investigation and remediation
- Environmental dynamics e.g., coastal erosion, sea level rise
- Environmental assessment tools, policy and management e.g., GIS, remote sensing, Environmental Management System (EMS)
- Environmental pollution and other novel solutions to pollution
- Remediation technology of contaminated environments
- Transboundary pollution
- Waste and wastewater treatments and disposal technology

Schedule
Environment and Natural Resources Journal (EnNRJ) is published 6 issues per year in January-February, March-April, May-June, July-August, September-October, and November-December.

Publication Fees
There is no cost of the article-processing and publication.

Ethics in publishing
EnNRJ follows closely a set of guidelines and recommendations published by Committee on Publication Ethics (COPE).

Environment and Natural Resources Journal (EnNRJ)

Volume 21, Number 4, July - August 2023 ISSN: 2408-2384 (Online)

Editorial Office Address
Research Management and Administration Section,
Faculty of Environment and Resource Studies, Mahidol University
999, Phutthamonthon Sai 4 Road, Salaya, Phutthamonthon, Nakhon Pathom, Thailand, 73170
Phone +662 441 5000 ext. 2108 Fax. +662 441 9509-10
Website: https://ph02.tci-thaijo.org/index.php/ennrj/index
E-mail: ennrjournal@gmail.com

Environment and Natural Resources Journal (EnNRJ)

Volume 21, Number 4, July - August 2023 ISSN: 2408-2384 (Online)

CONTENT

Factors Affecting Traffic Noise and Annoyance from Different Types of Roads: A Case Study in Nakorn Pathom Province, Thailand

Nattawat Siwapathomchai[1], Natnaree Aimyong[2], Withida Patthanaissaranukool[1,3], and Tanasri Sihabut[1,3*]

[1]Department of Environmental Health Sciences, Faculty of Public Health, Mahidol University, Bangkok, Thailand
[2]Department of Epidemiology, Faculty of Public Health, Mahidol University, Bangkok, Thailand
[3]Center of Excellence on Environmental Health and Toxicology, Bangkok, Thailand

ARTICLE INFO

Received: 9 Jan 2023
Received in revised: 21 Apr 2023
Accepted: 28 Apr 2023
Published online: 23 May 2023
DOI: 10.32526/ennrj/21/20230006

Keywords:
Annoyance/ Community/ Noise impact/ Noise sensitivity/ Road traffic noise

*** Corresponding author:**
E-mail: tanasri.sih@mahidol.ac.th

ABSTRACT

This study investigated factors associated with road traffic noise and residents' annoyance from three distinct types of roads (major arterial, minor arterial, and collector roads). Nine sampling locations in Thailand's Nakorn Pathom Province were chosen for the measurement of noise levels and three contributing characteristics: traffic volume, vehicle speed, and the proportion of heavy to total vehicles. Along with a housing survey, face to face interviews with a total of 387 roadside dwellers recorded their sociodemographic data, activity-based locations, and noise impacts experienced. A statistical analysis based on Spearman correlation revealed a positive relationship between traffic volume and traffic noise level on major arterial (r=0.607) and collector roads (r=0.885). Residents around collector roads were more sensitive than those along the main arterial road, in spite of having lower noise levels and less intense traffic patterns. Longer housing setbacks appeared to be a key factor in reducing noise annoyance from all road types, according to an exact logistic regression analysis (OR=0.11, 95% CI: 0.003, 0.73 for the major arterial road; OR=0.29, 95% CI: 0.10, 0.78 for the minor arterial road; and OR=0.32, 95% CI: 0.12, 0.84 for collector roads). However, performing activities in closed areas (OR=0.05, 95% CI: 0.01, 0.17 for the minor arterial road; OR=0.22, 95% CI: 0.54, 0.90 for collector roads) and living in soundproof structures (OR=0.05, 95% CI: 0.001, 0.31 for collector roads) played additional roles to reduce the annoyance of residents along the roads with shorter setback lines.

1. INTRODUCTION

Concerns about the health impacts of exposure to ambient noise have emerged as a result of the rapid global development of urbanization and transportation networks. Over 100 million people in Europe alone were subjected to excessive environmental noise, which had physical and psychological effects, particularly severe annoyance (22 million cases) and sleep disturbance (6.5 million) (EEA, 2020). Since up to 113 million people have been exposed to hazardous levels of road traffic noise, it can be determined that road traffic noise is a pollution source that poses a serious threat to environmental health (EEA, 2020). To begin alleviating the problem, we must first explore the road traffic noise characteristics and understand the annoyance of residents residing along the roads. While information on the former is useful for local authorities to implement appropriate control measures, findings on the latter imply the acceptable safety noise level of each culture which can be used for urban planning without stunting economic growth. As a result, investigations into the speed and volume of vehicles that contribute to road traffic noise have been conducted (Tripura and Sarkar, 2011; Miškinytė and Dėdelė, 2014; Halim et al., 2019), and studies into the annoyance in large and popular tourist cities around the world, including H. Matamoros and Tamaulipas in northeast Mexico, Sfax in Tunisia, Seoul and Ulsan in South Korea, Copenhagen, Aarhus, Odense and other cities in Denmark, and Phuket and

Citation: Siwapathomchai N, Aimyong N, Patthanaissaranukool W, Sihabut T. Factors affecting traffic noise and annoyance from different types of roads: A case study in Nakorn Pathom Province, Thailand. Environ. Nat. Resour. J. 2023;21(4):290-298. (https://doi.org/10.32526/ennrj/21/20230006)

Ayutthaya in Thailand, have been reported (Sung et al., 2016; DRD, 2016; Bunnakrid et al., 2017, Thareejit et al., 2020; Bouzid et al., 2020; Zamorano-González et al., 2021). No less significant than in these places, people in frontier areas have also complained about traffic noise brought on by town expansion and various types of nearby transit linkages going to large cities.

Although Nakorn Pathom is a small province with an area of 2,168.3 km^2 and a population of 920,729 individuals, it is currently ranked in the top 10 highest gross provincial product (GPP) in Thailand (NESDC, 2022). With seven adjacent provinces, including the capital Bangkok, and its proximity to the Myanmar border, Nakorn Pathom serves as a significant agricultural and industrial production hub as well as a gateway to other parts of Thailand. While Route 4 or Petchkasem Rd (the longest major arterial road in Thailand) serves as the only major highway to the south, and Route 321 or Malaiman Rd (an important minor arterial road for cargo transportation) serves as a shortcut to the west, many crowded collector roads serve as links between Nakorn Pathom communities and these arterial roads. Thus, to better understand how motor traffic affects the nearby inhabitants along each road, factors contributing to traffic noise and residents' annoyance were examined.

2. METHODOLOGY

2.1 Data collection

Road traffic noise levels, traffic characteristics, and information on residents along the roadsides were collected from January to April 2020. To avoid atypical traffic characteristics, we temporarily stopped collecting data a week before and after any town special event and public holiday.

2.1.1 Measurement of road traffic noise and its contributing factors

According to the community settlement, Route 4 from km 50 to km 61 (+100), Route 321 from km 0 to km 5 (+200) and three collector roads, Ying Pao, Thahan Bok, and Ratchamanka Rd, constituted the study territory. To measure noise levels, three sampling sites along each type of road were determined (Figure 1) and a calibrated class I SVAN971 sound level meter was installed 1.5 meters above the ground at a distance of approximately five meters, three meters, and two meters away from the roadsides of major arterial, minor arterial, and collector roads, respectively. At each site, hourly equivalent sound levels (L_{eq}) over 24 hours were measured for three days on both weekdays and weekends and the day-evening-night average sound level (L_{den}) was calculated using Equation 1.

$$L_{den} = 10\log\left[\frac{1}{24}\left(12 \times 10^{\frac{L_{day}}{10}} + 4 \times 10^{\frac{L_{evening}+5}{10}} + 8 \times 10^{\frac{L_{night}+10}{10}}\right)\right] \quad (1)$$

Where; L_{day}= the average sound level from 07.00 to 19.00; $L_{evening}$=the average sound level from 19.00 to 23.00; L_{night}=the average sound level from 23.00 to 07.00.

A video camera that covered a 100-meter radius around two reference stations, where the sound level meter was situated in the middle, also recorded traffic volumes and vehicle types in addition to the measurements. During the morning and evening rush hours, the number of motorcycles, motor tricycles, cars/vans, and buses/trucks were counted. The ratio of buses/trucks to all vehicles was then calculated. To determine the vehicle speed, the distance traveled between those two fixed points was divided by the time taken to complete the trip.

2.1.2 Social survey

Personal and housing factors were collected through a pre-tested survey form and questionnaire with the acceptable item-objective congruence index rated by three experts (0.9). Based on Cochran's formula (Cochran, 1977), a total of 387 households were chosen to participate. Forty-three residents of homes in the first row of buildings closest to the road verge made up 129 representative samples for each type of road surrounding each noise monitoring site. Along with the observation on their housing types, structures, and setbacks — residents aged between 18 and 65 years that have been residing in the area for more than one year and spending more than eight hours in their residence while having no hearing impairment were asked about their socioeconomic status (sex, age, education attainment, health status), activity-based locations (open/closed spaces), and noise impacts. Perceived annoyance was verbally rated according to the five-point International Commission on Biological Effects of Noise (ICBEN) scale: (1) not at all annoyed, (2) slightly annoyed, (3) moderately annoyed, (4) mostly annoyed, and (5) extremely annoyed (Fields et al., 2001). The ratio of the sum of respondents' rating scores to the total number of respondents was used to determine the average annoyance. The percentage of highly annoyed (%HA) participants included the number of residents

who felt mostly and extremely annoyed (Brink et al., 2021).

2.1.3 Ethical approval

The Ethics Review Committee for Human Research at Mahidol University granted ethics approval for this study (COA No. MUPH 2019-147 on November 28, 2019).

2.2 Data analysis

Statistical analysis was performed by R (R Core Team, 2019). The relationship between the traffic noise level measured during rush hours and three contributing factors, traffic volume, vehicle speed, and the proportion of bus/truck to total vehicles, was analyzed using Spearman correlation. Comparative community sensitivities were derived from the trends between the percentage of highly annoyed (%HA) and the day-evening-night average sound level (L_{den}). The exact logistic regression, which is better suited to a small sample size (Zamar et al., 2007), was used to quantify the relationships between personal and housing factors and residents' annoyance because the traditional logistic regression used the unconditional maximum likelihood estimation with asymptotic assumption.

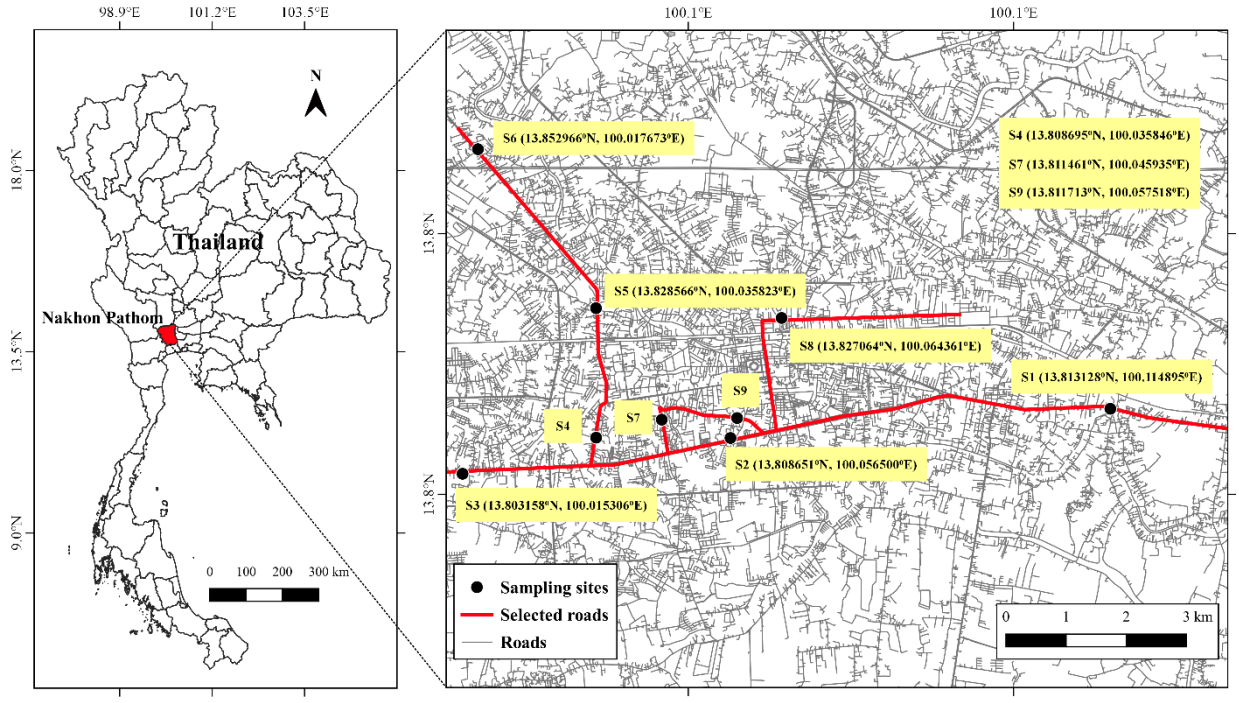

Figure 1. Sampling sites in Nakorn Pathom: Route 1 (S1, S2, S3), Route 321 (S4, S5, S6), and three collector roads, i.e., Ying Pao, Thahan Bok and Ratchamanka (S7, S8, S9)

3. RESULTS AND DISCUSSION

3.1 Road traffic characteristics, noise levels, and their contributing factors among different types of roads

In general, the major arterial road had the highest vehicle volumes, followed by minor arterial and collector roads, respectively (Table 1). According to the Thailand Road Traffic Act (Ministry of Interior, 1979; Ministry of Interior, 1981), heavy vehicles and cars/vans at several sites, especially on the minor arterial road, accelerated at speeds over the limit (inside city municipality: car/van ≤80 km/h, bus/truck ≤60 km/h; outside city municipality: car/van ≤90 km/h, bus/truck ≤80 km/h). As a result of engine noises combined with tire noises at higher speeds (Grubeša and Suhanek, 2021; Lechner et al., 2020), noise levels measured at these arterial roads were greater than those at collector roads (Table 2). Additionally, this pattern was seen in Delhi, India, and Phuket, Thailand (Ahmad and Sarkar; 2014, Bunnakrid et al., 2017).

Similar to many roads in large cities such as Doha in Qatar (Abdur-Rouf and Shaaban, 2022) and Sao Paulo in Brazil (Paiva et al., 2019), $L_{eq,\ 24h}$ at all sampling points on major and minor arterial roads in Nakorn Pathom exceeded the limit (70 dB(A)) determined by the Thailand Pollution Control Department, US Environmental Protection Agency,

and World Health Organization (Ministry of Natural Resources and Environment, 1997; CDC, 2019). Although L_{den} and L_{night} in our study were determined from traffic noise levels measured over a typical week, residents along the roads in Nakorn Pathom were exposed to a much higher noise threshold than that recommended by the Guideline Development Group (GDG) used in the European region — which accounted for added noises from special events throughout the year (WHO, 2018).

Table 1. Average of vehicle speeds, volumes and proportions of heavy to total vehicles in major arterial, minor arterial and collector roads in Nakorn Pathom Province

Road type	ID	Vehicle type								
		Motorcycle		Tricycle		Car/van		Bus/truck		Heavy to total vehicles*
		Speed (km/h)	Volume (veh/h)	Speed (km/h)	Volume (veh/h)	Speed (km/h)	Volume (veh/h)	Speed (km/h)	Volume (veh/h)	
Major arterial Rd	S1^{O}	57.6	913.3	39.0	8.2	85.9	10,332.3	61.0	515.2	0.051
	S2^{I}	60.1	747.2	41.4	9.0	85.5**	7,181.2	59.2	428.5	0.052
	S3^{O}	51.3	579.8	33.0	4.7	82.7	5,802.7	55.7	468.2	0.068
	Mean	56.3	746.8	37.8	7.3	84.7	7,772.1	58.6	470.6	0.057
	(SD)	(4.5)	(166.8)	(4.3)	(2.3)	(1.7)	(2,321.9)	(2.7)	(43.4)	(0.010)
Minor arterial Rd	S4^{I}	49.4	620.2	34.2	4.0	68.7	4,084.5	44.2	501.0	0.100
	S5^{I}	58.3	501.3	41.3	7.0	83.3**	2,754.7	62.4**	429.8	0.119
	S6^{O}	56.7	314.5	41.0	2.0	90.5**	2,361.3	71.2	389.8	0.127
	Mean	54.8	478.7	38.8	4.3	80.8	3,066.8	59.3	440.2	0.115
	(SD)	(4.7)	(154.1)	(4.0)	(2.5)	(11.1)	(903.0)	(13.8)	(56.3)	(0.014)
Collector Rd	S7^{I}	46.7	944.3	32.9	9.7	48.9	1,277.8	43.6	19.2	0.008
	S8^{I}	50.7	981.5	34.3	17.3	50.3	647.0	40.2	15.0	0.009
	S9^{I}	53.0	749.2	40.5	4.0	56.1	868.5	50.0	12.7	0.008
	Mean	50.1	891.7	35.9	10.3	51.8	931.1	44.4	15.6	0.008
	(SD)	(3.2)	(124.8)	(4.0)	(6.7)	(3.8)	(320.0)	(5.0)	(3.3)	(0.001)

I: located inside city municipality; O: located outside city municipality; *: the ratio of buses/trucks to all vehicles; **: over the speed limit as determined by the Thailand Road Traffic Act B.E.2522 (Ministry of Interior, 1979; Ministry of Interior, 1981)

Table 2. Average noise and annoyance levels and the percentage of highly annoyed (%HA) from road traffic noise in Nakorn Pathom Province

Road type	ID	Noise level (dB(A))					Annoyance level	%HA
		L_{day}	$L_{evening}$	L_{night}	L_{den}	$L_{eq,\ 24h}$		
Major arterial Rd	S1	79.4	77.2	76.1	83.2	78.4	2.8	53.5
	S2	77.4	75.3	72.8	80.3	76.0	2.2	34.9
	S3	76.2	74.9	72.5	79.8	75.1	1.8	25.6
Minor arterial Rd	S4	76.0	76.4	72.9	80.3	75.4	2.4	44.2
	S5	76.4	73.9	70.8	78.7	74.9	2.5	48.9
	S6	78.8	72.1	69.8	78.9	76.5	2.2	41.9
Collector Rd	S7	70.7	69.4	69.5	76.1	70.3	2.3	46.5
	S8	70.4	70.1	67.5	74.7	69.7	2.5	48.8
	S9	69.3	67.6	65.5	72.8	68.2	1.7	21.0

When the relationships between traffic noise level and its contributing factors were explored (Table 3), traffic volumes showed a significant correlation in regards to traffic noise, corresponding to several other studies (Halim et al., 2019; Peeters and Blokland, 2007; Miškinytė and Dėdelė, 2014). In contrast to normal circumstances, it was noted that traffic volume on the minor arterial road and vehicle speed on collector roads negatively correlated with noise level ($p=0.049$ and $p=0.002$, respectively).

The negative relation between traffic volume and noise level might be explained by road surface

condition and vehicle type. As shown in Table 1, the proportions of heavy to total vehicles on this minor arterial road were high since it served as a shortcut for cargo transport when traveling west of Thailand. Once the traffic volume was low, many truck drivers tended to accelerate their vehicle speeds. This resulted in higher noise levels from propulsion and tire rolling-contact surface (Peeters and Blokland, 2007; Grubeša and Suhanek, 2021) and rattling bodies from turbulence caused by the deteriorating pavements, which were commonly observed on arterial roads with a high number of trucks. Consequently, the noise level rose when the traffic volume was low, corresponding to a study of Anachkova et al. (2022).

For the latter case, a negative correlation could be elucidated by a traffic violation. Because collector roads had only two to four lanes with many vehicles parking along the roadsides, the drivers had to reduce their vehicle speeds which made vehicle volumes accumulate on the road. Thus, inverted relation was explored, possibly due to the influence of another factor. A similar condition was also observed in a congested area in Agartala City in India (Tripura and Sarkar, 2011).

Table 3. Spearman correlation coefficients between noise level ($L_{eq,1h}$) and its contributing factors

Road type		Traffic volume	Vehicle speed	Proportion of heavy to total vehicles
Major arterial	coefficient	0.607	0.269	-0.414
	p value	0.008	0.281	0.087
Minor arterial	coefficient	-0.469	0.444	-0.081
	p value	0.049	0.065	0.751
Collector	coefficient	0.885	-0.673	0.065
	p value	<0.001	0.002	0.797

3.2 Resident characteristics, noise impacts, and community sensitivities among different types of roads

As shown in Table 4, approximately one-half of the respondents were female. Most were middle-aged and their educational attainments were below college graduate levels. The majority performed their daily activities in open spaces and verbally described their physical status as healthy. Considering their housing characteristics, terraced houses along minor arterial and collector roads were common but relatively equal amounts of terraced and detached houses were observed along the major arterial road. The vast majority of housing was set back along the major arterial road further than 13 meters but only 0 to 6 and 0 to 5 meters away from the road verges for minor arterial and collector roads, respectively. Approximately 75% of the houses were made of cement, which was classified as effective soundproof structures, and the rest were either cement-wood-mixed or wood structures — which were classified as partially soundproof structures.

According to the interviews, adverse noise impacts involved annoyance (93.0-96.1%), conversation disturbance (42.6-86.8%), interference with hearing TV/Radio (38.8-60.0%), sleep disturbance (25.6-40.0%) and interference with working/reading (5.4-23.2%) (Figure 2). The average annoyance scores ranged from 1.7 to 2.8, and 21.0-53.5% of them felt highly annoyed (Table 2). Residents along arterial roads perceived trucks as the most annoying vehicle type while on collector roads were motorcycles. In this case, noise and vibration from a large number of trucks as previously discussed, as well as driving patterns, might be a cause. Since high proportions of heavy to total vehicles on arterial roads, especially on the minor arterial road, were observed — most truck drivers often touched the brake pads and used their unusually modified horns to avoid car accidents. The same reason can be used to account for residents' annoyance from collector roads. As a consequence of similar behaviors of riders, such as weird and distortedly loud accelerating, fast and aggressive riding, and group riding, this extreme annoyance response to motorcycles was also perceived by residents in Phuket, Thailand — as well as the Alpine valleys (Bunnakrid et al., 2017; Lechner et al., 2020).

Considering dose-response relationship, residents along collector roads with lower noise levels were more sensitive than the ones along the major arterial road (Figure 3). Although the significant correlations between road categories and noise-related impacts were indirectly described by noise levels in a previous study (González et al., 2023), the aforementioned noise characteristics together with shorter setback distance on collector roads might be an

explanation for our case. As confirmed by several studies, noise characteristics, in addition to noise levels, significantly increased traffic annoyance (Sung et al., 2016; Jeon et al., 2010; Erkan, 2017; Phan et al., 2009). Compared to other studies in Thailand (Bunnakrid et al., 2017; Thareejit et al., 2020), it was obvious that the traffic noise sensitivity among Thais who lived close to the same type of roads was alike. However, as a result of cultural differences, various sensitivities from many countries were observed (Bouzid et al., 2020; Sieber et al., 2018).

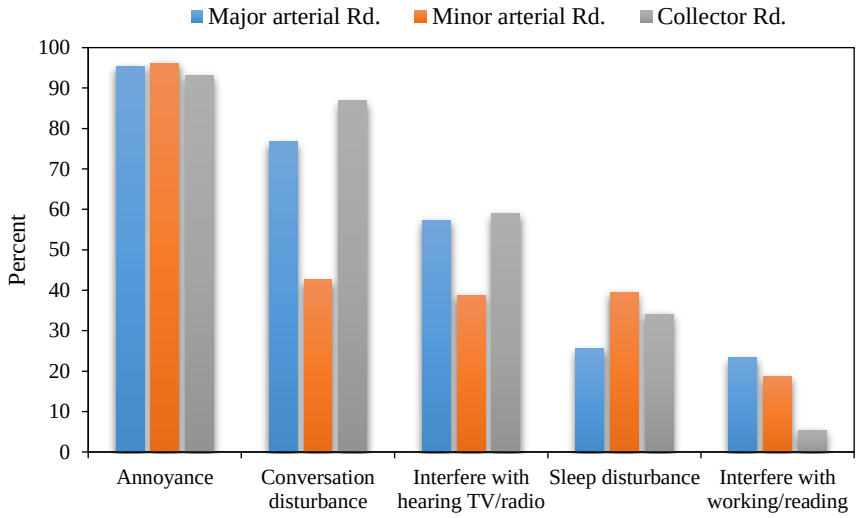

Figure 2. Noise impacts from major, minor and collector roads (n=129 individuals for each road)

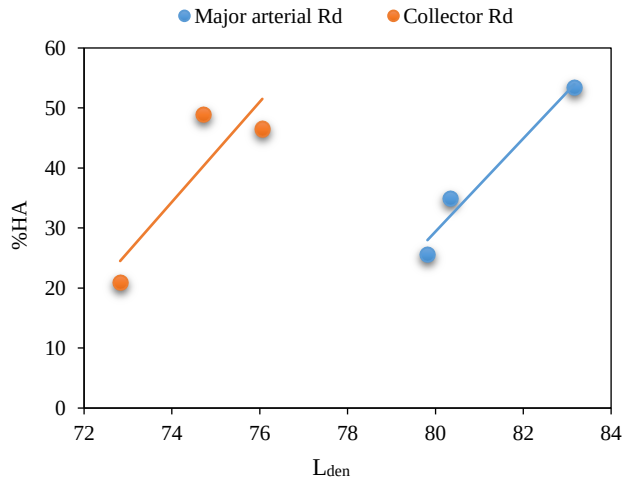

Figure 3. Noise sensitivities of residents living along different road types

3.3 Factors associated with residents' annoyance from different types of roads

As shown in Table 4, when the relations among variables were explored, two factors (sex and housing setback), three factors (age, housing setback, and activity-based location), and four factors (sex, housing setback, activity-based location, and housing structure) were significantly associated with residents' annoyance from the major arterial, minor arterial, and collector roads, respectively. From these findings, it consistently indicated that the further the housing setback distance, the lower the probability of being annoyed by traffic noise in every road type (OR=0.11, 95% CI: 0.003, 0.73 for the major arterial road; OR=0.29, 95% CI: 0.10, 0.78 for the minor arterial road and OR=0.32, 95% CI: 0.12, 0.84 for collector roads) (Table 4). As inverse relations between distance and noise levels have been confirmed in many studies (Miškinytė and Dėdelė, 2014; Azodo et al., 2019; Moshtaghie et al., 2012; Singhal et al., 2018), these may explain why activity-based locations and housing-related factors were insignificantly associated with residents' annoyance from the major arterial road. In contrast, these two factors played an important role in relieving noise disturbance to residents who lived in dwellings with the shorter setback distance. For instance, residents performing their daily activities in closed spaces along minor arterial (OR=0.05, 95% CI: 0.01, 0.17) and collector roads (OR=0.22, 95% CI: 0.54, 0.90) were less likely to be annoyed than those in open spaces. Another example was housing structure. The annoyance probability of residents living in houses with soundproof structures along collector roads was lower than among those in partially soundproof structures (OR=0.05, 95% CI: 0.001, 0.31). Although this relationship could not be explored from the minor

Table 4. Factors associated with annoyance of residents along different types of roads

Variable	Major arterial road					Minor arterial road					Collector roads				
	Total		Annoyance		p value OR (95% CI)	Total		Annoyance		p value OR (95% CI)	Total		Annoyance		p value OR (95% CI)
	n	%	n	%		n	%	n	%		n	%	n	%	
Total	129	100	103	79.8		129	100	104	80.6		129	100	93	72.1	
Sex					0.027					0.403					0.047
Female	67	51.9	59	88.1	1	69	53.5	58	84.1	1	77	59.7	61	79.2	1
Male	62	48.1	44	71.0	0.33 (0.11, 0.90)	60	46.5	46	76.7	0.63 (0.23, 1.64)	52	40.3	32	61.5	0.42 (0.18, 0.99)
Age					0.142					0.003					0.214
18-40	24	18.6	16	66.7	1	25	19.4	14	56.0	1	25	19.4	15	60.0	1
41-60	105	81.4	87	82.9	2.40 (0.77, 7.10)	104	80.6	90	86.5	4.97 (1.69, 14.73)	104	80.6	78	75.0	1.99 (0.71, 5.43)
Education					0.747					0.608					1.000
≥College	109	84.5	88	80.7	1	105	81.4	86	81.9	1	103	79.8	74	71.8	1
<College	20	15.5	15	75.0	0.72 (0.22, 2.81)	24	18.6	18	75.0	0.67 (0.21, 2.32)	26	20.2	19	73.1	1.06 (0.38, 3.32)
Health status					0.751					0.186					0.479
Unhealthy	10	7.8	9	90.0	1	18	14.0	17	94.4	1	21	16.3	17	81.0	1
Healthy	119	92.2	94	79.0	0.43 (0.01, 3.39)	111	86.0	87	78.4	0.22 (0.005, 1.52)	108	83.7	76	70.4	0.56 (0.13, 1.91)
Setback*					0.012					0.011					0.020
Inside cutoff	29	22.5	28	96.6	1	73	56.6	65	89.0	1	102	79.1	79	77.5	1
Outer	100	77.5	75	75.0	0.11 (0.003, 0.73)	56	43.4	39	69.6	0.29 (0.10, 0.78)	27	20.9	14	51.9	0.32 (0.12, 0.84)
Housing type					0.540					0.248					0.056
Detached	64	49.6	53	82.8	1	23	17.8	21	91.3	1	10	7.8	4	40.0	1
Terraced	65	50.4	50	76.9	0.69 (0.26, 1.79)	106	82.2	83	78.3	0.35 (0.04, 1.59)	119	92.2	89	74.8	4.39 (0.97, 22.64)
Soundproofing					0.148					0.248					<0.001
Partial	31	24.0	28	90.3	1	15	11.6	15	100.0	1	36	27.9	35	97.2	1
Effective	98	76.0	75	76.5	0.35 (0.06, 1.31)	114	88.4	89	78.1	0.24 (0.005, 1.71)	93	72.1	58	62.4	0.05 (0.001, 0.31)
Working space					0.250					<0.0001					0.001
Open	98	76.0	81	82.7	1	107	82.9	97	90.7	1	86	66.7	71	82.6	1
Closed	31	24.0	22	70.9	0.52 (0.19, 1.50)	22	17.1	7	31.8	0.05 (0.01, 0.17)	43	33.3	22	51.2	0.22 (0.54, 0.90)

* Due to different types of roadside characteristics, cutoff points for the major arterial, minor arterial and collector roads were 13, 6, and 5 meters, respectively.

arterial road, a high possibility of noise impact existed for the residents residing in houses with partly efficient soundproof structures, noticed by their consistent annoyance confirmation (Table 4).

For demographic factors, females residing along major arterial and collector roads and the older age group residing along the minor arterial road generally were more likely to be annoyed by road traffic noise. These resulted from higher environmental perceptions and awareness of females (Dratva et al., 2010) and loud noise acclimatization of younger respondents (Zamorano-González et al., 2021), respectively. However, as a result of individual factors, the relations could not be explored from some types of roads. The ground for these reasons should be explored further in-depth.

4. CONCLUSION

Road traffic noise levels at almost all sampling points in Nakorn Pathom Province exceeded the established limits. As a result, more than 90% of the respondents perceived slight to extreme annoyance. On collector roads, both the vehicle volume and the speed were significantly correlated with noise levels, while on major and minor arterial roads, vehicle volume was correlated with noise levels exclusively. According to the root causes, various legal measures, e.g., traffic flow and speed control should be implemented to alleviate the annoyance problem. For self-prevention, exact logistic regression analysis showed that housing setback potentially reduced noise annoyance from every road type. However, for minor arterial and collector roads, housing structure and activity-based location significantly played an additional role. Therefore, constructing houses with effective soundproof structures and performing activities in closed spaces were recommended.

ACKNOWLEDGEMENTS

The authors would like to thank the Mahidol University Alumni Association under the Royal Patronage of his Majesty the King for partial funding.

REFERENCES

Abdur-Rouf K, Shaaban K. Measuring, mapping, and evaluating daytime traffic noise levels at urban road intersections in Doha, Qatar. Future Transportation 2022;2:625-43.

Ahmad SA, Sarkar PK. Traffic noise studies on arterial and collector road in Delhi, India. International Journal of Structural and Civil Engineering Research 2014;3:138-50.

Anachkova M, Domazetovska S, Nikolovski F, Gavriloski V. Statistical analysis of urban noise measurement data: Case study for the city of Skopje. Proceedings of the Bi-annual Baltic Nordic-Acoustic Meetings; 2022 May 9-11; Aalborg: Denmark; 2022.

Azodo A, Onwubalili C, Mezue T. Assessment of observed building structure setback of shops along an arterial road and noise intrusion level. Journal of Engineering 2019;25:62-71.

Bouzid I, Derbel A, Elleuch B. Factors responsible for road traffic noise annoyance in the city of Sfax, Tunisia. Applied Acoustics 2020;168:Article No. 107412.

Bunnakrid K, Sihabut T, Patthanaissaranukool W. The relationship between road traffic noise and annoyance levels in Phuket Province, Thailand. Asia-Pacific Journal of Science and Technology 2017;22:1-9.

Brink M, Giorgis-Allemand L, Schreckenberg D, Evrard AS. Pooling and comparing noise annoyance scores and "High Annoyance" (HA) responses on the 5-point and 11-point scales: Principles and practical advice. International Journal of Environmental Research and Public Health 2021;18:Article No. 7339.

Centers for Disease Control and Prevention (CDC). What noises cause hearing loss? [Internet]. 2019 [cited 2022 Jun 1]. Available from: https://www.cdc.gov/nceh/hearing_loss/what_noises_cause_hearing_loss.html.

Cochran WG. The estimation of sample size. In: Cochran WG, editor. Sampling Techniques. 3rd ed. New York: John Wiley and Sons; 1977. p. 72-85.

Danish Road Directorate (DRD). Noise Annoyance from Urban Roads and Motorways. Copenhagen, Denmark: Vejdirektoratet; 2016.

Dratva J, Zemp E, Dietrich DF, Bridevaux P, Rochat T, Schindler C, et al. Impact of road traffic noise annoyance on health-related quality of life: Results from a population-based study. Quality of Life Research 2010;19:37-46.

Erkan İ. Horn sounds in transportation systems and a cognitive perspective on the instant mood-condition disorder. Procedia Engineering 2017;187:357-94.

European Environment Agency (EEA). Health risk caused by environmental noise in Europe [Internet]. 2020 [cited 2022 Aug 1]. Available from: https://www.eea.europa.eu/publications/health-risks-caused-by-environmental.

Fields JM, De Jong RG, Gjestland T, Flindell IH, Job RFS, Kurra S, et al. Standardized general-purpose noise reaction questions for community noise surveys: Research and a recommendation. Journal of Sound and Vibration 2001;242:641-79.

González DM, Morillas JMB, Rey-Gozalo G. Effects of noise on pedestrians in urban environments where road traffic is the main source of sound. Science of the Total Environment 2023;857:Article No.159406.

Grubeša S, Suhanek M. Traffic noise. In: Siano D, González E, editors. Noise and Environment. London, UK: IntechOpen; 2021. p. 1-21.

Halim H, Hamid NFN, Yusob MFM, Nor NAM, Hilmi NHFM, Sukor NSA, et al. Road traffic noise levels at different types of residential areas in Nibong Tebal, Penang. International Journal of Integrated Engineering 2019;11:101-12.

Jeon JY, Lee PJ, You J. Perceptual assessment of quality of urban soundscapes with combined noise source and water sound. Journal of Acoustic Society of America 2010;127:1357-66.

Lechner C, Schnaiter D, Siebert U, Böse-ÓReilly S. Effects of motorcycle noise on annoyance-a cross-sectional study in the Alps. International Journal of Environmental Research and Public Health 2020;17:Article No. 1580.

Ministry of Interior. Ministerial Regulations Issued under the Road Traffic Act, Royal Thai Government Gazette Volume 96, Part 95, Dated 14th Jun B.E. 2522. Bangkok, Thailand: Office of the Council of State; 1979.

Ministry of Interior. Ministerial Regulations Issued under the Road Traffic Act, Royal Thai Government Gazette Volume 98, Part 8, Dated 20th Jan B.E. 2524. Bangkok, Thailand: Office of the Council of State; 1981.

Ministry of Natural Resources and Environment. Notifications of National Environment Board RE: Prescribing Standard on Environmental Noise, Royal Thai Government Gazette Volume 114, Part 27d, Dated 3rd Apr B.E. 2540. Bangkok, Thailand: Office of the Council of State; 1997.

Miškinytė A, Dėdelė A. Evaluation and analysis of traffic noise level in Kaunas city. Proceedings of the 9th International Conference on Environmental Engineering; 2014 May 22-23; Vilnius: Lithuania; 2014.

Moshtaghie M, Kaboli M, Malekpouri P. Relationship between road vehicle traffic and noise pollution of Khojir National Park in the viewpoint of feasibility of fencing and soundproofing. International Journal of Environmental Health Engineering 2012;1:33-8.

Office of National and Economic and Social Development Council (NESDC). Gross Regional and Provincial Product: Chain Volume Measures 2020 Edition. Bangkok, Thailand: Office of National and Economic and Social Development Council; 2022.

Paiva KM, Cardoso MRA, Paulo PHT. Exposure to road traffic noise: Annoyance, perception and associated factors among Brazil's adult population. Science of the Total Environment 2019;650(Part 1):978-86.

Phan HAT, Yano T, Phan HYT, Nishimura T, Sato T, Hashimoto Y. Annoyance caused by road traffic noise with and without horn sounds. Acoustic Science and Technology 2009;30:327-37.

Peeters B, Blokland GV. The Noise Emission Model for European Road Traffic. Vught, Netherland: M+P-Consulting Engineers; 2007.

R Core Team. R: A language and environment for statistical computing [Internet]. 2019 [cited 2020 Nov 19]. Available from: https://www.R-project.org/.

Sieber C, Ragettli MS, Brink M, Olaniyan T, Baatjies R, Saucy A, et al. Comparison of sensitivity and annoyance to road traffic and community noise between a South African and a Swiss population sample. Environmental Pollution 2018;241:1056-62.

Singhal V, Jain S, Parida M. Train sound level detection system at unmanned railway level crossings. European Transport/ Trasporti Europei 2018;68:1-18.

Sung JH, Lee J, Park SJ, Sim CS. Relationship of transportation noise and annoyance for two metropolitan cities in Korea: Population based study. PLoS ONE 2016;11:1-10.

Thareejit M, Sihabut T, Patthanaissaranukool W. The association between road traffic noise and annoyance levels in residential and sensitive areas of Ayutthaya, Thailand. Asia-Pacific Journal of Science and Technology 2020;25:1-13.

Tripura DD, Sarkar PP. Traffic noise prediction model in Agartala City, India. International Review of Applied Engineering Research 2011;1:93-8.

World Health Organization (WHO). Environmental noise guidelines for the European region [Internet]. 2018 [cited 2022 Jun 20]. Available from: https://www.who.int/europe/publications/i/item/9789289053563.

Zamorano-González B, Pena-Cardenas F, Velázquez-Narváez Y, Parra-Siera V, Vargas-Martinez JI, Monreal-Aranda O, et al. Traffic noise annoyance in the population of North Mexico: Case study on the daytime period in the city of Matamoros. Frontiers in Psychology 2021;12:Article No. 657428.

Zamar D, McNeney B, Graham J. Elrm: Software implementing exact-like inference for logistic regression models. Journal of Statistical Software 2007;21:1-18.

Major Ion Chemistry of the Bheri (Snow-Fed) and the Babai (Rain-Fed) River Systems in Western Nepal: Implication on Water Quality

Kumar Khatri[1,2], Smriti Gurung[1*], Bibhuti Ranjan Jha[1], Milina Sthapit[3], and Udhab Raj Khadka[3]

[1]*Department of Environmental Science and Engineering, Kathmandu University, Dhulikhel, Nepal*
[2]*Mahendra Ratna Campus, Tribhuvan University, Kathmandu, Nepal*
[3]*Central Department of Environmental Sciences, Tribhuvan University, Kirtipur, Nepal*

ARTICLE INFO

Received: 17 Dec 2022
Received in revised: 21 Apr 2023
Accepted: 28 Apr 2023
Published online: 7 Jun 2023
DOI: 10.32526/ennrj/21/202200273

Keywords:
Babai River/ Bheri River/ Carbonate weathering/ Inter-basin water transfer/ Major ions

*** Corresponding author:**
E-mail: smriti@ku.edu.np

ABSTRACT

Inter Basin Water Transfer (IBWT) is a water resource stressor globally with negative environmental impacts. This study describes the major ions and hydrochemistry of the first ever ongoing IBWT from snow-fed Bheri River to rain-fed Babai River in Western Nepal. Water samples from 10 sites, five from each river system, were collected in HDPE bottles for major ions (Ca^{2+}, Mg^{2+}, Na^{+}, K^{+}, HCO_3^{-}, Cl^{-}, SO_4^{2-}, NO_3^{-}, CO_3^{2-}) along with the estimation of pH, temperature and conductivity encompassing winter, spring, summer, and autumn in 2018. $Ca^{2+}$and HCO_3^{-} were the most dominant cation and anion, respectively, with $Ca - Mg - HCO_3$ water type in both the river systems. Mann Whitney test revealed significant variation ($p<0.05$) between the two river systems with regard to Ca^{2+}, Mg^{2+}, HCO_3^{-}, and SO_4^{2-}. Kruskall Wallis test revealed significant variations between seasons in pH, temperature, Na^{+}, K^{+}, and Cl^{-} in Bheri River system, and in pH, TDS, temperature, Na^{+}, K^{+}, Cl^{-} and SO_4^{2-} in Babai River system. Carbonate weathering was the main mechanism of ionic sources with insignificant contribution from silicate weathering. Relatively higher concentrations of the major ions during the dry seasons probably indicate the dilution effect of monsoon. Higher concentrations of the ions in the Babai River system reflect the latter's bedrock geology with susceptibility to erosion. With Nepal's future plans of IBWTs and their environmental implications, this finding could be helpful in mitigating the negative consequences of IBWTs in the impact assessment and management of IBWT projects because of their implications on management of aquatic resources.

1. INTRODUCTION

Rivers are one of the main sources of freshwater that provide several ecosystem services and materials for human survival (Bolch et al., 2011). These include water for drinking and sanitation; fishery, irrigation and agriculture, hydropower generation, sand and gravel, transportation routes etc. (Tickner et al., 2017; WWF, 2018). These lotic systems are crucial components of hydrological cycles, climate regulation and material transport and cycling (Acreman, 1999; Kuchment, 2004). However, despite their huge significance, anthropogenic pressures associated with ever increasing dependency on river systems and their subsequent deterioration have become one of the major global environmental issues (MEA, 2005; Water UN, 2019). Major stressors on rivers include pollution, damming and diversion of rivers, and invasive species (Best, 2019). One of the major stressors in rivers is Inter Basin Water Transfer (IBWT) which involves construction of dams and diversion of naturally flowing waters. IBWTs are considered as crucial infrastructural developments to address the unequal distribution of crucial freshwater resources, however such transfers are associated with a range of negative environmental impacts in the upstream as well as downstream reaches of the rivers and their catchments (Snaddon et al., 1999; Lakra et al., 2011; Guo et al., 2020). Global reviews have shown their implications on terrestrial dynamics, biodiversity, and water quality (Ghassemi and White,

Citation: Khatri K, Gurung S, Jha BR, Sthapit M, Khadka UR. Major ion chemistry of the Bheri (snow-fed) and the Babai (rain-fed) River systems in Western Nepal: Implication on water quality. Environ. Nat. Resour. J. 2023;21(4):299-311. (https://doi.org/10.32526/ennrj/21/202200273)

2007; Snaddon et al., 1999; Zhuang, 2016) attributed to changes in water flow (Marak et al., 2020), which in turn affects transport capacity of the rivers, river water temperature, salinity, turbidity, mineral and nutrient concentrations, oxygenation, inorganic substrate composition, and sediment dynamics in both donor and recipient basins (Selge et al., 2016; Gallardo and Aldridge, 2018; Tian et al., 2019; Bui et al., 2020; de Lucena Barbosa et al., 2021).

Therefore, changes in natural flow due to IBWTs affect riparian eco-system health as it diminishes the water bodies' ability to assimilate pollutants and thus cause pollution, waterlogging, eutrophication, salinization, and acidification (Zhuang, 2016). Furthermore, water levels and renewal rates decline in downstream main channels (Pittock et al., 2009), disrupt river connectivity, and flood plains and channel connectivity (Bunn and Arthington, 2002; Grant et al., 2012). Changes in water transparency, nutrient and sediment loads, channel morphology and granulometry are some of the long-term physico-chemical effects of dams on downstream (Granzotti et al., 2018; Kamidis et al., 2021; Szatten et al., 2021; Yang et al., 2021), potentially leading to long-term oligotrophic-cation (Stockner et al., 2000; He et al., 2020). For instance, water transfer of São Francisco River in Brazil has been shown to cause algal blooms in receiving reservoirs (de Lucena Barbosa et al., 2021), decrease in dissolved oxygen content, and increased turbidity and salinity in Atibaia to Jundiaí transfer (Machado et al., 2018). These impacts in turn would affect the biodiversity (Schmidt et al., 2019), water quality (de Lucena Barbosa et al., 2021), and hydro-morphology of the river channels (Bui et al., 2020). Impacts on biodiversity include loss of biodiversity through blockade of migratory routes of fishes (ADB, 2018), interruption of life cycles (Pittock et al., 2009), introduction of invasive species (Gallardo and Aldridge, 2018), and change in biotic assemblages (Wang et al., 2021). For instance, blockade of salmon migratory routes in a large number of rivers is one of the well-known impacts of damming and diversion (Ferguson et al., 2011; Pringle et al., 2000). Likewise, water transfer from Orange River to Fish River resulted the replacement of dominant macro-invertebrate taxa like Chironomidae, Hydropsychidae, and Simuliidae by *Simulium chutteri* in Great Fish River, South Africa (O'keeffe and De Moor, 1988). In Great Berg River, reduction in macroinvertebrate taxa was reported where sensitive macroinvertebrate taxa, such as the Heptageniidae and Leptoceridae, were replaced by filter feeding Hydropsychidae (Snaddon et al., 1998). Thus, IBWTs compromise the ecological processes and benefits of the river systems (Machado et al., 2018) thereby making water quality assessments crucial prior to such transfers.

River water quality assessment often involves assessment of a range of physical, chemical, and biological parameters (MEA, 2005). Major ions, viz., calcium, magnesium, sodium, potassium, bicarbonate, sulphate, chloride, and nitrate in water are crucial components of water chemistry as they reflect the characteristics of ecological environment of the rivers and their catchments (Gergel, 2005; Novotny, 1999; Qishlaqi et al., 2016; Mallick, 2017). These ions form the bulk of the ionic composition in waters and account for salinity and conductivity, form important components of cellular structures and processes (Potasznik and Szymczyk, 2015), and play significant roles in osmoregulation and metabolism, and forms the basis for water quality for biotic assemblages and water use. For instance, elevated concentrations of major ions can induce osmotic stress in freshwater organisms (Ciparis et al., 2019), and affect soil properties (Biswas et al., 2018) and agricultural productivity. Thus, their presence and concentrations have important implications on the aquatic biodiversity, water quality and water use for various purposes such as irrigation, drinking and sanitation, and recreation (Moyel and Hussain, 2015).

The impact and consequences of IBWTs have been well documented in other parts of the world (Ghassemi and White, 2007). Nepal with its huge network of rivers possess tremendous potential for hydroelectricity and irrigation (WECS, 2011) and a number of IBWT projects are in pipeline to meet demands for irrigation water and electricity in the country (GoN/DWRI, 2019). This is also in line with the country's commitment to achieve Sustainable Development Goals (SDGs) 2016-2030 (GoN/NPC, 2017). The Bheri-Babai Diversion Multipurpose Project (BBDMP), is the first ever IBWT project of the country which aims to irrigate 51,000 ha of agricultural land in the southern districts of Bardiya and Banke and; generate 46 MW (Megawatt) of hydropower by transferring water from the snow-fed Bheri to the rain-fed Babai (GoN/BBDMP, 2018). Around two kilometers downstream of the proposed water release, the Babai River flows through one of the country's Protected Area harbouring rich and charismatic species of flora and fauna. Since the

BBDMP is the first of its kind project in the country, the study of IBWTs is important for Nepal as well. Considering the negative environmental impacts of such diversions, it is imperative to generate baseline data on major ions which can serve as a reference for future assessment of diversion. Therefore, the present study has focused on the status of major ions and hydrochemistry prior to water transfer from the Bheri to the Babai, which will be an important asset for managing IBWT projects with minimal negative impacts.

2. METHODOLOGY

2.1 Study area

The study was carried out in the Bheri and the Babai Rivers, respectively, lying in Surkhet and Dang Districts of Western Nepal (Figure 1). The Bheri River is about 264 km long originating from the permanent snow-capped mountains of the western Dhaulagiri range, and its basin covers an area of 13,900 km^2 with an elevational range of 200 to 7,746 m.a.s.l. (Mishra et al., 2018). The Babai River is about 400 km long originating from the low mountains in the Mahabharat hills, has springs, monsoon river water, and underground water, and has water all year, but the volume of water is low during the dry season and its basin covers an area of 3,250 km^2 extended between from 147 to 2,880 m.a.s.l. (Mishra et al., 2021). The BBDMP aims to transfer surplus water from the Bheri River to the Babai River through a 12.7 km tunnel which is expected to provide year-round irrigation facility with generation of electricity (GoN/BBMDP, 2018). In the lowlands, the Babai flows through the Bardiya National Park harbouring several of Nepal's most charismatic and endangered wildlife fauna (Chhetri et al., 2020).

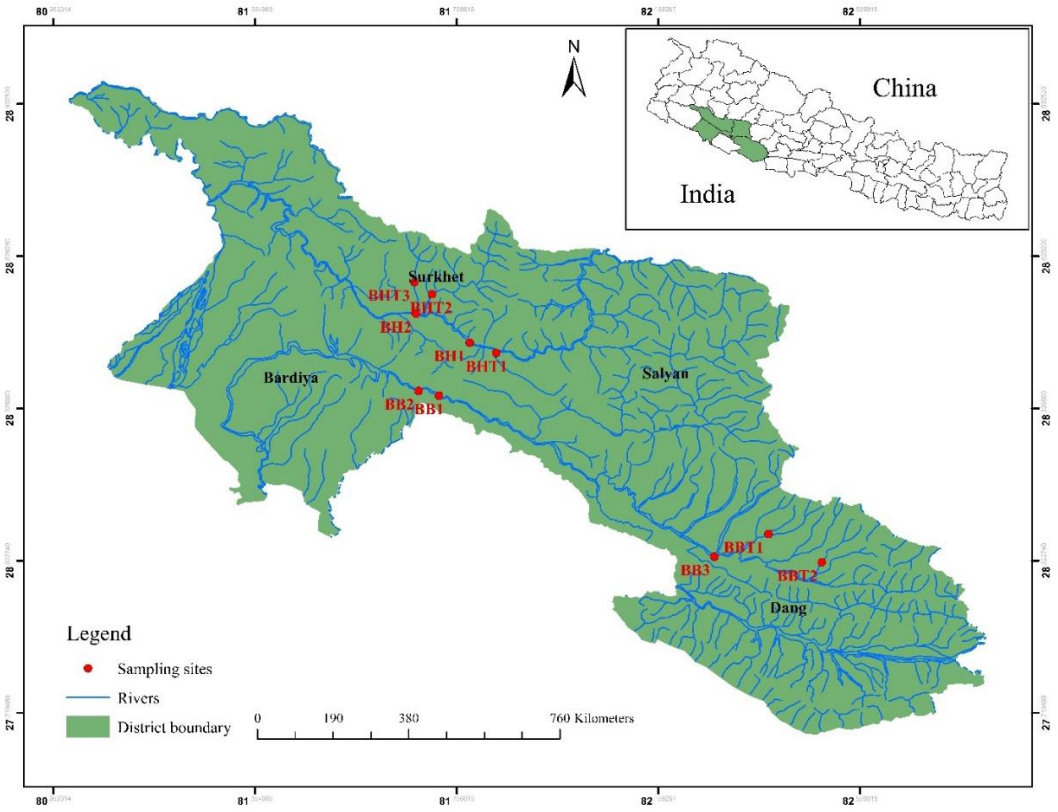

Figure 1. Study area map showing sampling sites

2.2 Sampling

Sampling was conducted in 2018 during January (winter), March-April (spring), June (summer), and November (autumn). A total of 10 sites (five from each river system) were selected based on strategic occurrence, accessibility, and retention of water in the tributaries throughout the year (Figure 1). Upstream and downstream sites of water transfer at the Bheri (BH1 and BH2 respectively) and water release at the Babai (BB1 and BB2 respectively), three tributaries from the Bheri, namely, Goche (BHT1), Chingad (BHT2); and Jhupra (BHT3); and one upstream main stem at the Babai (BB3) and two

tributaries, viz., Patre (BBT1) and Katuwa (BBT2) were sampled.

From each site, 1,000 mL of water samples were collected in high density polyethylene (HDPE) bottles and the samples were stored at 4°C in an icebox until laboratory analyses at the Department of Environmental Science and Engineering, Kathmandu University, to determine the concentrations of Ca^{2+}, Mg^{2+}, Na^{+}, K^{+}, HCO_3^-, Cl^-, SO_4^{2-}, NO_3^-, and CO_3^{2-} following standard methods (APHA, 2005). Water pH, dissolved oxygen (DO), conductivity, total dissolved solids (TDS), and temperature were measured on-site using a Multi-parameter Hannah probe (Model: HI98193).

2.3 Data analysis

Descriptive statistical analysis for the major ions was computed. Because of the skewness of the obtained data, non-parametric statistical tests were used to assess significant variations between seasons and between two rivers. Mann Whitney U test was performed to compare the statistically significant variations between various parameters in the two river systems. Kruskal-Wallis H test was used to determine significant seasonal variations within each river systems. Piper trilinear diagram which is used to analyze the chemical composition of river water (Piper, 1944) was plotted. Gibbs diagram (Gibbs, 1970) which categorizes the ion sources of surface waters into rock weathering type, precipitation control type and evaporation crystallization was also plotted to show the relationships between the total dissolved solids (TDSs) and ions (anions and cations). In addition, scatter plots were also generated to identify the main sources and processes controlling the major ion chemistry in the Bheri and the Babai River systems. All mathematical and statistical analyses of the data were performed in OriginPro 2022.

3. RESULTS AND DISCUSSION

3.1 Major ions and their seasonal variation

The mean concentrations of major ions in the Bheri and the Babai rivers during different seasons are presented in Table 1. The concentration of cations in both the river systems was in the order of $Ca^{2+} > Mg^{2+} > Na^{+} > K^{+}$, whereas those of the anions were in the order of $HCO_3^- > SO_4^{2-} > Cl^- > NO_3^-$ in the Bheri system, and $HCO_3^- > Cl^- > SO_4^{2-} > NO_3^-$ in the Babai system. Mann Whitney test revealed significant variation ($p<0.05$) between the Bheri and the Babai River systems with regard to Ca^{2+}, Mg^{2+}, HCO_3^- and SO_4^{2-} (Figure 2). Ca^{2+} and HCO_3^- are often the most dominant cation and anion in freshwater systems globally (Wetzel, 2001) and a large number of studies across Nepal and elsewhere have reported the dominance of these ions in different freshwater bodies (Lacoul and Freedman, 2005; Bajracharya et al., 2020; Bhatta et al., 2022). In contrast, the concentrations of K^{+} ions were lowest in both the water bodies. K^{+} is known to be absorbed by plants thereby making its concentrations lower in water (Skowron, 2018). The Kruskal Wallis test for pH, temperature, Na^{+}, K^{+}, and Cl^- in the Bheri revealed significant variation between seasons; and in the Babai system, significant variation between seasons was observed in pH, TDS, temperature, Na^{+}, K^{+} , Cl^-, and SO_4^{2-} (Table 1). In both the river systems, concentrations of most of the ions were higher during autumn except for SO_4^{2-}. Seasons tend to affect concentrations of ions in water bodies (Kannel et al., 2011) and seasonal variations in ion concentrations have been reported by various authors (Pant et al., 2018; Khadka and Ramanathan, 2021). Lower concentrations of ions during summer could be because of dilution effect attributed to heavy precipitation and glacial meltwater as summer months of June, July, August and September are characterized by monsoon in South Asia including Nepal (Shrestha and Aryal, 2011; Zhu et al., 2021).

pH was alkaline in both the river systems (Table 1). A large number of studies conducted in Nepalese rivers have also reported similar findings (Jha et al., 2018; Ghimire et al., 2021; Singh et al., 2021). Alkalinity is attributed to dissolved carbon dioxide, bicarbonate, and carbonate (Domenico and Schwartz, 1998; Ewaid, 2016), which in turn is affected by pH. The TDS was higher in the Babai River system. TDS values are usually attributed to natural as well as anthropogenic sources (Mikalsen, 2005). Bedrock geology and weathering are natural sources of dissolved ions (Singh et al., 2016), whereas drainage systems particularly in urbanized watersheds, wastewater leakages and fertilizer runoffs are the anthropogenic sources which contribute to increased TDS concentrations in water bodies (Mikalsen, 2005). The higher TDS concentrations indicate the presence of an appreciable quantities of bicarbonates, sulphates and chlorides of Ca^{2+}, Mg^{2+}, and Na^{+} (Hossain et al., 2017). The higher TDS concentrations in the Babai system particularly in sites BB3, BBT1, and BBT2 probably reflects the use of fertilizer run off, urbanized watershed and catchment geology. In both the river

Table 1. Seasonal variation of the major ions concentrations in the Bheri and the Babai River systems (units in mg/L except for pH)

Parameters	Bheri River system				Babai River System			
	Winter	Spring	Summer	Autumn	Winter	Spring	Summer	Autumn
pH	8.47±0.16^{ab}	8.65±0.17^{a}	7.88±0.35^{b}	7.80±0.44^{b}	8.46±0.20^{a}	8.31±0.25^{a}	7.69±0.39^{b}	7.69±0.19^{c}
TDS	141.00±36.52^{a}	154.93±28.47^{a}	152.40±32.34^{a}	188.13±42.07^{a}	186.40±32.94^{abc}	175.13±17.99^{a}	169.33±58.54^{ac}	263.33±49.80^{b}
Ca^{2+}	33.24±3.53^{a}	36.64±8.75^{a}	36.96±8.61^{a}	31.52±9.97^{a}	44.16±8.62^{a}	37.12±5.56^{a}	33.12±8.50^{a}	41.60±7.48^{a}
Mg^{2+}	14.56±2.43^{a}	15.90±2.49^{a}	14.06±1.41^{a}	14.14±3.92^{a}	22.24±3.98^{a}	19.68±3.05^{a}	15.50±4.15^{a}	20.40±4.02^{a}
K^{+}	1.67±0.37^{ab}	1.92±0.47^{a}	0.54±0.03^{c}	1.17±0.13^{bc}	1.73±0.19^{a}	2.06±0.30^{a}	0.64±0.15^{c}	1.61±0.17^{ac}
Na^{+}	5.22±1.68^{a}	4.33±0.68^{a}	0.39±0.02^{b}	3.38±0.99^{ab}	4.62±1.32^{ab}	8.03±2.75^{c}	0.33±0.02^{a}	4.77±0.42^{bc}
HCO_3^{-}	143.83±53.48^{a}	136.01±41.03^{a}	125.29±29.61^{a}	156.02±42.30^{a}	184.67±22.96^{a}	165.84±34.69^{a}	154.00±25.47^{a}	196.49±34.47^{a}
Cl^{-}	11.33±3.09^{a}	14.15±6.88^{a}	2.50±0.00^{b}	6.50±2.38^{ab}	13.13±1.87^{a}	13.50±1.92^{a}	6.00±4.18^{b}	7.83±1.51^{b}
NO_3^{-}	0.46±0.24^{a}	0.25±0.31^{a}	0.26±0.15^{a}	0.23±0.13^{a}	0.44±0.34^{a}	0.44±0.29^{a}	0.17±0.07^{a}	0.46±0.58^{a}
SO_4^{2-}	20.08±8.36^{a}	21.97±9.48^{a}	15.29±10.01^{a}	16.15±11.96^{a}	12.02±1.50^{ab}	12.83±1.72^{a}	4.43±0.45^{c}	6.34±1.63^{cb}

Note: Values followed by different letters are statistically significant ($p<0.05$).

systems, Ca^{2+} concentrations exceeded 15 mg/L which is higher than the concentrations in natural waters. This may be associated with carbonate-rich rocks (Bisht et al., 2018). The concentrations of Mg^{2+}, K^{+}, and Na^{+} are within the range of natural concentrations and thus, suitable for agricultural purposes (Boyd, 2020). The excess of K^{+} enters freshwaters with industrial discharges and runoffs from agricultural land as potassium is widely used in industry and fertilizers (Best, 2019; Mukate et al., 2020). Concentration of Cl^{-} in winter and spring from both the river systems surpassed the pristine limit of <10 mg/L. SO_4^{2-} concentrations were within range of concentrations in natural waters (Chapman, 1996). SO_4^{2-} is naturally present in surface waters though it can arise from the atmospheric deposition of oceanic aerosols, leaching of sulphur compounds, from sedimentary rocks, and industrial and atmospheric precipitation can add significant amounts of SO_4^{2-} to surface waters (Kurdi et al., 2015).

3.2 Hydrochemistry and mechanisms controlling water chemistry

The hydrochemical facies of both river systems is shown in a Piper plot (Figure 3). In the Bheri River system, Ca^{2+} accounted for the highest total cationic equivalent charge of 55.25% followed by Mg^{2+} with 38.95%, Na^{+} and K^{+} covering 5.80%. Among the anions, HCO_3^{-} contributed 78.30% of the total anionic equivalent charge followed by SO_4^{2-} with 13.71% and Cl^{-} covering 7.99%. In the Babai system also, Ca^{2+} accounted for the highest total cationic equivalent charge of 51.72% followed by Mg^{2+} with 42.38%, Na^{+} and K^{+} covering 5.89%. HCO_3^{-} contributed 86% of the total anionic equivalent charge followed by Cl^{-} with 8.38% and SO_4^{2-} covering 5.62%. Dominance of Ca^{2+} and HCO_3^{-} in both the river systems indicates their origin from carbonate weathering (Singh et al., 2005). The dominance of these ions has been reported in a number of freshwater bodies across the earth including Nepal (Reynolds et al., 1995; Wetzel, 2001; Gurung et al., 2018; Sharma et al., 2020). The points in ternary plots appear to support from the Ca^{2+} apex to the Mg^{2+} side accompanied by drifting from the Cl^{-} side to the HCO_3^{-} and SO_4^{2-} domain indicating general direction of progression from carbonate weathering in both the river systems (Figure 3). HCO_3^{-} mainly originates from carbonate weathering, reflecting the dominance of carbonates rocks as controls of water chemistry (Jiang et al., 2015).

Hence, the total cations and anions in both rivers in the Ca^{2+}, Mg^{2+}, HCO_3^- corners suggest a Ca^{2+}-Mg^{2+}-HCO_3^- river water (Khadka and Ramanathan, 2012; Qu et al., 2019).

Gibbs plots (Gibbs, 1970) reflecting the ratio of $Na^+/(Na^+ + Ca^{2+})$ and $Cl^-/(Cl^- + HCO_3^-)$ as a function of TDS further revealed that all the water samples fall in the dominated area of rock weathering indicating that various rock forming minerals as the primary factor controlling the water chemistry of the Bheri and the Babai River systems (Figures 4 and 5).

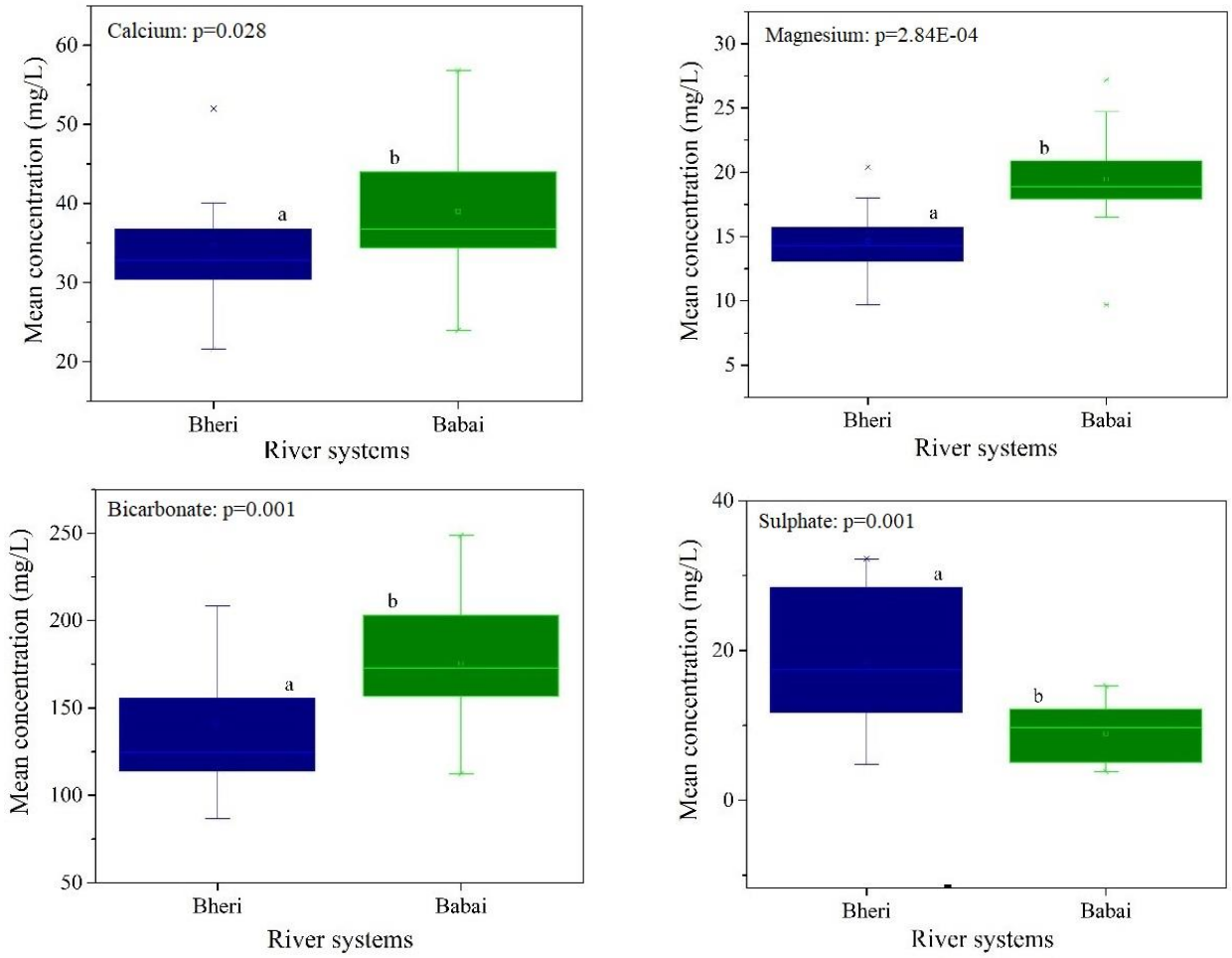

Figure 2. Mean concentration of different physico-chemical parameters of the Bheri and the Babai River system (Values followed by different letters are statistically significant ($p<0.05$).)

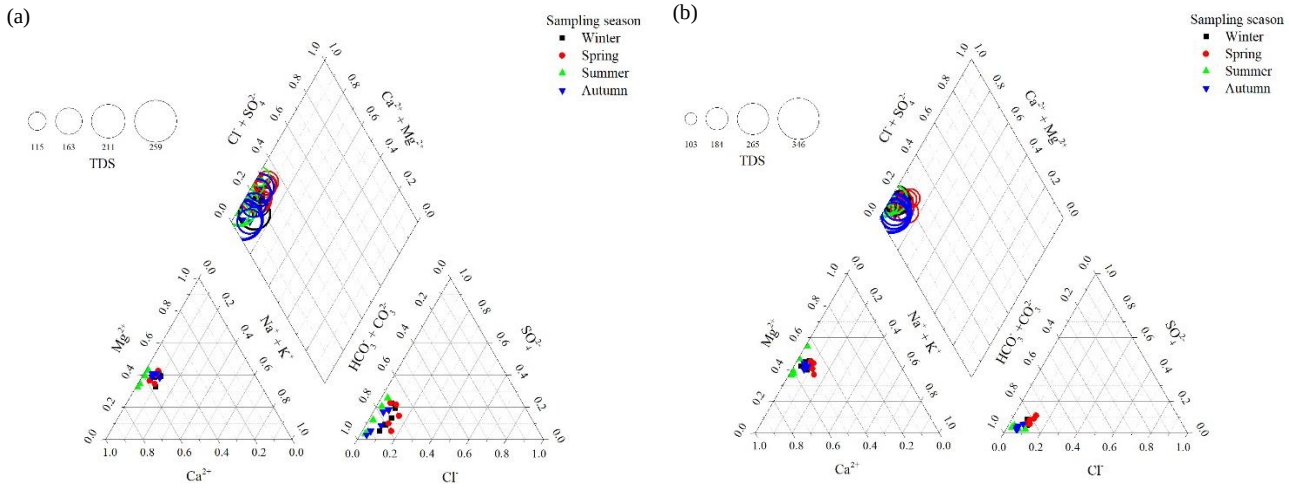

Figure 3. Ternary plots of cation and anion concentrations of the Bheri (a) and the Babai (b) River systems

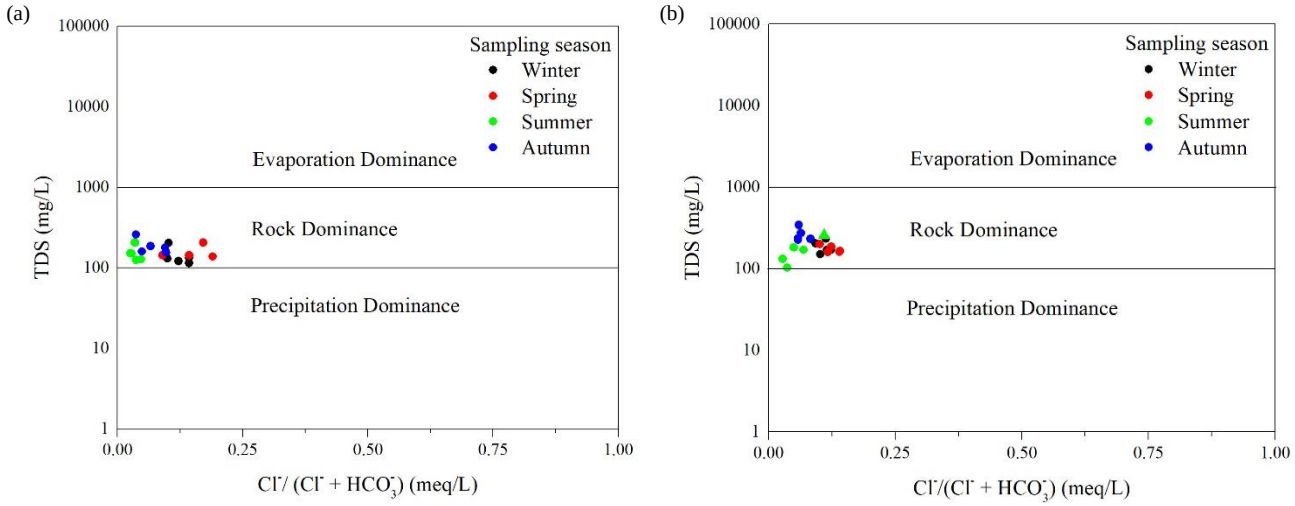

Figure 4. Gibbs diagrams indicating the Bheri (a) and the Babai (b) River system natural evolution mechanisms TDS vs. $Cl^-/(Cl^-+HCO_3^-)$.

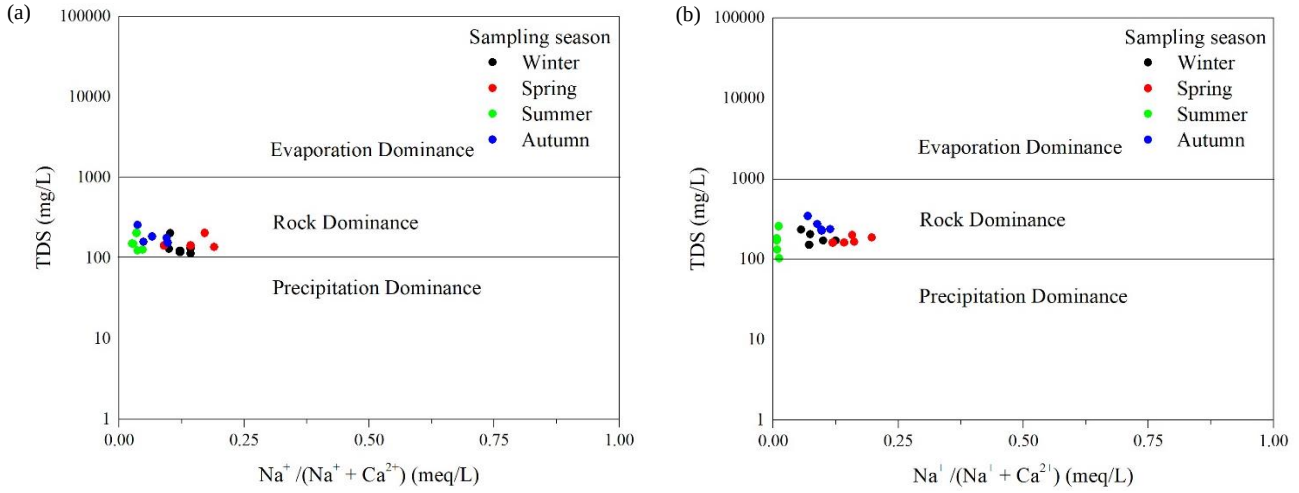

Figure 5. Gibbs diagrams indicating the Bheri (a) and the Babai (b) River system natural evolution mechanisms TDS vs. $Na^+/(Na^+ + Ca^{2+})$.

The hydrochemical facies reflect the chemical interactions on the lithological environment (Vasanthavigar et al., 2013). The high concentration of Ca^{2+} for all the water bearing units can probably be due to water-rock interaction as most of the rocks contain mineral species such as calcite, gypsum, and anhydrite (Dhital, 2015). The low level of K^+ relative to Ca^{2+}, Mg^{2+}, and Na^+ may be due to the fact that it can easily be fixed by clay minerals (Shakeri and Abtahi, 2020). Dominance of HCO_3^- indicates chemical weathering inferred from silicate and carbonate weathering rocks present in the river basin (Nisha et al., 2021). Dissolution of CO_2 in the surface water through natural gas exchange from atmosphere, respiration of riparian plants, and microbial activity in sediments results into the formation of CO_3^- and HCO_3^-, which in turn are mainly accountable for rock weathering, particularly carbonate rocks and alumino-silicate minerals (Gupta et al., 2022). Dominance of CO_3^- and HCO_3^- in both the river systems thus reflect carbonate weathering and atmospheric carbon oxide exchange. Furthermore, dominance of Ca^{2+} and HCO_3^- (weak acid) over SO_4^{2-} and Cl^- (strong acids) in both the river systems indicate the dominance of alkaline earth metals over alkaline elements thereby confirming bedrock geology as the main contributor to major ions (Tiwari et al., 2021). All analyzed samples are classified as calcium-magnesium-bicarbonate water. All the water samples are mainly towards carbonate and silicate end-members, indicating the main mechanism controlling the water chemistry of both river systems, and reflects the dissolution of minerals such as pyroxene, calcite, gypsum, anhydrite, and dolomite (Wanty et al., 2009). The sources of these minerals are associated with limestone, marl, dolerite, and pyroclastic materials associated with the slate rocks in the study area (Zaw et al., 2014). Chemical weathering has been identified as the major

source of major ions in the rivers draining the Himalaya where carbonate weathering plays the dominant role in river hydrochemistry (Tsering et al., 2019). The weathering of carbonates is greater in most river systems in Western Nepal than the weathering of silicates (Quade et al., 2003). In the glaciated Himalayan regions, more than 90% of HCO_3^- and Ca^{2+} is derived from carbonate weathering, though the carbonates represent only ~1.0 wt% in fresh glacial till (Jacobson et al., 2002). The Bheri catchment consists of very thick (more than 5 m) alternating beds of red-purple, yellow, brown, and grey-green mudstone, calcareous mudstone, and shale with siltstone and medium to fine-grained grey and green-grey sandstone intercalations (Arita et al., 1984; Kafle et al., 2019). The Babai River system in the Dang Valley is filled up with Pleistocene to Holocene fluvial sediments, consisting of clay and peat, fluvial deposits, mixed up with various crush rocks silt soils with pebbles, cobbles, and boulders (up to 1 m) of quartzite, slate, and limestone. This also explains higher TDS in the Babai system particularly at sites BB3 (Babai River), BBT1 (Patre River), and BBT2 (Katuwa River). Most of these materials are highly weathered, resulting in the development of red soils and badlands (Kono, 1974). The Himalayan region has a high frequency of physical erosion and chemical weathering triggered by relief and elevation (Singh et al., 2005; Lupker et al., 2012). Calcareous rocks are predominantly carbonate rocks, usually limestone or dolostone with chemical compositions of $CaCO_3$ (Dhital, 2015) and $CaMg(CO_3)_2$ (Tamrakar and Shrestha, 2008), respectively. Presence of such calcite and dolomite rich geology explains the higher concentrations of Ca^{2+}, Mg^{2+}, and HCO_3^- in the Bheri and the Babai River waters.

The values of the ionic ratios also support the origin of major ions generated by chemical weathering. Scatter plots showing ionic source and mechanism controlling hydrochemistry of the Bheri and the Babai systems are shown in Figures 6, 7, 8, and 9. The ratio of $Ca^{2+}+Mg^{2+}/(Tz^+)$ (Figure 6) in the Bheri and the Babai Rivers with the regression line having slope values of 0.95 and 0.90, respectively, suggests the majority of contributions from Ca^{2+} and Mg^{2+}. The ratio of $Ca^{2+}+Mg^{2+}/HCO_3^-+SO_4^{2-}$ (Figure 7) in both the systems with slope values of 0.58 and 1.24, respectively, suggests the dominant role of carbonate weathering, suggesting calcite, dolomite, and gypsum dissolution to be dominating reactions. In both river systems, most of the sites have higher values of $(Ca^{2+}+Mg^{2+})$ than HCO_3^- which requires additional anions such as SO_4^{2-} for ionic balance indicating the probable role of sulfuric acid in carbonate weathering in both river systems. However, $Ca^{2+}+Mg^{2+}/HCO_3^-$ ratio (Figure 8) with the regression line showing slope values of 0.56 and 1.19 in the Bheri and the Babai respectively, also suggests the contribution from silicate weathering in addition to carbonate weathering. Few samples appear below the equiline in both river systems indicating an excess of HCO_3^- over Ca^{2+} probably derived from silicate weathering (Vinnarasi et al., 2021). The $(Na^++K^+)/Tz^+$ ratio in the Bheri and the Babai River systems (Figure 9) with the regression line having a slope value of 0.046 and 0.096, respectively, further confirms carbonate weathering indicating that there is no significant contribution of cations to the river waters from of alumino-silicate weathering. Little ionic contribution from silicate weathering has been reported in several water bodies from Nepal for instance, from Dudh Koshi and Indrawati Rivers (Paudyal et al., 2016), lakes of Pokhara (Khadka and Ramanathan, 2012; Khadka and Ramanathan, 2021; Kafle et al., 2023), Chandragiri-Payaswini River system in India (Nisha et al., 2021), and Teesta River in Sikkim, India (Tsering et al., 2019).

Ca^{2+} and HCO_3^- are the most dominant cation and anion in both the river systems. Furthermore, the scatter plots revealed that carbonate weathering of sedimentary rocks rich in calcium minerals with limestone and gypsum is the main source of dissolved calcium in river water (Bhateria and Jain, 2016). The ionic composition of surface waters is usually considered to be relatively stable and is governed by exchanges with the underlying geology of the drainage basin and atmospheric deposition. Magnesium, sodium, and potassium concentrations tend not to be heavily influenced by metabolic activities of aquatic organisms, whereas calcium can exhibit marked seasonal and spatial dynamics as a result of biological activity (Wetzel, 2001; Carr and Neary, 2008). Similarly, chloride concentrations are not heavily influenced by biological activity, whereas sulphate and inorganic carbon (carbonate and bicarbonate) concentrations can be driven by production and respiration cycles of the aquatic biota (Carr and Neary, 2008). External forces such as climatic events that govern evaporation and discharge regimes and anthropogenic inputs can also drive patterns in ionic concentrations.

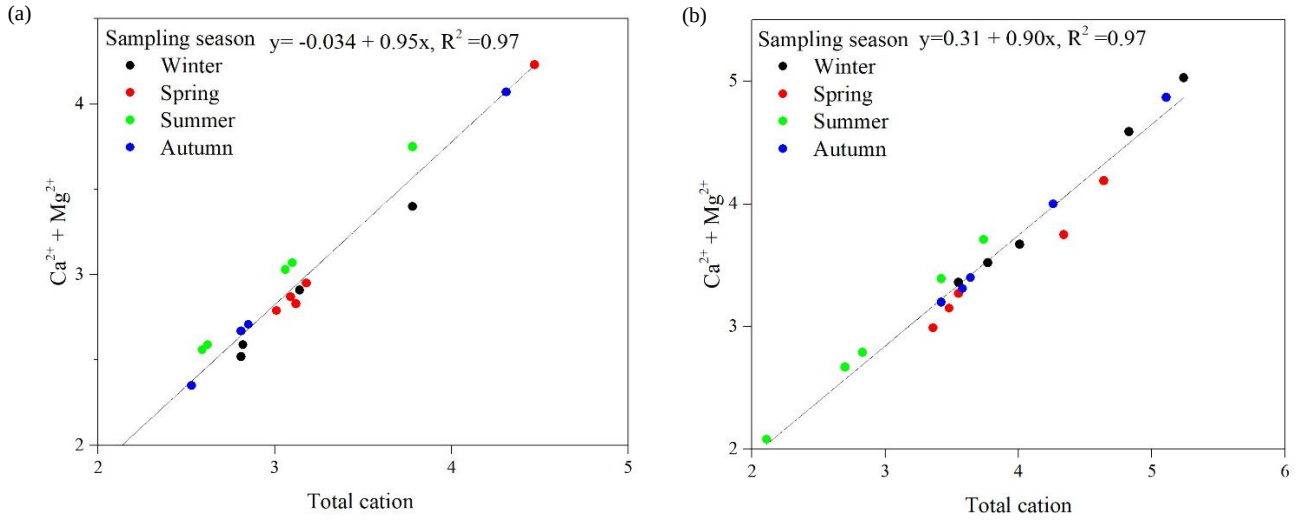

Figure 6. Scatter diagram of $(Ca^{2+}+Mg^{2+})/Tz^{+}$ of the Bheri (a) and the Babai (b) River systems

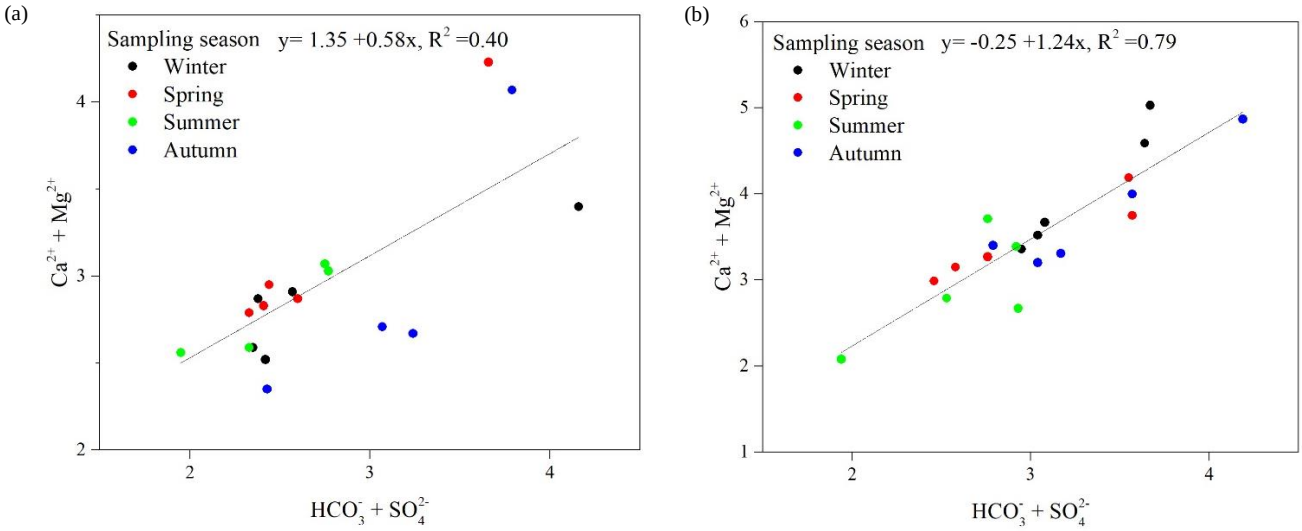

Figure 7. Scatter diagram of $(Ca^{2+}+Mg^{2+})/(HCO_3^- + SO_4^{2-})$ of the Bheri (a) and the Babai (b) River systems

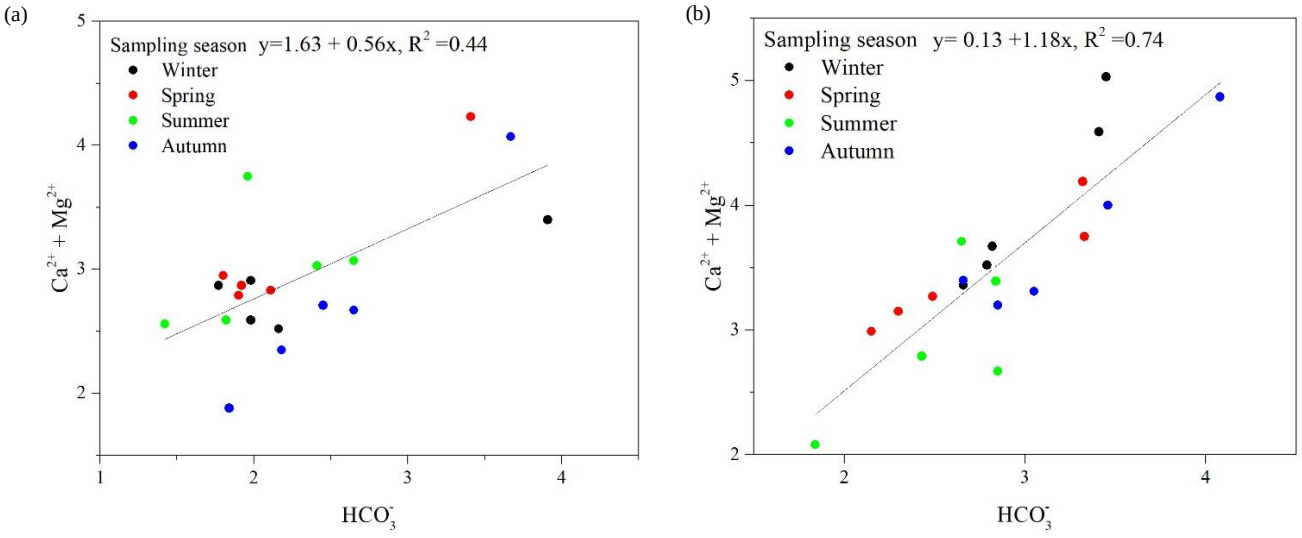

Figure 8. Scatter diagram of $(Ca^{2+}+Mg^{2+})/HCO_3^-$ of the Bheri (a) and the Babai (b) River systems

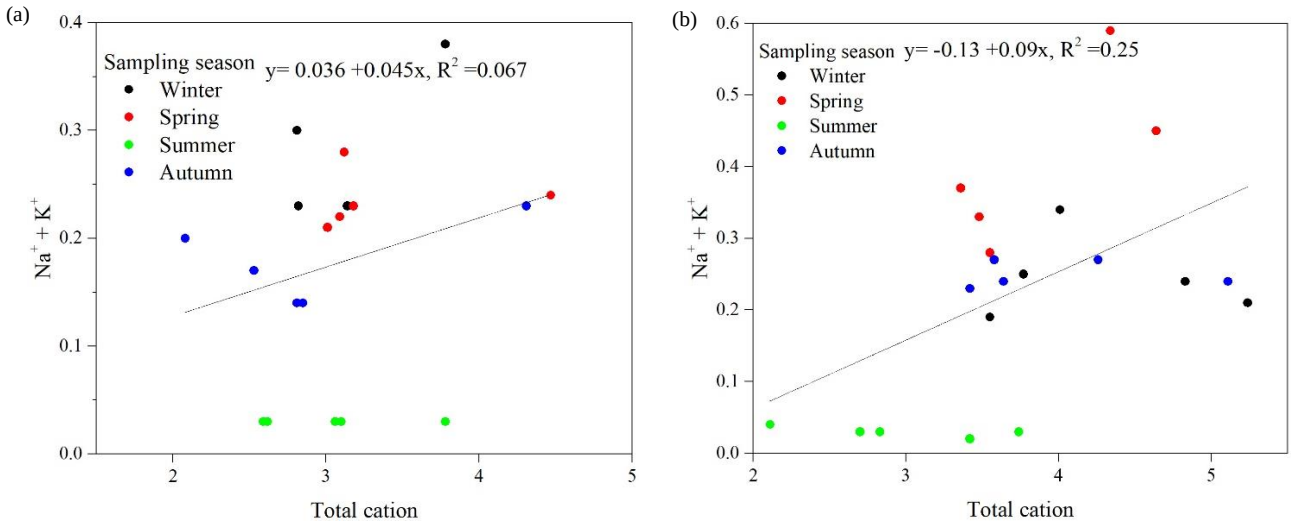

Figure 9. Scatter diagram of $(Na^+ + K^+)/Tz^+$ of the Bheri (a) and the Babai (b) River systems

4. CONCLUSION

This study has generated the status of major ions and hydrochemistry of the Bheri and the Babai Rivers in Western Nepal prior to inter-basin water transfer. In both rivers, Ca^{2+} and HCO_3^- were the most dominant cation and anion respectively. Carbonate weathering was the main mechanism of ionic sources with insignificant contribution from silicate weathering. Relatively higher concentrations of major ions during the dry seasons probably indicate the dilution effect of monsoon. Apart from this, higher concentrations of the ions in the Babai systems reflect the latter's bedrock geology which is susceptible to erosion. In order to balance the distribution of crucial water resource from water abundant river basin to the water deficit river basin, the IBWTs will be a common practice in the future. However, there will be the widespread impacts of such transfers, both positive and negative. While, the positives such as the redistribution of water, thereby helping water cycle and climate regime, protecting biota and repairing disrupted ecological system are most welcome, the information this study has gathered is more important in mitigating the negative consequences of such initiatives in the future. These findings are crucial baseline data particularly in the impact assessment of inter-basin water transfer and management of IBWT projects because of their implications on management of water quality and aquatic resources.

ACKNOWLEDGEMENTS

This research was financially supported by the University Grants Commission (UGC) (Faculty Collaborative Research Grant for F.Y. 2072/73) of Nepal. The authors would like to acknowledge the Department of National Park and Wildlife Conservation (DNPWC), Nepal for giving us permission to sample at Mulghat, Bardiya National Park.

REFERENCES

Acreman M. Water and ecology linking the earth's ecosystems to its hydrological cycle. In: Revista CIDOB d'Afers Internacionals 45-46. Barcelona Centre for International Affairs; 1999. p. 129-144.

Asian Development Bank (ADB). Impact of Dams on Fish in the Rivers of Nepal. Manila, Philippines: ADB; 2018. p. 95-110.

American Public Health Association (APHA). Standard Methods for the Examination of Water and Wastewater. 21st ed. Washington DC, USA: American Public Health Association, American Water Works Association, and Water Environment Federation; 2005.

Arita K, Shiraishi K, Hayashi D. Geology of western Nepal and a comparison with Kumaun, India. Journal of the Faculty of Science, Hokkaido University. Series 4, Geology and Mineralogy 1984;21:1-20.

Bajracharya R, Nakamura T, Ghimire S, Shakya BM, Tamrakar NK. Identifying groundwater and river water interconnections using hydrochemistry, stable isotopes, and statistical methods in Hanumante river, Kathmandu Valley, Central Nepal. Water 2020;12(6):Article No. 1524.

Best J. Anthropogenic stresses on the world's big rivers. Nature Geoscience 2019;12:7-21.

Bhateria R, Jain D. Water quality assessment of lake water: A review. Sustainable Water Resources Management 2016; 2:161-73.

Bhatta R, Gurung S, Joshi R, Tuladhar S, Regmi D, Kafle BK, et al. Spatio-temporal hydrochemistry of two selected Ramsar sites (Rara and Ghodaghodi) of west Nepal. Heliyon 2022;8(11):e11243.

Bisht H, Arya PC, Kumar K. Hydro-chemical analysis and ionic flux of meltwater runoff from Khangri Glacier, West Kameng, Arunachal Himalaya, India. Environmental Earth Sciences 2018;77:1-16.

Biswas B, Qi F, Biswas JK, Wijayawardena A, Khan MAI, Naidu R. The fate of chemical pollutants with soil properties and processes in the climate change paradigm: A review. Soil Systems 2018;2(3):Article No. 51.

Bolch T, Pieczonka T, Benn DI. Multi-decadal mass loss of glaciers in the Everest area (Nepal Himalaya) derived from stereo imagery. The Cryosphere 2011;5:349-58.

Boyd CE. Water Quality: An Introduction. 3rd ed. Cham, Switzerland: Springer Nature; 2020.

Bui DT, Asl DT, Ghanavati E, Al-Ansari N, Khezri S, Chapi K, et al. Effects of inter-basin water transfer on water flow condition of destination basin. Sustainability 2020;12(1):Article No. 338.

Bunn SE, Arthington AH. Basic principles and ecological consequences of altered flow regimes for aquatic biodiversity. Environmental Management 2002;30(4):492-507.

Carr GM, Neary JP. Water Quality for Ecosystem and Human Health. 2nd ed. UNEP GEMS/Water Programme; 2008.

Chapman DV. Water Quality Assessments: A Guide to the Use of Biota, Sediments and Water in Environmental Monitoring. 2nd ed: CRC Press; 1996.

Chhetri TB, Dhital YP, Tandong Y, Devkota LP, Dawadi B. Observations of heavy rainfall and extreme flood events over Banke-Bardiya Districts of Nepal in 2016-2017. Progress in Disaster Science 2020;6:Article No. 100074.

Ciparis S, Rhyne G, Stephenson T. Exposure to elevated concentrations of major ions decreases condition index of freshwater mussels: Comparison of metrics. Freshwater Mollusk Biology and Conservation 2019;22:98-108.

de Lucena Barbosa JE, dos Santos Severiano J, Cavalcante H, de Lucena-Silva D, Mendes CF, Barbosa VV, et al. Impacts of inter-basin water transfer on the water quality of receiving reservoirs in a tropical semi-arid region. Hydrobiologia 2021;848:651-73.

Dhital MR. Geology of the Nepal Himalaya: Regional Perspective of the Classic Collided Orogen. Cham, Switzerland: Springer; 2015.

Domenico PA, Schwartz FW. Physical and Chemical Hydrogeology. New York: John Wiley and Sons, Inc.; 1998.

Ewaid SH. Water quality evaluation of Al-Gharraf River by two water quality indices. Applied Water Science 2016;7:3759-65.

Ferguson JW, Healey M, Dugan P, Barlow C. Potential effects of dams on migratory fish in the Mekong River: Lessons from salmon in the Fraser and Columbia Rivers. Environmental Management 2011;47:141-59.

Gergel SE. Spatial and non-spatial factors: When do they affect landscape indicators of watershed loading? Landscape Ecology 2005;20:177-89.

Gibbs RJ. Mechanisms controlling world water chemistry. Science 1970;170:1088-90.

Ghassemi F, White I. Inter-Basin Water Transfer: Case Studies from Australia, United States, Canada, China and India. UK: Cambridge University Press; 2007.

Ghimire NP, Adhikari N, Pant RR, Thakuri S. Characterizations of water quality in West-Seti and Tamor River Basins, Nepal. Scientific World 2021;14:106-14.

Gallardo B, Aldridge DC. Inter-basin water transfers and the expansion of aquatic invasive species. Water Research 2018;143:282-91.

Government of Nepal, Babai Bheri Diversion Multipurpose Project (GoN/BBDMP). Strategic plan of BBDMP [Internet]. 2018 [retrived 2018 Nov 14]. Available from: http://www.bbdmp.gov.np.

Government of Nepal, Department of Water Resources and Irrigation (GoN/DWRI). Irrigation Master Plan 2019. Singha Durbar, Kathmandu, Nepal: GoN/DWRI; 2019.

Government of Nepal, National Planning Commission (GoN/NPC). Nepal's Sustainable Development Goals, Status and Roadmap: 2016-2030. Singha Durbar, Kathmandu, Nepal: GoN/NPC; 2017.

Grant EH, Lynch HJ, Muneepeerakul R, Arunachalam M, Rodriguez-Iturbe I, Fagan WF. Interbasin water transfer, riverine connectivity, and spatial controls on fish biodiversity. PLoS ONE. 2012;7(3):e34170.

Granzotti RV, Miranda LE, Agostinho AA, Gomes LC. Downstream impacts of dams: Shifts in benthic invertivorous fish assemblages. Aquatic Sciences 2018;80(3):1-14.

Guo C, Chen Y, Gozlan RE, Liu H, Lu Y, Qu X, et al. Patterns of fish communities and water quality in impounded lakes of China's south-to-north water diversion project. Science of the Total Environment 2020;713:Article No. 136515.

Gupta D, Kaushik S, Shukla R, Mishra VK. Mechanisms controlling major ion chemistry and its suitability for irrigation of Narmada River, India. Water Supply 2022;22:3224-41.

Gurung S, Gurung A, Sharma CM, Jüttner I, Tripathee L, Bajracharya RM, et al. Hydrochemistry of Lake Rara: A high mountain lake in western Nepal. Lakes and Reservoirs: Science, Policy and Management for Sustainable Use 2018;23:87-97.

He T, Deng Y, Tuo Y, Yang Y, Liang N. Impact of the dam construction on the downstream thermal conditions of the Yangtze River. International Journal of Environmental Research and Public Health 2020;17(8):Article No. 2973.

Hossain MA, Zakir H, Kumar D, Alam M. Quality and metallic pollution level in surface waters of an urban industrialized city: A case study of Chittagong City, Bangladesh. Journal of Industrial Safety Engineering 2017;4:9-18.

Jacobson AD, Blum JD, Chamberlain CP, Poage MA, Sloan VF. Ca/Sr and Sr isotope systematics of a Himalayan glacial chronosequence: carbonate versus silicate weathering rates as a function of landscape surface age. Geochimica et Cosmochimica Acta 2002;66:13-27.

Jha BR, Gurung S, Khatri K, Gurung A, Thapa A, Mamta KC, et al. Patterns of diversity and conservation status of freshwater fishes in the glacial fed and rain fed rivers of Eastern Nepal. Environmental Biology of Fishes 2018;101:1295-305.

Jiang L, Yao Z, Liu Z, Wang R, Wu S. Hydrochemistry and its controlling factors of rivers in the source region of the Yangtze River on the Tibetan Plateau. Journal of Geochemical Exploration 2015;155:76-83.

Lacoul P, Freedman B. Physical and chemical limnology of 34 lentic waterbodies along a tropical-to-alpine altitudinal gradient in Nepal. International Review of Hydrobiology 2005;90(3):254-76.

Kafle BK, Sharma CM, Gurung S, Raut N, Kafle KR, Bhatta R, et al. Hydrogeochemistry of two major mid-hill lentic water bodies for irrigation of the Central Himalaya, Nepal. Environment and Natural Resources Journal 2023;21(2):171-85.

Kafle N, Dhungel LR, Acharya KK, Dhital MR. A Balanced geological cross-section along Kohalpur-Surkhet Area of Sub-Himalayan Range, Mid-Western Nepal. Journal of Science and Engineering 2019;6:1-8.

Kamidis N, Koutrakis E, Sapounidis A, Sylaios G. Impact of river damming on downstream hydrology and hydrochemistry: The case of lower Nestos River Catchment (NE. Greece). Water 2021;13(20):Article No. 2832.

Kannel PR, Kanel SR, Lee S, Lee Y-S, Gan TY. A review of public domain water quality models for simulating dissolved oxygen in rivers and streams. Environmental Modeling and Assessment 2011;16:183-204.

Khadka UR, Ramanathan AL. Hydrogeochemical analysis of Phewa Lake: A lesser Himalayan Lake in the Pokhara Valley, Nepal. Environment and Natural Resources Journal 2021;19:68-83.

Khadka UR, Ramanathan AL. Major ion composition and seasonal variation in the Lesser Himalayan lake: Case of Begnas Lake of the Pokhara Valley, Nepal. Arabian Journal of Geosciences 2012;6:4191-206.

Kono M. Gravity anomalies in east Nepal and their implications to the crustal structure of the Himalayas. Geophysical Journal International 1974;39:283-99.

Kuchment LS. The Hydrological Cycle and Human Impact on It. Water Resources Management, Encyclopedia of Life Support Systems (EOLSS); 2004. p. 40.

Kurdi M, Eslamkish T, Seyedali M, Ferdows MS. Water quality evaluation and trend analysis in the Qareh Sou Basin, Iran. Environmental Earth Sciences 2015;73:8167-75.

Lakra WS, Sarkar UK, Dubey VK, Sani R, Pandey A. River inter linking in India: Status, issues, prospects and implications on aquatic ecosystems and freshwater fish diversity. Reviews in Fish Biology and Fisheries 2011;21:463-79.

Lupker M, France-Lanord C, Galy V, Lavé J, Gaillardet J, Gajurel AP, et al. Predominant floodplain over mountain weathering of Himalayan sediments (Ganga basin). Geochimica et Cosmochimica Acta 2012;84:410-32.

Machado FH, Gontijo ESJ, Beghelli FGDS, Fengler FH, de Medeiros GA, Filho AP, et al. Environmental impacts of inter-basin water transfer on water quality in the Jundiaí-Mirim River, south-east Brazil. International Journal of Environmental Impacts 2018;1(1):80-91.

Mallick J. Hydrogeochemical characteristics and assessment of water quality in the Al-Saad Lake, Abha Saudi Arabia. Applied Water Science 2017;7:2869-82.

Marak JDK, Sarma AK, Bhattacharjya RK. Assessing the impacts of interbasin water transfer reservoir on streamflow. Journal of Hydrologic Engineering 2020;25(10):Article No. 05020034.

Mikalsen T. Causes of increased total dissolved solids and conductivity levels in urban streams in Georgia. Proceedings of the 2005 Georgia Water Resources Conference; 2005 April 25-27; Athens, Georgia; 2005.

Millennium Ecosystem Assessment (MEA). Ecosystems and Human Well-Being: Wetlands and Water Synthesis. Washington, DC, USA: World Resources Institute; 2005.

Mishra Y, Babel MS, Nakamura T, Mishra B. Impacts of climate change on irrigation water management in the Babai River Basin, Nepal. Hydrology 2021;8(2):Article No. 85.

Mishra Y, Nakamura T, Babel MS, Ninsawat S, Ochi S. Impact of climate change on water resources of the Bheri River Basin, Nepal. Water 2018;10(2):Article No. 220.

Moyel MS, Hussain NA. Water quality assessment of the Shatt Al-Arab River, Southern Iraq. Journal of Coastal Life Medicine 2015;3:459-65.

Mukate SV, Panaskar DB, Wagh VM, Baker SJ. Understanding the influence of industrial and agricultural land uses on groundwater quality in semiarid region of Solapur, India. Environment, Development and Sustainability 2020;22:3207-38.

Nisha BK, Balakrishna K, Udayashankar HN, Manjunatha BR. Chemical weathering and carbon dioxide consumption in a small tropical river catchment, southwestern India. Aquatic Geochemistry 2021;27:173-206.

Novotny V. Diffuse pollution from agriculture: A worldwide outlook. Water Science and Technology 1999;39(3):1-13.

O'keeffe J, De Moor F. Changes in the physico-chemistry and benthic invertebrates of the Great Fish River, South Africa, following an interbasin transfer of water. Regulated Rivers: Research and Management 1988;2(1):39-55.

Quade J, English N, DeCelles PG. Silicate versus carbonate weathering in the Himalaya: A comparison of the Arun and Seti River Watersheds. Chemical Geology 2003;202(3-4):275-96.

Pant RR, Zhang F, Rehman FU, Wang G, Ye M, Zeng C, et al. Spatiotemporal variations of hydrogeochemistry and its controlling factors in the Gandaki River Basin, Central Himalaya Nepal. Science of the Total Environment 2018;622-623:770-82.

Paudyal R, Kang S, Sharma CM, Tripathee L, Huang J, Rupakheti D, et al. Major ions and trace elements of two selected rivers near Everest region, Southern Himalayas, Nepal. Environmental Earth Sciences 2016;75:1-11.

Piper AM. A graphic procedure in the geochemical interpretation of water-analyses. Eos, Transactions American Geophysical Union 1944;25(6):914-28.

Pittock J, Meng J-h, Chapagain AK. Interbasin Water Transfers and Water Scarcity in a Changing World: A Solution or a Pipedream? Germany: World Wildlife Fund Germany; 2009. p. 61.

Potasznik A, Szymczyk S. Magnesium and calcium concentrations in the surface water and bottom deposits of a river-lake system. Journal of Elementology 2015;20(3):677-92.

Pringle CM, Freeman MC, Freeman BJ. Regional effects of hydrologic alterations on riverine macrobiota in the new world: Tropical-temperate comparisons. BioScience 2000; 50(9):807-23.

Qishlaqi A, Kordian S, Parsaie A. Hydrochemical evaluation of river water quality: A case study. Applied Water Science 2016;7:2337-42.

Qu B, Zhang Y, Kang S, Sillanpaa M. Water quality in the Tibetan Plateau: Major ions and trace elements in rivers of the "Water Tower of Asia". Science of the Total Environment 2019; 649:571-81.

Reynolds B, Chapman P, French M, Jenkins A, Wheater H. Major, minor, and trace element chemistry of surface waters in the Everest region of Nepal. Proceedings and Reports-Intern Assoc Hydrological Sciences 1995;228:405-12.

Schmidt BV, Wang Z, Ren P, Guo C, Qin J, Cheng F, et al. A review of potential factors promoting fish movement in inter-basin water transfers, with emergent patterns from a trait-based risk analysis for a large-scale project in china. Ecology of Freshwater Fish 2019;29:790-807.

Selge F, Matta E, Hinkelmann R, Gunkel G. Nutrient load concept-reservoir vs. bay impacts: A case study from a semi-arid watershed. Water Science and Technology 2016;74:1671-9.

Sharma CM, Kang S, Tripathee L, Paudyal R, Sillanpää M. Major ions and irrigation water quality assessment of the Nepalese Himalayan Rivers. Environment, Development and Sustainability 2020;23:2668-80.

Shakeri S, Abtahi A. Potassium fixation capacity of some highly calcareous soils as a function of clay minerals and alternately wetting-drying. Archives of Agronomy and Soil Science 2020;66(4):445-57.

Shrestha AB, Aryal R. Climate change in Nepal and its impact on Himalayan glaciers. Regional Environmental Change 2011; 11:65-77.

Singh R, Kayastha SP, Pandey VP. Water quality of Marshyangdi River, Nepal: An assessment using water quaity index (WQI). Journal of Institute of Science and Technology 2021;26:13-21.

Singh SK, Sarin MM, France-Lanord C. Chemical erosion in the eastern Himalaya: Major ion composition of the Brahmaputra and δ13C of dissolved inorganic carbon. Geochimica et Cosmochimica Acta 2005;69:3573-88.

Singh VB, Ramanathan A, Mandal A. Hydrogeochemistry of high-altitude lake: A case study of the Chandra Tal, Western Himalaya, India. Arabian Journal of Geosciences 2016;9:1-9.

Skowron P, Skowrońska M, Bronowicka-Mielniczuk U, Filipek T, Igras J, Kowalczyk-Juśko A, et al. Anthropogenic sources of potassium in surface water: The case study of the Bystrzyca River catchment, Poland. Agriculture, Ecosystems and Environment 2018;265:454-60.

Snaddon CD, Davies BR, Wishart M, Meador M, Thoms M. A Global Overview of Inter-Basin Water Transfer Schemes, with an Appraisal of their Ecological, Socio-Economic and Socio-Political Implications, and Recommendations for their Management. Water Research Commission Report No TT120/00 Pretoria: Water Research Commission; 1999.

Snaddon CD, Wishart M, Davies BR. Some implications of inter-basin water transfers for river ecosystem functioning and water resources management in southern Africa. Aquatic Ecosystem Health and Management 1998;1(2):159-82.

Stockner J, Rydin E, Hyenstrand P. Cultural oligotrophication: causes and consequences for fisheries resources. Fisheries 2000;25(5):7-14.

Szatten D, Habel M, Babiński Z. Influence of hydrologic alteration on sediment, dissolved load and nutrient downstream transfer continuity in a river: Example lower Brda River Cascade Dams (Poland). Resources 2021;10(7):Article No. 70.

Tamrakar NK, Shrestha MB. Relationship between fluvial clastic sediment and source rock abundance in Rapti River Basin of Central Nepal Himalayas. Boletin de Geologia 2008;30:63-75.

Tian J, Liu D, Guo S, Pan Z, Hong X. Impacts of inter-basin water transfer projects on optimal water resources allocation in the Hanjiang River Basin, China. Sustainability 2019;11(7): Article No. 2044.

Tickner D, Parker H, Moncrieff CR, Oates NEM, Ludi E, Acreman M. Managing rivers for multiple benefits: A coherent approach to research, policy and planning. Frontiers in Environmental Science 2017;5:Article No. 4.

Tiwari AK, Singh AK, Phartiyal B, Sharma A. Hydrogeochemical characteristics of the Indus River water system. Chemistry and Ecology 2021;37:780-808.

Tsering T, Abdel Wahed MSM, Iftekhar S, Sillanpää M. Major ion chemistry of the Teesta River in Sikkim Himalaya, India: Chemical weathering and assessment of water quality. Journal of Hydrology: Regional Studies 2019;24:Article No. 100612.

Vasanthavigar M, Srinivasamoorthy K, Prasanna MV. Identification of groundwater contamination zones and its sources by using multivariate statistical approach in Thirumanimuthar sub-basin, Tamil Nadu, India. Environmental Earth Sciences 2013; 68:1783-95.

Vinnarasi F, Srinivasamoorthy K, Saravanan K, Gopinath S, Prakash R, Ponnumani G, et al. Chemical weathering and atmospheric carbon dioxide (CO_2) consumption in Shanmuganadhi, South India: Evidences from groundwater geochemistry. Environmental Geochemistry and Health 2021;43:771-90.

Wang J, Soininen J, Heino J. Ecological indicators for aquatic biodiversity, ecosystem functions, human activities and climate change. Ecological Indicators 2021;132:Article No. 108250.

Wanty RB, Verplanck PL, San Juan CA, Church SE, Schmidt TS, Fey DL, et al. Geochemistry of surface water in alpine catchments in central Colorado, USA: Resolving host-rock effects at different spatial scales. Applied Geochemistry 2009;24:600-10.

Water UN. Climate Change and Water: UN-Water Policy Brief. Geneva, Switzerland: Water UN; 2019.

Water and Energy Commission Secretariat (WECS). Water Resources of Nepal in the Context of Climate Change. Kathmandu, Nepal: WECS and Government of Nepal; 2011.

Wetzel RG. Limnology: Lake and River Ecosystems. 3rd ed. Academic Press; 2001.

World Wildlife Fund (WWF). Valuing Rivers: How the Diverse Benefits of Healthy Rivers Underpin Economies. WWF; 2018.

Yang N, Zhang C, Wang L, Li Y, Zhang W, Niu L, et al. Nitrogen cycling processes and the role of multi-trophic microbiota in dam-induced river-reservoir systems. Water Research 2021; 206:Article No. 117730.

Zaw K, Meffre S, Lai CK, Burrett C, Santosh M, Graham I, et al. Tectonics and metallogeny of mainland Southeast Asia: A review and contribution. Gondwana Research 2014;26:5-30.

Zhu M, Kuang X, Feng Y, Hao Y, He Q, Zhou H, et al. Hydrochemistry of the Lhasa River, Tibetan Plateau: Spatiotemporal variations of major ions compositions and controlling factors using multivariate statistical approaches. Water 2021;13:Article No. 3660.

Zhuang W. Eco-environmental impact of inter-basin water transfer projects: A review. Environmental Science and Pollution Research 2016;23(13):12867-79.

Microbiological Quality and Sanitation of Food Stalls and Drinking Water Vending Machines

Rapeepan Yongyod*, Phatcharaporn Phusomya, and Peechanika Chopjitt

Faculty of Public Health, Kasetsart University Chalermphrakiat Sakon Nakhon Campus, Sakon Nakhon, Thailand

ARTICLE INFO

Received: 13 Jan 2023
Received in revised: 25 Arp 2023
Accepted: 28 Arp 2023
Published online: 23 Jun 2023
DOI: 10.32526/ennrj/21/20230014

Keywords:
Drinking water/ Food stall/ Microbiological quality/ Sanitation

*** Corresponding author:**
E-mail: rapeepan.y@ku.th

ABSTRACT

Consumption of food from food stalls and water from vending machines has recently increased in Sakon Nakon Province, Thailand. This study investigated the microbial quality of food stalls and the sanitation of drinking water distributed through water vending machines. *Escherichia coli*, *Salmonella* spp., *Staphylococcus aureus*, and *Vibrio cholerae* were detected using polymerase chain reaction. In total, 33 food samples were collected from food stalls and 63 drinking water samples were collected from water vending machines. The results identified *E. coli* in 6.06% of the food and 11.11% of the drinking water samples. *Salmonella* spp., *S. aureus*, and *V. cholerae* were not detected in any of the food or drinking water samples. Food sanitation assessment indicated 21 (63.64%) of the food stalls did not meet the standards for drinking water as it was not stored in clean and closed containers equipped with a tap or nozzle. Regarding the sanitation of the water vending machines, the businesses failed to inspect the physical, chemical and biological aspects of water quality and never used a simple bacterial test kit to check water quality. It is concluded that the relevant government officials should educate the vender on food safety and hygiene as well as enforcing regular monitoring of the quality of food stall and drinking water vending machines.

1. INTRODUCTION

At present, the expansion of food stalls and water vending machines is growing to respond to the increasing needs of people, as these outlets provide convenience, are time saving, and offer goods at a cheaper price compared to bottled water. Additionally, the food items sold by food stalls are highly popular because of the limited time for cooking and the daily rush in many modern lifestyles. Therefore, if people choose non-standard drinking water and food contaminated with germs, they may encounter illness. According to data from the Bureau of Epidemiology (USA) in 2017, 1,038,349 patients had diarrhea with two deaths. Furthermore, eight patients had cholera and 110,396 patients had food poisoning with three deaths, with the causes being poisonous or pathogenic bacteria, possibly in food or drinks initially, or from contamination from the surrounding environment, especially due to personal hygiene. In 2017, the most detected pathogenic bacteria were *Vibrio*, *Staphylococcus*, *Salmonella* spp., and *Escherichia coli* (Feng et al., 2022; CDC, 2022).

Foodborne illnesses are usually infectious or toxic in nature and are caused by bacteria, viruses, parasites, or chemical substances entering the body through contaminated food. Chemical contamination can lead to acute poisoning or long-term diseases, such as cancer, while many foodborne diseases may lead to long-lasting disability or death. *Salmonella* and enterohaemorrhagic *Escherichia coli* are some of the most common foodborne pathogens that affect millions of people annually, sometimes with severe and fatal outcomes. Symptoms include fever, headache, nausea, vomiting, abdominal pain, and diarrhea. Foods involved in outbreaks of salmonellosis include eggs, poultry, and other products of animal origin. Enterohaemorrhagic *Escherichia coli* is associated with unpasteurized milk, undercooked meat, and contaminated fresh fruits, vegetables, and drinking water. *Vibrio cholerae* can infect people

Citation: Yongyod R, Phusomya P, Chopjitt P. Microbiological quality and sanitation of food stalls and drinking water vending machines. Environ. Nat. Resour. J. 2023;21(4):312-321. (https://doi.org/10.32526/ennrj/21/20230014)

through contaminated water or food. Rice, vegetables, millet gruel, and various types of seafood have been implicated in cholera outbreaks (WHO, 2022).

Of most concern for health is naturally occurring toxins and environmental pollutants. Naturally occurring toxins include mycotoxins, marine biotoxins, cyanogenic glycosides, and toxins occurring in poisonous mushrooms. Staple foods, such as corn or cereals can contain high levels of mycotoxins, such as aflatoxin and ochratoxin, produced by mold on grain and long-term exposure can affect the immune system and normal development, or cause cancer. Persistent organic pollutants are compounds that accumulate in the environment and human body. Known examples are dioxins and polychlorinated biphenyls, which are unwanted by-products of industrial processes and waste incineration. They are found worldwide in the environment and accumulate in animal food chains. Dioxins are highly toxic and can cause reproductive and developmental problems, damage the immune system, interfere with hormones, and cause cancer. Other chemical hazards in food can include radioactive nucleotides (that can be discharged into the environment from industries and from civil or military nuclear operations), food allergens, residues of drugs, and other contaminants incorporated in the food during the process (WHO, 2022).

Chiang Khruea Sub-District, Mueang District, Sakon Nakon Province surrounds the Kasetsart University Chalermphrakiat, Sakon Nakon Province Campus, where there are many student dormitories; consequently, entrepreneurs and residential owners have installed water vending machines and food stalls to gain more income (Yongyod, 2018). Food and drinking water stores that open for service will focus on food quantity and speed to meet the limited time and the daily rush in many modern lifestyles, especially of students. As a result, the quality of food and drinking water served may be neglected.

Food and drinking water quality are essential to human health. Therefore, for the safety of consumers, contamination with *Escherichia coli*, *Salmonella* spp., *Staphylococcus aureus*, and *Vibrio cholerae* in food stalls and water from drinking water vending machines was examined using polymerase chain reaction (PCR) analysis. Furthermore, sanitation was evaluated in accordance with the requirements regarding food sanitation for food stalls and drinking water vending machines. The results could be used as fundamental information and for the development of guidelines for the sectors responsible for supervising and monitoring food and drink quality. The development and enforcement of guidelines regarding sanitation standards for food stall vendors and drinking water vending machine providers should provide assurance to consumers that these products are safe and clean.

2. METHODOLOGY

In order to evaluate the microbial quality of food stall and drinking water in Chiang Khruea Sub-District, Mueang District, Sakon Nakon Province were selected (Figure 1). Thirty three food samples were collected from food stalls and 63 water samples were collected from drinking water vending machines using a standard method (APHA, 2012) and examined for *Escherichia coli*, *Salmonella* spp., *Staphylococcus aureus*, and *Vibrio cholerae* by multiplex PCR method.

2.1 Study area and sampling sites

The study area for sampling was the Chiang Khruea Sub-District, Mueang District, Sakon Nakon Province, Thailand (Figure 1). Sample sites were selected to represent different locations of drinking water and of various type of foods (ready-to-eat items, such as curry, soup, and broiled and fried products).

In total, 63 water samples were collected from drinking water vending machines and tested for *E. coli*, *Salmonella* spp., *S. aureus*, and *V. cholerae*, while 33 food samples were collected from food stalls using a standard method (APHA, 2012) and examined for *E. coli*, *Salmonella* spp., and *S. aureus*.

At each sampling point, approximately 500 mL of water was collected in two plastic bottles of 600 mL each, while 50 g of food was collected in a plastic bag. All samples were transported to the microbiology laboratory in a cold box within 24 h.

2.2 Microbiological analysis

2.2.1 Food samples were prepared following Kim et al. (2007)

2.2.2 Enrichment and identification of bacterial pathogens

For isolation of *E. coli*, 25 g of food sample was homogenized with 225 mL of EC broth (HIMEDIA, Nashik, India) for two minutes with a stomacher (BagMixer, interscience, France). The suspension was first incubated at 35±2°C for 16 h, then 100 µL of suspension was streaked on RAPID' *E. coli* 2 agar (Bio-Rad, CA, USA) and further incubated at 35±2°C

for 24 h. Violet colonies were selected as presumptive *E. coli* and confirmed by using multiplex PCR. *E. coli* ATCC 25922 was used as a positive control.

For the isolation of *Salmonella* spp., 25 g of food sample was homogenized with 225 mL of buffered peptone water (BPW; Oxoid, Hampshire England) in a stomacher apparatus for two minutes. The mixture was incubated at 35±2°C for 18 h and 100 µL of suspension was streaked on *Salmonellla Shigella* Agar (HIMEDIA, Nashik, India) and was further incubated at 35±2°C for 24 h. Black colony were presumptive as *Salmonella* and confirmed by using multiplex PCR. *Salmonella Typhimurium* ATCC14028 was used as a positive control.

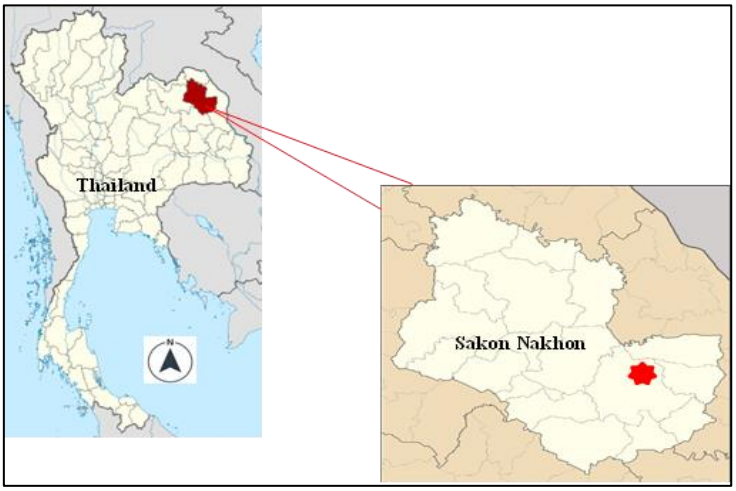

Figure 1. Map of the study area in Chiang Khruea Sub-District, Mueang District, Sakon Nakon Province, Thailand

S. aureus was isolated by homogenizing 25 g of food sample with 225 mL of tryptic soy broth with 10% NaCl (TSB; HIMEDIA, Nashik, India) for two minutes with a stomacher. The suspension was incubated at 35±2°C for 18 h, then 100 µL of suspension was streaked on mannitol salt agar (MSA; SIGMA-ALDRICH, Switzerland) incubated at 35±2°C for 24 h. Yellow colonies were selected as presumptive *S. aureus* and confirmed by using multiplex PCR. *S. aureus* ATCC 25923 was used as a positive control.

2.2.3 Water samples

A standard membrane filtration technique was used for the isolation of *E. coli*, *Salmonella* spp., and *Vibrio cholerae* by modifying APHA 9222 (2012), the presence. Briefly, 1,000 mL of water samples were filtered through a 0.22 µM pore size membrane filter (Millipore, MA, USA), then pre-enriched in BPW for *E. coli* and *Salmonella* spp., and incubated in alkaline peptone water (APW; HIMEDIA, Nashik, India) for *V. cholerae*. All enrichment samples were incubated at 35±2°C for 18 h. A loop full of broth culture was streaked on RAPID' *E. coli* 2 Agar, SS Agar, and thiosulfate citrate bile salts sucrose (TCBS; Sigma-Aldrich, Switzerland) for isolation of *E. coli*, *Salmonella* spp., and *V. cholera*, respectively. Suspected colonies (5-10 colonies) were sub-cultured on those media again. All isolates were cultured on TSA to extract genomic DNA and confirmed by multiplex PCR.

2.2.4 Identification of E. coli, S. aureus, Salmonella spp., and V. cholerae by multiplex PCR

DNA form all isolates were extracted using the heat-lysis method (Liu et al., 2002). All primers used in this study were shown in Table 1. An in-house multiplex PCR reaction mixture was performed using a total volume of 25 µL containing 1X PCRBIO Taq Mix Red (12.5 µL) (PCR Biosystemm, London, UK.), 0.2 µM of each primer for *E. coli*, *S. Typhimurium*, *V. cholerae* and 0.5 µM of each primer for *S. aureus*, sterile deionized water 5 µL, and the 50-100 ng DNA sample. A negative control containing the same reaction mixture except the DNA template was included in every experiment. The PCR amplifications were conducted using a T100 Thermal cycler (BioRad, Singapore). The PCR condition consisted of initial denaturation at 95°C for five min, followed by 30 cycles of denaturation at 95°C for one min, annealing at 56°C for 30 s, extension at 72°C for one min, and final extension at 72°C for five min. PCR products

were evaluated in 1.5% agarose gels (Bioline Reagents Ltd, UK) at 100 V for 30 min. Gels were stained with ethidium bromide (Wako pure chemical industries, Ltd., Japan) for 20 min. Amplicon sizes were estimated by comparison with a DNA ladder (GeneRuler 100 bp Plus DNA Ladder, Thermo-scientific, Lithuania), visualized and photographed under ultraviolet light using gel documentation (Syngene, UK).

Table 1. Sequences of primers and expected product size used in this study

Bacterium	Primers	Sequence (5'→3')	Product size (bp)	Reference
E. coli	EC uidA-F	AAAACGGCAAGAAAAAGCAG	147	Bej et al. (1991)
	EC uidA-R	ACGCGTGGTTAACAGTCTTGCG		
V. cholerae	VC-F	GAATTAGGGTCCTGTGCAGG	248	Kong et al. (2002)
	VC-R	ATCGCTTGGCGCATCAGTGCCC		
Salmonella spp.	Salmo-F	GAGGAAAAAGAAGGGTCG	780	Radhika et al. (2014)
	Salmo-R	CTCAACTTCAGCAGATACCA		
S. aureus	FamA-F	CGATCCATATTTACCATATCA	450	Al-Talib et al. (2009)
	FamA-R	ATCACGCTCTTCGTTTAGTT		

2.3 Drinking water and food sanitation evaluation

Evaluation of the water from the drinking water vending machines was based on six items and the food sanitation requirements for food stalls were based on 12 items specified by the Bureau of Food and Water Sanitation, Department of Health, Ministry of Public Health, Thailand (Ministry of Public Health, 2013). The six water vending machine items were: (1) Location; (2) Characteristics of the vending machine; (3) Water source and water quality improvement; (4) Drinking water quality control; (5) Maintenance and hygiene; and (6) Recording and reporting.

The criteria for assessing the sanitation and the vending machine surrounds were categorized as: covering all items listed=good level; covering some items listed=poor level; and covering none of the items listed=should-improve level.

3. RESULTS

The results from the PCR testing of the 33 food stalls for the three types of bacteria (*E. coli*, *Salmonella* spp., and *S. aureus*) and the 63 drinking water samples for three types of bacteria (*E. coli*, *Salmonella* spp., *and V. cholera*) are shown in Tables 2 and 3, respectively.

Some food samples contained *E. coli* at a level exceeding the standard (Figure 2). All food samples were negative for the presence of *Salmonella* spp. or *S. aureus*. The drinking water samples were generally within the WHO standard levels, except for seven (11.11%) samples that exceeded the standard for *E. coli*. No *Salmonella* spp. or *V. cholera* was found in any of the drinking water samples.

Table 2. Presence of tested bacteria in samples of food stalls (N=63)

Indicator bacterium	Number of food samples tested (%)	Food standard*
Escherichia coli	2 (6.06)	Not detected
Salmonella spp.	0	Not detected
Staphylococcus aureus	0	Not detected

*Food stalls standard from the Ministry of Public Heath, Thailand

Table 3. Presence of tested bacteria in samples of drinking water (N=33)

Indicator bacterium	Number of drinking water samples tested (%)	Drinking water standard*
Escherichia coli	7 (11.11)	Not detected
Salmonella spp.	0	Not detected
Vibrio cholera	0	Not detected

*Drinking water standard from WHO

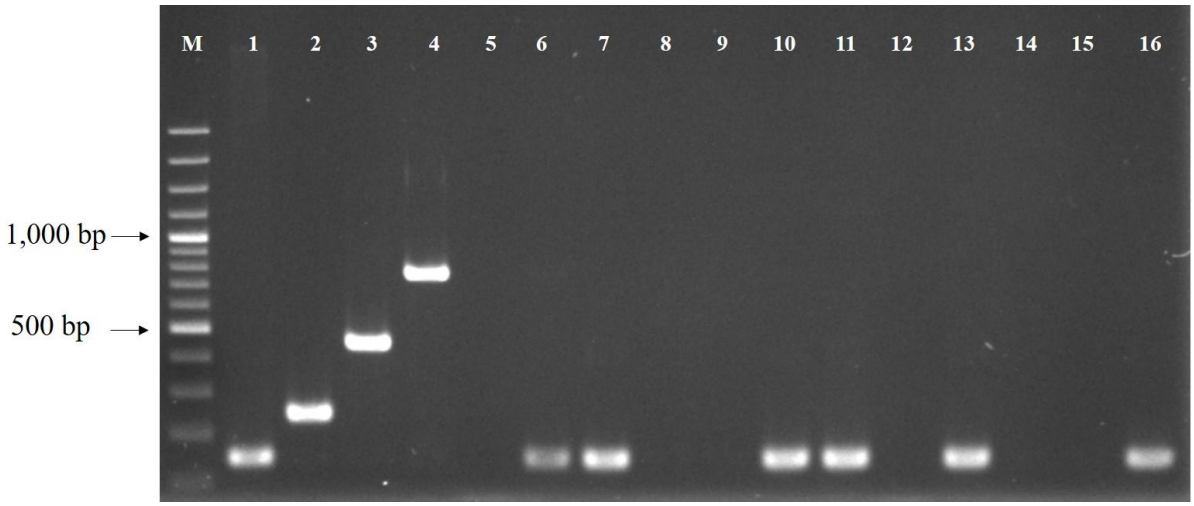

Figure 2. Multiplex PCR reaction of four pathogens detection. Lane M: DNA marker 100 bp, Lane 1: *E. coli* ATCC25922 (147 bp), Lane 2: *V. cholerae* ATCC 14035 (248 bp), Lane 3: *S. aureus* ATCC25923 (450 bp), Lane 4: *Salmonellas Typhimurium* ATCC14028 (780 bp), Lane 5: Negative control, Lane 6-16: samples isolated from food and water

3.1 Evaluation of sanitation conditions of food stalls

Table 4 shows the food sanitation evaluation for the 33 food stalls based on the 12 physical criteria from the food sanitation manual and sanitation requirements for food stalls produced by the Bureau of Food and Water Sanitation, Department of Health, Ministry of Public Health, Thailand (Ministry of Public Health, 2013).

The food sanitation evaluation in accordance with the requirements for food sanitation for food stalls requires stalls to be made from easily cleaned materials and to be kept in good and orderly condition and at least 60 cm above the ground. Food additives with FDA (Food and Drug Administration) number are required, and containers must be cleaned with dishwashing liquid and rinsed in clean water twice, with the washing equipment being at least 60 cm above the ground. It was found that solid waste was gathered and disposed of daily, and entrepreneurs must have any wound covered tightly and must use utensils to handle cooked food. It was found that 32 stalls (96.96%) had equipment for picking up food and the entrepreneurs were cleanly dressed and used an apron with a hat or hair net in 28 stalls (84.84%). Furthermore, 27 (81.81%) stalls had a container for spoons, forks or chopsticks with the handles upward in a transparent container kept at least 60 cm above the ground. The requirement that the stalls adhered to the least was not having cooked food covered or protected from insects, with 16 stalls (48.48%) at fault regarding this point (Figure 3).

Table 4. Evaluation of sanitation conditions of food stalls (N=33)

Item	Food sanitation	
	Number (%) Passed	Number (%) Not passed
1. Food vendor stall must be made of non-toxic and non-corrosive materials and installed to be easily cleaned. Food preparation areas must be at least 60 cm above the floor.	33 (100)	0
2. All cooked food must be kept in covered containers to protect from dirt, vermin, and other contamination.	16 (48.48)	17 (51.52)
3. All food additives or seasonings must be approved and registered with an FDA food number.	33 (100)	0
4. Drinking water must be stored in a clean and closed container equipped with a tap or nozzle.	12 (36.36)	21 (63.64)
5. Beverage or other drinks must be stored in clean and closed containers equipped with a tap or nozzle, or use a long-handled spoon/scoop for serving.	17 (51.52)	16 (48.48)

Table 4. Evaluation of sanitation conditions of food stalls (N=33) (cont.)

Item	Food sanitation	
	Number (%) Passed	Number (%) Not passed
6. Potable ice must be supplied and kept in a clean and closed container placed at least 60 cm above the floor. The ice must not be used to store raw or other food in the same container. Proper utensil (long handle spoon/scoop) must be used to pick up ice for serving.	13 (39.39)	20 (60.61)
7. All equipment and utensils must be washed with detergent and rinsed twice with clean tap water. The washing area must be set at least 60 cm above the floor.	33 (100)	0
8. Spoons, forks, and chopsticks must be kept with handle up or laid down neatly in a clean and covered container or basket, placed at least 60 cm above the floor.	27 (81.81)	6 (18.19)
9. Food waste and garbage must be disposed of in a sanitary manner.	33 (100)	0
10. Food handlers must wear suitable protective clothing including short or long sleeves clothes, apron and hair covering (hat or net).	28 (84.84)	5 (15.16)
11. Proper utensils (tongs, spoon, spatula, or any other utensil) must be used for picking up food.	32 (96.96)	1 (3.04)
12. Any cut or wound on food handlers' hands or skin must be completely protected by waterproof covering to avoid transmission of diseases.	33 (100)	0

Figure 3. Food stalls in study area around Kasetsart University Chalermphrakiat, Sakon Nakon Province Campus

3.2 Evaluation of sanitation conditions of drinking water vending machines

The 63 vending machines in operation were evaluated for sanitation and surrounding conditions detrimental to health according to the Public Health Act 1992 and the Ministry of Public Health announcement (No. 362) of 2013 (Ministry of Public Health, 2013), The results are shown in Table 5.

Table 5. Evaluation of sanitation conditions of drinking water vending machines (N=63)

Item	Number of machines (%)			Evaluation level
	Good	Poor	Should improve	
Location				
1. Should be at least 30 m away from water drainage	62 (98.41)	1 (1.58)	0 (0)	Good
2. There should be no drainage around the water vending machines	35 (55.56)	14 (22.22)	14 (22.22)	Good
3. The vending machines should be covered with a cap on the inlet to prevent insect entry	44 (69.84)	13 (20.63)	6 (9.52)	Good
4. The vending machines should be installed at least 10 cm above the ground as indicated by stability, to prevent short-circuit	24 (36.36)	34 (53.97)	5 (9.09)	Good
5. The container should be above the ground	39 (61.90)	22 (34.92)	2 (3.17)	Good

Table 5. Evaluation of sanitation conditions of drinking water vending machines (N=63) (cont.)

Item	Number of machines (%)			Evaluation level
	Good	Poor	Should improve	
Condition of machines				
6. No rust and stable to prevent a short-circuit	26 (41.27)	30 (47.62)	7 (11.11)	Poor
7. Parts exposed directly to the water are made of suitable materials without odor, color, or taste that may affect water quality	40 (63.49)	20 (31.74)	3 (4.76)	Good
8. The outlet and container resting at least 60 cm above the ground so that neither insects nor infectious animals could enter	40 (63.49)	13 (20.63)	10 (15.87)	Good
9. Parts exposed directly to the water have no evidence of thallophytic plants	30 (47.27)	20 (32.72)	13 (20.00)	Good
Water resources and quality improvement				
10. Water resources and quality are clean with no contamination, adverse color, smell, or taste	53 (84.13)	10 (15.87)	0 (0.00)	Good
11. Water resources are satisfactorily clean (water supply and ground water)	45 (71.43)	18 (28.57)	0 (0.00)	Good
12. Water quality meets the standards for drinking water	28 (44.44)	31 (49.21)	4 (6.35)	Poor
Drinking water standardized quality control				
13. Water sampling testing for physical and chemical characteristics and bacteria carried out at least once per year	12 (19.05)	2 (3.17)	49 (77.78)	Should improve
14. Use of a simple test kit to check for coliform bacteria at least once per month	10 (15.87)	3 (4.76)	50 (79.37)	Should improve
Maintenance and servicing				
15. Machines checked by the machine company	20 (31.75	25 (39.63)	18 (28.57)	Good
16. Machines cleaned every day to prevent dust spreading	25 (39.68)	26 (41.27)	12 (19.05)	Poor
17. Outlet and water container cleaned every day to prevent dust spreading	19 (30.16)	26 (41.27)	18 (28.57)	Poor
18. Water storage cleaned at least once per month	15 (23.81)	20 (31.75)	28 (44.44)	Should improve
19. Cleaning and changing filter by the machine company	20 (31.75)	14 (22.22)	29 (46.03)	Should improve
Recording and reporting				
20. Water quality record and maintenance record	5 (7.94)	10 (15.87)	48 (76.19)	Should improve
21. Inform customers of water quality	3 (4.76)	20 (31.75)	40 (63.49)	Should improve
22. Monitor drinking water quality	8 (12.70)	10 (15.87)	45 (71.43)	Should improve

3.2.1 Location

The sanitation evaluation for the location of drinking water vending machine was at the good level, with the location of the drinking water vending machine stable being strong and stable with no waterlogged or dirty surfaces. The water drainage was sanitarily suitable, with the machines were installed at least 10 cm above the ground and water pick-up point closure was provided to control and prevent contamination from insects and animals as disease carriers from entering the machine (Figure 4).

3.2.2 Characteristics of water machine

The evaluation result of the characteristics of the drinking water vending machines was at the good level except for poor wiring (47.62%) which could be dangerous due to a short circuit affecting users of the water vending machine (Figure 5).

Figure 4. Typical location of drinking water vending machine

Figure 5. Characteristics of water machine

3.2.3 Water source and water quality improvement

The evaluation result for water sources and water quality improvement of the water vending machines was at the good level (84.13%), with good quality, clean water without any undesirable color, odor, or flavor. Most water in the vending machines was from a local water supply.

3.2.4 Drinking water quality standard control

The entrepreneurs were unaware of water quality analysis for physical, chemical, and biological aspects (77.78%) and were also uninformed about an easy test kit for examining coliform bacteria for biological water quality testing by themselves (79.37%).

3.2.5 Maintenance and cleaning

The evaluation result for maintenance and cleaning of the water vending machines was at the fair level because the entrepreneurs were uneducated about cleaning water tanks and changing filters and so had to wait for the drinking water vending machine company to replace the filter annually. Additionally, some machines had never been cleaned and their filters had never been replaced (Figure 6).

Figure 6. Maintenance and cleaning of water vending machines

3.2.6 Recording and reporting

The evaluation result of the recording and reporting for the drinking water vending machines was at the poor level because most entrepreneurs had failed to identify the date of filter replacement and record water quality inspections for service users. There was only identification of the filter system and the brand of the manufacturer.

4. DISCUSSION

While only a few cases of *E. coli* (a bacterium indicating below-standard drink and food sanitation) were identified, this was dangerous because the standard for drink and food quality requires zero presence. In fact, *E. coli* inhabits the intestines of humans and warm-blooded animals, and some kinds of *E. coli* can result in illnesses, such as diarrhea (WHO, 2022). Food contamination with *E. coli* may result from the distribution of uncovered cooked food that is not protected from dust or animals as disease carriers, or be present in nearly cooked, uncooked, or unheated food which could be more exposed to bacteria or microorganisms than thoroughly cooked food (Ghosh et al., 2007). Food stalls usually operate in small units, perhaps lacking hygiene, and appropriate food management, such as preparation, storage, and handling practices (Seo and Lee, 2021).

Most entrepreneurs did not have containers covering the cooked food which may cause contamination from insects and dust, while some stalls provided spoons, forks, and chopsticks without the handle up, so that when the cooks used them, contamination of the food could result in adverse effects on consumers (Pratum and Khananthai, 2017). Additionally, the cooks at some stalls failed to wear an apron, hat, or hairnet, which may have resulted in contamination by loose hairs and dirt in food, which again may have affected consumers (Bereda et al., 2016). Despite there being only a few observed occurrences, such failures could negatively affect the consumers. Cooked food should be clean and safe for all consumers.

Some aspects regarding the sanitation of the water vending machines required improvement as entrepreneurs failed to inspect the physical, chemical, and biological aspects of water quality and never used a simple bacterial test kit to check the water quality (Dorothy et al., 2010). Furthermore, there were some factors affecting water quality, such as cleaning and filter replacement on time based on water quality data records, and vending machine repair and maintenance (Tan et al., 2016; WHO, 2017; Phusomya and Yongyod, 2022). At present, there is no law clearly controlling food and water quality, as only water quality is monitored (Yongyod, 2018).

We concluded that food safety and hygiene interventions with embedded hand washing with soap at critical times could have important effect on reducing publicly transmitted diarrheal disease (WHO, 2019). As such, the promotion of food hygiene practices using a behavior-centerd approach should be integrated into nutrition, such as the “Scaling Up Nutrition” and “WASH” (Community Led Total Sanitation)” intervention policies and programming. Although limited benefits were seen from the addition of feces and water management interventions, it should be considered that these may have been impacted by the existing environmental contamination in the household yard. Integration can be achieved through existing structures using locally available expertise with appropriate support and supervision (Morse et al., 2020).

5. CONCLUSION

Out of the total of 63 drinking water samples taken from the vending machines, seven samples (11.11%) were positive for *E. coli* and two food samples (6.06%) were detected with *E. coli*. There was no contamination of *Salmonella* spp., *Staphylococcus aureus*, or *Vibrio cholera* in any of the drinking water samples. All of food samples were negative for *Salmonella* spp., and *Staphylococcus aureus.* Generally, drinking water sanitation was at the good level; however, improvements were needed in cleanliness, orderly wiring to prevent electric shock, and recording and monitoring water quality. Sanitation at a level below the standards could lead to bacterial contamination in food and drinks.

The sanitation evaluation revealed that 14 stalls (42.42%) met the relevant standards for food sanitation of food stalls, while 19 stalls (57.58%) failed to meet the standards. The stall practice that was at the least achieved level was the failure to use covered containers for cooked food to protect the food from animals. Therefore, the concerned authorities should monitor the stalls and strictly impose the regulations to ensure safe drinking water quality and food safety.

ACKNOWLEDGEMENTS

The Faculty of Public Health, Kasetsart University Chalermphrakiat Sakon Nakhon Campus provided support during the laboratory analysis.

REFERENCES

Al-Talib H, Yean CY, Al-Khateeb A, Hassan H, Singh KK, Al-Jashamy K, et al. A pentaplex PCR assay for the rapid detection of methicillin resistant *Staphylococcus aureus* and Panton-Valentine Leucocidin. BMC Microbiology 2009; 9(1):1-8.

American Public Health Association (APHA). Standard Methods for the Examination of Water and Wastewater: Volume 22nd. Washington, DC, USA: American Public Health Association; 2012.

Bej AK, Dicesare JL, Haff L, Atlas RM. Detection of *Escherichia coli* and *Shigella* spp. in water by using the polymerase chain reaction and gene probes for uid. Applied and Environmental Microbiology 1991;57(4):1013-7.

Bereda TW, Emerie YM, Reta MA, Asfaw HS. Microbiological safety of street vended foods in Jigjiga City, Eastern Ethiopia. Ethiopian Journal of Health Sciences 2016;26(2):163-72.

Center for Disease Control (CDC). Waterborne diseases [Internet]. 2022 [cited 2022 Oct 28]. Available from: https://www.cdc.gov/healthywater/surveillance/drinking-surveillance-reports.html.

Dorothy YM, Grace SK, Moses A, Langbong B. Bacteriological quality of ready to eat foods sold on and around university of Ghana Campus. Research Journal of Microbiology 2010; 5(2):130-6.

Feng P, Weagant SD, Jinneman K. Diarrhea genic *Escherichia coli* [Internet]. 2022 [cited 2022 Oct 28]. Available from: https://www.fda.gov/food/laboratory-methods-food/bam-chapter-4a-diarrheagenic- escherichia-coli.

Ghosh M, Wahi S, Kumar M, Ganguli A. Prevalence of enterotoxigenic *Staphylococcus aureus* and *Shigella* spp. in some raw street vended Indian foods. International Journal of Environmental Health Research 2007;17(2):151-6.

Ministry of Public Health. Handbook of Drinking Water Vending Machines. Business Detrimental to Health, in Public Health Act 1992 and the Ministry of Public Health. Bangkok, Thailand: Ministry of Public Health; 2013 (in Thai).

Kim JS, Lee GG, Park JS, Jung YH, Kwak HS, Kim SB, et al. A novel multiplex PCR assay for rapid and simultaneous detection of five pathogenic bacteria: *Escherichia coli* O157:H7, *Salmonella*, *Staphylococcus aureus*, *Listeria monocytogenes*, and *Vibrio parahaemolyticus*. Journal of Food Protection 2007:70(7):1656-62.

Kong RY, Lee SK, Law TW, Law SH, Wu RS. Rapid detection of six types of bacterial pathogens in marine waters by multiplex PCR. Water Research 2002;36(11):2802-12.

Liu L, Coenye T, Burns JL, Whitby PW, Stull TL, LiPuma JJ. Ribosomal DNA-directed PCR for identification of *Achromobacter (Alcaligenes) xylosoxidans* recovered from sputum samples from cystic fibrosis patients. Journal of Clinical Microbiology 2002;40(4):1210-3.

Morse T, Tilley E, Chidziwisano K, Malolo R, Musaya J. Health outcomes of an integrated behaviour-centred water, sanitation, hygiene and food safety intervention: A randomised before and after trial. International Journal of Environmental Research and Public Health 2020;17(8):Article No. 2648.

Phusomya P, Yongyod R. Application of hazard analysis and critical control points concept for rural bottled drinking water production process. Urban Water Journal 2022;19(10):1060-5.

Pratum C, Khananthai N. Assessment of factors affecting drinking water quality from free water dispenser in the higher education institution. International Journal of Environmental and Science Education 2017;12:787-97.

Radhika M, Saugata M, Murali HS, Batra HV. A novel multiplex PCR for the simultaneous detection of *Salmonella enterica* and *Shigella* species. Brazilian Journal of Microbiology 2014;45: 667-76.

Seo KH, Lee JH. Understanding risk perception toward food safety in street food: The relationships among service quality, values, and repurchase intention. International Journal of Environmental Research and Public Health 2021;18(13): Article No. 6826.

Tan EY, Arifullah M, Soon JM. Identification of *Escherichia coli* strains from water vending machines of Kelantan, Malaysia using 16S rRNA gene sequence analysis. Exposure and Health 2016;8(2):211-6.

World Health Organization (WHO). Guidelines for Drinking Water Quality. 4th ed. Geneva, Switzerland: The World Health Report; 2017. p. 110-2.

World Health Organization (WHO). Water, Sanitation, Hygiene, and Health: A Primer on WASH and Health for Health Professionals. Geneva, Switzerland: WHO; 2019.

World Health Organization (WHO). Food safety [Internet]. 2022 [cited 2022 Jan 24]. Available from: https://www.who.int/news-room/fact-sheets/detail/food-safety.

Yongyod R. Drinking water quality and evaluation of environmental conditions of water vending machines. Asia-Pacific Journal of Science and Technology 2018;23(1):1-5.

$MgFe_2O_4$ Magnetic Catalyst for Photocatalytic Degradation of Congo Red Dye in Aqueous Solution Under Visible Light Irradiation

Fahma Riyanti[1,2], Nurhidayah[1], Widia Purwaningrum[1,2], Nova Yuliasari[1], and Poedji Loekitowati Hariani[1,2*]

[1]*Department of Chemistry, Faculty of Mathematics and Natural Sciences, Universitas Sriwijaya, Jalan Palembang-Prabumulih, Indralaya, Ogan Ilir 30662, Indonesia*

[2]*Research Group on Magnetic Materials, Department of Chemistry, Faculty of Mathematics and Natural Sciences, Jalan Palembang-Prabumulih, Indralaya, Ogan Ilir 30662, Indonesia*

ARTICLE INFO

Received: 3 Jan 2023
Received in revised: 13 May 2023
Accepted: 15 May 2023
Published online: 23 Jun 2023
DOI: 10.32526/ennrj/21/20230002

Keywords:
$MgFe_2O_4$/ Photocatalytic degradation/ Visible light irradiation/ Congo red

*** Corresponding author:**
E-mail:
puji_lukitowati@mipa.unsri.ac.id

ABSTRACT

In this study, $MgFe_2O_4$ was successfully synthesized through the coprecipitation method using the precursors $Fe(NO_3)_3 \cdot 9H_2O$ and $Mg(NO_3)_2 \cdot 6H_2O$. The $MgFe_2O_4$ product was characterized using XRD, SEM-EDS, VSM, UV-DRS, and FTIR. The catalyst was used for the photocatalytic degradation of Congo red dye under visible light irradiation. The variables of the photocatalytic degradation included solution pH, Congo red concentration, H_2O_2 concentration, and irradiation time. The $MgFe_2O_4$ synthesized has magnetic properties, with a saturation magnetization value of 17.78 emu/g and a band gap of 1.88 eV. A degradation efficiency of 99.62% was achieved under specific conditions, including a Congo red concentration of 10 mg/L, a solution pH of 6, an H_2O_2 concentration of 2.5 mM, and an irradiation time of 180 min. The degradation efficiency without H_2O_2 was observed to be 83.45%. The photocatalytic degradation of Congo red followed the pseudo-first-order kinetics model with a rate constant (k) of 0.0167 min^{-1} and a half-life ($t_{1/2}$) of 41.49 min. The total organic carbon (TOC) removal of 84.58% indicated that the mineralization of Congo red had occurred. The effectiveness of photocatalytic degradation decreased from 99.62% to 94.50% (<5%) after five cycles of photocatalytic degradation. The results demonstrated that $MgFe_2O_4$ has a high Congo red dye degradation efficiency, can be regenerated, and is readily separated from the solution using a permanent magnet.

1. INTRODUCTION

Dyes are widely produced by industries of, among others, textiles, pharmaceuticals, soap, plastics, cosmetics, paper, and food (Wang et al., 2012; Ali et al., 2020). Azo dyes are the most widely used by industry, reaching 35% (Argote-Fuentes et al., 2021). They contain aromatic and N=N groups (Mezohegyi et al., 2012). The dyes have high toxicity and can even bioaccumulate in the food chain (Robinson et al., 2001; El Gaini et al., 2009). One of the azo dyes that is often used is Congo red. The dye has a structure that is resistant to oxidation and is difficult to degrade naturally, enabling it to survive in the environment for quite a long time (Sharma et al., 2021; Harja et al., 2022). Congo red has an aromatic structure that causes it to be carcinogenic and mutagenic (Saha and Mukhopadhyay, 2020). For this reason, an effective method for treating industrial wastewater containing dyes is necessary.

Various methods, such as adsorption (Harja et al., 2022), coagulation-flocculation (Habiba et al., 2017), ion exchange (Gao et al., 2021), photo-degradation (Jha and Chakraborty, 2020), electro-chemical oxidation (Sathiskumar et al., 2019), and direct membrane (Khumalo et al., 2019) have been used to reduce dyes. Some of the methods used have limitations. The dyes only undergo physical transformation without structural change, resulting in secondary pollutants that must be treated using other methods (Lum et al., 2020).

Advanced Oxidation Processes (AOPs) refer to methods that are inexpensive, effective, and capable of

Citation: Riyanti F, Nurhidayah, Purwaningrum W, Yuliasari N, Hariani PL. $MgFe_2O_4$ magnetic catalyst for photocatalytic degradation of Congo red dye in aqueous solution under visible light irradiation. Environ. Nat. Resour. J. 2023;21(4):322-332. (https://doi.org/10.32526/ennrj/21/20230002)

converting organic contaminants into smaller, harmless molecules (Jarariya, 2022). These methods use destructive techniques based on oxidation-reduction reactions with the help of photon energy. When a catalyst gains photon energy, electrons are excited from the valence band (VB) to the conduction band (CB) and leave the photo-generated hole (h^+). Furthermore, electron pairs/holes allow oxidation and reduction processes to occur on the surface of the photocatalyst (Valenzuela et al., 2002; Augugliaro et al., 2012) which can also be used for photocatalytic degradation processes repeatedly.

The effectiveness of degradation depends on the catalyst type and the irradiation source used (Oliveira et al., 2020). Semiconductor materials with wide band gaps (>3.0 eV), such as SnO_2, ZnO, and TiO_2, are corrosion-resistant but technically less effective at absorbing light in the UV region; only about 5% (Boudiaf et al., 2021). They are also unsuitable for the solar spectrum because it contains UV light and visible light irradiation of only 4.0% and 45%, respectively (Shahid et al., 2013). Thus, developing a photocatalyst capable of absorbing light in the visible region for practical applications is necessary.

Spinel ferrites have the general chemical formula AB_2O_4 where A is a metal ion, such as Co, Cu, Zn, Mg, Ni, Fe, Cd, or another metal, while B is iron(III) oxide (Fe_2O_3). These materials have narrow band gaps, thus effectively absorbing light in the visible region (Shahid et al., 2013). One of the ferrite compounds is $MgFe_2O_4$, which is an n-type semiconductor with a band gap between 1.7-2.4 eV (McDonald and Barlett, 2021). $MgFe_2O_4$ is a soft magnet with chemical and thermal stability (Shahjuee et al., 2019; Jarariya, 2022). The magnetic properties of ferrite compounds are advantageous in photocatalytic degradation processes because the photocatalyst can be removed from the solution quickly using a permanent magnet.

Combining a photocatalyst of ferrite compounds with H_2O_2 can increase degradation performance (Hariani et al., 2021). For example, the effectiveness of the photocatalytic degradation of $CoFe_2O_4$ with H_2O_2 on rhodamine B dyes was greater than that of $CoFe_2O_4$ under visible light irradiation (Nguyen et al., 2019). Likewise, the photocatalytic degradation of naphthalene using Fe_3O_4+H_2O_2 had greater effectiveness than without H_2O_2 (Zhang et al., 2019). H_2O_2 is an oxidant that can increase the number of hydroxyl radicals, thereby increasing the degradation efficiency. In addition, it is safe and does not threaten the environment because it decomposes into water and oxygen easily.

In this research, $MgFe_2O_4$ was synthesized using the coprecipitation method and applied to reduce the concentration of Congo red from solution. Several photocatalytic degradation variables, namely pH, initial concentration of dye, irradiation time, and H_2O_2 concentration, were investigated. An analysis of total organic carbon was carried out to prove the occurrence of dye mineralization. The photocatalyst was used repeatedly for the photocatalytic degradation of dyes to investigate their effectiveness and stability.

2. METHODOLOGY

2.1 Materials

Iron(III) nitrate nonahydrate $Fe(NO_3)_3{\cdot}9H_2O$, magnesium(II) nitrate hexahydrate ($Mg(NO_3)_2{\cdot}6H_2O$), ethanol (C_2O_6O), sodium hydroxide (NaOH), hydrochloride acid (HCl solution 37%), and Congo red dye ($C_{32}H_{22}N_6Na_2O_6S_2$) were obtained from Merck, Germany.

2.2 $MgFe_2O_4$ preparation

As much as 8.08 g $Fe(NO_3)_3{\cdot}9H_2O$ and 2.56 g $Mg(NO_3)_2{\cdot}6H_2O$ were dissolved in 120 mL of distilled water. Under nitrogen gas flow, a 1 M NaOH solution was dripped into the solution and stirred using a magnetic stirrer until the pH reached ±10. The precipitate was filtered, washed repeatedly with distilled water until pH 7, then dried in an oven at 100°C for 4 h and calcined at 500°C for 3 h to produce $MgFe_2O_4$ powder.

2.3 Characterization of $MgFe_2O_4$

The crystal structure and phase of the $MgFe_2O_4$ were characterized using X-Ray Diffraction (XRD PANalytical), CuKα radiation was performed at a wavelength (λ=0.15418 nm) and an accelerated voltage of 30 kV in the range of 2θ=10-90°. The functional groups before and after the photocatalytic degradation were characterized by Fourier Transform Infra-Red (FTIR Prestige 21 Shimadzu), obtained using the KBr pellet technique and scanning from 4,000-400 cm^{-1}. The elemental morphology and composition were characterized using a Scanning Electron Microscope-Energy Dispersive Spectrometer (SEM-EDS JOEL JSM 6510 LA). The magnetic properties were determined using a Vibrating Sample Magnetometer (VSM Oxford Type 1.2 T). UV-Vis Diffuse Reflectance Spectroscopy (UV-Vis DRS Pharmaspec UV-1700) was used to determine

absorption and band gaps. The optical band gap value can be calculated by the equation (Equation 1):

$$(\alpha hv)^n = A\,(hv - Eg) \quad (1)$$

Where; hv is the photon energy, A is the optical constant, h is the Planck constant, and n indicates 2 or ½ for the direct and indirect transitions, respectively.

The absorbance of Congo red was determined using a UV-Vis Spectrophotometer (Type Orion Aquamate 8000). The λ_{max} for measurement of Congo red concentration was obtained at 498 nm. The mineralization was determined using Total Organic Carbon (TOC Teledyne Tekmar).

2.4 Determination of pHpzc

As much as 25 mL of 0.01 M $NaNO_3$ solution was prepared, and its pH was adjusted to range from 2 to 12 by adding 0.1 M HNO_3 or NaOH. Then, 0.1 g of $MgFe_2O_4$ was added to each Erlenmeyer flask and shaken using a shaker at 150 rpm for 48 h (Hariani et al., 2022). The pH of each solution was then determined using a pH meter (HI 2211 Hanna). A graph of ΔpH versus initial pH is used to calculate the pH pzc. The pHpzc measurement was repeated three times.

2.5 Photocatalytic degradation

The photocatalytic degradation process was carried out in a closed reactor at room temperature. The light source used was visible light irradiation (150 w Xenon lamp) at a distance of 30 cm from the sample. The dye was placed in a quartz pipe (50 mL). Congo red dye was used in a volume of 25 mL at a concentration of 50 mg/L. Then, 0.02 g of $MgFe_2O_4$ was added. The variables of photocatalytic degradation studied were pH effects (3-9), concentrations of Congo red (10, 20, 30, 40, and 50 mg/L), and H_2O_2 concentrations (0.5, 1.0, 1.5, 2.0, and 2.5 mM) over a time range of 0-210 min. Photocatalytic degradation was carried out with three repetitions. The degradation efficiency was determined by the formula (Equation 2).

$$\text{Efficiency}\ (\%) = \frac{C_o - C_t}{C_o} \quad (2)$$

Where; C_o and C_t are the initial and final concentrations of Congo red (mg/L).

After the degradation process, the catalyst is separated from the solution using an external magnet. The reusability of $MgFe_2O_4$ was determined by washing it with ethanol and distilled water, drying it in an oven for 60 min at 70ºC, and reusing it for other photocatalytic degradation processes. The reusability process is carried out according to the optimum conditions of photocatalytic degradation obtained. The experiment was repeated five times to determine the degradation efficiency (Ajabshir and Niasari, 2019; Hariani et al., 2022). Figure 1 shows a schematic diagram of a photocatalytic reactor for the degradation of Congo red dye.

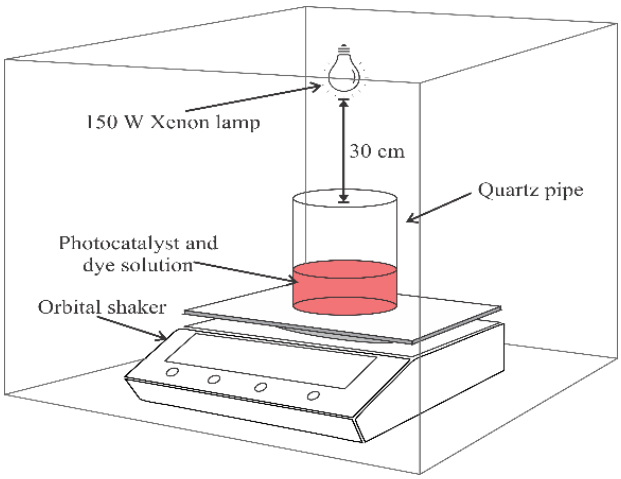

Figure 1. Schematic diagram of a photocatalytic reactor for the degradation of Congo red dye

3. RESULTS AND DISCUSSION

3.1 Characterization of the synthesized $MgFe_2O_4$

The XRD pattern of $MgFe_2O_4$ at 2θ=10-90º is presented in Figure 2. The 2θ angles were observed at 30.19º, 35.55º, 43.13º, 53.95°, 57.70º, 62.64º, and 74.95º, which were of the planes (220), (311), (400), (422), (511), (440), and (553), according to JCPDS card 36-0398, namely cubic spinel structure. The crystallite size of $MgFe_2O_4$ was calculated to be 14.38 nm using the Debye-Scherrer formula on the (311) reflection plane (Shahjuee et al., 2019).

Figure 3(a) shows the absorbance of $MgFe_2O_4$ as determined using UV-DRS. The UV-DRS spectra indicate the wavelength region of the catalyst absorbing light (Fu et al., 2019). It can be seen that the maximum absorption appears at a wavelength of 420 nm which indicates that $MgFe_2O_4$ is more suitable to be used as a catalyst in the visible light region. Based on the extrapolation of the $(\alpha hv)^n$ versus hv curve, the band gap value of $MgFe_2O_4$ was 1.88 eV (Figure 3(b)). The band gap is similar to $MgFe_2O_4$ synthesized using the sol-gel method (1.87 eV) (Vaish et al., 2019) and $MgFe_2O_4$ synthesized using solution combustion (1.91 eV) (Sripiya et al., 2019).

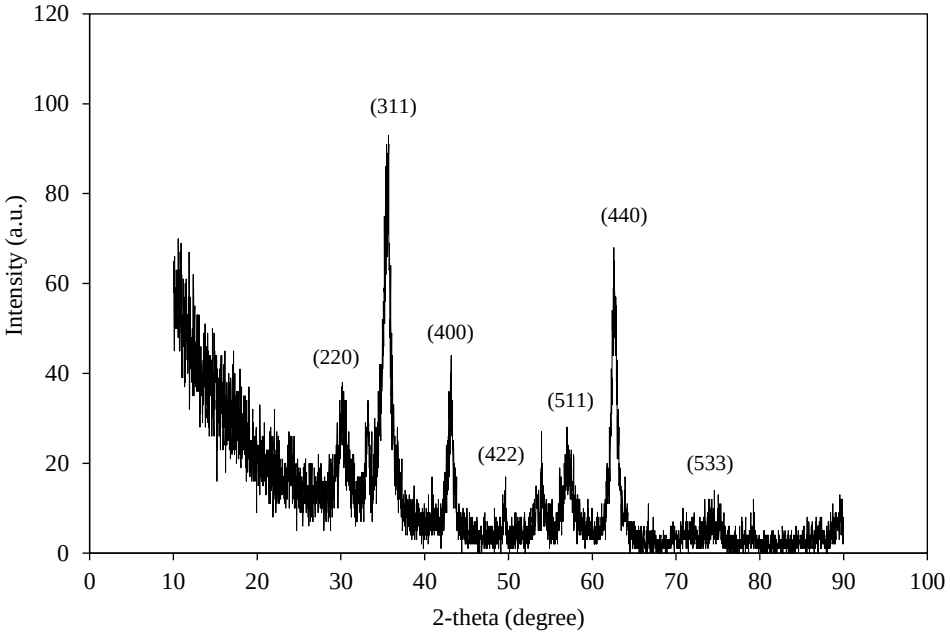

Figure 2. XRD pattern of $MgFe_2O_4$

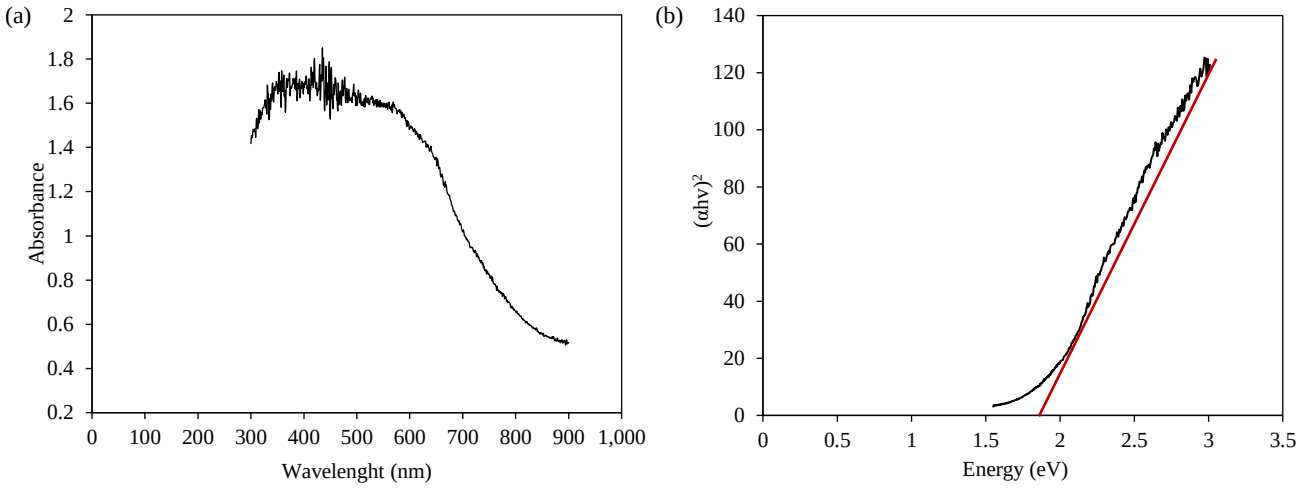

Figure 3. (a) UV-DRS spectrum and (b) band gap of $MgFe_2O_4$

The morphology of $MgFe_2O_4$ is presented in Figure 4. The morphology of $MgFe_2O_4$ appeared to be inhomogeneous; agglomeration occurs in some of it. SEM mapping revealed that Fe (blue) dominated the surface, Mg (red) was almost uniformly distributed, and Oxygen (O) was covered by Fe. The mass percentage of Fe was the highest (59.06%), while O and Mg were 30.26% and 10.68%, respectively. The presence of elements Fe, Mg, and O indicated that the synthesis of $MgFe_2O_4$ was successful.

Figure 5 shows the $MgFe_2O_4$ magnetization curves analysis using VSM. The magnetization curves show superparamagnetic properties. The saturation magnetization value of $MgFe_2O_4$ was 17.78 emu/g, more significant than that of $MgFe_2O_4$ synthesized using tragacanth gum (TG) by the sol-gel method (14 emu/g) (Fardood et al., 2019). $MgFe_2O_4$ is classified as a soft magnetic semiconductor material of the n-type (Maensiri et al., 2009). The saturation magnetization of bulk $MgFe_2O_4$ is approximately 26.9 emu/g (Sepelak et al., 2003). The magnetic property of $MgFe_2O_4$ is an advantage of the catalyst in a photocatalytic degradation process. $MgFe_2O_4$ can be separated from the solution quickly and easily with a permanent magnet after the degradation photocatalytic process.

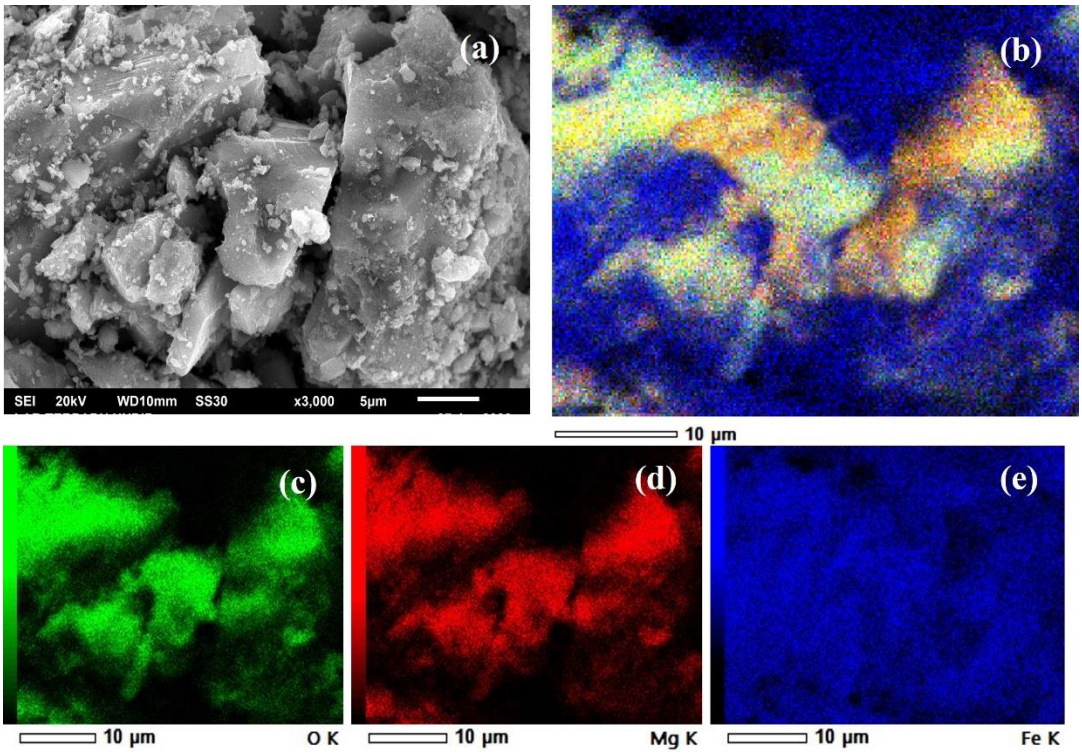

Figure 4. SEM images of (a) $MgFe_2O_4$, (b) elemental mapping of $MgFe_2O_4$, (c) O element, (d) Mg element, and (e) Fe element

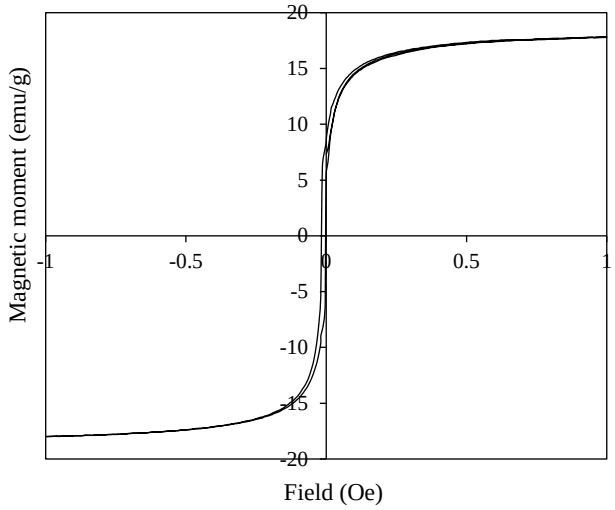

Figure 5. Saturation magnetization curves of $MgFe_2O_4$

3.2 Photocatalytic activity

The pH of the solution affects the interaction between the dye and the catalyst. In a photocatalytic degradation process, the first step is the attraction between the dye and the catalyst. The next step is the decomposition of the dye by two active species, namely superoxide anion ($\bullet O_2^-$) and hydroxyl radical ($\bullet OH$). In a solution with pH > pHpzc, $MgFe_2O_4$ is negatively charged. $MgFe_2O_4$ is positively charged if the pH of the solution < pHpzc. This study found a pHpzc of 6.8 (Figure 6(a)). pH effect was studied using a dye concentration of 50 mg/L in as much as 25 mL with 0.02 g of $MgFe_2O_4$ in the pH range of 3-9 and irradiation time of 0-210 min, as shown in Figure 6(b). The degradation efficiency increases with increasing pH of the solution, with a maximum degradation efficiency of 68.45% at pH 6. The pKa of Congo red dye at room temperature (25°C) is 4.1. Congo red dissociates into a polar group, specifically a negatively charged sulfonate group (R-SO_3-), under acidic conditions (Lafi et al., 2019). At a solution pH < pHpzc, $MgFe_2O_4$ is positively charged, increasing the attraction between the dye and $MgFe_2O_4$ (Shaban et al., 2019). Conversely, there is repulsion between $MgFe_2O_4$ and dyes at an alkaline pH because both are negatively charged (Hariani et al., 2021; Saleh and Taufik, 2019).

The effect of Congo red concentration was observed in the concentration range of 10-50 mg/L in as much as 25 mL with a mass of 0.02 g of $MgFe_2O_4$ and a pH of 6, as shown in Figure 6(c). The highest degradation efficiency occurred at a concentration of 10 mg/L. The elevated dye concentration results in an increased quantity of dye molecules that require decomposition by a restricted quantity of hydroxyl radicals. There is an inverse relationship between dye concentrations and degradation efficiency, whereby higher concentrations of dye lead to lower degradation efficiency (Boudiaf et al., 2021). In addition, the high

dye concentration can block light from interacting with the catalyst, thereby reducing the hydroxyl radicals generated (Vasiljevic et al., 2020; Jha and Chakraborty, 2020). This is similar to other research for the degradation of Congo red using $CoAl_2O_4$/ZnO under visible light irradiation. The photocatalytic degradation reactions are as follows (Jarariya, 2022; Ammar et al., 2020):

$$MgFe_2O_4 + hv \rightarrow MgFe_2O_4 (e_{CB^-} + h_{VB^+}) \quad (3)$$

$$e_{CB^-} + O_2 \rightarrow {}^{\bullet}O_2^- \quad (4)$$

$$h_{VB^+} + H_2O \rightarrow H^+ + {}^{\bullet}OH \quad (5)$$

$${}^{\bullet}O_2^- + H^+ \rightarrow {}^{\bullet}OH_2 \quad (6)$$

$${}^{\bullet}O_2^- + H_2O \rightarrow {}^{\bullet}HO_2 + OH^- \quad (7)$$

$${}^{\bullet}OH_2 + H_2O \rightarrow H_2O_2 + {}^{\bullet}OH \quad (8)$$

$$H_2O_2 \rightarrow 2\ {}^{\bullet}OH \quad (9)$$

$${}^{\bullet}O_2^- + \text{Congo red} \rightarrow CO_2 + H_2O + \text{other products} \quad (10)$$

$${}^{\bullet}OH + \text{Congo red} \rightarrow CO_2 + H_2O + \text{other products} \quad (11)$$

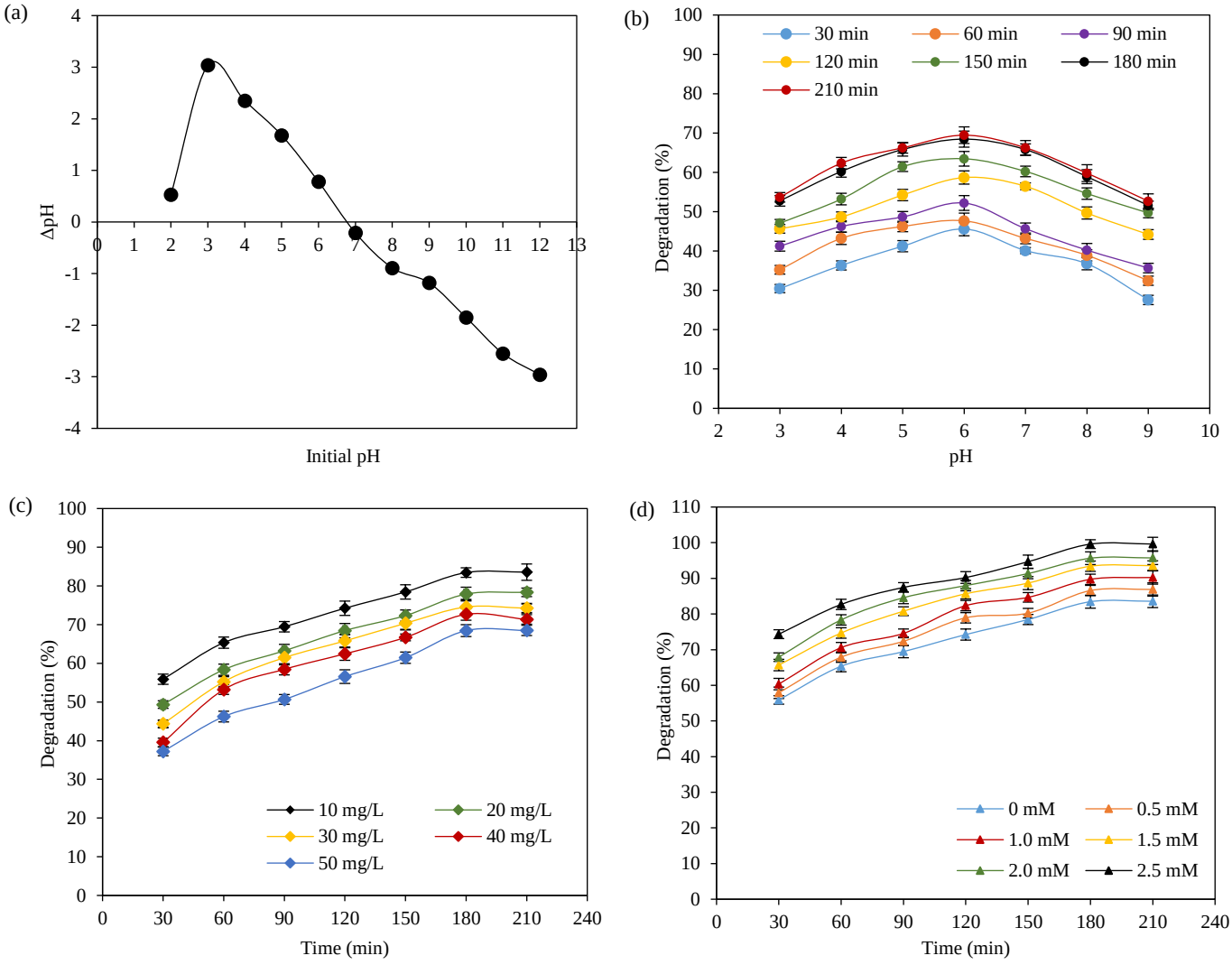

Figure 6. (a) pHpzc of $MgFe_2O_4$ and degradation photocatalytic of Congo red as a function of (b) pH, (c) initial concentration, and (d) H_2O_2 concentration

Figure 6(d) shows the effect of H_2O_2 on the degradation efficiency of Congo red. The dye concentration used was 10 mg/L with a volume of 25 mL, 0.02 g of $MgFe_2O_4$, a solution pH of 6, and H_2O_2 concentrations ranging from 0.5 to 2.5 mM. At 30 to 180 min, it is demonstrated that the greater the H_2O_2 concentration, the more efficient the degradation. No significant difference was observed in the degradation efficiency between the 180 and 210 irradiation times.

The increasing concentration of H_2O_2 also caused the degradation process to become less effective because the ${}^{\bullet}OH$ produced reacted with H_2O_2

reduced the probability of $^{\bullet}OH$ to attack the dye (Saleh and Taufik, 2019). The reactions that occurred were as follows (Flores et al., 2014):

$$^{\bullet}OH + H_2O_2 \rightarrow HO_2^{\bullet} + H_2O \quad (12)$$

$$^{\bullet}OH + HO_2^{\bullet} \rightarrow H_2O_2 + \tfrac{1}{2}O_2 \quad (13)$$

Figure 7 shows the comparison of the degradation efficiency of $MgFe_2O_4$, visible light, H_2O_2, $MgFe_2O_4$ + visible light, and $MgFe_2O_4$ + H_2O_2 + visible light. Sequentially, visible light irradiation (photolysis) < $MgFe_2O_4$ < H_2O_2 < $MgFe_2O_4$ + visible light irradiation < $MgFe_2O_4$ + H_2O_2 + visible light irradiation. The Congo red used had a concentration of 10 mg/L, a volume of 25 mL, 0.02 g $MgFe_2O_4$, a pH of 6, a concentration of H_2O_2 of 2.5 mM, and an irradiation time of 180 min. The results of this study suggest that the $MgFe_2O_4$ and visible light irradiation had the greatest impact on combined effects on degradation efficiency. However, it was also observed that the inclusion of H_2O_2 led to an increase in degradation efficiency. In this study, without the addition of H_2O_2 with an irradiation time of 180 min, the degradation efficiency was 83.45%. Adding H_2O_2 with a concentration of 2.5 mM increased the degradation efficiency to 99.60%. Another study, with an increase in H_2O_2 concentration, revealed that the photocatalytic degradation efficiency of acid orange 7 dye using a ZnO catalyst increased. With the addition of 1.25 mM H_2O_2, its degradation efficiency increased from 38 to 78.9% (Rahmati et al., 2021). Table 1 shows that combined degradation using $MgFe_2O_4$, visible light irradiation and H_2O_2 has the highest degradation efficiency compared to other studies.

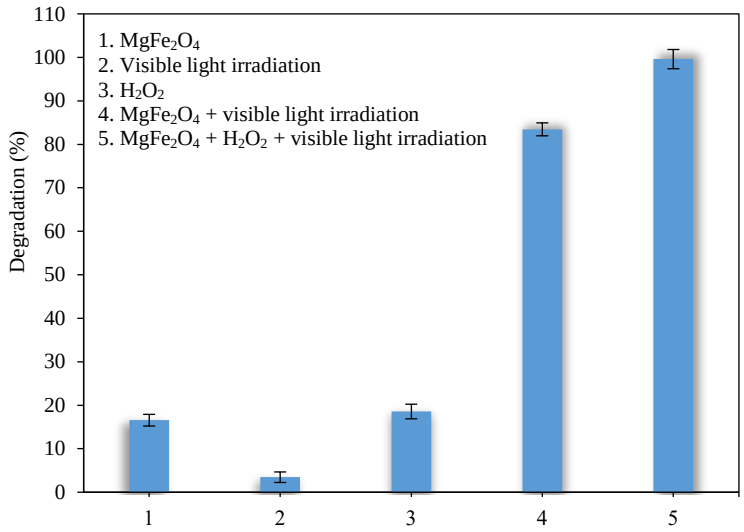

Figure 7. The comparison of the degradation efficiency of $MgFe_2O_4$, visible light irradiation, H_2O_2, $MgFe_2O_4$ + visible light irradiation, and $MgFe_2O_4$ + H_2O_2 + visible light irradiation

Table 1. Comparison of degradation of Congo red using several catalysts

Catalyst	pH	Dose (g/L)	Concentration (mg/L)	Efficiency (%)	References
Cellulose/PVC/ZnO	-	0.6	50	90	Linda et al. (2016)
Bs-$CoFe_2O_4$	9	0.03	5	84	Ali et al. (2020)
Ni-TiO_2	2	0.8	80	92.31	Indira et al. (2021)
$CoAl_2O_4$/ZnO	-	0.1	20	97	Boudiaf et al. (2021)
TiO_2/CoC@SiO_2bipy	4	0.045	10	95.80	Hammud et al. (2022)
SnO_2-Fe_3O_4 + H_2O_2	6	0.03	18	50.76	Said et al. (2022)
$MgFe_2O_4$ + H_2O_2	6	0.02	10	99.62	In this work

3.3 The kinetics of photocatalytic degradation

The kinetics of photocatalytic degradation of Congo red is expressed using the pseudo-first-order kinetics equation as follows (Mahboob et al., 2023; Boudiaf et al., 2021):

$$\ln\left(\frac{C_0}{C}\right) = kt \quad (14)$$

Where; C_o and C is the initial concentration and the concentration after the photocatalytic degradation of Congo red at each time (t), rate constant (k), respectively. Figure 8 shows the kinetics of photocatalytic degradation of Congo red using $MgFe_2O_4$ at a dye concentration of 10 mg/L in as much as 25 mL volume, 0.02 g $MgFe_2O_4$, and pH 6, H_2O_2 2.5 mM under visible light irradiation.

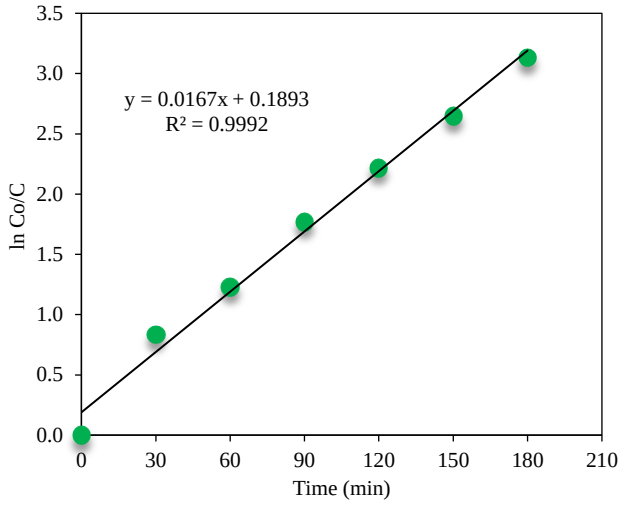

Figure 8. Kinetic photocatalytic degradation of Congo red using $MgFe_2O_4$

The correlation coefficient (R^2) obtained was 0.9992, close to 1, indicating that the photocatalytic degradation was in accordance with the pseudo-first-order. This study determined a k of 0.0167 min^{-1} and a half-life value ($t_{1/2}$=0.693/k) of 41.49 min. Other investigations have demonstrated that the photocatalytic degradation of Congo red employing P-ZrO_2CeO_2ZnO nanoparticles follows a pseudo-first-order with a k of 0.0069 min^{-1} and a $t_{1/2}$ of 100.46 min (Hokonya et al., 2022). Several variables influence the disparity between degradation rates, including catalyst particle size, surface area, work function value (eV), and dye structure (Mandal et al., 2023).

3.4. FTIR spectra before and after photocatalytic degradation

Figure 9 presents the FTIR spectra of $MgFe_2O_4$ before and after being used for Congo red photocatalytic degradation. The broad peak at the wavenumber around 3,400 cm^{-1} represented the O-H vibrations of the adsorbed water molecules. This result was reinforced by the peak at the wavenumber of around 1,630 cm^{-1}, namely H-O-H bending vibrations (Samiei et al., 2018). The characteristics of $MgFe_2O_4$ were observed at wavenumbers in the range 400-800 cm^{-1} attributed to M-O-M stretching (M=Mg and Fe). Wavenumbers around 580 cm^{-1} and 400 cm^{-1} confirm the presence of ferrite structure (Mohdi et al., 2006). The peaks of $MgFe_2O_4$ before and after photocatalytic degradation showed the same characteristics, namely, the wavenumbers appearing at 563 cm^{-1} and 567 cm^{-1} were Fe-O vibrations of tetrahedral and octahedral sites, while those in the area around 422 cm^{-1} and 418 cm^{-1} were the vibrations of octahedral sites. However, some Congo red was adsorbed on $MgFe_2O_4$, as evidenced by the peak at wavenumbers 1,043 cm^{-1} and 1,167 cm^{-1} that was (SO_3) stretching of the sulphonate groups in Congo red dye (Hammud et al., 2022).

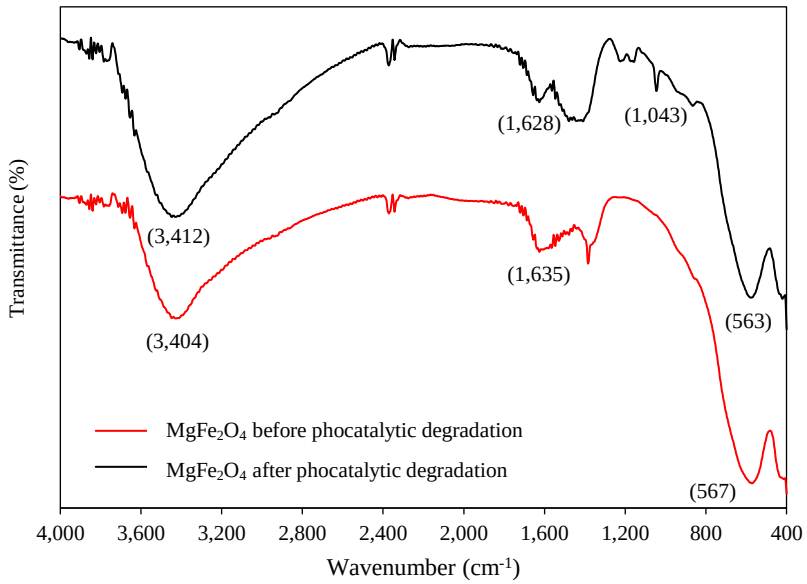

Figure 9. FTIR spectrum of $Mg_2Fe_2O_4$ before and after photocatalytic degradation

3.5. Reusability of the photocatalyst

Determining a catalyst's performance requires testing its regeneration and reuse. $MgFe_2O_4$, after use in the photocatalytic degradation process, was washed and dried in an oven to be reused for photocatalytic degradation at the optimum conditions obtained, namely, Congo red at a concentration of 10 mg/L in a volume of 25 mL, 0.02 g $MgFe_2O_4$, a pH of 6, 2.5 mM H_2O_2, and an irradiation time of 180 min. Figure 10 presents the effectiveness of degradation after five cycles. After five cycles, the effectiveness of photocatalytic degradation decreased from 99.62% to 94.50% (<5%). Such a reduction in the degradation effectiveness can occur during the photocatalytic degradation processes, such as separation, washing, drying processes, and the catalyst can undergo agglomeration (Hariani et al., 2022).

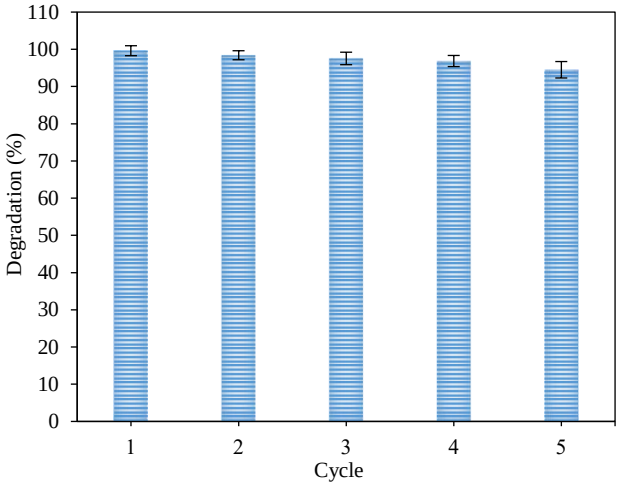

Figure 10. Reusability of $MgFe_2O_4$ as photocatalyst

The level of mineralization of Congo red as a result of photocatalytic degradation is determined from the total organic carbon (TOC) value. Mineralization levels are usually not fully developed (Pourzad et al., 2020). In this study, the TOC values were determined before and after photocatalytic degradation with a dye concentration of 10 mg/L, pH 6, H_2O_2 concentration of 2.5 mM, and irradiation time of 180 min. The TOC removal obtained was 84.58%. Other research indicated that the longer the irradiation time, the higher the effectiveness of TOC. Congo red photocatalytic degradation using $CoAl_2O_4$/ZnO under visible light irradiation obtained a maximum TOC of 66.9% (Boudiaf et al., 2021). A reduction in the TOC value proves that dye mineralization has occurred.

4. CONCLUSION

$MgFe_2O_4$ has been successfully synthesized by the coprecipitation method. The results show that $MgFe_2O_4$ has magnetic properties and, after being used as a photocatalyst, is easily separated from the solution using a permanent magnet. The efficiency of photocatalytic degradation is affected by the pH of the solution, the concentration of dye, and the addition of H_2O_2. The optimum photocatalytic degradation was obtained at a solution pH of 6, a dye concentration of 10 mg/L, a concentration of 2.5 mM H_2O_2, and irradiation time of 180 min under visible light irradiation, with a degradation efficiency of 99.62%. $MgFe_2O_4$ has high stability and reusability because, after five cycles, the degradation efficiency is above 90%. The study indicated that $MgFe_2O_4$ has the potential to be used for wastewater treatment, especially for treating wastewater containing dyes.

ACKNOWLEDGEMENTS

This research was funded by the DIPA of Public Service Agency of Universitas Sriwijaya 2022, SP DIPA-023.17.2.677515/2022 (SATEKS scheme), on December 13th, 2021, in accordance with the Rector's Decree Number: 0110/UN9.3.1/SK/2022, on April 28th, 2022.

REFERENCES

Ajabshir SZ, Niasari MS. Preparation of magnetically retrievable $CoFe_2O_4$-SiO_2-$Dy_2Ce_2O_7$ nanocomposites as novel photocatalyst for higly efficient degradation of organic contaminants. Composites Part B: Engineering 2019;174:1-9.

Ali N, Said A, Ali F, Razig F, Ali Z, Bilil M, et al. Photocatalytic degradation of Congo red dye from aqueous environment using cobalt ferrite nanostructures: Development, characterization, and photocatalytic performance. Water, Air, and Soil Pollution 2020;231(50):1-16.

Ammar SH, Elaibi AI, Mohamme IS. Core/shell Fe_3O_4@Al_2O_3-PMo magnetic nanocatalyst for photocatalytic degradation of organic pollutants in an internal loop airlift reactor. Journal of Water Process Engineering 2020;37:Article No.101240.

Argote-Fuentes S, Feria-Reyes R, Ramos-Ramirez E, Gutierrez-Ortega N, Cruz-Jimenez G. Photoelectrocatalytic degradation of Congo red dye with activated hydrotalcites and copper anod. Catalysts 2021;11(211):1-19.

Augugliaro V, Bellardita M, Loddo V, Palmisano G, Palmisano L, Yurdakal S. Overview on oxidation mechanisms of organic compounds by TiO_2 in heterogeneous photocatalysis. Journal of Photochemistry and Photobiology C: Photochemistry Reviews 2012;3(3):224-45.

Boudiaf S, Nasrallah N, Mellal M, Belhamdi B, Belabed C, Djilali MA, et al. Kinetic studies of congo red photodegradation on the hetero-system $CoAl_2O_4$/ZnO with a stirred reactor under solar light. Journal of Environmental Chemical Engineering 2021;9(4):Article No.105572.

El Gaini L, Lakraimi M, Sebbar E, Meghea A, Bakasse M. Removal of indigo carmine dye from water to Mg-Al-CO_3-calcined layered double hydroxides. Journal of Hazardous Materials 2009;161(2-3):627-32.

Fardood ST, Moradnia F, Mostafaei M, Afshari Z, Faramarzi V. Biosynthesis of $MgFe_2O_4$ magnetic nanoparticles and their application in photodegradation of malachite green dye and kinetic study. Nanochemistry Research 2019;4(1):86-93.

Flores A, Nesprias K, Vitale P, Tasca J, Lavat A, Eyler N, et al. Heterogeneous photocatalytic discoloration/degradation of rhodamine B with H_2O_2 and spinel copper ferrite magnetic nanoparticles. Australian Journal of Chemistry 2014;67:609-14.

Fu C, Liu X, Wang Y, Li L, Zhang Z. Preparation and characterization of Fe_3O_4@SiO_2@TiO_2-Co/rGO magnetic visible light photocatalyst for water treatment. RSC Advances 2019;9:20256-65.

Gao HJ, Wang SF, Fang LM, Sun GA, Chen XP, Tang SN, et al. Nanostructured spinel-type M (M=Mg, Co, Zn) Cr_2O_4 oxides: Novel adsorbents for aqueous Congo red removal. Materials Today Chemistry 2021;22:Article No.100593.

Habiba U, Siddique TA, Joo TC, Salleh A, Ang BC, Afifi AM. Synthesis of chitosan/polyvinyl alcohol/zeolite composite for removal of methyl orange, Congo red and chromium(VI) by flocculation/adsorption. Carbohydrate Polymers 2017;157: 1568-76.

Hammud HH, Traboulsi H, Karnati RK, Bakir EM. Photodegradation of Congo red by modified P25-titanium dioxide with cobalt-carbon supported on SiO_2 matrix, DFT studies of chemical reactivity. Catalyst 2022;12(248):1-14.

Hariani PL, Said M, Rachmat A, Riyanti F, Pratiwi HC, Rizki WT. Preparation of $NiFe_2O_4$ nanoparticles by solution combustion method as photocatalyst of Congo red. Bulletin of Chemical Reaction Engineering and Catalysis 2021;16:481-90.

Hariani PL, Said M, Salni, Aprianti N, Naibaho YALR. High efficient photocatalytic degradation of methyl orange dye in an aqueous solution by $CoFe_2O_4$-SiO_2-TiO_2 magnetic catalyst. Journal of Ecological Engineering 2022;23:118-28.

Harja M, Buema G, Bucur D. Recent advances in removal of Congo red dye by adsorption using an industrial waste. Scientific Reports 2022;12(6087):1-18.

Hokonya N, Mahamadi C, Mukaratirwa-Muchanyereyi N, Gutu T, Zvinowanda C. Green synthesis of P-ZrO_2CeO_2ZnO nanoparticles using leaf extracts of *Flacourtia indica* and their application for the photocatalytic degradation of a model toxic dye, Congo red. Heliyon 2022;8:1-18.

Indira K, Shanmugam S, Hari A, Vasantharaj S, Sathiyavimal S, Brindhadevi K, et al. Photocatalytic degradation of Congo red dye using nickel-titanium dioxide nanoflakes synthesized by *Mukia madrasapatna* leaf extract. Environmental Research 2021;202:1-8.

Jarariya R. A review based on spinel ferrite nanomaterials-$MgFe_2O_4$-synthesis of photocatalytic dye degradation in visible light response. Journal of Environmental Treatment Techniques 2022;10(2):149-56.

Jha AK, Chakraborty S. Photocatalytic degradation of Congo red under UV irradiation by zero valent iron nano particles (nZVI) synthesized using *Shorea robusta* (Sal) leaf extract. Water Science and Technology 2020;82(11):2491-502.

Khumalo NP, Nthunya LN, De Canck E, Derese S, Verliefde AR, Kuvarega AT, et al. Congo red dye removal by direct membrane distillation using PVDF/PTFE membrane. Separation and Purification Technology 2019;211:578-86.

Lafi R, Montasser I, Hafiane A. Adsorption of Congo red dye from aqueous solutions by prepared activated carbon with oxygen-containing functional groups and its regeneration. Adsorption Science and Technology 2019;37(1-2):160-81.

Linda T, Muthupoongodi S, Shajan XS, Balakumur S. Photocatalytic degradation of Congo red and crystal violet dyes on cellulose/PVC/ZnO composites under UV light irradiation. Materials Today: Proceedings 2016;3:2035-41.

Lum PT, Foo KY, Zakaria NA, Palaniandy P. Ash based nanocomposites for photocatalytic degradation of textile dye pollutants: A review. Materials Chemistry and Physics 2020;241:Article No.122405.

Maensiri S, Sangmanee M, Wiengmoon A. Magnesium Ferrite ($MgFe_2O_4$) nanostructures fabricated by electrospinning. Nanoscale Research Letter 2009;4:221-8

Mandal RK, Mondal AS, Ghosh S, Halder A, Majumder TP. Synthesis, characterisation and optical studies of CdO-NiO NCs for comparative dye degradation study between two hazardous dyes Congo red and rose bengal. Results in Chemistry 2023;5:Article No.100810.

Mahboob I, Shafig I, Shafique S, Akhter P, Munir M, Saeed M, et al. Porous Ag_3VO_4/KIT-6 composite: Synthesis, characterization and enhanced photocatalytic performance for degradation of Congo red. Chemosphere 2023;311:Article No.137180.

McDonald KD, Bartlett BM. Microwave synthesis of spinel $MgFe_2O_4$ nanoparticles and the effect of annealing on photocatalysis. Inorganic Chemistry 2021;60:8704-9.

Mezohegyi G, Van Der Zee FP, Font J, Fortuny A, Fabregat A. Towards advanced aqueous dye removal processes: A short review on the versatile role of activated carbon. Journal of Environmental Management 2012;102:148-64.

Mohdi KB, Chhantbar MC, Joshi HH. Study of elastic behavior of magnesium ferri aluminates. Ceramics International 2006; 32(2):111-4.

Nguyen LTT, Nguyen LTH, Manh NC, Quoc DN, Quang HN, Nguyen HTT, et al. A facile synthesis, characterization, and photocatalytic activity of magnesium ferrite nanoparticles via the solution combustion method. Journal of Chemistry 2019;2019:Article No.3428681.

Oliveira TP, Marques GN, Castro MAM, Costa RCV, Rangel JHG, Rodrigues SF, et al. Synthesis and photocatalytic investigation of $ZnFe_2O_4$ in the degradation of organic dyes under visible light. Journal of Materials Research and Technology 2020;9(6):15001-15.

Pourzad A, Sobhi HR, Behbahani M, Esrafili A, Kalantary RR, Kermani M. Efficient visible light-induced photocatalytic removal of paraquat using N-doped TiO_2@SiO_2@Fe_3O_4 nanocomposite. Journal of Molecular Liquids 2020;299: Article No.112167.

Rahmati R, Nayebi B, Ayati B. Investigating the effect of hydrogen peroxide as an electron acceptor in increasing the capability of slurry photocatalytic process in dye removal. Water Science and Technology 2021;83(10):2414-23.

Robinson T, McMullan G, Marchant R, Nigam P. Remediation of dyes in textile effluent: A critical review on current treatment technologies with a proposed alternative. Bioresource Technology 2001;77(3):247-55.

Saha R, Mukhopadhyay M. Elucidation of the decolorization of Congo red by trametes versicolor laccase in presence of ABTS through cyclic voltammetry. Enzyme and Microbial Technology 2020;135:Article No.109507.

Said M, Rizki WT, Asri WR, Desnelli D, Rachmat A, Hariani PL. SnO_2-Fe_3O_4 nanocomposites for the photodegradation of the Congo red dye. Heliyon 2022;8:1-8.

Saleh R, Taufik A. Degradation of methylene blue and Congo red dyes using Fenton, photo-Fenton, sono-Fenton, and sonophoto-Fenton methods in the presence of iron (II,III) oxide/zinc oxide/graphene (Fe_3O_4/ZnO/graphene) composites. Separation and Purification Technology 2019;210:563-73.

Samiei S, Pakpur F, Ghanbari D. Synthesis of magnesium ferrite-silver nanostructures and investigation of its photocatalyst and magnetic properties. Journal of Nanostructures 2018; 8(1):37-46.

Sathiskumar K, Alsalhi MS, Sanganyado E, Devanesan S, Arulprakash A, Rajasekar A. Sequential electrochemical oxidation and bio-treatment of the azo dye Congo red and textile effluent. Journal of Photochemistry and Photobiology B: Biology 2019;200:Article No.111655.

Sepelak V, Baabe D, Mienert D, Litterst FJ, Becker KD. Enhanced magnetisation in nanocrystalline high-energy milled $MgFe_2O_4$. Scripta Materialia 2003;48:961-6.

Shaban M, Ahmed AM, Shehata N, Betiha MA, Rabie AM. Ni-doped and Ni/Cr co-doped TiO_2 nanotubes for enhancement of photocatalytic degradation of methylene blue. Journal of Colloid and Interface Science 2019;555:31-41.

Shahid M. Jingling L, Ali Z, Shakir I, Warsi MF, Parveen R, et al. Photocatalytic degradation of methylene blue on magnetically separable $MgFe_2O_4$ under visible light irradiation. Materials Chemistry and Physics 2013;139:566-71.

Shahjuee T, Masoudpanah SM, Mirkazemi SM. Thermal decomposition synthesis of $MgFe_2O_4$ nanoparticles for magnetic hyperthermia. Journal of Superconductivity and Novel Magnetism 2019;32:1347-52.

Sharma G, Algarni TS, Kumar PS, Bhogal S, Kumar A, Sharma S, et al. Utilization of Ag_2O-Al_2O_3-ZrO_2 decorated onto rGO as adsorbent for the removal of Congo red from aqueous solution. Environmental Research 2021;197:Article No.111179.

Sripiya R, Mahendiran M, Madahavan J, Raj MVA. Enhanced magnetic properties of $MgFe_2O_4$ nanoparticles. Materials Today: Proceedings 2019;8:310-4.

Vaish G, Kripal R, Kumar L. EPR and optical studies of pure $MgFe_2O_4$ and ZnO nanoparticles and $MgFe_2O_4$-ZnO nanocomposite. Journal of Materials Science: Materials in Electronics 2019;30:16518-26.

Valenzuela MA, Bosch P, Jimenez-Becerrill J, Quiroz O, Paez AI. Preparation, characterization and photocatalytic activity of ZnO, Fe_2O_3 and $ZnFe_2O_4$. Journal of Photochemistry and Photobiology A: Chemistry 2002;148(1-3):177-82.

Vasiljevic ZZ, Dojcinovic MP, Vujancevic JD, Jankovic-Casvan I, Ognjanovic M, Tadic NB, et al. Photocatalytic degradation of methylene blue under natural sunlight using iron titanate nanoparticles prepared by a modified sol-gel method. Royal Society Open Science 2020;7:1-14.

Wang L, Li J, Wang Y, Zhao L, Jiang Q. Adsorption capability for Congo red on nanocrystalline MFe_2O_4 (M=Mn, Fe, Co, Ni) spinel ferrites. Chemical Engineering Journal 2012;181-182:72-9.

Zhang J, Fan S, Lu B, Cai Q, Zhao J, Zang S. Photodegradation of naphthalene over Fe_3O_4 under visible light irradiation. Royal Society Open Science 2019;6:1-15.

Individual and Combined Effects of Pesticides with Active Ingredients of Mancozeb and Methomyl on the DNA Damage of *Daphnia magna* (Straus, 1820; Cladocera, Daphniidae)

Rania Nawra Thifali Izdihar, Diah Ariyanti Perdana, Farial Alwaini, and Andhika Puspito Nugroho*

Faculty of Biology, Universitas Gadjah Mada, Special Region of Yogyakarta 55281, Indonesia

ARTICLE INFO

Received: 3 Feb 2023
Received in revised: 21 May 2023
Accepted: 24 May 2023
Published online: 3 Jul 2023
DOI: 10.32526/ennrj/21/20230036

Keywords:
Biomonitoring/ Comet Assay/ *Daphnia magna*/ DNA damage/ Eco-genotoxicity/ Mancozeb/ Methomyl

*** Corresponding author:**
E-mail: andhika_pn@ugm.ac.id

ABSTRACT

Mancozeb and methomyl are active ingredients commonly contained in pesticides applied in shallot farming. Surface runoff can carry pesticide residues that enter water bodies and affect non-target organisms, such as *Daphnia magna*. This study evaluated the genotoxicity effects of individual and combined mancozeb and methomyl on the DNA damage of *D. magna*. Organisms at 24 h old and 48 h old were exposed to individual and combined concentrations of mancozeb and methomyl for 24 h to obtain the LC50-24 h values. These values were used to evaluate DNA damage by calculating the tail intensity (TI) (%), tail moment (TM), and tail factor (TF). Results showed that based on the LC50-24 h values, methomyl has the highest toxicity level, followed by the mancozeb:methomyl combination, and then mancozeb. The combination index of mancozeb:methomyl for both *D. magna* ages (24 h and 48 h) indicated that the two pesticides antagonistically interact (CI>1). However, based on TI%, TM, and TF values, the level of damage was almost the same between the individual and combined pesticide concentrations, and the DNA damage was more massive with increased pesticide concentration. The DNA damage of 24 h old and 48 h old *D. magna* did not significantly differ. Increased DNA damage in *D. magna* indicated that this parameter was sensitive to the presence of pesticides. In application, DNA damage can be used as a biomarker for biomonitoring pesticide pollution in the aquatic ecosystem.

1. INTRODUCTION

Methomyl and mancozeb are carbamate pesticides that control foliage and soil-borne insect pests on various food and feed crops. Mancozeb is a fungicide that can inhibit the growth of fungi and spores prior to the development of mycelium in plant tissues. This fungicide is effective against external contamination caused by fungi (Asita and Makhalemele, 2009). Meanwhile, methomyl is a broad-spectrum and systemic anticholinesterase carbamate insecticide used worldwide to protect crops from invading organisms. Unfortunately, this carbamate insecticide can also affect non-target organisms (Seleem, 2019).

These pesticides can leave residues on the soil surface that are carried away by surface water that flows into aquatic ecosystems, where they are absorbed by non-target organisms. Therefore, an unpredictable ecological risk is posed based on the individual concentrations of pesticides. The interaction of various pesticides can have toxic effects, which are additive, synergistic, or antagonistic in organisms (Aktar et al., 2009; Kaur and Kaur, 2018; Vasiljević et al., 2012). Furthermore, *Daphnia magna*, an essential planktonic crustacean in the aquatic ecosystem, is exposed to these pesticides individually or in combination (Kretschmann et al., 2011). Pesticides also affect the survival, growth, and fecundity of *D. magna* (Rajini et al., 2016). The exposure of these organisms to 0.58 ppm of mancozeb resulted in a mortality rate of 50%. This pesticide also causes damage to the nucleus, and chromosomal and micronuclear aberrations (Christin et al., 2015). According to Mayer and Ellersieck (1986), exposure

Citation: Izdihar RNT, Perdana DA, Alwaini F, Nugroho AP. Individual and combined effects of pesticides with active ingredients of mancozeb and methomyl on the DNA damage of *Daphnia magna* (Straus, 1820; Cladocera, Daphniidae). Environ. Nat. Resour. J. 2023;21(4): 333-344. (https://doi.org/10.32526/ennrj/21/20230036)

to 7.3-20.0 g/L of methomyl caused the death of *D. magna*. Both pesticides (mancozeb and methomyl) induce damage and break chromosomal abrasion, sister-chromatid exchanges, micronuclei, and DNA bonds in terms of single- and double-strand (Hart et al., 1978; Pellegri et al., 2014). Through the food chain, the accumulation of such pesticides in *Daphnia* can lead to biomagnification, which can have detrimental effects on other aquatic organisms and humans as one of the top predators. A study of mancozeb effects on the test organism, Sprague Dawley rats, indicated that it induced genotoxic effects, metabolic alterations, and histological changes in the colon and liver (Yahia et al., 2019). In humans, carbamate pesticides, such as methomyl, can inhibit various types of esterase. The toxic effect of this pesticide is the inhibition of acetylcholinesterase, leading to excessive cholinergic overstimulation. The symptoms of pesticide poisoning include muscle twitching and weakness, decreased levels of consciousness, excessive salivation and tearing, seizures, respiratory failure, and constricted pupils (Liang et al., 2023).

D. magna is a selective filter feeder organism that feeds on unicellular algae and various organic detritus. The organism becomes a food source for the next trophic level in the aquatic ecosystems because it is naturally essential for fish larvae (Antunes et al., 2016). However, this food chain also leads to the biomagnification of pesticides. Therefore, humans become exposed to high toxic concentrations at the top of the food chain (Castro et al., 2019; Mahmood et al., 2015).

Biological responses at the molecular level provide early sensitive and specific warnings regarding environmental pollutants. In polluted environments, DNA damage of aquatic organisms is considered a sensitive biomarker to evaluate genotoxicity and ecogenotoxicological risks (Liyan et al., 2005; Pellegri et al., 2014). Furthermore, single-cell gel electrophoresis (SCGE) or comet assay is often used in DNA damage analysis because it is a simple procedure. This assay can detect damages caused by genotoxic agents, especially in eukaryotic cells, including *D. magna* (Pellegri et al., 2020; Jha, 2008). *Daphnia* sp. is widely used for water quality testing due to its characteristics, which satisfy the requirement of a model organism for ecotoxicological studies. This organism has a wide distribution range, is easily cultured in the laboratory with relatively high sensitivity to pollutants, and has known biological data (Surtikanti et al., 2017).

Previous studies using comet assays with *D. magna* (Jha, 2008; Pellegri et al., 2020) have shown and emphasized the advantage of using the comet assay method in assessing the genotoxicity of toxicants on aquatic organisms. However, studies with agricultural pesticides, such as methomyl and mancozeb (and their combination), still need to be explored. Evaluation of DNA damage of the organism upon exposure to the pesticides will reveal the pesticide risks on aquatic ecosystems. Furthermore, the age selection of *D. magna* is closely related to its high sensitivity to pollutants (Pellegri et al., 2014). Therefore, this study aims to evaluate the genotoxicity of individual and combined effects of mancozeb and methomyl on the DNA damage of 24 h old and 48 h old *D. magna*.

2. METHODOLOGY

2.1 Chemical materials

The chemicals used in the study were of analytical grade (Merck). An artificial medium (Klüttgen et al., 1994) was used as the *Daphnia* growth medium. For the individual and combined exposure experiments, stock solutions of methomyl and mancozeb were prepared in 500 mL of bidistilled water by first dissolving 50 mg methomyl PESTANAL, analytical grade (CAS 16752-77-5, Merck) in acetonitrile (5 mL), and 50 mg mancozeb PESTANAL, analytical grade (CAS 8018-01-7, Merck) in dimethyl sulfoxide (2.5 mL), respectively, yielding a concentration of 100 mg/L each.

2.2 Breeding *D. magna*

D. magna was obtained from the Center for Aquaculture Technology Development (BPTPB), Cangkringan, Sleman, Special Region of Yogyakarta, Indonesia. The culture process was carried out by maintaining female organisms in an aerated artificial medium for 24 h, with a population density of three individuals/100 mL medium. This process provided nutrition in maltose, with aeration for water circulation. The offspring were maintained for 24 h and 48 h to obtain individuals within the age range. The offspring were further used in individual or combined tests to evaluate the toxicity of mancozeb and methomyl and analyze their effects on DNA damage. For toxicity tests and analysis of DNA damage, 10 individuals of *D. magna* (24 h old and 48 h

old) were obtained from the culture and separately transferred to a glass beaker filled with artificial medium without being fed.

2.3 Acute toxicity test

The acute toxicity test consisted of preliminary and definitive tests to obtain the LC50-24 h of mancozeb, methomyl, and a combination of both pesticides on *D. magna*. For the initial examination, mancozeb and methomyl were added to the *D. magna* culture (10 individuals, n=3). Administration of both pesticides produced concentrations of 0.0, 0.1, 1.0, 10.0, and 100.0 mg/L. The mortality of the organisms was recorded after 24 h. The concentration range that produced the mortality rate of 50% was further used as the definitive test range.

Ten individuals were used for each definitive test (Table 1), and the mortality of *D. magna* was recorded after 24 h. Probit analysis was performed based on definitive test results to obtain the LC50-24 h for individual and combined pesticides.

To evaluate the effects of the pesticides in combination, e.g., additive, synergism, or antagonism, the combination index (CI) was calculated using the following classic isobologram combination index:

$$\frac{Am}{Ai} + \frac{Bm}{Bi}$$

Where; Am is the LC50-24 h value of mancozeb in combination, Bm is LC50-24 h value of methomyl in combination, Ai is LC50-24 h value of individual mancozeb, and Bi is LC50-24 h value of individual methomyl.

The values of CI are defined as synergism (CI<1), additive (CI=1), or antagonism (CI>1). If the values were plotted graphically, then the CI point position on the above additive line represents an antagonistic effect, the under-additive line being synergistic (Markovsky et al., 2014).

2.4 DNA damage analysis

The *D. magna* cultures of age 24 h and 48 h were prepared in a 250 mL glass beaker, with a density of 10 individuals/100 mL, to evaluate the effects of mancozeb and methomyl pesticides on DNA damage. The test organisms were treated with different toxicant concentrations, with three repetitions for each concentration (Table 2). The differences in the pesticide concentrations between the two age groups of *D. magna* were due to the LC50-24 h values.

Table 1. Concentrations of mancozeb, methomyl, and combination of mancozeb:methomyl in the 24-h definitive test for two age groups of *D. magna*

Pesticides	Age of *D. magna*	Concentration (mg/L)
Mancozeb	24 h	0.0
		0.1
		0.4
		0.7
		1.0
	48 h	0.0
		0.1
		0.4
		0.7
		1.0
Methomyl	24 h	0.00
		0.01
		0.04
		0.07
		0.10
	48 h	0.00
		0.01
		0.04
		0.07
		0.10
Mancozeb: Methomyl	24 h	0:0
		0.10:0.01
		0.40:0.04
		0.70:0.07
		1.00:0.10
	48 h	0:0
		0.10:0.01
		0.40:0.04
		0.70:0.07
		1.00:0.10

2.4.1 D. magna hemolymph extraction

After exposure of *D. magna* to the pesticides, the DNA damage was analyzed following the method of Pellegri et al. (2014). The organisms were obtained from the medium, crushed by a mortar, combined with 2 mL of Buffer P solution (0.1 M phosphate buffer, 0.2% citric acid, 0.1 M NaCl, 1 mM EDTA, and pH 7.8 (Pellacani et al., 2006)) and placed into a 15 mL conical tube to maintain the viability of the extraction result. The extract was then centrifuged at a speed of 45xg for 5 min. The supernatant was discarded, and the hemolymph extract pellet was washed twice using

2 mL Buffer P and centrifuged at a speed of 45xg for 5 min. The resulting pellet (hemolymph extract) was then placed in a 2 mL microtube, added with 1 mL of PP Buffer solution (0.1 M phosphate buffer, 0.2% citric acid, 0.1 M NaCl, 1 mM EDTA, and pH 7.8) and stored in the freezer (-80°C).

Table 2. Concentrations of mancozeb, methomyl, and combination of mancozeb:methomyl in the DNA damage analysis of the two age groups of *D. magna*

Pesticides	Age of *D. magna*	Concentration (mg/L)
Mancozeb	24 h	0.0
		0.3
		0.5
		0.7
	48 h	0.000
		0.080
		0.100
		0.012
Methomyl	24 h	0.00
		0.04
		0.06
		0.08
	48 h	0.000
		0.014
		0.024
		0.034
Mancozeb: Methomyl	24 h	0:0
		0.066:0.066
		0.086:0.086
		0.106:0.106
	48 h	0:0
		0.018:0.018,
		0.028:0.028
		0.038:0.038

2.4.2 Preparations

Microscope slides were placed into a 100 mL glass beaker containing 100 mL of 1% normal melting agarose (NMA) solution until two-thirds of the slide was coated. The slides were then covered with aluminum foil and stored in the refrigerator at 4°C for 24 h.

An aliquot of 10 µL hemolymph cell extract was combined with 90 µL 0.7% low melting agarose (LMA) on parafilm and mixed two to three times using a micropipette with an angle of 45°. The mixture was carefully placed on a microscope slide coated with NMA, covered with a cover glass, and stored in a refrigerator at 4°C for 24 h. The cover glass was removed by slowly sliding until detachment was achieved.

2.4.3 Lysis

The microscope slides were vertically placed into the staining jar as the lysis solution was added (2.5 M NaCl, 100 mM Na_2EDTA, 10 mM Tris-HCl, 1% Triton X-100, and 10% DMSO at pH 10) at a temperature of 4°C. The staining jar was then closed and placed in the refrigerator at 4°C for 24 h.

2.4.4 Electrophoresis

The microscope slides were removed from the lysis solution for unwinding by immersing in an alkaline buffer (1 mM Na_2EDTA, 300 mM NaOH, and pH > 13) for 10 min. The slide was then placed horizontally in an electroporator comet assay tank and filled with alkaline buffer until entirely submerged. This tank was placed in a refrigerator at 4°C, and the power supply was regulated at 300 mA and 25 V for 10 min.

2.4.5 Neutralization

Each slide was neutralized by immersion in a neutralization buffer (0.4 M Tris-HCl and pH 7.5). This process was carried out thrice, removing the remaining alkaline buffer, with the slide being soaked for 5 min in each washing. The slides were then dried and stored in a refrigerator at 4°C until the staining process.

2.4.6 Image analysis

The electrophoresed comet assay slides were stained with SYBR Safe dissolved in DMSO at a 10,000-fold dilution. Each slide was stained with 70 µL SYBR Safe and observed under a fluorescent microscope (526 nm wavelength and 5×10 magnification). These observations were calculated with at least 50 nuclei per sample with five fields of view. In this study, the DNA damage was evaluated with the parameters of the percentage tail intensity (TI%, % of DNA in the tail), tail moment (TM, tail length x% of DNA in the tail), and tail factor (TF, a measure for the degree of DNA fragmentation in a cell population) by using the Comet Score: Automatic Comet assay Software series 2.0.0.38, which displayed the TI% and TM results.

For the TF, *D. magna* nuclei were grouped into five categories (A-E) according to the amount of DNA in the tail. Category A showed 2.5% of DNA in the

tail. It was accompanied by categories B, C, D, and E, which showed cells with DNA in the tail of 12.5%, 30%, 67.5%, and 97.5%, respectively (Focke et al., 2010). Furthermore, the grade A damage indicated that the cells were primarily undamaged, with B-E representing higher levels of DNA fragmentation (Focke et al., 2010).

2.5 Data analysis

The DNA damage data (TI% and TM) were analyzed by one-way analysis of variance, with pesticide concentrations as the independent variable. When the results showed a significant difference, the Dunnett multiple comparison tests were performed between the control and pesticide concentrations in each age group, where the comet category of TF was tested by Duncan Multiple Range Test. In addition, an independent sample T-test was performed to evaluate the effect of *D. magna*'s age on DNA damage. Linear regression analysis was performed to assess the relationships between pesticide concentrations and DNA damage (TI% and TM), followed by Pearson correlation analysis to test the strength of linear relationships.

3. RESULTS AND DISCUSSION

3.1 Acute toxicity

The acute toxicity test showed that the LC50-24 h of methomyl was lower than the methomyl: mancozeb combination and mancozeb alone (Table 3). This finding indicated that methomyl has the highest toxicity level (Alwaini, 2021; Ariyanti, 2021; Izdihar, 2021). The acute toxicity tests resulted in LC50-24 h values below 1 mg/L. Based on the European Commission (EC, 2003), an LC50 value of less than 1 mg/L is extremely toxic to aquatic organisms.

Table 3. LC50-24 h of methomyl, mancozeb, and mancozeb:methomyl combination against *D. magna*

Pesticides	Age of *D. magna*	LC50-24 h (mg/L)
Methomyl	24 h	0.060
	48 h	0.024
Mancozeb	24 h	0.529
	48 h	0.141
Mancozeb:Methomyl	24 h	0.086
	48 h	0.028

According to USEPA (2005), the LC50-24 h of mancozeb toward *D. magna* was 0.058 mg/L, which was lower than the results of this study. For methomyl, Ren et al. (2017) suggested that the LC50-24 h on *D. magna* ranged from 0.0073-0.0200 mg/L, whereas Menconi and Beckman (1996) obtained 0.0317 mg/L, results that are also lower than those obtained in this study. The LC50 values may be influenced by parent nutrition, individual genotype and size, neonate qualities, and food availability (Pellegri et al., 2014). The combination index of mancozeb:methomyl for both *D. magna* ages (24 h and 48 h) showed a value of >1, indicating that the two pesticides antagonistically interacted. In the isobologram, the values of CI are above the additive line (Figure 1).

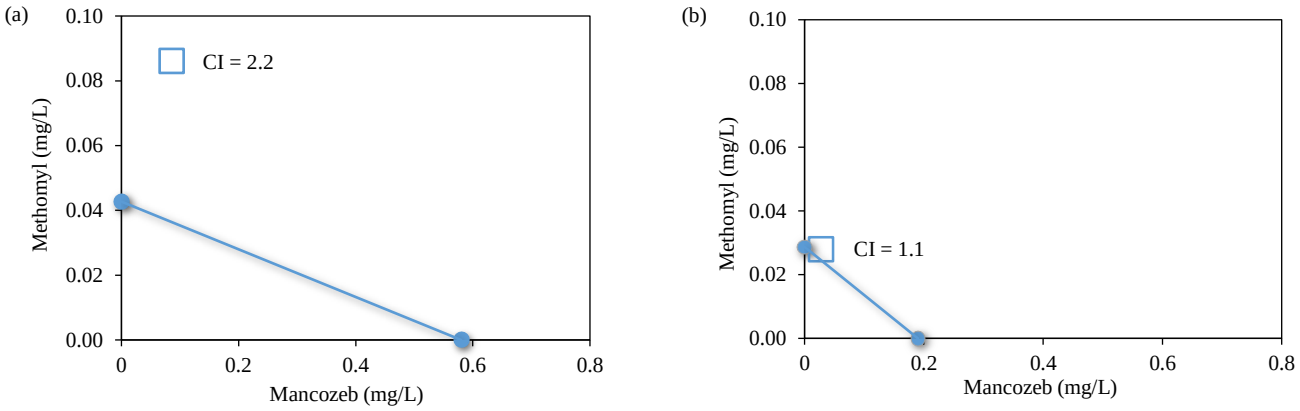

Figure 1. Isobolograms that represent the antagonistic activity of mancozeb and methomyl on (a) 24 h old and (b) 48 h old *D. magna*

Based on the toxicity test, methomyl, mancozeb, and mancozeb:methomyl combination affected the movement of *Daphnia*, which became weaker and slower. These pesticides also caused the death of some *D. magna*, which were found to have paler body color. According to Lushchak et al. (2018), pesticide exposure causes several damages to the physiological features of the organism, such as molting and the destruction of the antennae and internal body structure. This exposure also affected

reproduction, feeding, and breathing abilities, which decreased due to reduced oxygen consumption levels (Araujo et al., 2019). Furthermore, mancozeb interfered with lipid metabolism and respiration, with methomyl affecting the physiology of *D. magna*, by binding to acetylcholinesterase (AChE) and inhibiting cholinesterase at the synapse (Pereira and Goncalves, 2007). These enzymes play a role in acetylcholine (ACh) hydrolysis, the primary neurotransmitter in the peripheral and central nervous systems. The inhibition also interfered with the enzyme's ability to bind substrates by typically accumulating ACh at the nerve endings. It leads to overstimulation and the desensitization of muscarinic and nicotinic ACh receptors. Inhibition of the AChE also occurred after phosphorylation of the hydroxyl group on serine, which was observed at the enzyme's active site. In addition, cholinergic stimulation causes hyperactivity of excited tissues, fasciculations, seizures, muscle paralysis, coma, and death (Hertika and Baghaz, 2019).

D. magna at 24 h old and 48 h old were used in this research because both ages have high sensitivity to pollutants. Therefore, the organism was suitable for toxicity tests and comet assay analysis (Pellegri et al., 2014). Generally, the toxicity results on 24 h old *D. magna* produced a higher mortality percentage than the other age group. According to Pellegri et al. (2014), the 24 h old organism had more carapace fragility because it is newly hatched and possessing higher sensitivity. Therefore, the toxicants penetrated the body and carapace more easily. However, the finding is contrary to that of the present study, which found that the 48 h old *D. magna* had a higher mortality rate than the other age group. The result is consistent with that of Traudt et al. (2017), indicating that newly hatched neonates had more robust physiological defense mechanisms than older organisms, with the abilities decreasing along with their ages. Furthermore, the 24 h old *D. magna* still had leftover food reserves for body nutrition, which protected against some metals. Therefore, it indicated lower sensitivity given that 48 h old organisms no longer had yolks in their body structure (Traudt et al., 2017).

The acute toxicity test showed that the LC50-24 h for *D. magna* aged 24 h was higher than that for 48 h (Table 1). For genotoxicity analysis, the determination of individual pesticide concentrations referred to the LC50 values at, above, and below the LC50 concentrations. Thus, the individual pesticide concentration for *D. magna* aged 24 h was higher than that of 48 h. If the two age groups had the same concentration, then the organism's death is more likely to be immediate in the 48 h age group.

3.2 Genotoxicity

3.2.1 Qualitative analysis

The exposure of mancozeb, methomyl, and mancozeb:methomyl combination to the age groups at varying concentrations induced DNA damage by forming comet structures (Figures 2 and 3) (Alwaini, 2021; Ariyanti, 2021; Izdihar, 2021). The damage generally began to occur at the lowest pesticide concentration. The comet's tail increased in size with increasing concentration. Comets with a small nucleoid head and a large and long tail indicated high amounts of damaged cells and also apoptosis (Lorenzo et al., 2013). Therefore, the smaller size of the comet head indicates higher level of DNA damage.

Darlina et al. (2018) stated that the mancozeb, methomyl, and combined exposures directly caused changes in DNA structure through the indirect breakdown of strands, thereby enabling the cleavage of water molecules to produce reactive oxygen species (ROS). The presence of ROS species oxidatively damaged the DNA molecules. Therefore, the damage to the strand created a comet-like structure.

3.2.2 TI%

The TI%, which indicates the percentage of DNA in the tail, increased significantly in all individual and combined concentrations of pesticides and age groups compared with the control ($p<0.05$) (Figure 4) (Alwaini, 2021; Ariyanti, 2021; Izdihar, 2021). The increase in TI% started from the lowest level of pesticides, indicating that the lowest concentration could induce DNA damage. The greater TI value (%) indicates higher DNA fragmentation occurrence. This condition indicates that the damage was more massive in the cell. The highest values of TI%, ranging from 12.5%-13.6%, was observed at concentrations of 0.08 mg/L methomyl (*D. magna* 24 h old), 0.034 mg/L methomyl (*D. magna* 48 h old), and 0.106:0.106 mg/L mancozeb:methomyl (*D. magna* 24 h old). The regression analysis on the age group of *D. magna* 24 h and 48 h indicated the concentration-dependent effects of mancozeb (r^2=0.96 and 0.94), methomyl (r^2=0.97 and 0.99), and mancozeb: methomyl (r^2=0.93 and 0.99) on TI%. In the control, the TI value was below 10%. This level of damage is generally considered minimum (Mitchelmore et al., 1998).

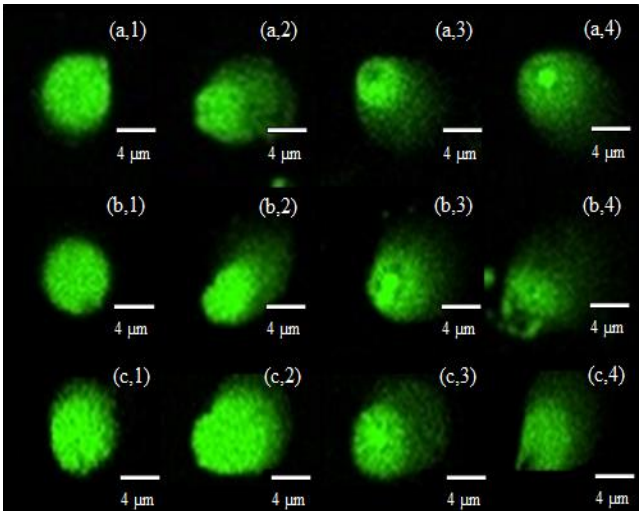

Figure 2. Comet of cell *D. magna* 24 h exposed to (a) methomyl (a,1) 0 mg/L, (a,2) 0.04 mg/L, (a,3) 0.06 mg/L, and (a,4) 0.08 mg/L; (b) mancozeb (b,1) 0 mg/L, (b,2) 0.3 mg/L, (b.,3) 0.5 mg/L, and (b,4) 0.7 mg/L; (c) mancozeb:methomyl combination (c,1) 0 mg/L, (c,2) 0.066:0.066 mg/L, (c,3) 0.086:0.086 mg/L, and (c,4) 0.106:0.106 mg/L for 24 h (5×10 magnification).

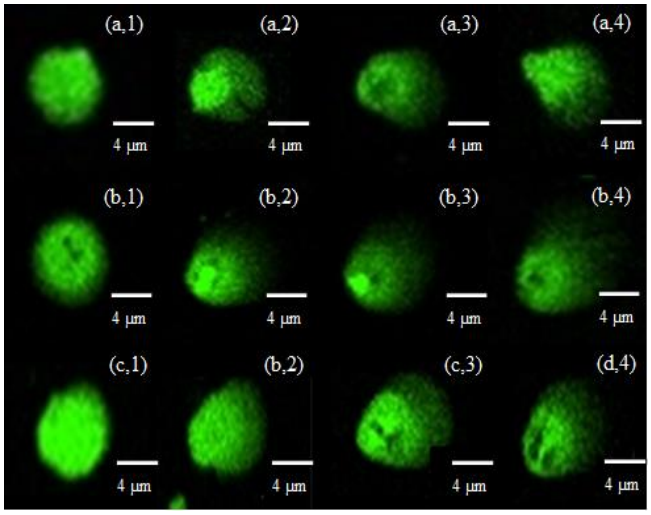

Figure 3. Comet of cell *D. magna* aged 48 h with exposure of (a) methomyl (a,1) 0 mg/L, (a,2) 0.014 mg/L, (a,3) 0.024 mg/L, and a,4) 0.034 mg/L; (b) mancozeb (b,1) 0 mg/L, (b,2) 0.08 mg/L, (b,3) 0.1 mg/L, and (b,4) 0.12 mg/L; (c) combination of mancozeb: methomyl (c,1) 0 mg/L, (c,2) 0.018:0.018 mg/L, (c,3) 0.028:0.028 mg/L, and (c,4) 0.038:0.038 mg/L for 24 h (5×10 magnification).

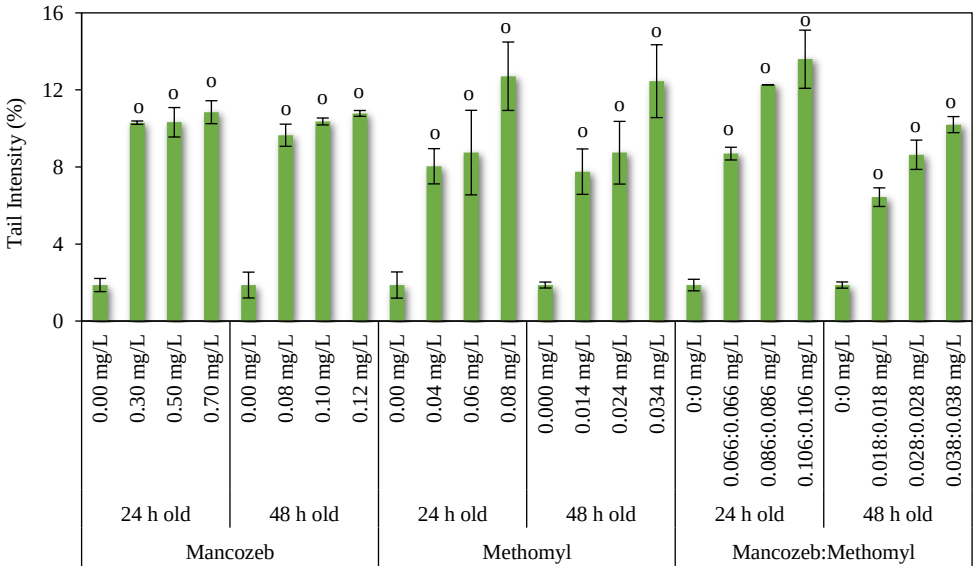

Figure 4. TI% of 24 h old and 48 h old *D. magna* upon exposure to mancozeb, methomyl, and mancozeb:methomyl combination. Significant differences in comparison to control within each age group of pesticide exposure were indicated by letter "o".

Exposure of *D. magna* to the individual pesticide showed that methomyl was more toxic to DNA than mancozeb because the concentration of methomyl was much lower than that of mancozeb but produced a similar level of TI%. A similar result was also observed in the combined pesticide exposure, confirming that the combined exposure had an antagonistic effect. Surprisingly, in 48 h old *D. magna*, the combined exposure produced the lowest impact, mainly compared with the individual pesticide (Alwaini, 2021; Ariyanti, 2021; Izdihar, 2021). Silva et al. (2019) suggested that the exposure of *D. magna* to the combination of triclosan and carbendazim also resulted in an antagonistic effect. In the *Daphnia* age group, the individual and combined pesticide concentrations administered on the 48 h old *D. magna* were two to three times lower than those of the 24 h old group. Nevertheless, the TI% of the two age groups had similar values. This finding may indicate that the 24 h old group exposed to higher

concentrations used leftover food reserves as protection from the toxicity of the pesticides (Traudt et al., 2017). However, no significant difference ($p>0.05$) was observed between the TI% of both age groups. Pellegri et al. (2014) also stated that using *D. magna* with different ages resulted in a TI% value similar to the comet assay. Knapik and Ramsdorf (2020) reported that exposure of *D. magna* to malathion at 0.23 and 0.47 µg/L for 48 h increased the intensity of fragmented DNA materials. According to Li et al. (2022) and Srivastava and Singh (2020), this genotoxic effect is caused by an increase in ROS upon exposure to pesticides, causing cell membrane damage.

3.2.3 TM

The TM values for *D. magna* 24 h old tended to be higher than the other age group (Figure 5) (Alwaini, 2021; Ariyanti, 2021; Izdihar, 2021). However, there was no significant difference ($p>0.05$) between the values of both age groups. Nebeker et al. (1986) also observed the effect of Zn on the damage of *D. magna*, as the results showed no significant difference in the genetic destruction of young and old organisms. Furthermore, the *D. magna* between the ages of 1 to 7 d had a level of DNA damage that was not significantly different; however, older organisms had lower sensitivity. Therefore, the level of DNA damage was down.

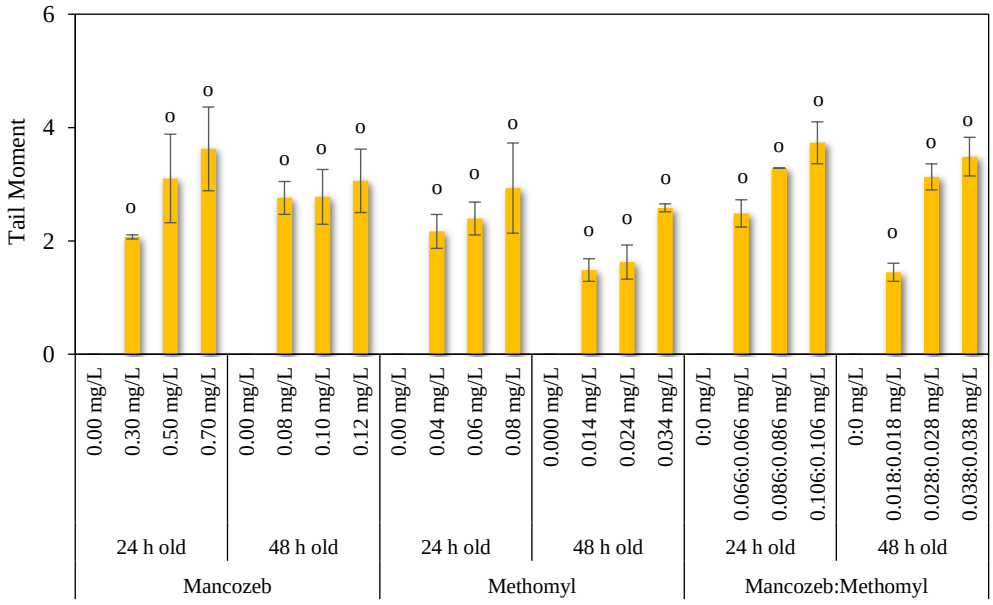

Figure 5. TM of 24 h old and 48 h old *D. magna* upon exposure to mancozeb, methomyl, and mancozeb:methomyl combination. Significant differences in comparison to control within each age group of pesticide exposure were indicated by letter "o".

The TM values also increased with higher exposure concentration. Significant differences between 0 ppm and the lowest pesticide concentration were observed in all pesticide concentrations ($p<0.05$) (Figure 5). The regression analysis represented the strong relationship between TM and pesticide concentrations. In the age groups of 24 h and 48 h, the r^2 values for mancozeb were 0.97 and 0.95, respectively; the r^2 values were 0.97 and 0.98 for methomyl, and 0.99 and 0.95 for mancozeb:methomyl combination. A concentration of 0 ppm produced a TM value below 1. This value indicated low DNA damage with a short migration distance of genetic material. For individual pesticides, exposure to methomyl generated slightly lower TM values than mancozeb and combined pesticides; it also confirmed the highest toxicity of methomyl. Combined pesticides also produced similar results to individual exposure, ensuring that combined exposure had an antagonistic effect. Prasath et al. (2016) suggested that the TM values of *Daphnia carinata* increase significantly upon exposure to 2, 4-dinitroanisole, its metabolites (2-amino 4- nitroanisole and 2,4-dinitroanisole), and 2, 4, 6-trinitro toluene for 48 h. The production of ROS due to oxidative stress is attributed to genotoxicity.

According to Shaposhnikov et al. (2008), the formation of TM was caused by areas on the double strands which experienced relaxation. This area contained double- and single-strand breaks, which migrated toward the positive pole to form a tail during electrophoresis. The migration distance of this DNA genetic material developed a TM, indicating

considerable DNA damage. At the same time, the finding suggests that the further migration distance of genetic material indicates a higher TM value.

3.2.4 TF

The TF is a parameter in the comet assay that is based on the DNA tail percentage value. Furthermore, the tail DNA indicated the percentage of DNA in the comet of a cell. This relative percentage showed the frequency of DNA breaks after the comet assay (Azqueta and Collins, 2013).

For all exposures, a concentration of 0 mg/L (24 h old and 48 h old *D. magna*) showed only a few cells that fall into category A, whereas some cells were lightly destroyed in B (Figure 6) ($p<0.05$) (Alwaini, 2021; Ariyanti, 2021; Izdihar, 2021). Based on the research of Phromchaloem et al. (2018), the value of tail DNA (%) for the control exposure of Cd toxicant against *Moina macrocopa* for 48 h belonged to categories A and B. Nunes et al. (2018) reported that upon exposure of *D. magna* to ciprofloxacin at a concentration of 0.078 mg/L, the number of damaged cells increases from category A to D. In this study, most cells belonged to category D at all concentrations, indicating the presence of DNA in the tail by 40%-95%. The percentage of cells in category D exposed to the highest concentration of pesticides was higher than those in lower concentrations ($p<0.05$). It also revealed that pesticides at lower concentrations could induce DNA damage. Category E was not observed in the cell comets at all concentrations, indicating that no cells were severely fragmented. According to Focke et al. (2010), categories A to D indicated the stress of DNA replication, whereas category E showed the apoptotic process. Thus, in this study, *D. magna* cells experienced genetic replication stress, which caused the accumulation of DNA in the tail with no apoptotic processes.

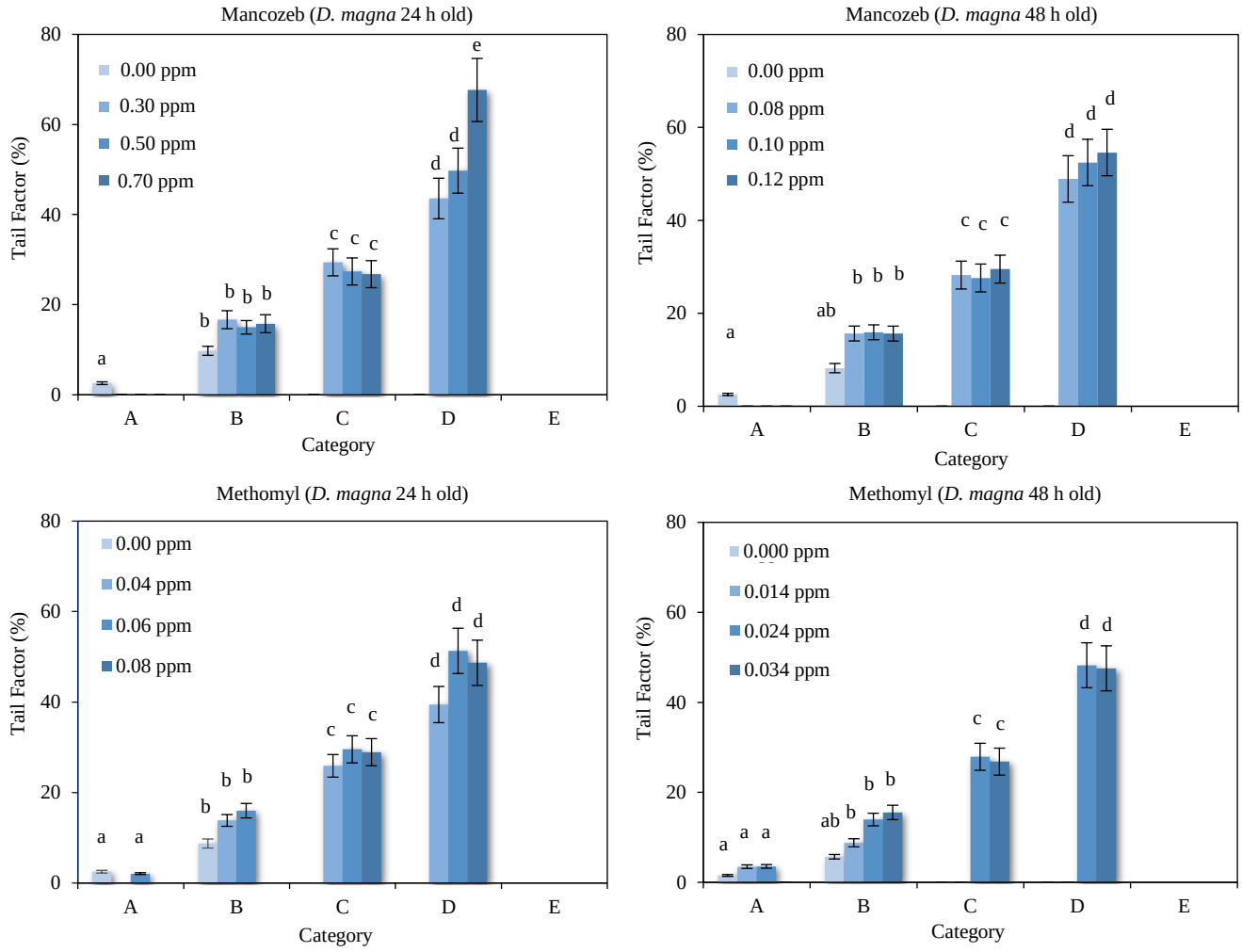

Figure 6. Percentage of *D. magna*'s cells (24 h and 48 h) in comet categories A-E upon exposure to mancozeb, methomyl, and mancozeb:methomyl. Similar letters indicate that the differences of TF were not significant.

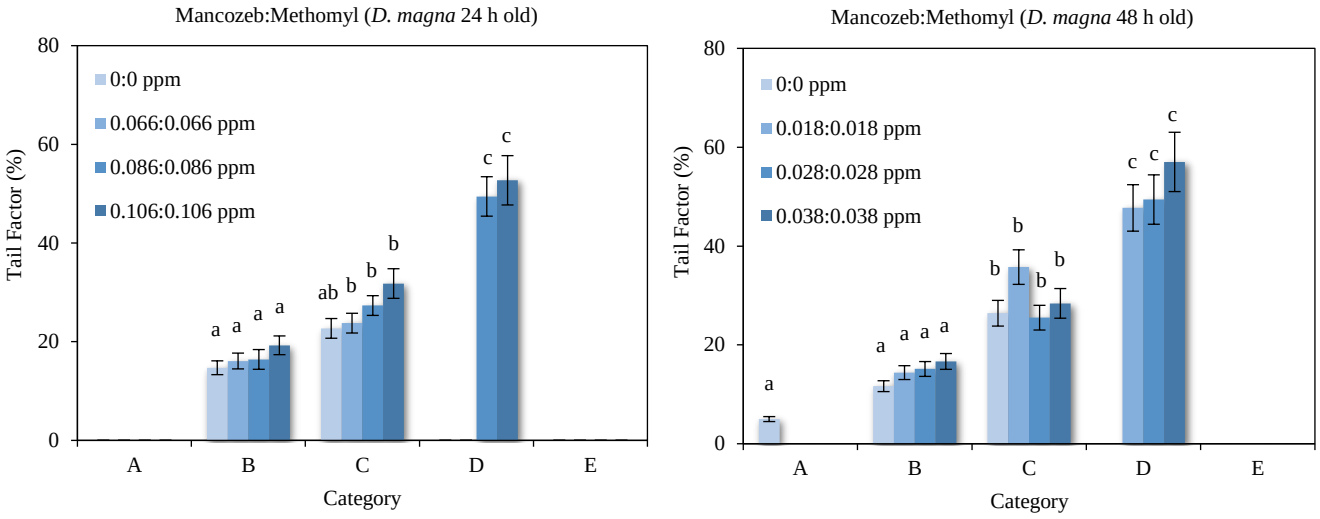

Figure 6. Percentage of *D. magna*'s cells (24 h and 48 h) in comet categories A-E upon exposure to mancozeb, methomyl, and mancozeb:methomyl. Similar letters indicate that the differences of TF were not significant (cont.).

The TF values increased with higher exposure concentration (Figure 7). In all treatments, the TF values were generally significantly different from the control. The highest TF value with the highest concentration was observed in *D. magna* upon pesticide exposure. The TI% and TM values were relatively the same between individual and combined exposures. However, the TF value indicating the level of DNA fragmentation showed that the combined exposure resulted in a slightly higher level of DNA fragmentation, followed by methomyl and mancozeb treatments. Furthermore, the TF of the 24 h old *D. magna* was more severe than that of the 48 h old *D. magna*, but the differences were insignificant ($p>0.05$).

The result of this present study indicates that, in response to the exposure to individual and combined pesticides, the values of each parameter of DNA damage, i.e., TI%, TM, and TF, showed a function of pesticide concentrations. Although the interaction of pesticides in combined exposure led to an antagonistic effect, DNA damage was massive linearly given the increasing combined concentration of pesticides. Furthermore, the three parameters can be used as sensitive biomarkers for pesticide pollution.

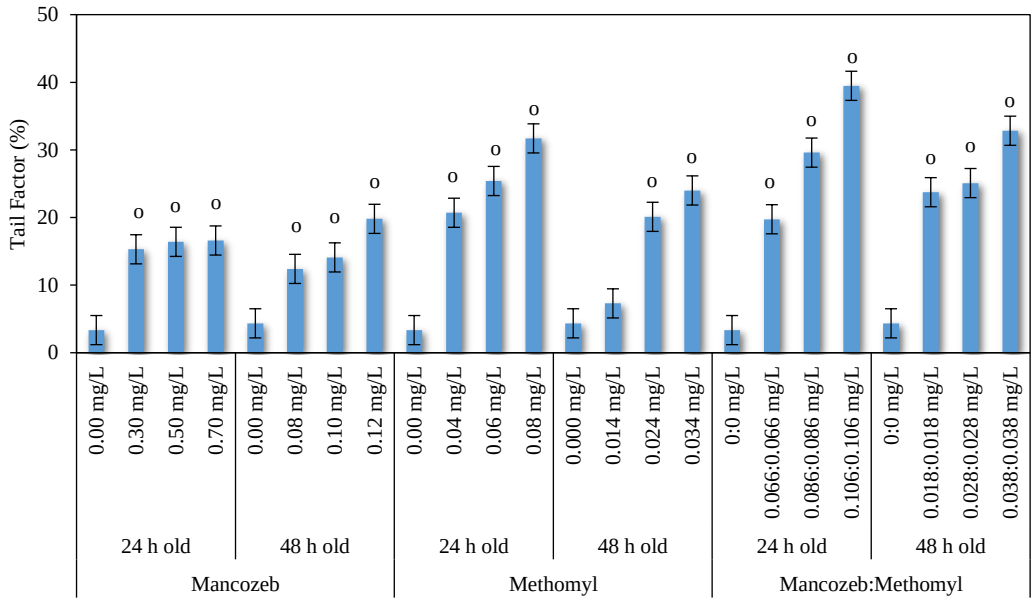

Figure 7. TF of *D. magna*'s cells (24 and 48 h old) in comet assay upon exposure to mancozeb, methomyl, and mancozeb:methomyl. Significant differences in comparison to control within each age group of pesticide exposure were indicated by letter "o".

4. CONCLUSIONS

The toxicity levels of mancozeb, methomyl, and mancozeb:methomyl combination were categorized as extremely toxic. The combination index of mancozeb:methomyl for both *D. magna* ages (24 h and 48 h) indicated that the two pesticides were antagonistically interacted (CI>1). Exposure of *D. magna* to the pesticides individually and in combination induced DNA damage. Based on TI%, TM, and TF values, the level of damage was almost the same between the individual and combined pesticide concentrations; the level of DNA damage increased with higher pesticide concentration. However, the DNA damage of 24 h old and 48 h old *D. magna* did not significantly differ. Increased DNA damage in *D. magna* indicated that this parameter was sensitive to the presence of pesticides. This study greatly contributes to the current issue of environmental pollution and environmental risk assessment in freshwater ecosystems via pesticide danger. In application, DNA damage can be used as a biomarker for biomonitoring pesticide pollution in the aquatic ecosystem. However, further field research is required to study the genotoxicity of multiple pesticides to *D. magna* in the agricultural area using the comet assay.

ACKNOWLEDGEMENTS

We thank all the people who worked alongside us on this study. We are grateful for your help. Thank you for your support, hard work, and dedication.

REFERENCES

Aktar MW, Sengupta D, Chowdhury A. Impact of pesticides use in agriculture: Their benefits and hazards. Interdisciplinary Toxicology 2009;2(1):1-12.

Alwaini F. Genotoxic Effects of Mancozeb on DNA Damage of *Daphnia magna* (Straus, 1820; Cladocera, Daphniidae) [dissertation]. Indonesia, Universitas Gadjah Mada; 2021 (in Indonesian)

Antunes SC, Almeida RA, Carvalho T, Lage OM. Feasibility of planctomycetes as a nutritional or supplementary food source for *Daphnia* spp. International Journal of Limnology 2016; 52:317-25.

Araujo GS, Pinheiro C, Pestana JLT, Soares AMVM, Abessa DMS, Loureiro S. Toxicity of lead and mancozeb differs in two monophyletic *Daphnia* species. Ecotoxicology and Environmental Safety 2019;178:230-8.

Ariyanti DP. Genotoxic Effects of Methomyl on DNA Damage of *Daphnia magna* (Straus, 1820; Cladocera, Daphniidae) [dissertation]. Indonesia, Universitas Gadjah Mada; 2021 (in Indonesian).

Asita OA, Makhalemele R. Genotoxic effects of dithane, malathion, and garden ripcord on onion root tip cells. African Journal of Food Agriculture Nutrition and Development 2009;9(4):1191-209.

Azqueta A, Collins AR. The essential comet assay: A comprehensive guide to measuring DNA damage and repair. Archives of Toxicology 2013;87(6):949-68.

Castro M, Sobek A, Yuan B, Breitholtz M. Bioaccumulation potential of CPs in aquatic organisms: Uptake and depuration in *Daphnia magna*. Environmental Science and Technology 2019;53(16):9533-41.

Christin F, Elystia S, Yenie E. Acute toxicity test of tofu liquid waste against *Daphnia magna* with the renewal test method. Jurnal Teknik 2015;2(2):1-9 (in Indonesian).

European Commission (EC). Technical Guidance Document in Support of Commission Directive 93/67/EEC on Risk Assessment for New Notified Substances, Commission Regulation (EC) No. 1488/94 on Risk Assessment for Existing Substances and Directive 98/8/EC of the European Parliament and of the Council Concerning the Placing of Biocidal Products on the Market. Ispra, Italy: European Commission Joint Research Centre; 2003.

Darlina, Rahardjo T, Syaifudin M. Evaluation of the relationship of radiation dose to DNA damage of lymphocyte cells by using the comet test. Jurnal Sains dan Teknologi Nuklir Indonesia 2018;19(1):13-20 (in Indonesia).

Focke F, Schuermann D, Kuster N, Schar P. DNA fragmentation in human fibroblast under extremely low electromagnetic field exposure. Mutation Research 2010;683:74-83.

Hart RW, Hall KY, Daniel FB. DNA repair and mutagenesis in mammalian cells. Photochemistry and Photobiology 1978; 28:131-55.

Hertika AMS, Baghaz R. Ecotoxicology for Aquatic Environments. Malang, Indonesia: UB Press; 2019 (in Indonesian).

Izdihar RNT. Genotoxic Effects of Methomyl and Mancozeb on DNA Damage of *Daphnia magna* (Straus, 1820; Cladocera, Daphniidae) [dissertation]. Indonesia, Universitas Gadjah Mada; 2021 (in Indonesian).

Jha AN. Ecotoxicological applications and significance of the comet assay. Mutagenesis 2008;23:207-21.

Kaur K, Kaur R. Occupational pesticide exposure, impaired DNA repair, and disease. Indian Journal of Occupational and Environmental Medicine 2018;22(2):74-81.

Klüttgen B, Dülmer U, Engels M, Ratte HT. ADaM, an artificial freshwater for the culture of zooplankton. Water Research 1994;28:743-6.

Knapik LFO, Ramsdorf W. Ecotoxicity of malathion pesticide and its genotoxic effects over the biomarker comet assay in *Daphnia magna*. Environmental Monitoring and Assessment 2020;192(264):1-9.

Kretschmann A, Ashauer R, Preuss TG, Spaak P, Escher BI, Hollender J. Toxicokinetic model describing bioconcentration and biotransformation of diazinon in *Daphnia magna*. Environmental Science and Technology 2011;45:4995-5002.

Liang CA, Chang SS, Chen HY, Tsai KF, Lee WC, Wang IK, et al. Human poisoning with methomyl and cypermethrin pesticide mixture. Toxics 2023;11(372):1-10.

Li X, Naseem S, Hussain R, Ghaffar A, Li K, Khan A. Evaluation of DNA damage, biomarkers of oxidative stress, and status of antioxidant enzymes in freshwater fish (*Labeo rohita*) exposed to pyriproxyfen. Oxidative Medicine and Cellular Longevity 2022;2022:Article No. 5859266.

Liyan Z, Ying H, Guangxing L. Using DNA damage to monitor water environment. Chinese Journal of Oceanology and Limnology 2005;23:340-8.

Lorenzo Y, Costa S, Collins AR, Azqueta A. The comet assay, DNA damage, DNA repair, and cytotoxicity: Hedgehogs are not always dead. Mutagenesis 2013;28(4):427-32.

Lushchak VI, Matviishyn TM, Husak VV, Storey JM, Storey KB. Pesticide toxicity: Mechanistic approach. EXCLI Journal 2018;17:1101-36.

Mahmood I, Imadi SR, Shazadi K, Gul KA. Effects of pesticides on environment. In: Hakeem K, Akhtar M, Abdullah S, editors. Plant, Soil and Microbes. Switzerland: Springer, Cham; 2015. p. 260.

Markovsky E, Baabur-Cohen H, Satchi-Fainaro R. Anticancer polymeric nanomedicine bearing synergistic drug combination is superior to a mixture of individually-conjugated drugs. Journal of Controlled Release 2014;187:145-57.

Mayer FR, Ellersieck MR. Manual of Acute Toxicity: Interpretation and Data Base for 410 Chemicals and 66 Species of Freshwater Animals. Columbia, USA: U.S. Department of the Interior, Fish and Wildlife Service; 1986.

Menconi M, Beckman J. Hazard Assessment of the Insecticide Methomyl to Aquatic Organism in the San Joaquin River System. California, USA: State of California the Resources Agency Department of Fish and Game; 1996.

Mitchelmore CL, Birmelin C, Livingstone DR, Chipman JK. Detection of DNA strand breaks in isolated mussel (*Mytilus edulis* L.) digestive gland cells using the "comet" assay. Ecotoxicology and Environmental Safety 1998;41(1):51-8.

Nebeker AV, Ciarns MA, Onjukka ST, Titus RH. Effect of age on sensitivity of *D. magna* to cadmium, copper and cyanazine. Environmental Toxicology and Chemistry 1986;55:527-30.

Nunes B, Leal C, Rodrigues S, Antunes SC. Assessment of ecotoxicological effects of ciprofloxacin in *Daphnia magna*: Life-history traits, biochemical and genotoxic effects. Water Science and Technology 2018;2017(3):835-44.

Pellacani C, Buschin A, Furlini M, Poli P, Rossi C. A battery of in vivo and in vitro tests useful for genotoxic pollutant detection in surface waters. Aquatic Toxicology 2006;77:1-10.

Pellegri V, Gorbi G, Buschini A. Comet assay on *D. magna* in eco-genotoxicity testing. Aquatic Toxicology 2014;155:261-8.

Pellegri V, Gorbi G, Buschini A. DNA damage detection by comet assay on *Daphnia magna*: Application in freshwater bio-monitoring. Science of the Total Environment 2020;705:1-11.

Pereira JL, Goncalves D. Effects of food availability on the acute and chronic toxicity of the insecticide methomyl on *Daphnia* spp. Science of the Total Environment 2007;386(1-3):9-20.

Phromchaloem C, Nakphlaiphan A, Piriyamasakul S, Pruksarojanakul W, Pewnim T. Single cell gel electrophoresis of microcrustaceans *Moina macrocopa* exposed to cadmium. Veridian E-Journal Science and Technology Silpakorn University 2018;5(1):36-45.

Prasath A, Panneerselvan L, Provatas A, Naidu R, Megharaj M. Genotoxicity assessment of acute exposure of 2, 4-dinitroanisole, its metabolites and 2, 4, 6-trinitrotoluene to *Daphnia carinata*. Ecotoxicology 2016;25:1873-9.

Rajini A, Revathy K, Chitrikha T. Toxicity and reproductive effect of combination pesticide to *Daphnia magna*. Indian Journal of Science and Technology 2016;9(3):1-5.

Ren Q, Zhao R, Wang C, Li S, Zhang T, Ren Z, et al. The role of AChE in swimming behavior of *Daphnia magna*: Correlation analysis of both parameters affected by deltamethrin and methomyl exposure. Journal of Toxicology 2017;2017: Article No. 3265727.

Shaposhnikov SA, Salenko VB, Brunborg G, Nygren J, Collins AR. Single-cell gel electrophoresis (the comet assay): Loops or fragments. Electrophoresis 2008;29:3005-12.

Silva ARR, Cardoso DN, Cruz A, Mendo S, Soares AMVM. Long-term exposure of *Daphnia magna* to carbendazim: How it affects toxicity to another chemical or mixture. Environmental Science and Pollution Research 2019;26: 16289-302.

Srivastava A, Singh D. Assessment of malathion toxicity on cytophysiological activity, DNA damage and antioxidant enzymes in root of *Allium cepa* model. Scientific Reports 2020;10:Article No. 886.

Surtikanti HK, Juansah R, Frisda D. Optimization of *Daphnia* cultures as test animals in ecotoxicology. Jurnal Biodjati 2017:2(2):83-8.

Seleem AA. Teratogenicity and neurotoxicity effects induced by methomyl insecticide on the developmental stage of *Bufo arabicus.* Neurotoxicology and Teratology 2019;72:1-9.

Traudt EM, Ranville JF, Meyer JS. Effect of age on acute toxicity of cadmium, copper, nickel, and zinc in individual-metal exposure to *Daphnia magna* neonates. Environmental Toxicology Chemistry 2017;36(1):113-9.

United States Environmental Protection Agency (USEPA). Registration Eligibility Decision for Mancozeb. Washington, USA: USEPA; 2005.

Vasiljević T, Grujić S, Radišić M, Dujaković N, Laušević M. Pesticide residues in surface water and groundwater. In: Rathore HS, Nollet LML, editors. Pesticides: Evaluation of Environmental Pollution. Boca Raton, USA: CRC Press; 2012. p. 259-98.

Yahia D, El-Amir YO, Rushdi M. Mancozeb fungicide-induced genotoxic effects, metabolic alterations, and histological changes in the colon and liver of Sprague Dawley rats. Toxicology and Industrial Health 2019;35(4):265-76.

Effect of Oxide Presence in Activated Carbon on Arsenic Removal

Thearak Vong[1], Korea Phat[1], Seunghee Lee[1], Shinhoo Kang[1,2], and Jinhwan Oh[3,*]

[1]Department of Physics, Royal University of Phnom Penh, Phnom Penh, Cambodia
[2]Department of Materials Science and Engineering, Seoul National University, Seoul, Korea
[3]Graduate School of International Studies, Ewha Woman's University, Seoul, Korea

ARTICLE INFO

Received: 15 Mar 2023
Received in revised: 29 May 2023
Accepted: 6 Jun 2023
Published online: 4 Aug 2023
DOI: 10.32526/ennrj/21/20230066

Keywords:
Arsenic removal/ Adsorbent/ Activated carbon/ Nano oxide particles/ SDDC/ Spectrophotometry/ Cambodia

*** Corresponding author:**
E-mail: joh@ewha.ac.kr

ABSTRACT

This study investigated the effect of oxides on the removal of As when present in simple mixtures with granular activated carbon (GAC) particles. The performance of these mixtures was compared with other reported GAC-based adsorbents. A standard curve for ultraviolet adsorption vs. As concentration was obtained using the silver diethyldithiocarbamate (SDDC) method to evaluate various samples. A preliminary study was carried out to find the optimal conditions for experiments. For 50 mL samples with 2.35 ppm As, the optimal values of pH, adsorption time, and amount of adsorbent were pH 7, 30 min, and 50 mg, respectively. The ratio between the amount of adsorbent and well water in this study showed a superior As adsorption capacity (1 g/L, 2.1 mg/g) compared to similar adsorbents reported previously (12.5 g/L, 1.0-1.4 mg/g). Among the adsorbents, KOH-treated AC-Mn_3O_4 exhibited the best performance in As removal with an efficiency of ~95%. The oxide particles had a synergistic effect with GAC on As removal. This was primarily due to the change in the potential of partially agglomerated nano Mn_3O_4 particles on the ACK surface. The influence of the surface area of the adsorbents was not pronounced. All results were explained in terms of microstructure, specific surface area, and zeta potential. This finding could be extended to other activated carbons (AC) obtained from different sources.

1. INTRODUCTION

Groundwater needs to be completely protected from pollution and purified for use as a drinking water source (Gil and Vicente, 2019). Significant research efforts have been made to remove heavy metals, especially arsenic, and dye materials from water (Mahmoodi, 2014; Mahmoodi et al., 2017; Mousavi et al., 2020). Arsenic (As, hereafter) in drinking water is poisonous, mutagenic, and carcinogenic (WHO, 2010). In addition to acute poisoning, chronic exposure to modest doses of As over an extended period of time may seriously affect human health (López-Guzmán et al., 2019). In aquatic systems, inorganic As can be found in the 3^-, 0, 3^+, and 5^+ oxidation states. While the 3^+ and 5^+ oxidation states are frequently observed, the elemental states of 3^- and 0 are incredibly uncommon (Tallman and Shaikh, 1980). Inorganic As (III) and As (V) pose a potential threat to the environment, human health, and animal health. High doses of As can cause damage to the liver, skin, and central nervous, as well as cause various malignancies, including lung, skin, hyperkeratosis, and prostate cancer (Hudak, 2010; Mostafapour et al., 2013).

Although water usually contains very little As, it has a cumulative impact. Thus, numerous monitoring techniques have been developed for As, including the silver diethyldithiocarbamate (SDDC) spectrophotometric approach and novel silver salt spectrophotometry (Stratton and Whitehead, 1962; Liang and Lai, 2010; Vašák and Šedivec, 1953). The SDDC spectrophotometric approach is superior to other methods for measuring As. It is especially ideal for measuring the As concentration in large volumes of surface water and wastewater because of its excellent precision and accuracy, and cheap input costs (Liang and Lai, 2010).

Arsenic has been discovered in more than 70 nation, predominantly in Asia, but previous studies have tended to focus on Bangladesh and West Bengal (Ahmad et al., 2018). The problem in Southeast Asia,

Citation: Vong T, Phat K, Lee S, Kang S, Oh J. Effect of oxide presence in activated carbon on arsenic removal. Environ. Nat. Resour. J. 2023;21(4):345-357. (https://doi.org/10.32526/ennrj/21/20230066)

notably in Cambodia, where the highest As concentrations have been observed in the Mekong River Basin, has just been recently discovered (Pravalprukskul et al., 2018). The World Health Organization (WHO) states that the maximum allowable level of As is 10 µg/L (Yao et al., 2014). However, Cambodia maintains a much higher limit of 50 µg/L (WHO, 2011) than that of WHO.

Numerous studies have investigated the use of activated carbon (AC) for enhancing the water quality of polluted water. In addition to the As (Wong et al., 2018) cationic methylene blue dye (Jiang et al., 2021), and synthetic heavy metal ions (Pb^{2+}, Cu^{2+}, and Zn^{2+}), and Pb(II) have also been removed from an aqueous solution using AC as an adsorbent. Fe combined with Granular AC (GAC) has been used in As(V) solutions to increase the As removal efficiency (Kalaruban et al., 2019). Compared to GAC (1,013 µg/g), GAC-Fe has a greater Langmuir maximum adsorption capacity at pH 6 (1,430 µg/g) with 12.5 g/L of adsorbent in 2 h.

Another Fe-incorporated AC from a biomass combination has been fabricated via $FeSO_4$ impregnation (Rahman et al., 2020). The adsorption capacity was 42.92 mg/g. A study combining Fe_3O_4 particles with AC made from sugarcane bagasse via a chemical activation process was also reported (Joshi et al., 2019). The maximum As removal capacity of 6.69 mg/g was observed at pH 8, 1.8 g/L of adsorbent dosage, and 60 min of contact time.

Arsenic was also removed using a hybrid technique combining oxidation with ozone (Rusmana et al., 2019). Adsorption with the adsorbent doses of 12.5 g/L was 69% and 55% for GAC and zeolite, respectively. Furthermore, AC made from Tamarix leaves (Koohzad et al., 2019) showed an optimal pH of 7. With contact times of 40 min, starting concentrations of 10 mg/L, and adsorbent dosages of 3 g/L, the maximum removal efficiency was attained for As ions (96.18%). Many researchers have reported maximum As removal capacities of AC-based adsorbents that vary significantly (1-140 mg/g) (Kalaruban et al., 2019; Esmaeili et al., 2021; Jha and Maharjan, 2022). The value is presumed to be very much dependent on the manufacturing process for AC.

In this study we attempted to evaluate simple mixtures of oxide-GAC as adsorbents and compared them with other GAC-based adsorbents reported previously. Further, we made an effort to understand the effect of oxides, such as Fe_2O_3 and Mn_3O_4, in the presence of GAC on the As removal. Prior to this, an optimal condition in terms of pH, adsorption time, and amount of adsorbent was obtained. The performance was interpreted with microstructure and zeta potential.

2. METHODOLOGY

2.1 Materials and equipment

Commercial coconut GAC with a size of <2 mm was used as a raw material for As removal and purchased from Unitech Water Co., Ltd. (Cambodia). Various standard sample solutions were prepared for SDDC analysis, using a standard solution of 1,000 ppm As (Inorganic Ventures, USA). SDDC ($C_5H_{10}AgNS_2$) was procured from Shanghai Zhanyun Chemical Co., Ltd., China. A glass arsine generator was procured from Scilab Co., Ltd., Korea.

A Lamda 365 UV-VIS spectrophotometer (PerkinElmer, Korea) was used to measure the As removal efficiency. XRD (D8 Advance, Bruker, Germany) and FESEM (AUGIGA, Carl Zeiss, Germany) were employed to identify the phases and microstructures of the adsorbents, respectively. The surface area, pore size, and volume were measured using a BELSORP-MAX analyzer (Bel Japan Inc., Japan).

2.2 Preparation of adsorbents and standard curve

Iron oxide was synthesized via the copre-cipitation method, using $FeCl_3{\cdot}6H_2O$ and $FeCl_2{\cdot}4H_2O$ in DI water with 0.414 M NaOH solution. The resultant black precipitates obtained from the reaction were centrifuged, washed, and dried in an oven. For the synthesis of manganese oxide, manganese (II) nitrate tetrahydrate, $Mn(NO_3)_2{\cdot}4H_2O$, and ammonia (NH_4OH) were used (Chang and Shih, 2018). The precipitates obtained from the reaction were washed and dried in an oven. The dried manganese oxide powder was calcined in a tube furnace for 1 h at 350°C to enhance the crystallinity of the oxide precipitates (Dehmani and Abouarnadasse, 2020).

GAC powder with size of 0.8-2.0 mm was washed with 0.1 M H_2SO_4 and DI water. Then, the samples were dried at 100°C for 24 h in a dry oven. Then, KOH was mixed according to the AC:KOH weight ratio of 1:6 to improve the surface condition of GAC. The mixture was heated at 5°C/min to 750°C and cooled at 10°C/min. The resultant GAC was termed as ACK (1:6). The adsorbents were simply prepared by mixing the oxide powder with the granular ACK powder in DI water, in weight ratio of 10:1. Details of the experimental procedure are described in elsewhere (Chang and Shih, 2018; Thearak, 2023).

Various samples with known As concentrations were prepared from a standard solution of 1,000 ppm

As and DI water. Regression analysis was done to establish a standard curve of As concentration vs. UV absorbance. Then, the SDDC colorimetric technique was employed to analyze the samples treated with various adsorbents. The average values of 4-12 measurements are reported herein and the range of the variation in the values is presented with error bars.

3. RESULTS AND DISCUSSION

3.1 Characteristics and morphology of raw materials

Figure 1 shows the FESEM micrographs of as-received AC and oxides, α-Fe_2O_3 and Mn_3O_4. The as-received and as-screened AC had an irregular and granular shape with many internal pore channels, and the particle size of the as-screened AC was in the range of 0.8-2.0 mm. Iron oxide produced by co-precipitation had a diameter of 100-500 nm and was somewhat faceted. The particle size of manganese oxide differed greatly from that of iron oxide. It was in the range of 50-100 nm. Both oxides were agglomerated due to their small sizes.

In the XRD analysis of as-received AC, typical carbon peaks were observed with peak broadening (Figure 2). It indicates a low level of crystallinity of the phase. The iron and manganese oxides were identified as α-Fe_2O_3 and Mn_3O_4, respectively, with some unidentified peaks. The peak broadening is clearly reduced for the oxides, confirming the high level of crystallinity.

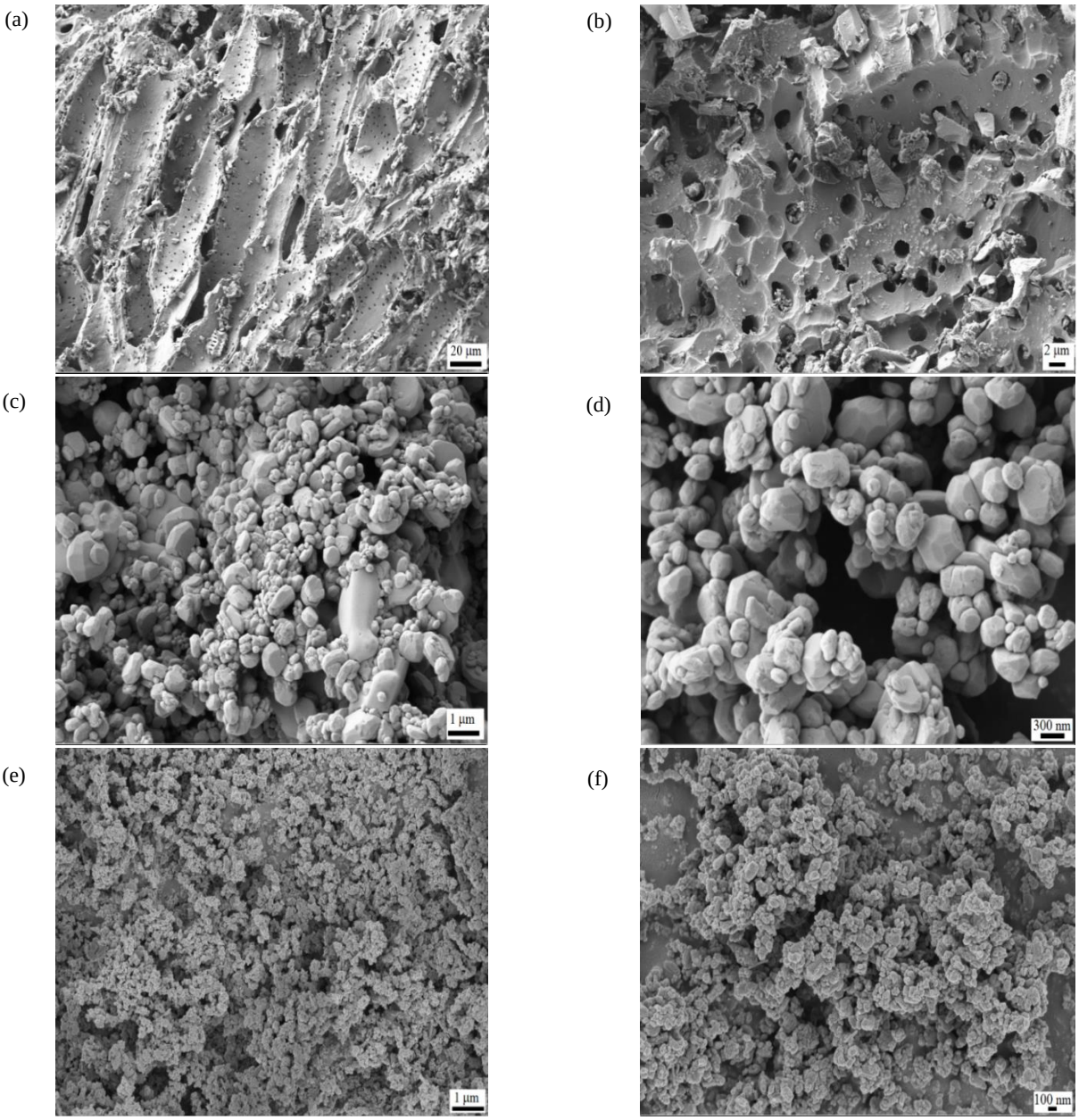

Figure 1. FE-SEM Micrographs of (a,b) As-received AC, (c,d) Fe_2O_3 and (e,f) Mn_3O_4

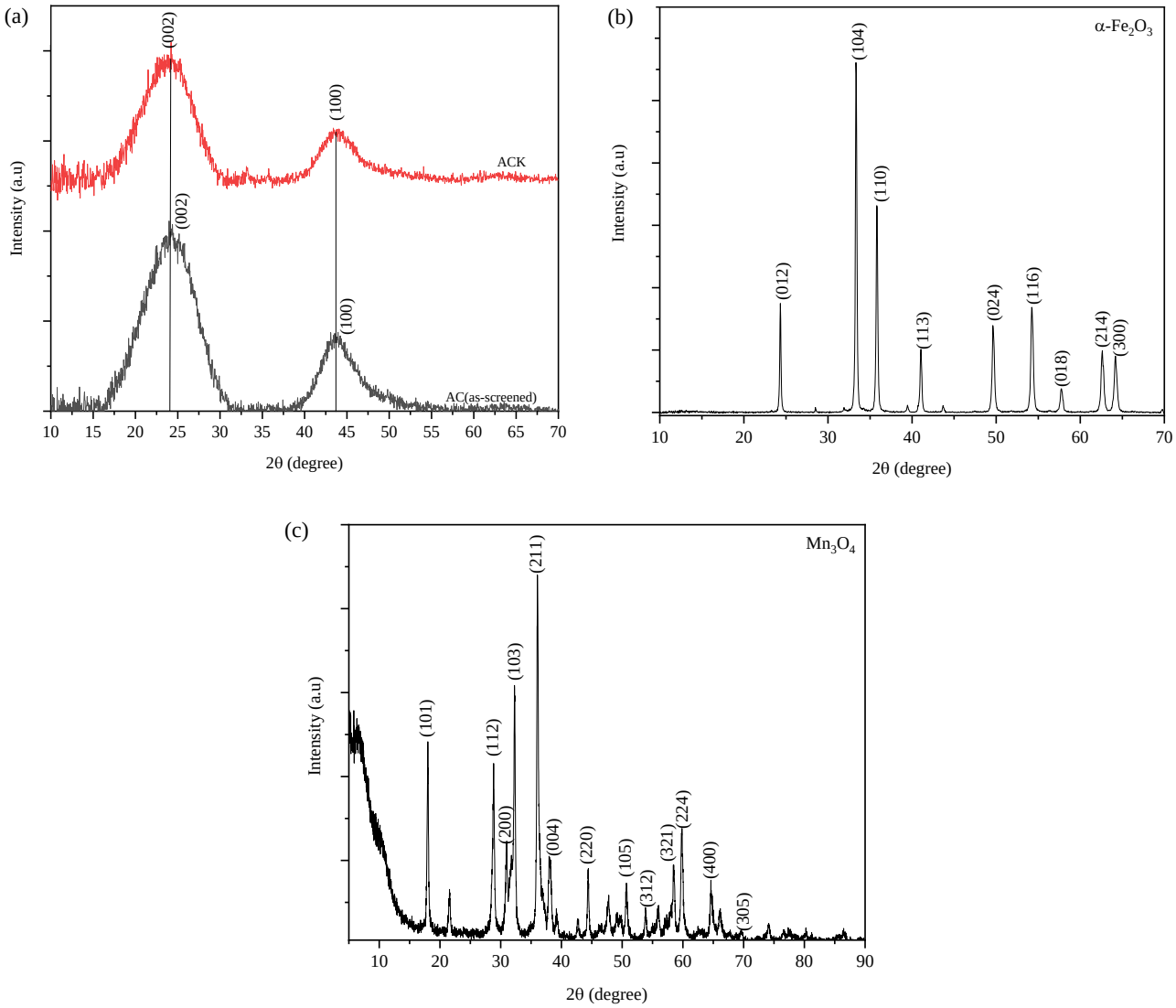

Figure 2. XRD Results from (a) AC(as-screened) and ACK, (b) α-Fe_2O_3, and (c) Mn_3O_4

Figure 3 presents the optical (a) and FESEM micrographs (b-d) of the as-screened AC and ACK (1:6). AC is commonly treated with KOH to increase the specific surface area. However, the treatment in this study did not change the surface morphology noticeably. It might be due to the large size of the employed GAC powder. But it removed most debris from the surface of the As-screened AC.

Table 1 shows the powder characteristics of the raw materials (1-4) and candidate adsorbents (5,6). The AC selected herein provides the most surface area with a high volume of nano pores. The surface area of ACK was reduced slightly compared to that of the as-screened AC. This indicates that the KOH treatment did not increase the volume of the nano pores, resulting in little increase in the surface area.

Interestingly, the BET values of both oxides were relatively small despite their nano sizes. This is attributed to the high degree of agglomeration of the powders after the co-precipitation. The powder mixture of ACK with the oxides, candidate adsorbents, showed interesting results: the BET values were considerably higher (15%~20%) than the arithmetic averages of the raw materials. Since the surface area of ACK remains constant, the increase in the area must have resulted from the oxides. That is, the oxide particles became somewhat deagglomerated during the mixing process with ACK in DI water.

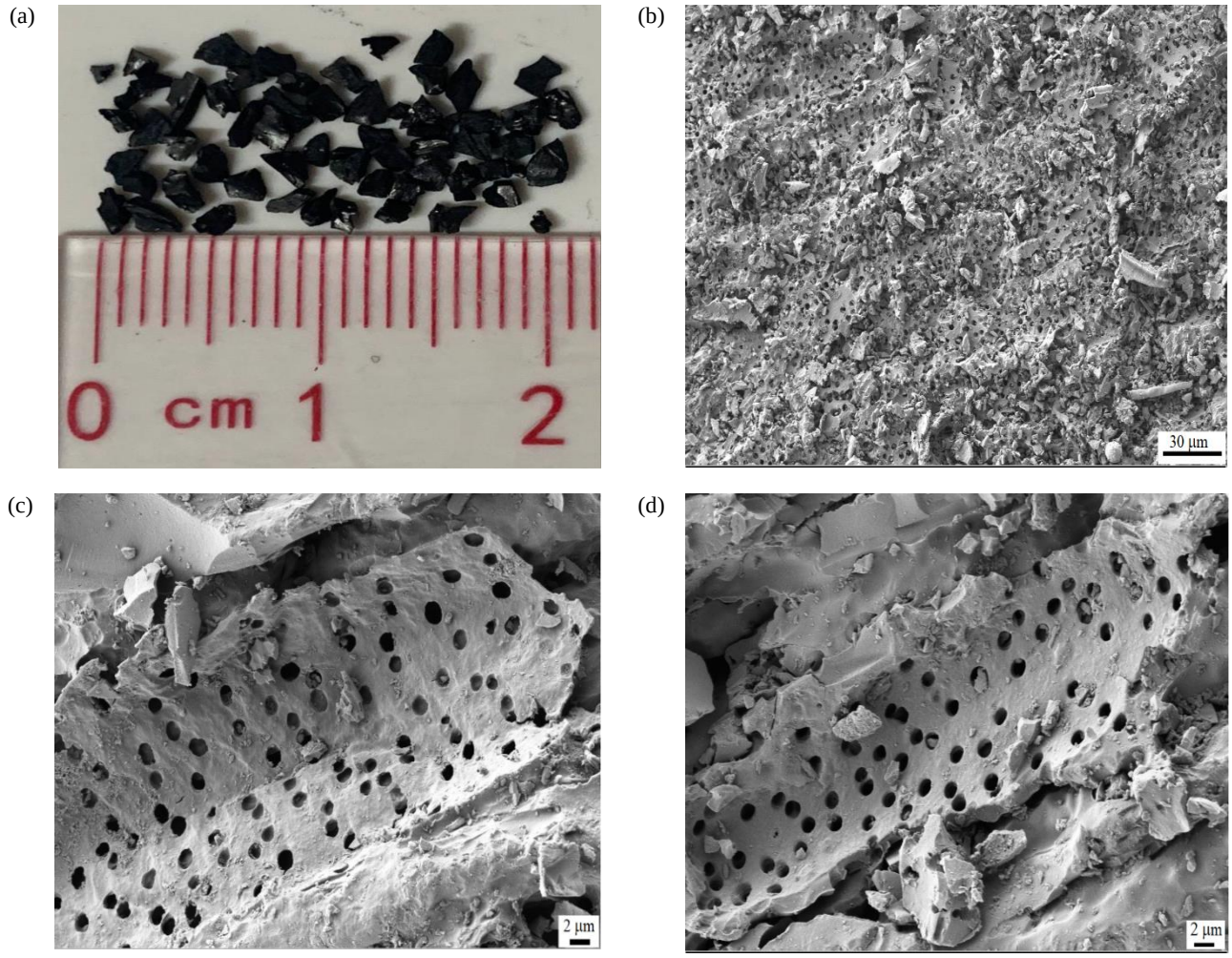

Figure 3. Microstructures of (a,b) As-screened AC and (c,d) ACK

Table 1. BET results of various AC, oxides, and their mixtures

Nº	Sample name	Surface area (m^2/g)	Total pore volume (cm^3/g)	Average pore diameter (nm)
1	AC(as-screened)	953.24	0.3855	1.6175
2	ACK (1:6)**	940.16	0.3775	1.6059
3	Fe_2O_3	2.2583	0.0011	1.9527
4	Mn_3O_4	15.463	0.1592	41.171
5	ACK-Fe_2O_3 (10:1)**	1008.10 (854.90)*	0.4086	1.6213
6	ACK-Mn_3O_4 (10:1)**	953.86 (856.10)*	0.4136	1.7342

(* Number in parentheses) Calculated BET based on the weight ratio from ** and surface area of individual sample material

3.2 Optimal conditions for As adsorption

Figure 4 is the plot of absorbance vs. As concentration obtained by SDDC method with standard samples: SDDC reacted with $AsH_{3(g)}$ that evaporated from the As-containing solution (Vašák and Šedivec, 1953). The intercept, slope of the curve, and the regression coefficient (R^2) were 0.017, 0.983, and 0.994, respectively. This demonstrates the validity of the SDDC method as it confirms the excellent linear relationship between the As concentration and As absorbance measured via spectrometry. The difference in As contents between the original solution and SDDC was calculated as the As removal amount (in %) by the adsorbent employed.

A study was conducted as a function of pH, adsorption (contact) time, and amount of adsorbent to determine the optimal and practical conditions for water purification. The sample water was obtained from a well in Kaoh Thum District, Kandal Province, Cambodia. Water was initially pumped out for five min to avoid stagnant well water. The well water of pH ~7 was immediately acidified after it was taken

from the well to pH <2 using H_2SO_4 to preserve the As concentration (Liang and Lai, 2010). The pH value of the water was adjusted later according to the experimental needs.

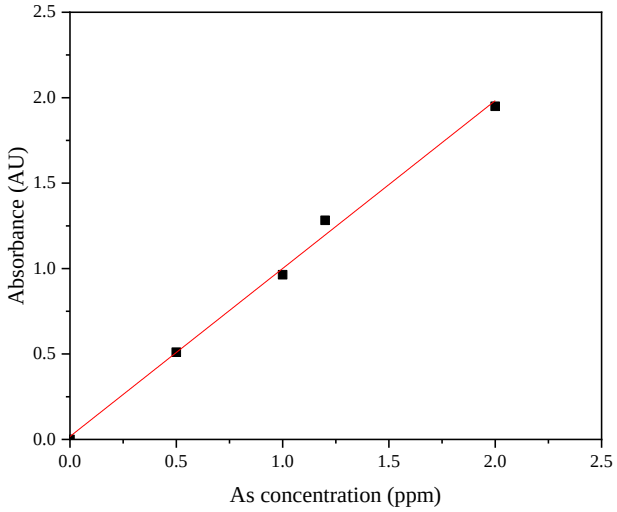

Figure 4. A plot of absorbance vs As concentration in ppm by SDDC method

Chemical analysis was done on the well water. Harmful elements such as F, B, CN, Cr, Pb, Cd, and Hg were present within the allowed limits. It was found that the As content was exceedingly high (460 µg/L) compared to the suggested WHO limit (<10 µg/L) and the Cambodian limit (<50 µg/L). For this study, the well water was condensed to a high As concentration, 2.35 ppm, by drying. Detailed results can be found in the reference (Thearak, 2023).

3.2.1 Effect of pH

The effect of pH was investigated with the candidate adsorbents. 50 mg of various adsorbents were added to 50 mL of well water, and the adsorption process was conducted for 30 min. Figure 5(a) shows the removal efficiency of the raw materials, i.e., AC, ACK (1:6), α-Fe_2O_3, and Mn_3O_4. In general, the As adsorption was not favorable in an acidic environment except for α-Fe_2O_3, as reported in previous studies (Kalaruban et al., 2019; Joshi et al., 2019).

AC (as-screened) and ACK (1:6) exhibited their best performances at pH 7, while α-Fe_2O_3 and Mn_3O_4 did at pH 5 and 9, respectively. This was expected since the ZPC of AC is normally in the pH range of 2-5 (Kalaruban et al., 2019). Further, most oxide surfaces are hydrated and result in positively and negatively charged surfaces at low and high pH values, respectively (Rahaman, 2017). ACK (1:6), which has a high surface area as presented in Table 1, exhibited ~70% As adsorption at pH 7. The performances of the two oxides were about the same.

The removal efficiency of the mixture absorbents made of the raw materials was also compared with that of ACK (Figure 5(b)). In general, a neutral water of pH 7 and/or a base water exhibited a superior performance among this limited number of samples. The highest removal of As (~95%) was observed at pH 7.0 with ACK-Mn_3O_4. Thus, pH 7.0 was chosen as the optimum condition for further experiment.

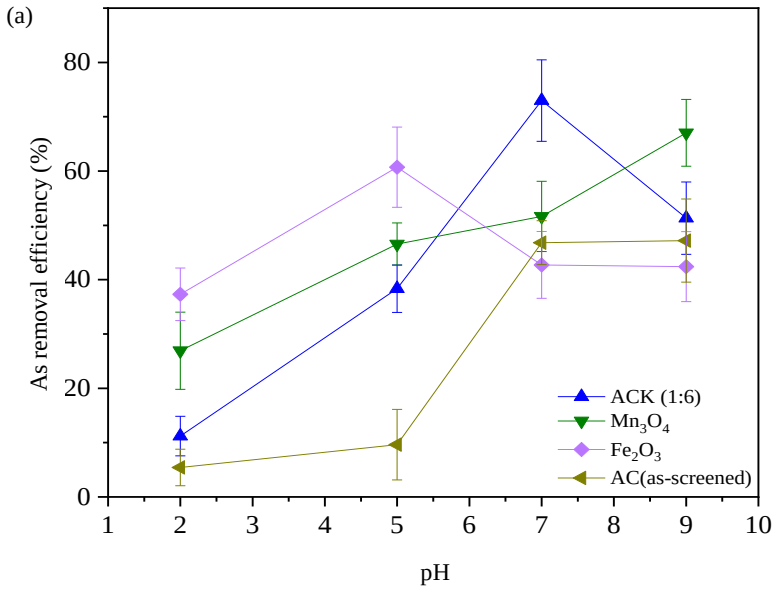

Figure 5. The effect of solution pH on Arsenic removal efficiency of (a) the raw materials and (b) the mixtures

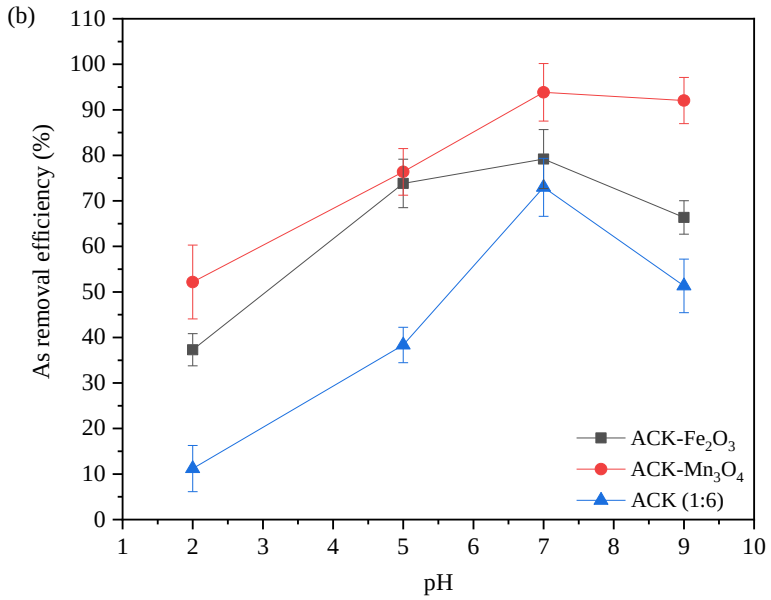

Figure 5. The effect of solution pH on Arsenic removal efficiency of (a) the raw materials and (b) the mixtures (cont.)

3.2.2 Effect of adsorption time

The removal process was conducted at pH 7 as a function of time and the amount of KOH used for AC. The maximum efficiency of 40-75% was observed within 20-60 min for various AC as shown in Figure 6(a), as was observed in previous studies (Jiang et al., 2021; Kalaruban et al., 2019; Joshi et al., 2019; Rahman et al., 2020; Rusmana et al., 2019; Koohzad et al., 2019). Considering the ratio of AC and KOH, the weight ratio of 1:6 exhibited a steady increase in the adsorption, reaching up to 70-75%. Most AC showed little improvement after 30 min. That is, the rate of removal is initially high and then stabilizes after 30 min.

A similar trend was noted from the individual oxide and candidate adsorbents (Figure 6(b)). This might be related to the intrinsic adsorption behavior that occurs on the adsorbent surface as in a Langmuir model (Tan et al., 2008). From the materials aspect, the mixtures of ACK with oxides demonstrated 75-95% efficiency in 30 min. Especially, ACK-Mn_3O_4 outperformed the others with 90-95% efficiency for the well water. Thus, a time period of 30 min was found sufficient at pH 7 for the As adsorption.

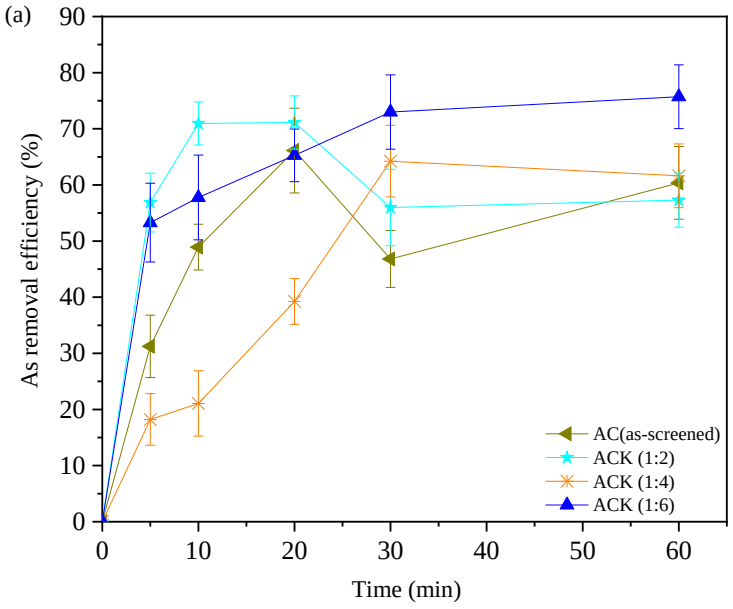

Figure 6. Arsenic removal efficiency As a function of adsorption time at pH 7 from (a) AC treated by various KOH amounts and (b) the mixtures and raw materials

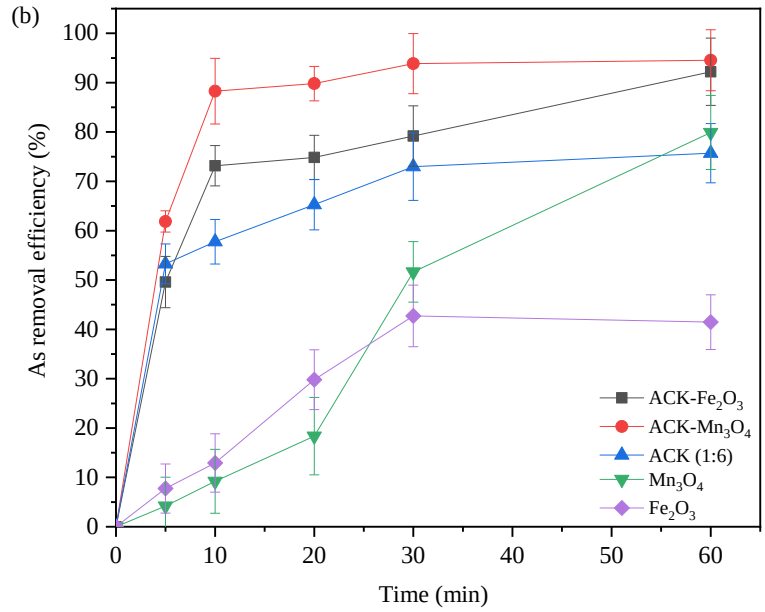

Figure 6. Arsenic removal efficiency As a function of adsorption time at pH 7 from (a) AC treated by various KOH amounts and (b) the mixtures and raw materials (cont.)

3.2.3 Effect of adsorbent amount

Figure 7 shows how various adsorbents behave, at pH 7 in 30 min of adsorption time, as a function of the adsorbent amount (10-100 mg). In most cases, the As removal rate in ppm/mg sec is high when the amount of adsorbent is relatively small (up to 50 mg). Thus, 50 mg of adsorbent was chosen for 50 ml of well water as the proper adsorption amount. In this study the as-received AC and the individual oxide showed the low rates of adsorption while the rates of ACK, ACK-Fe_2O_3, and ACK-Mn_3O_4 were high in this range (10-50 mg). It indicates that the surface morphologies of ACK, ACK-Fe_2O_3, and ACK-Mn_3O_4 offer more sites for As adsorption than those of the as-received AC and the oxides. It is to be noted that the ratio between the amount of adsorbent and well water was 1 g/L. This ratio is considerably less than the values commonly observed in other studies (1.8-12.5 g/L) (Joshi et al., 2019; Rusmana et al., 2019; Koohzad et al., 2019), demonstrating the effectiveness in practical applications and performance.

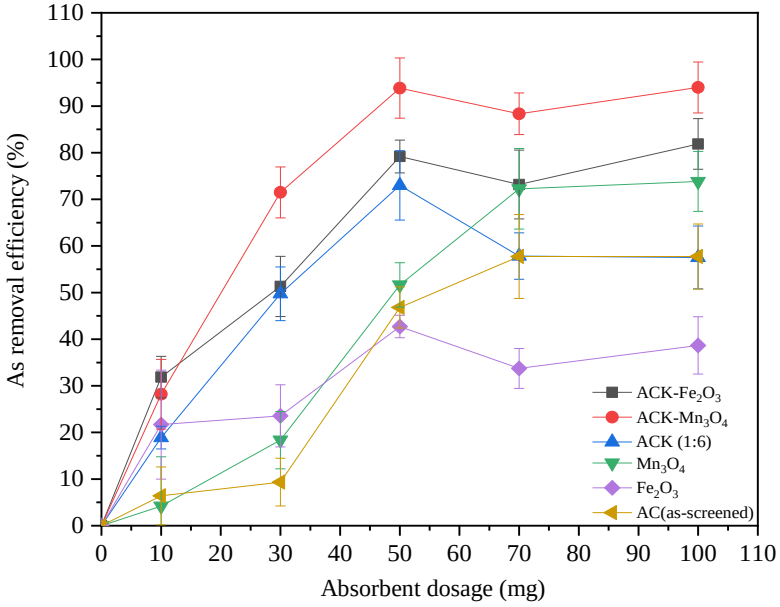

Figure 7. Arsenic removal efficiency as a function of adsorbent amount for various adsorbents at pH 7 for 30 min adsorption time

3.3 Effect of oxide presence with ACK on adsorption performance

Figure 8 presents the performance curves of ACK-Fe_2O_3 and ACK-Mn_3O_4 along with the calculated data. The dotted and dashed lines were calculated based on the weight ratio (10:1) and the surface area, respectively, of the raw materials shown in Figure 7 and Table 1. ACK-Fe_2O_3 and ACK-Mn_3O_4 performed much better than the arithmetic sums of each contribution from the constituent ACK and oxides. The simple addition of an oxide to ACK increased the As removal rate and the efficiency by 10-40% in most ranges of pH, adsorption time, and adsorbent amount. It can be concluded that the addition of oxides, especially Mn_3O_4, to ACK demonstrate a synergetic effect on the As removal.

According to Table 1, the surface areas of ACK-Fe_2O_3 and ACK-Mn_3O_4 (10:1) increased by 154 and 99 m^2/g, respectively, more than the calculated surface areas in parenthesis. As mentioned, the oxides must be responsible for the increase, which is due to deagglomeration of oxide particles. However, the addition of nano Mn_3O_4 to ACK did not result in as significant an increase in the surface area as Fe_2O_3. It means that nano Mn_3O_4 still exhibits a stronger agglomeration tendency than Fe_2O_3 due to its high surface energy associated with nano size particles.

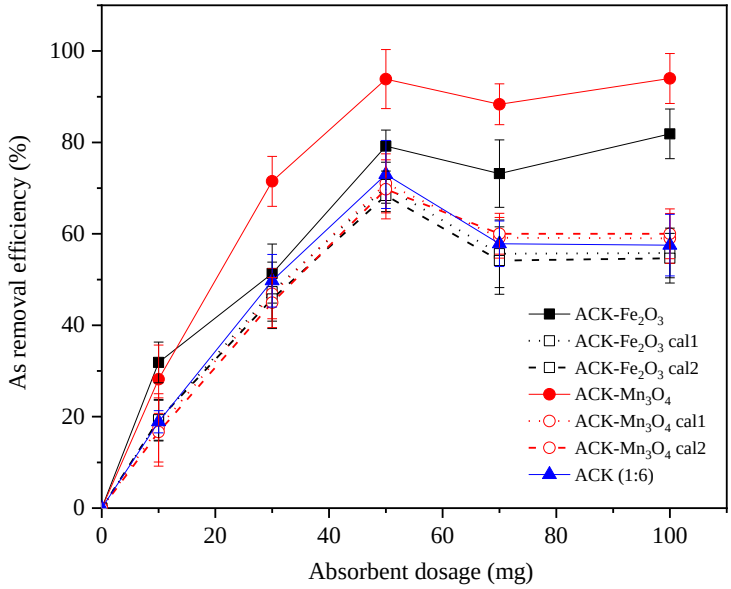

Figure 8. Effect of composition and surface area on the As removal (Calculations were done based on the weight ratio (dotted lines) and the ratio of surface areas (dashed lines) of individual constituent materials.)

Based on the results above, the colloidal states of ACK-Fe_2O_3 and ACK-Mn_3O_4 could be speculated during As adsorption. Since ACK-Fe_2O_3 exhibited a higher increase in the surface area than ACK-Mn_3O_4, Fe_2O_3 particles are expected to disperse more freely in the well water than Mn_3O_4 particles. In addition, ACK-Fe_2O_3 resulted in little improvement in the performance compared to that of ACK. Thus, it is reasonable to say that Fe_2O_3 did not enhance the number of adsorption sites for As significantly. On the other hand, Mn_3O_4 particles of nano size have a tendency to retain the state of agglomeration and deposit on the ACK surface more than Fe_2O_3 to reduce the surface energy effect. Agglomeration of powder in solid state is an equivalent term to flocculation tendency in colloidal science. Figure 9 shows the schematics of the mixture adsorbents, i.e., ACK-Fe_2O_3 and ACK-Mn_3O_4, before and after mixing the oxides with ACK in a solution.

In order to understand this issue, zeta, ζ, potential was measured for each material as a function of pH. The potential is electric, which is normally in the range of -100 to 100 mV in the interfacial double layer at the location of the slipping plane. It is normally used to estimate the dispersion tendency of particles in a solution (Dukhin and Goetz, 2017). Fast flocculation is known to occur in a solution if the potential falls in the range of 0-5 mV, while an incipient instability (low flocculation) occurs when the potential is in the range of 10-30 mV (Kumar and Dixit, 2017).

(a) ACK-Fe_2O_3

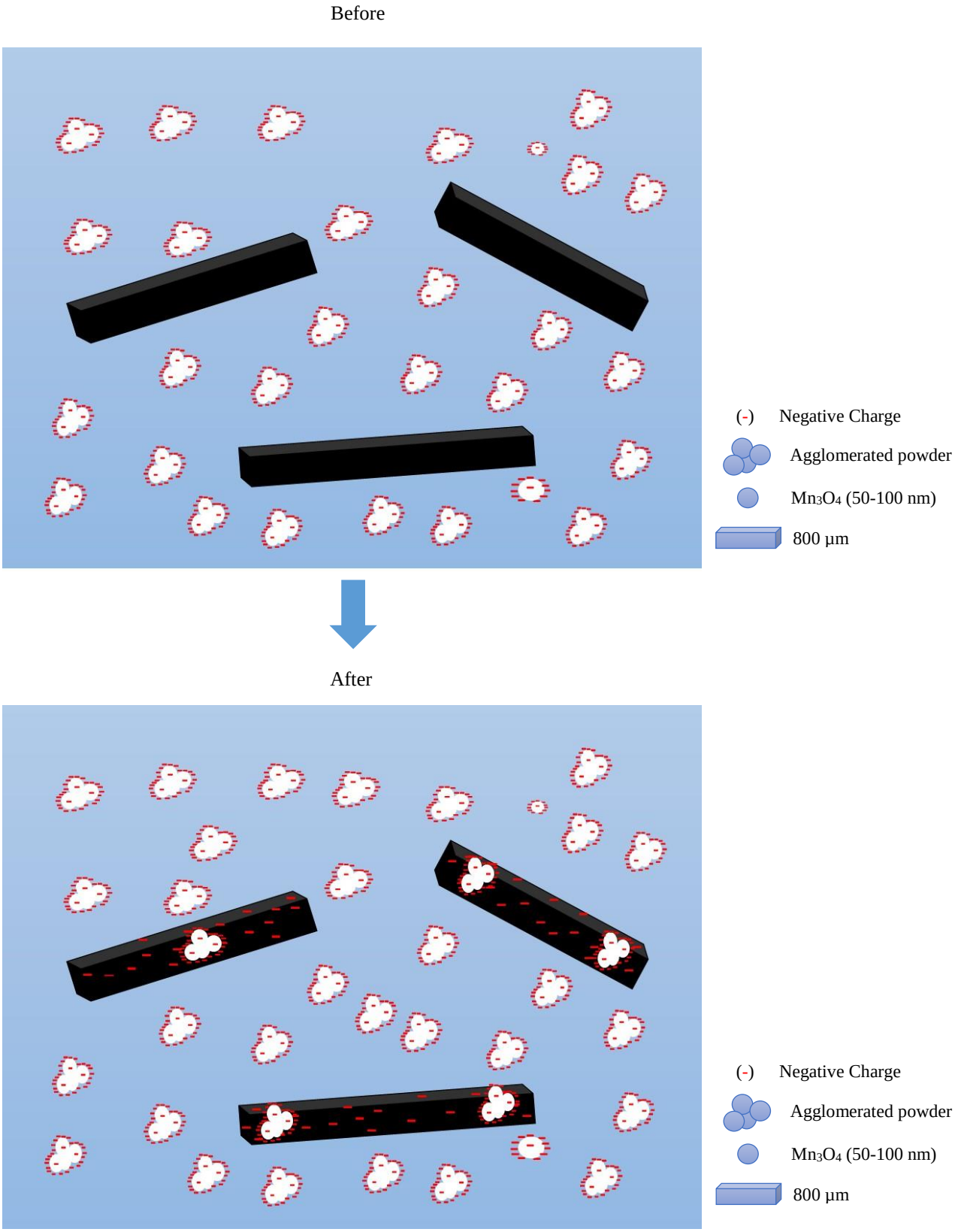

Figure 9. Schematics of (a) ACK-Fe_2O_3 and (b) ACK-Mn_3O_4 in the colloidal state before and after interactions of the mixtures

(b) ACK-Mn_3O_4

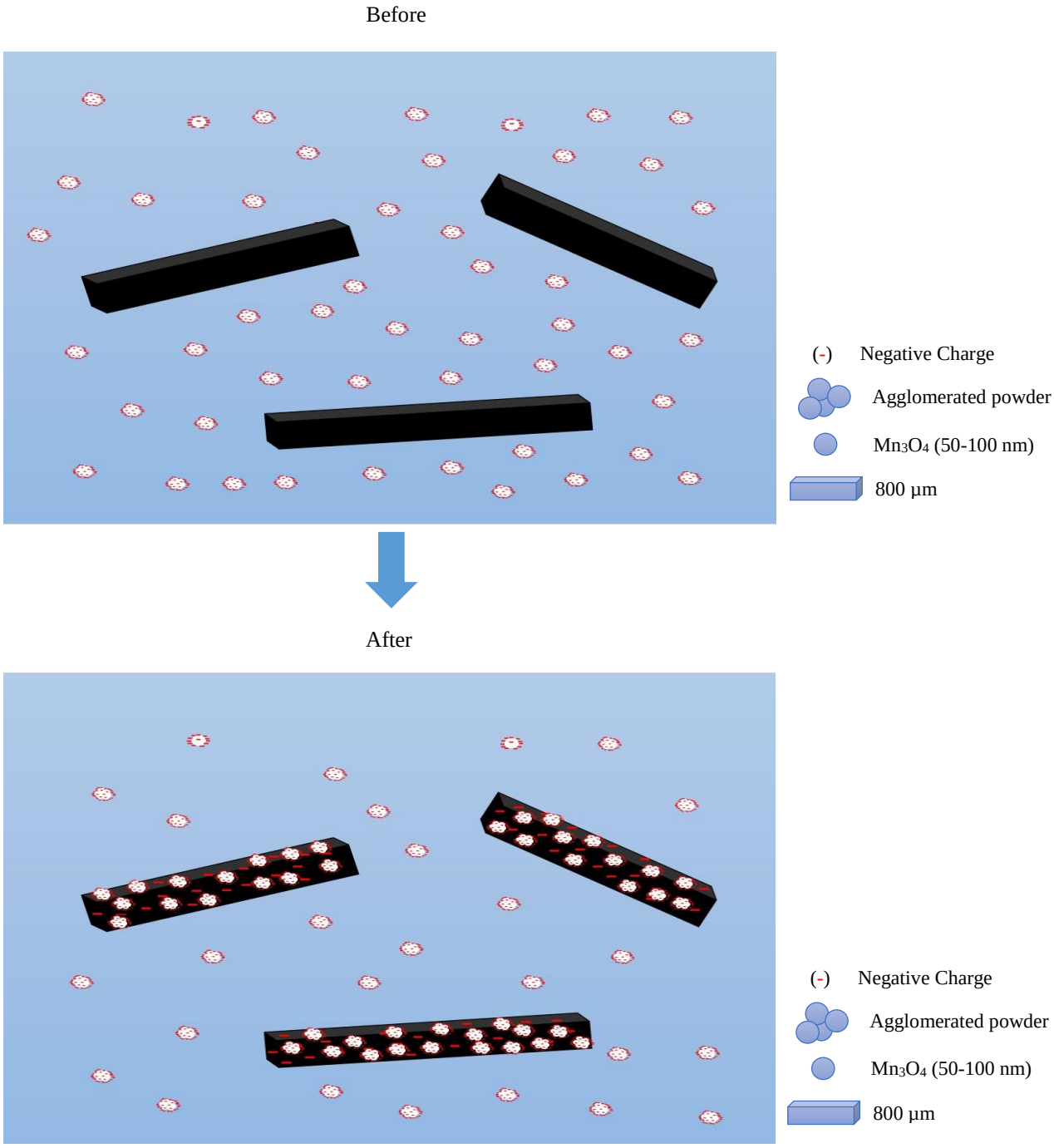

Figure 9. Schematics of (a) ACK-Fe_2O_3 and (b) ACK-Mn_3O_4 in the colloidal state before and after interactions of the mixtures (cont.)

As shown in Figure 10, the net electrical charge bounded by the slipping plane of each material ranged from 0 to -14 mV in the well water of pH 7. The zeta potential of AC and ACK was -11 mV and that of each oxide was about -12.5 mV. On the other hand, ACK-Fe_2O_3 and ACK-Mn_3O_4 had zeta potentials of -13 and -5 mV, respectively. Note that the zeta potential of ACK-Fe_2O_3 (-13 mV) is much more negative than that of ACK-Mn_3O_4 (-5 mV).

The potential of the electrical double layers is determined greatly by the surface charges of individual constituent particles, the morphology and the interactions among them. The zeta potential of ACK-Fe_2O_3 (-13 mV) is not much different from its raw materials, ACK (-11 mV), and Fe_2O_3 (-12 mV). This indicates that ACK and Fe_2O_3 particles are dispersed freely in the well water. In contrast the zeta potential of ACK-Mn_3O_4 (-5 mV) is much lower than

those of constituent materials, ACK (-11 mV) and Mn_3O_4 (-12.5 mV). It suggests that there must be intimate interactions between ACK and Mn_3O_4, providing a new environment for As adsorption.

With the known contribution of ACK in the potential, this result is in good agreement with the schematics suggested (Figure 9). The new morphology of ACK-Mn_3O_4 mixture provided the highest number of adsorption sites. A notable synergetic effect between ACK and Mn_3O_4 on As removal was observed and was reasoned by the surface charge and surface energy of the nano-sized oxide particles.

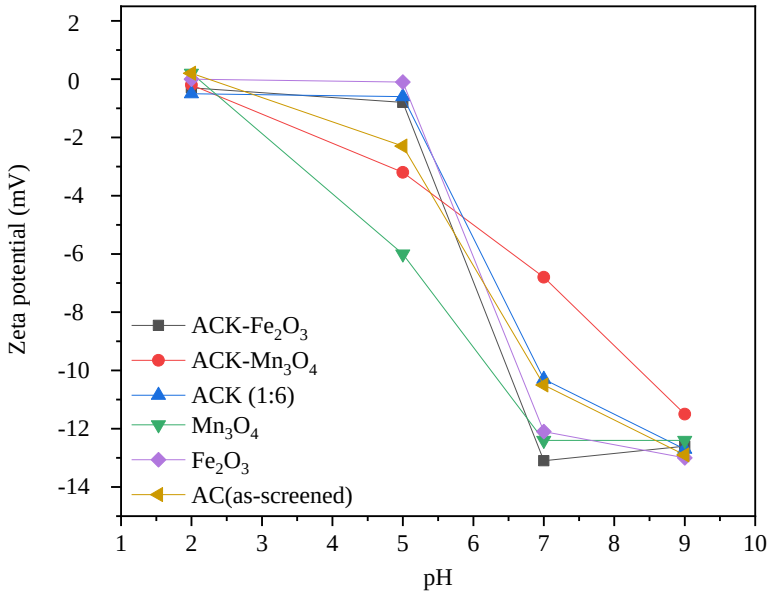

Figure 10. Zeta(ζ) potentail of various absorbents

4. CONCLUSION

The microstructure and characteristics of various AC-based adsorbents were investigated and evaluated in terms of their As removal efficiency. Overall, the study results demonstrate that adsorbents comprising ACK, Mn_3O_4, and Fe_2O_3 could be considered as economical and effective adsorbents for As removal. The summary and conclusions of this study are as follows:

(1) For 50 mL As-containing well water, the optimal values of pH, adsorption time, and amount of adsorbent were pH 7, 30 min, and 50 mg, respectively. The ratio between the amount of adsorbent and well water (1 g/L) of this study offered equivalent or superior performance efficiency compared to those reported previously (1.8-12.5 g/L). The adsorbents consisting of ACK and oxides are advantageous in performance and cost over other GAC-based adsorbents.

(2) A strong synergetic effect of Mn_3O_4 with granular ACK was observed on As removal (~95%). This is primarily due to the change in the potential of partially agglomerated nano Mn_3O_4 particles on the ACK surface. The influence of the surface area of the adsorbents was not pronounced.

Once As-removal absorbents are developed, making them widely available to public is another important task, where the role of the Cambodian government is important. Given that arsenic issues are inherently inter-disciplinary between environment and health, together with education (for raising public awareness) and coordination (between the central government and local provinces), a number of ministries (Ministry of Environment, Ministry of Health, Ministry of Rural Development, etc.) should establish systematic channels for effective communications and implementations, including communications with international communities. This should be reserved as a topic for a further study.

ACKNOWLEDGEMENTS

This work was supported by the Ministry of Education of the Republic of Korea and the National Research Foundation of Korea (NRF-2022S1 A5A2A01045555), and partially supported by the Swedish International Development Cooperation Agency (SIDA) through Sweden and Royal University of Phnom Penh (RUPP)'s Pilot Research Cooperation Program (Sida Contribution No. 11599) and We acknowledge the experimental assistance of Mr.

Piseth Lim from RUPP and Prof. GH. Lee, Dr. CH. Kim from Seoul National University.

REFERENCES

Ahmad SA, Khan MH, Haque M. Arsenic contamination in groundwater in Bangladesh: Implications and challenges for healthcare policy. Risk Management and Healthcare Policy 2018;11:251-61.

Chang M, Shih YH. Synthesis and application of magnetic iron oxide nanoparticles on the removal of Reactive Black 5: Reaction mechanism, temperature and pH effects. Journal of Environmental Management 2018;224:235-42.

Dehmani Y, Abouarnadasse S. Study of the adsorbent properties of nickel oxide for phenol depollution. Arabian Journal of Chemistry 2020;13(5):5312-25.

Dukhin AS, Goetz PJ. Characterization of Liquids, Dispersions, Emulsions, and Porous Materials Using Ultrasound. 3rd ed. Elsevier; 2017.

Esmaeili H, Mousavi SM, Hashemi SA, Chiang WH, Abnavi SA. Activated carbon@ MgO@ Fe_3O_4 as an efficient adsorbent for As (III) removal. Carbon Letters 2021;31:851-62.

Gil A, Galeano LA, Vicente MÁ. Applications of Advanced Oxidation Processes (AOPs) in Drinking Water Treatment. Cham: Springer International Publishing; 2019.

Hudak PF. Nitrate, arsenic and selenium concentrations in the pecos valley aquifer, West Texas, USA. International Journal of Environmental Research 2010;4(2):229-36.

Jha VK, Maharjan J. Activated carbon obtained from banana peels for the removal of AS (III) from water. Scientific World 2022;15(15):145-57.

Jiang W, Zhang L, Guo X, Yang M, Lu Y, Wang Y, et al. Adsorption of cationic dye from water using an iron oxide/activated carbon magnetic composites prepared from sugarcane bagasse by microwave method. Environmental Technology 2021;42(3):337-50.

Joshi S, Sharma M, Kumari A, Shrestha S, Shrestha B. Arsenic removal from water by adsorption onto iron oxide/nano-porous carbon magnetic composite. Applied Sciences 2019;9(18):Article No. 3732.

Kalaruban M, Loganathan P, Nguyen TV, Nur T, Johir MA, Nguyen TH, et al. Iron-impregnated granular activated carbon for arsenic removal: Application to practical column filters. Journal of Environmental Management 2019;239:235-43.

Koohzad E, Jafari D, Esmaeili H. Adsorption of lead and arsenic ions from aqueous solution by activated carbon prepared from tamarix leaves. ChemistrySelect 2019;4(42):12356-67.

Kumar A, Dixit CK. Methods for characterization of nanoparticles. In: Advances in Nanomedicine for the Delivery of Therapeutic Nucleic Acids. United Kingdom: Woodhead Publishing; 2017.

Liang M, Lai Y. Determination of the arsenic content in surface water by silver diethyldithiocarbamate spectrophotometry. Proceedings of the 4th International Conference on Bioinformatics and Biomedical Engineering; 2010 Jun 18-20; Chengdu: China; 2010.

López-Guzmán M, Alarcón-Herrera MT, Irigoyen-Campuzano JR, Torres-Castañón LA, Reynoso-Cuevas L. Simultaneous removal of fluoride and arsenic from well water by electrocoagulation. Science of the Total Environment 2019; 678:181-7.

Mahmoodi NM, Ghezelbash M, Shabanian M, Aryanasab F, Saeb MR. Efficient removal of cationic dyes from colored wastewaters by dithiocarbamate-functionalized graphene oxide nanosheets: From synthesis to detailed kinetics studies. Journal of the Taiwan Institute of Chemical Engineers 2017;81:239-46.

Mahmoodi NM. Synthesis of magnetic carbon nanotube and photocatalytic dye degradation ability. Environmental Monitoring and Assessment 2014;186(9):5595-604.

Mostafapour FK, Bazrafshan E, Farzadkia M, Amini S. Arsenic removal from aqueous solutions by *Salvadora persica* stem ash. Journal of Chemistry 2013;2013:Article No. 740847.

Mousavi SR, Asghari M, Mahmoodi NM. Chitosan-wrapped multiwalled carbon nanotube as filler within PEBA thin film nanocomposite (TFN) membrane to improve dye removal. Carbohydrate Polymers 2020;237:Article No. 116128.

Pravalprukskul P, Aung MT, Wichelns D. Arsenic in Rice: State of Knowledge and Perceptions in Cambodia. Stockholm: Stockholm Environment Institute; 2018.

Rahaman MN. Ceramic Processing and Sintering. Boca Raton: CRC Press; 2017.

Rahman HL, Erdem H, Sahin M, Erdem M. Iron-incorporated activated carbon synthesis from biomass mixture for enhanced arsenic adsorption. Water, Air, and Soil Pollution 2020;231:1-7.

Rusmana YF, Notodarmojo S, Helmy Q. Arsenic removal in groundwater by integrated ozonation and adsorption by activated carbon and zeolite. IOP Conference Series: Materials Science and Engineering 2019;536(1):Article No. 012073.

Stratton G, Whitehead HC. Colorimetric determination of arsenic in water with silver diethyldithiocarbamate. Journal-American Water Works Association 1962;54(7):861-4.

Tallman DE, Shaikh AU. Redox stability of inorganic arsenic (III) and arsenic (V) in aqueous solution. Analytical Chemistry 1980;52(1):196-9.

Tan IA, Ahmad AL, Hameed BH. Adsorption of basic dye on high-surface-area activated carbon prepared from coconut husk: Equilibrium, kinetic and thermodynamic studies. Journal of Hazardous Materials 2008;154(1-3):337-46.

Vašák V, Šedivec V. Colorimetric determination of arsenic. Collection of Czechoslovak Chemical Communications 1953;18(1):64-72.

Thearak V. Oxides and Activated Carbon on Removal of Arsenic from Cambodian Well Water [dissertation]. Phnom Penh, Royal University of Phnom Penh; 2023.

World Health Organization (WHO). Hardness in Drinking-Water: Background Document for Development of WHO Guidelines for Drinking-Water Quality. WHO; 2010.

World Health Organization (WHO). Guidelines for Drinking-Water Quality: WHO Chronicle. Switzerland: WHO; 2011.

Wong S, Ngadi N, Inuwa IM, Hassan O. Recent advances in applications of activated carbon from biowaste for wastewater treatment: A short review. Journal of Cleaner Production 2018;175:361-75.

Yao S, Liu Z, Shi Z. Arsenic removal from aqueous solutions by adsorption onto iron oxide/activated carbon magnetic composite. Journal of Environmental Health Science and Engineering 2014;12:1-8.

Bacteriological Assessment of Fecal Contamination in the Sediments of the Gulf of Annaba (Southern Mediterranean): A Preliminary Investigation

Mouna Boufafa[1*], Fatma Zohra Guellati[1], Hassen Touati[2], Skander Kadri[1], and Mourad Bensouilah[1]

[1]*Laboratory of Eco-Biology for Marine Environment and Coastlines, Faculty of Science, Badji Mokhtar University, BP 12 Annaba 23000, Algeria*

[2]*Faculty of Natural Sciences, Life Sciences, Earth and the Universe, 8 Mai 1945 University, BP 401 Guelma 24000, Algeria*

ARTICLE INFO

Received: 8 Mar 2023
Received in revised: 29 May 2023
Accepted: 8 Jun 2023
Published online: 18 Jul 2023
DOI: 10.32526/ennrj/21/20230057

Keywords:
Fecal indicators/ Gulf of Annaba/ Pathogenic bacteria/ Physicochemical variables/ Seawater/ Sediments

*** Corresponding author:**
E-mail: mouna_boufafa@yahoo.fr

GRAPHICAL ABSTRACT

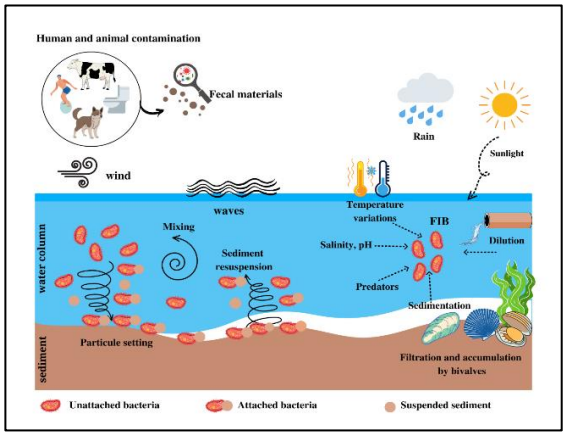

ABSTRACT

This study investigated the bacteriological and physicochemical quality of seawater and sediment samples collected from four sampling sites in the Gulf of Annaba (Northeastern Algeria) over a one-year period. Culture-based techniques were used to quantify and assess Fecal Indicator Bacteria (FIB) and potentially pathogenic bacteria. Additionally, various physicochemical parameters including temperature, pH, salinity, dissolved oxygen, and suspended solids were measured. The results revealed seasonal variations in the physicochemical variables, reflecting the influence of environmental conditions in the research area. The highest concentrations of FIB were observed in samples obtained from Sidi Salem and Rezgui Rachid, indicating a possible association with sewage contamination. Furthermore, the sediments collected from all sites exhibited higher levels of FIB and potentially pathogenic bacteria compared to the seawater samples, particularly during the summer and fall seasons.

1. INTRODUCTION

Coastal ecosystems are continuously subjected to significant anthropogenic impacts, including bacterial contamination from urban, agricultural, and industrial activities (Basili et al., 2021). This form of pollution can harbor harmful pathogenic bacteria, which can detrimentally impact human health and aquatic ecosystems, leading to severe environmental, economic, and health consequences, notably a deterioration in recreational water quality (Curran et al., 2022).

In polluted coastal waters, a wide range of bacterial species, including Fecal Indicator Bacteria (FIB), can be found alongside the most dangerous pathogens (Zhang et al., 2019). FIB, which are highly prevalent in human feces, tend to occur in higher

Citation: Boufafa M, Guellati FZ, Touati H, Kadri S, Bensouilah M. Bacteriological assessment of fecal contamination in the sediments of the Gulf of Annaba (Southern Mediterranean): A preliminary investigation. Environ. Nat. Resour. J. 2023;21(4):358-369. (https://doi.org/10.32526/ennrj/21/20230057)

concentrations in wastewater compared to many pathogens, making them reliable indicators for identifying sewage inputs (O'Mullan et al., 2019; González-Fernández et al., 2021).

Once introduced into coastal environments, FIB have a remarkable ability to persist, thereby increasing the potential for human disease transmission. Moreover, under specific hydrological conditions, these bacteria can migrate to nearby areas such as bathing and shellfish zones (Luna et al., 2016), thus, exposing humans to heightened susceptibility of contracting various illnesses, including skin diseases, gastrointestinal infections, acute respiratory infections, and allergies (Karbasdehi et al., 2017; Valério et al., 2022).

Since its implementation in 1993, the bathing water quality requirements derived from the Official Journal of the Algerian Republic (OJAR, 1993) has played a crucial role in evaluating the quality of coastal bathing waters by assessing the levels of FIB such as *Escherichia coli* (*E. coli*) and fecal streptococci (FS). These bacterial standards are established based on extensive research that estimates the risk of enteric bacteria-related diseases among bathers when exposed to different concentrations of these indicators in water (Aragonés et al., 2016).

Regrettably, the primary shortcoming of the previous standards lies in their restricted scope, as they solely focus on assessing the quality of coastal waters while neglecting the crucial role of sediments. Research studies conducted by Zimmer-Faust et al. (2017), Fang et al. (2018), and Chávez-Díaz et al. (2020) have consistently demonstrated the critical role of sediments in harboring bacteria and serving as a potential source of contamination.

Sediments play a crucial role in the fate of FIB due to several factors, including the abundant availability of organic carbon and nutrients, minimal temperature variations, reduced exposure to sunlight, and protection against predators (Fang et al., 2018). These favorable conditions in sediments contribute to the survival and potential proliferation of FIB (Chávez-Díaz et al., 2020). However, the presence of these bacteria can have significant implications for both human health and the overall quality of coastal ecosystems, particularly when sediments are disturbed and re-suspended. This re-suspension can arise from human activities, such as recreational water activities, as well as natural phenomena like tides and heavy rainfall, leading to high levels of contamination (Luna et al., 2012).

The Gulf of Annaba is a region of particular interest for environmental research due to its exposure to various natural and anthropogenic pressures (Amri et al., 2017). Previous monitoring surveys in this area have primarily focused on assessing the quality of seawater and marine organisms, such as bivalves (Hidouci et al., 2014; Kadri et al., 2015; Kadri et al., 2017; Boufafa et al., 2021), while largely overlooking the crucial role of sediments as a potential reservoir of fecal bacteria in coastal ecosystems. Consequently, our research aims to bridge this gap by undertaking the first comprehensive investigation to (1) evaluate the abundance and distribution of FIB and pathogenic bacteria in the sediments and (2) assess the impact of environmental variables in the seawater on the abundance of FIB in the Gulf of Annaba.

2. METHODOLOGY

2.1 Description of the sampling zone

The Gulf of Annaba is one of the most valued regions in Algeria due to its strategic geographic position and socioeconomic importance. Situated in the extreme northeast of the country, it stretches approximately 40 km between Cap de Garde in the west (7°16'E - 36°68'N) and Cap Rosa in the east (8°15'E - 36°38'N) (Figure 1). This coastal area is permanently threatened by various anthropogenic activities, including the discharge of agricultural and industrial effluents, untreated wastewater, and fishing practices, etc. Additionally, it receives a substantial inflow of freshwater from Oued Bedjima and, notably, Oued Seybouse (Figure 1), which is the second longest river in Algeria with a catchment area of about 6,470 km^2 (Amri et al., 2017).

For this study, four sampling sites (Figure 1) were selected according to their proximity to the different sources of contamination in these areas, as well as their accessibility and importance in tourism. The characteristics of the selected sites are shown in Table 1.

2.2 Sampling strategy

Seawater and sediment samples were collected monthly early in the morning at each site over a one-year survey period from January to December 2018. To minimize bacterial exposure to solar irradiation, seawater samples were obtained from a depth of approximately 30-50 cm using sterilized glass bottles. Subsequently, sediment samples weighing approximately 50 g were collected by scraping the top few centimeters of the surface (2-5 cm) and carefully

placed in sterile bags. All samples were immediately stored in a cool box maintained at a low temperature (4°C to 6°C) and transported to the laboratory for analysis within 2-3 h.

Directly after sampling, seawater environmental variables including temperature (T), pH salinity (Sal), and dissolved oxygen (DO) were measured *in situ* at each site using a multiparameter probe (Multi 340i/SET-82362, WTW®, Germany). Suspended solids (SS) were determined in the laboratory by the differential weighing method (Aminot and Kérouel, 2004).

Figure 1. Map showing the location of the Gulf of Annaba and sampling sites. The small map shows the overall location of Annaba with respect to Algeria and the Mediterranean Sea. The large map shows the exact locations of the four sampling sites (S1=Cap de Garde; S2=Rezgui Rachid; S3=Sidi Salem; S4=Lahnaya).

Table 1. Characteristics of the four sampling sites in the Gulf of Annaba

Name and coordinates of sampling site	Location in the study area and characteristics of the sampling sites
S1: Cap de Garde (36°96′N, 7°79′E)	Located in the western part of the study area and characterized by the presence of bathers in summer
S2: Rezgui Rachid (36°91′N, 7°76′E)	Located in the center of Annaba City and receives urban waste
S3: Sidi Salem (36°86′N, 7°76′E)	Located in the east of Annaba City, close to Wadi Seybouse and Bedjima and receives a mixture of industrial, urban agricultural and wastes
S4: Lahnaya (36°93′N, 8°20′E)	Located at 45 km from the city of Annaba and relatively unaffected by urban interference

2.3 Bacteriological analysis

2.3.1 Fecal indicator bacteria enumeration

A volume of 100 mL of seawater was directly analyzed without any pre-treatment. In the case of sediment samples, a detachment step was conducted prior to bacterial enumeration. Samples of approximately 10 g were homogenized and diluted in 90 mL of peptone water supplemented with 1 mL of Tween 80 ® (Biopack). The mixture was continuously stirred for 10 to 15 min to ensure thorough dispersion of the bacteria from the sediment particles.

For all samples, the density of FIB, including total coliform (TC), *E. coli*, and fecal streptococci were enumerated by a multiple tube dilution method using the three tube Most Probable Number (MPN) method (standard V 08-020 (1994)/ISO 7251 and 08-021 V (1993)/ISO 7402). The results were statistically expressed as MPN of bacteria per 100 mL or g according to the Mac Grady's tables.

2.3.2 Isolation and identification of potentially pathogenic bacteria

The isolation and identification of potentially pathogenic bacteria were carried out following the methods described by Rodier et al. (2009). Selected isolates were presumptively identified based on their morphological and cultural characteristics. Subsequently, they were further identified up to the species level using the Analytical Profile Index API 20E, API 20NE, and API staph systems, according to the manufacturer's recommendations. Additionally, enzymatic tests including oxidase, catalase, and staphylocoagulase tests were performed to confirm their characteristics and ascertain their enzymatic profiles. These enzymatic tests were conducted in accordance with standard protocols and guidelines.

The relative bacterial abundance is calculated by dividing the number of each bacterium by the total number of bacteria for each site and for each compartment. The results are expressed as a percentage.

2.4 Statistical analysis

Statistical analyses were carried out on the physicochemical and bacteriological variables using R software. Correlation analyses for seawater samples were estimated to analyze the intensity of the relationships between the data sets using the Spearman correlation coefficient. Finally, principal component analysis (PCA) was used as a descriptive method to characterize the pattern of the four sampling sites in the Gulf of Annaba.

3. RESULTS

3.1 Physicochemical variables

Five physicochemical variables were measured in all seawater samples during the sampling period. As expected, seawater temperature at the four study sites was strongly influenced by air temperature, reaching its highest value (27.7°C) in summer at S2 and its lowest value (11°C) in winter at S4 (Figure 2). Salinity showed a similar seasonal pattern to the temperature, where the maximum value was recorded at S4 (41 g/L) in summer (Figure 2). According to the Spearman correlation coefficient, these two variables were strongly correlated with each other ($r=0.76$, $p<0.0001$) (Table 2). In contrast, DO levels exhibited an inverse relationship with water temperature, with the highest values observed in winter and the lowest values during summer and fall (Figure 2). The highest correlation in this study was revealed between DO and temperature ($r=-0.85$, $p<0.0001$) (Tables 2).

Regarding the pH, the measurements remained relatively alkaline and consistent across the four seasons. The highest value (8.8) of this variable was recorded at S4 in spring (Figure 2). Maximum levels of suspended solids (0.4 mg/L) were reached twice, in the winter and the fall, at S2 and S3, respectively (Figure 2).

3.2 Bacteriological analysis of fecal indicator bacteria

The levels of TC, *E. coli*, and FS in both seawater and sediment samples at each sampling site and season are reported in Figure 3.

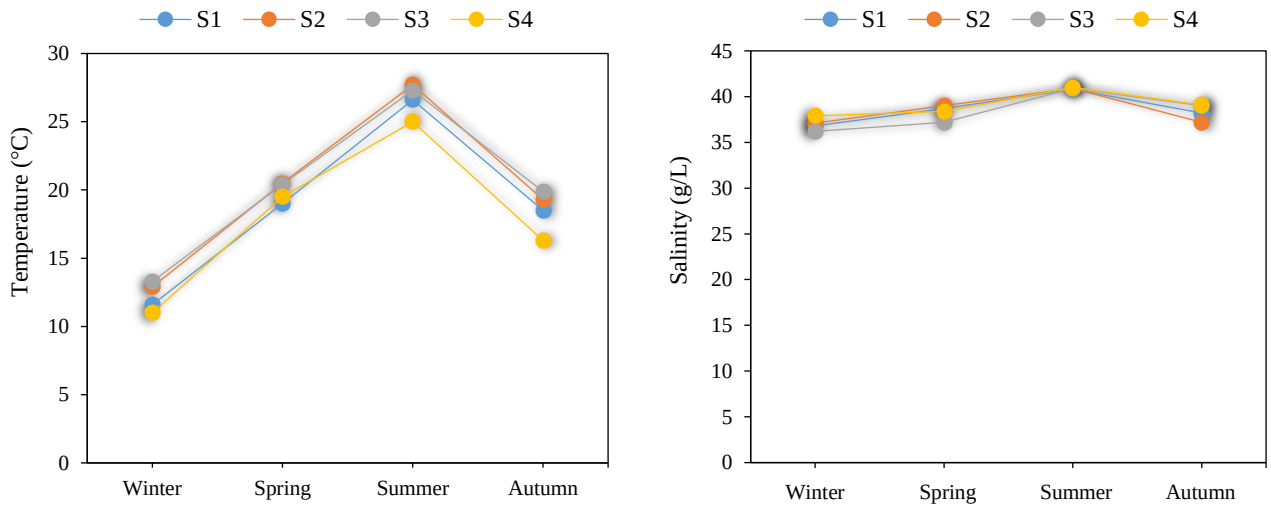

Figure 2. Results of the physicochemical analysis of seawater samples at the four sampling sites

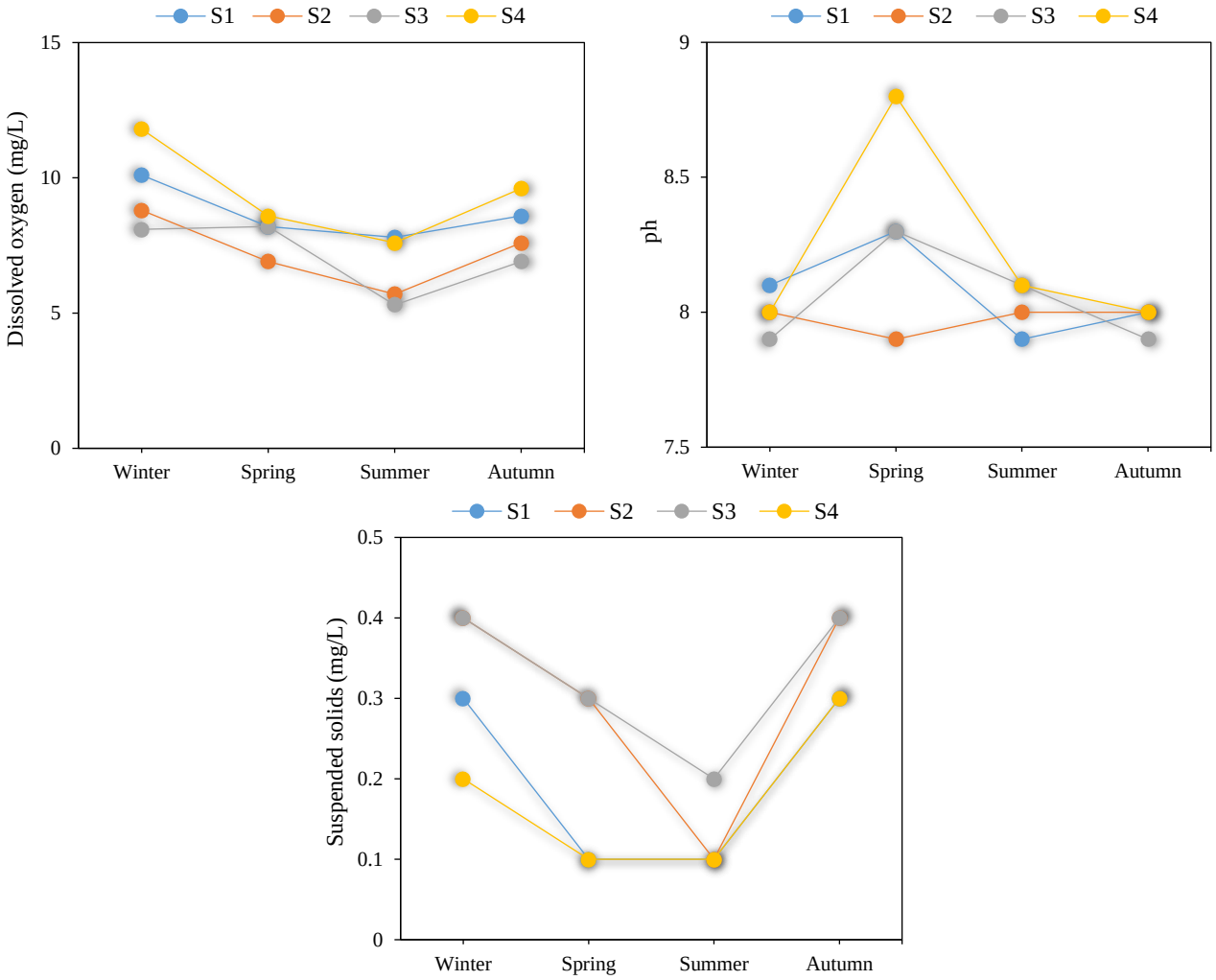

Figure 2. Results of the physicochemical analysis of seawater samples at the four sampling sites (cont.)

Total coliforms were consistently detected throughout the research period. The abundance of these bacteria was above the regulatory limits established by the Algerian legislation for recreational water (500 MPN/100 mL of water) (OJAR, 1993) at all sampling sites and seasons, with the exception of S4, where the lowest levels were observed in spring (340 TC/100 mL) and autumn (380 TC/100 mL) (Figure 3).

E. coli concentrations ranged from 23.3 *E. coli*/100 mL at S4 in spring to 853.3 *E. coli*/100 g at S3 in autumn (Figure 3). FS were consistently present in all seawater samples collected throughout the study year (Figure 3), mainly due to their high resistance to severe environmental stress. The highest amount of these bacteria (1500 FS/100 mL) was detected in seawater from S3 (Figure 3).

Unlike water, FIB were found in all sediment samples, and were obviously and comparatively higher than in seawater samples (Figure 3). Levels of 1.8×10^5 TC/100 g and 1.4×10^5 TC/100 g were recorded at S3 and S2 in spring and summer, respectively. The sediments in all the sites, were heavily contaminated by *E. coli*; values of 1.3×10^5 *E. coli*/100 g and 1.1×10^5 *E. coli*/100 g were obtained in winter at S3 and summer at S2, respectively (Figure 3). The lowest concentration of *E. coli* (2.1×10^4 *E. coli*/100g) was detected at S4 in winter. Regarding FS, the highest level was recorded in summer at S2 (1.5×10^5 FS/100 g) (Figure 3).

3.3 Identification of potentially pathogenic bacteria

During the study period, a total of 164 bacteria were isolated and identified. Investigation of the occurrence and abundance of potentially pathogenic bacteria showed higher sediment (56.76% of isolates) than seawater (40.23% of isolates) contamination in the Gulf of Annaba.

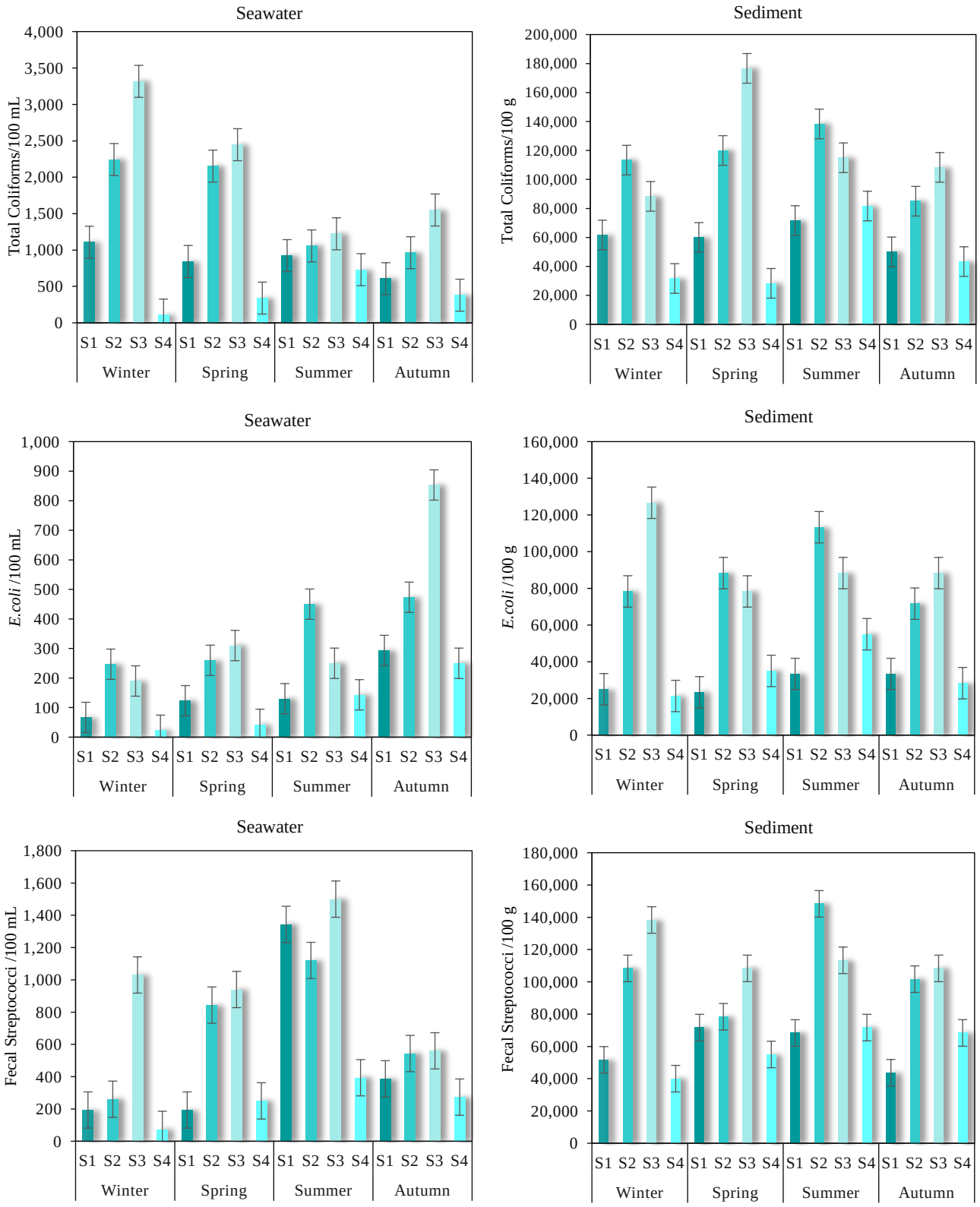

Figure 3. Spatial and temporal variations of FIB in seawater and sediments

Several potentially pathogenic bacteria, mostly associated with fecal and sewage contamination, were found in seawater and sediment samples. *E.coli* (36.6%) showed the maximum occurrence in all sampling sites and environmental samples, followed by *Aeromonas hydrophila* (5.49%), *Enterobacter cloacae* (5.48%), *Burkholderia cepacia* (4.27%), *Klebsiella pneumoniae*, *Vibrio parahaemolyticus* (3.66%), *Pseudomonas aeruginosa*, and *Staphylococcus sciuri*

(3.59%). The relative abundance of all species identified in this research is shown in Figure 4.

Figure 5 illustrates the seasonal distribution of potentially pathogenic bacteria in the Gulf of Annaba, indicating that the diversity of these species exhibited an increase during the warm season (summer and fall) in comparison to the cold season (winter and spring) in both compartments (seawater and sediment).

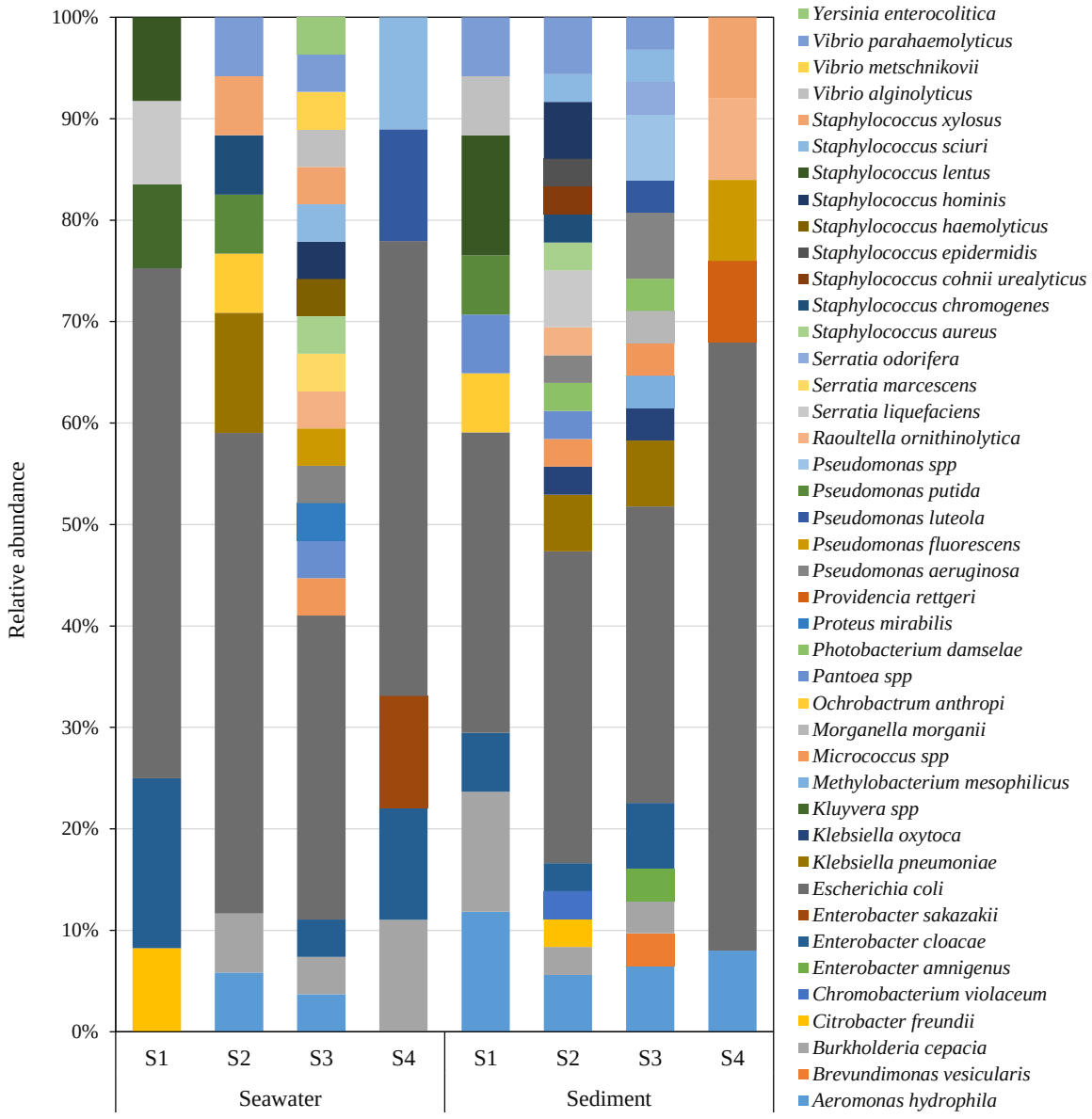

Figure 4. Relative abundance of potential pathogenic bacteria in seawater and sediments samples

3.4 Influence of physicochemical variables on FIB in the Gulf of Annaba

Spearman correlation analysis revealed that the levels of FIB were significantly related to physicochemical variables: seawater temperature, salinity, dissolved oxygen, and suspended solids (Table 2). No significant correlations were found between FIB and pH in all the sampling sites.

Dissolved oxygen, suspended solids, and seawater temperature were found to show the strongest correlations with the levels of FIB (Table 2). According to the correlation analysis, the highest and most significant correlations were found between FS and DO ($r=-0.79$, $p<0.0001$), as well as temperature ($r=0.75$, $p<0.0001$). TC showed a positive correlation with suspended solids (SS) ($r=0.51$, $p<0.05$), whereas *E. coli* exhibited a negative correlation with dissolved oxygen ($r=-0.57$, $p<0.05$) (Table 2).

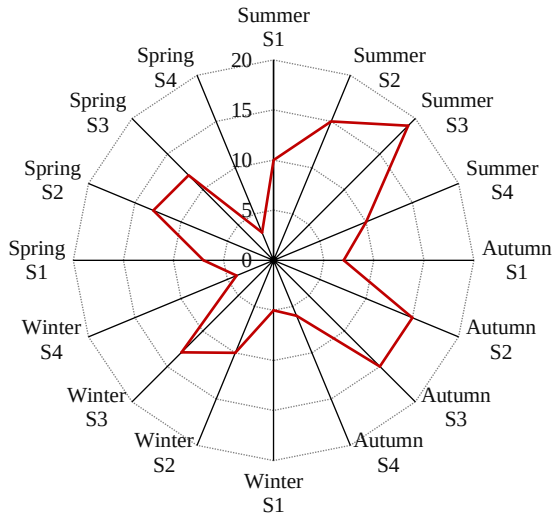

Figure 5. Seasonal distribution of potential pathogenic bacteria in seawater and sediments samples

3.5 Principal component analysis (PCA)

PCA analysis of seawater variables produced two main axes accounting for 74% of the total information in the data set (Figure 6).

The projection into the first axis accounting for 56.3% of the variance opposed the variables seawater temperature (r=-0.53), salinity (r=0.47), and FS (r=-0.41) to the variable DO (r=0. 46) (Figure 6). This suggests that the differences in these variables are most likely due to seasonal changes. Instead, PC2 accounted for 31% of the variation and exhibited negative associations with TC (r=-0.51), SS (r=-0.48), *E. coli* (r=-0.43), and positive correlation with pH (r=0.41) (Figure 6).

Table 2. Spearman's correlation matrix of the seawater quality

	T	Sal	pH	DO	SS	TC	EC
Sal	0.76 ***						
pH	0.00	-0.02					
DO	-0.85***	-0.59*	0.24				
SS	-0.52*	-0.66**	-0.47	0.18			
TC	0.14	-0.34	-0.29	-0.38	0.51*		
EC	0.41*	0.15	-0.34	-0.57*	0.45	0.44	
FS	0.75***	0.38	-0.39	-0.79***	-0.06	0.53*	0.55*

* p≤0.05; ** p≤0.01; *** p≤ 0.001

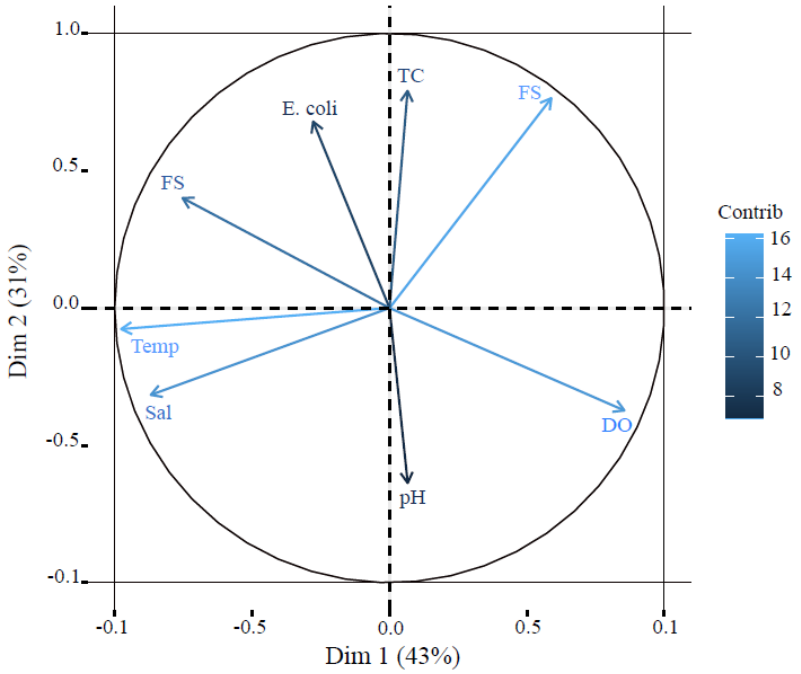

Figure 6. Principal component analysis performed on data from seawater samples. Correlation of environmental variables with the first axis of the standard PCA. Temp: seawater temperature, Sal: salinity, DO: dissolved oxygen, SS: Suspended solids. *E. coli*: *Escherichia coli*, TC: total coliforms and FS: fecal streptococci.

4. DISCUSSION

4.1 Physicochemical variables

The measurements of physicochemical variables of seawater samples showed that temperature, salinity, pH, DO, and SS present seasonal fluctuations in all sites at the Gulf of Annaba. Peak values for seawater temperature coincided with the summer-fall period. As previously observed, variations of this abiotic variable are broadly related to the local climatic conditions, particularly to ambient temperature (Gutiérrez-Cacciabue et al., 2014).

Salinity, similar to water temperature, exhibited its highest values during the warm season, as shown in Figure 2. This pattern is likely attributed to the combined effects of elevated temperatures, which promote significant evaporation, and reduced precipitation, resulting in decreased freshwater inflow (Mihanović et al., 2021). The inflow of freshwater into the sea through the Oueds plays an important role in seawater dilution and, consequently, the reduction in salinity, particularly during winter. Notably, our findings are consistent with the observations reported by Lamine et al. (2019) in Morocco.

The pH levels in the Gulf were predominantly alkaline, fluctuating between 7.3 and 8.9 (Figure 2). It is worth noting that, according to Chapman (1996), pH values within the range of 6 to 9 are generally considered safe for aquatic life and fisheries.

The annual cycle of dissolved oxygen in the Gulf revealed a pronounced oxygenation of the Gulf water during the cold season, primarily due to the decrease in water temperature and the occurrence of high wind speeds. These factors contribute to continuous mixing of the water mass, resulting in an enrichment of dissolved oxygen during the winter season (Hébert and Légaré, 2000). Conversely, the low levels of this variable observed during the dry season indicate elevated bacterial growth and oxygen consumption, alongside a reduction in the self-purification capacity of the seawater (Rodier et al., 2009).

Regarding suspended solids, their concentrations showed higher values during winter in comparison to summer. These variations appear to be related with climatic conditions, particularly the increased precipitation during winter. The abundance of rainfall leads to soil leaching and substantial allochthonous inputs, contributing to elevated suspended solids in the Gulf.

4.2 Bacteriological analysis

4.2.2 Seawater

The spatial-temporal variations of FIB revealed a distinct seasonal pattern across the four study sites. Significantly higher levels of these bacteria were observed during the summer and fall seasons (Figure 3) probably due to the influence of high temperatures, which are recognized as one of the key environmental factors promoting the persistence of FIB. Barreras et al. (2019) suggest that elevated temperatures can prolong the duration of FIB presence in the water, a hypothesis supported by our study. Notably, our findings demonstrated significant positive correlations between FIB and temperature, as confirmed by Spearman's correlation and multivariate analysis ($p \leq 0.05$) (Table 2). These results are in line with the studies conducted by Lamine et al. (2019) and Chávez-Díaz et al. (2020).

Moreover, in areas designated for swimming, where the average depth of the seawater column does not exceed 2 meters, sediments are constantly in motion due to factors such as recreational activities of bathers and coastal currents. This dynamic environment facilitates the migration of a portion of FIB present in the sediments into the water column, leading to elevated levels of contamination (Garrido-Pérez et al., 2008).

As expected, the central zone sites of the Gulf (S2 and S3) exhibited the highest concentrations of fecal bacteria (Figure 1). These sites are characterized by high population density, animal husbandry, and extensive anthropogenic activities, including industries, recreational practices, coastal tourism, and the presence of fishermen and swimmers, among others (Kadri et al., 2017; Boufafa et al., 2021). Importantly, it should be noted that, according to the Algerian Bathing Water executive decrees (OJAR, 1993), the seawater at these two sites is considered to have an unacceptable sanitary quality. In contrast, the strong hydrodynamic conditions, coupled with limited sewage discharge at S1 and S4, have contributed to relatively lower levels of fecal contamination compared to the other two sites (Boufafa et al., 2021).

4.2.3 Sediments

FIB densities were shown to be heavily concentrated in sediments compared to seawater samples (Figure 3), confirming their prolonged survival and persistence in this compartment. Our

results corroborate previous studies conducted at different marine beaches worldwide, which have consistently reported significantly higher average concentrations of FIB in sediments compared to water samples (Crabill et al., 1999; Davies and Bavor, 2000; Karbasdehi et al., 2017). This difference in concentration could be explained by significant dilution of FIB within the water column due to mixing processes, resulting in lower concentrations. Additionally, adsorption and sedimentation processes play a crucial role in removing bacteria from suspension and facilitating their accumulation in bottom sediments (Rozen and Belkin, 2001; Mote et al., 2012).

Our results also revealed a correlation between high bacterial loads during the warm season and elevated FIB levels in sediments. This suggests that the variations in bacterial concentrations were most likely related to the temperature of the sediments, particularly the warming of the surface layer, which creates favorable conditions for bacterial growth. These findings are consistent with the studies conducted by Whitman et al. (2014) and Abreu et al. (2016). According to Zhang et al. (2015), higher temperatures during the summer can stimulate increased concentrations of fecal indicators. This poses a potential concern for bathers, especially children, who tend to have more frequent and active interactions with sediment, making them more susceptible to fecal bacteria (Abreu et al., 2016).

In contrast, the important concentrations of FIB during winter would be probably due to the high levels of organic matter resulting from untreated wastewater drained by heavy rainfall. Our findings support earlier research that highlights the role of organic matter in the persistence and long-term survival of these indicators in sediments (Malham et al., 2014; Perkins et al., 2014; Chávez-Díaz et al., 2020). A study conducted by Craig et al. (2004) demonstrated higher survival levels of *E. coli* in sediments compared to water, and that the presence of substantial organic matter in sediments further enhanced the survival of this bacteria.

The association of bacteria with sediments has been demonstrated to circumvent the negative effects of environmental stresses, such as protection from UV light, salinity, and seasonal variations, resulting in higher survival of indicator bacteria (Zimmer-Faust et al., 2017). Bacteria attach themselves to clays, such as montmorillonite, and utilize the abundant organic and mineral elements present in sediments as a source of nutrients (Malham et al., 2014). This attachment to sediments protect bacteria from predators and bacteriophage attacks. Consequently, sediments can be considered as important accumulation zones for FIB, and in extreme cases, they can even serve as naturalized habitats (O'Mullan et al., 2019).

4.3 Pathogenic bacteria

Pathogenic bacteria were abundant in seawater and sediment samples collected from the Gulf of Annaba, which is comparable to previously reported contaminated coastal areas (Karbasdehi et al., 2017; Chávez-Díaz et al., 2020). Similar to FIB, these species were higher in sediments than in seawater samples, which validates their significant role in assessing pathogen's abundance in these coastal environments.

As can be seen in Figure 4, biochemical tests revealed the presence of different potentially pathogenic species. While many of these species belong to the family *Enterobacteriaceae*, commonly found in the gut microbiota of humans and animals, some are environmental bacteria that are typically isolated from clinical settings. Several studies have reported the association of these species with human outbreaks, including meningitis, urinary and pulmonary tract infections, nosocomial infections, and gastroenteritis (Wang et al., 2020; Hespanha et al., 2021; Soumastre et al., 2022). According to Mohammed et al. (2012), in the lack of optimal indicators of non-fecal health hazards, certain bacteria such as Pseudomonas, may be beneficial in assessing the health conditions of the coastal environments.

Following the *Enterobacteriaceae* family, *Staphylococcus* spp., predominated in seawater and sediment samples, especially in heavily contaminated sites (S2 and S3). These bacteria are considered opportunistic pathogens, and certain strains have the potential to cause illness (including skin infections), even in healthy individuals (Whitman et al., 2014). Interestingly, *Staphylococcus* spp. exhibited higher abundance in the sediment than in the surrounding water during the summer, which is consistent with findings from other studies (Esiobu et al., 2004; Shah et al., 2011).

The results of our study also revealed that *Vibrio* spp. showed the highest occurrence during the summer, which is in agreement with several studies carried out on sediment and seawater samples (Abia et al., 2016; Baron et al., 2017; Rincé et al., 2018; Debnath et al., 2019). According to Arab et al. (2021),

the significant increase in water temperature and salinity during the summer season creates favorable conditions for the proliferation of *Vibrio* spp., which can cause several infectious diseases and pose a significant threat to the health of bathers.

5. CONCLUSION

The findings of the current study demonstrated the significant role played by sediment as a reservoir of FIB and potentially pathogenic bacteria in the Gulf of Annaba. It has been confirmed that the bacteriological quality of both seawater and sediment samples in the study area was strongly influenced by a range of anthropogenic activities, environmental factors, and seasonal variations. In particular, it was observed that during the hot season, the concentration of FIB often exceeded the maximum permissible limits recommended by Algerian regulations for recreational water. Notably, the site of Sidi Salem was found to be the most contaminated, followed by Rezgui Rachid, due to the presence of multiple untreated wastewater outfalls and domestic animals in the vicinity. Consequently, regular and stringent monitoring of water quality in the Gulf is crucial to mitigate the risks to public health and the environment.

ACKNOWLEDGEMENTS

This work was supported by the General Directorate for Scientific Research and Technological Development (DGRSDT), Algeria.

REFERENCES

Abia ALK, Ubomba-Jaswa E, Momba MNB. Competitive survival of *Escherichia coli*, *Vibrio cholerae*, *Salmonella typhimurium*, and *Shigella dysenteriae* in riverbed sediments. Microbial Ecology 2016;72:881-9.

Abreu R, Figueira C, Romão D, Brandão J, Freitas MC, Andrade C, et al. Sediment characteristics and microbiological contamination of beach sand: A case-study in the archipelago of Madeira. Science of the Total Environment 2016;573:627-38.

Aminot A, Kérouel R. Hydrology of Marine Ecosystems: Parameters and Analyses. Paris, France: Ifremer; 2004 (in French).

Amri S, Samar MF, Sellem F, Ouali K. Seasonal antioxidant responses in the sea urchin *Paracentrotus lividus* (Lamarck 1816) used as a bioindicator of the environmental contamination in the SouthEast Mediterranean. Marine Pollution Bulletin 2017;122:392-402.

Arab S, Nalbone L, Giarratana F, Berbar A. *Vibrio* spp. in wild and farmed *Mytilus galloprovincialis* along the Algerian Mediterranean Coast: Evidence of *V. cholerae* 01 Serotype Ogawa. Journal of Aquatic Food Product Technology 2021;30:774-83.

Aragonés L, López I, Palazón A, López-Úbeda R, García C. Evaluation of the quality of coastal bathing waters in Spain through fecal bacteria *Escherichia coli* and *Enterococcus*. Science of the Total Environment 2016;566:288-97.

Baron S, Larvor E, Chevalier S, Jouy E, Kempf I, Granier SA, et al. Antimicrobial susceptibility among urban wastewater and wild shellfish isolates of non-O1/Non-O139 *Vibrio cholerae* from La Rance Estuary (Brittany, France). Frontiers in Microbiology 2017;8:Article No. 1637.

Barreras H Jr, Kelly EA, Kumar N, Solo-Gabriele HM. Assessment of local and regional strategies to control bacteria levels at beaches with consideration of impacts from climate change. Marine Pollution Bulletin 2019;138:249-59.

Basili M, Campanelli A, Frapiccini E, Luna GM, Quero GM. Occurrence and distribution of microbial pollutants in coastal areas of the Adriatic Sea influenced by river discharge. Environmental Pollution 2021;285:Article No. 117672.

Boufafa M, Kadri S, Redder P, Bensouilah M. Occurrence and distribution of fecal indicators and pathogenic bacteria in seawater and *Perna perna* mussel in the Gulf of Annaba (Southern Mediterranean). Environmental Science and Pollution Research 2021;28:46035-52.

Chapman D. Water Quality Assessments: A Guide to the Use of Biota, Sediments and Water in Environmental Monitoring. London and New York: Taylor and Francis; 1996.

Chávez-Díaz LV, Gutiérrez-Cacciabue D, Poma HR, Rajal VB. Sediments quality must be considered when evaluating freshwater aquatic environments used for recreational activities. International Journal of Hygiene and Environmental Health 2020;223:159-70.

Crabill C, Donald R, Snelling J, Foust R, Southam G. The impact of sediment fecal coliform reservoirs on seasonal water quality in Oak Creek, Arizona. Water Research 1999;33:2163-71.

Craig DL, Fallowfield HJ, Cromar NJ. Use of microcosms to determine persistence of *Escherichia coli* in recreational coastal water and sediment and validation with in situ measurements. Journal of Applied Microbiology 2004;96:922-30.

Curran JF, Zaggia L, Quero GM. Metagenomic characterization of microbial pollutants and antibiotic- and metal-resistance genes in sediments from the Canals of Venice. Water 2022; 14:Article No. 1161.

Davies CM, Bavor HJ. The fate of storm water-associated bacteria in constructed wetland and water pollution control pond systems. Journal of Applied Microbiology 2000;89:349-60.

Debnath A, Mizuno T, Miyoshi SI. Comparative proteomic analysis to characterize temperature-induced viable but non-culturable and resuscitation states in *Vibrio cholerae*. Microbiology 2019;165:737-46.

Esiobu N, Mohammed R, Echeverry A, Green M, Bonilla T, Hartz A, et al. The application of peptide nucleic acid probes for rapid detection and enumeration of eubacteria, *Staphylococcus aureus* and *Pseudomonas aeruginosa* in recreational beaches of S. Florida. Journal of Microbiological Methods 2004; 57:157-62.

Fang T, Cui Q, Huang Y, Dong P, Wang H, Liu WT, et al. Distribution comparison and risk assessment of free-floating and particle-attached bacterial pathogens in urban recreational water: Implications for water quality management. Science of the Total Environment 2018;613:428-38.

Garrido-Pérez MC, Anfuso E, Acevedo A, Perales-Vargas-Machuca JA. Microbial indicators of faecal contamination in waters and sediments of beach bathing zones. International Journal of Hygiene and Environmental Health 2008;211:510-7.

González-Fernández A, Symonds EM, Gallard-Gongora JF, Mull B, Lukasik JO, Navarro PR et al. Relationships among microbial indicators of fecal pollution, microbial source tracking markers, and pathogens in Costa Rican coastal waters. Water Research 2021;188:Article No. 116507.

Gutiérrez-Cacciabue D, Teich I, Poma HR, Cruz MC, Balzarini M, Rajal VB. Strategies to optimize monitoring schemes of recreational waters from Salta, Argentina: A multivariate approach. Environmental Monitoring and Assessment 2014;186:8359-80.

Hébert S, Légaré S. Monitoring the water quality of rivers and small streams [Internet]. 2000 [cited 2017 Nov 13]. Available from: https://belsp.uqtr.ca/id/eprint/1288/ (in French).

Hespanha AC, Minto BW, Cardozo MV, Menezes MP, Tasso JB, Moraes PC. Contamination by antimicrobial-resistant enterobacteria isolated from cell phones and hands in a veterinary hospital. Acta Veterinaria Hungarica 2021;69: 216-22.

Hidouci S, Djebar AB, Amara R, Sahraoui EH. Bacterial quality of coastal waters of Annaba (East Algeria). European Journal of Scientific Research 2014;120:488-93.

Official Journal of the Algerian Republic (OJAR). OJAR Guidelines for Bathing Water Quality Requirements: Volume 46. Algeria: OJAR; 1993 (in French).

Kadri S, Dahel A, Djebbari N, Barour C, Bensouilah M. Environmental parameters influence on the bacteriological water quality of the Algerian North East coast. International Journal of Biosciences 2015;11:151-65.

Kadri S, Belhaoues S, Touati H, Boufafa M, Djebbari N, Bensouilah M. Environmental parameters and bacteriological quality of the *Perna perna* mussel (North East Algerian coast). International Journal of Biosciences 2017;11:151-65.

Karbasdehi VN, Dobaradaran S, Nabipour I, Ostovar A, Arfaeinia H, Vazirizadeh A, et al. Indicator bacteria community in seawater and coastal sediment: The Persian Gulf as a case. Journal of Environmental Health Science and Engineering 2017;15:1-15.

Lamine I, Alla AA, Bourouache M, Moukrim A. Monitoring of physicochemical and microbiological quality of Taghazout Seawater (Southwest of Morocco): Impact of the new tourist resort "Taghazout Bay". Journal of Ecological Engineering 2019;20(7):79-89.

Luna GM, Dell'Anno A, Pietrangeli B, Danovaro R. A new molecular approach based on qPCR for the quantification of fecal bacteria in contaminated marine sediments. Journal of Biotechnology 2012;157:446-53.

Luna GM, Quero GM, Perini L. Next generation sequencing reveals distinct fecal pollution signatures in aquatic sediments across gradients of anthropogenic influence. Advances in Oceanography and Limnology 2016;7:115-24.

Malham SK, Rajko-Nenow P, Howlett E, Tuson KE, Perkins TL, Pallett DW, et al. The interaction of human microbial pathogens, particulate material and nutrients in estuarine environments and their impacts on recreational and shellfish waters. Environmental Science: Processes and Impacts 2014;16:2145-55.

Mihanović H, Vilibić I, Šepić J, Matić F, Ljubešić Z, Mauri E, et al. Observation, preconditioning and recurrence of exceptionally high salinities in the Adriatic Sea. Frontiers in Marine Science 2021;8:Article No. 834.

Mohammed RL, Echeverry A, Stinson CM, Green M, Bonilla TD, Hartz A, et al. Survival trends of *Staphylococcus aureus*, *Pseudomonas aeruginosa*, and *Clostridium perfringens* in a sandy South Florida beach. Marine Pollution Bulletin 2012;64:1201-9.

Mote BL, Turner JW, Lipp EK. Persistence and growth of the fecal indicator bacteria enterococci in detritus and natural estuarine plankton communities. Applied and Environmental Microbiology 2012;78:2569-77.

O'Mullan GD, Juhl AR, Reichert R, Schneider E, Martinez N. Patterns of sediment-associated fecal indicator bacteria in an urban estuary: Benthic-pelagic coupling and implications for shoreline water quality. Science of the Total Environment 2019;656:1168-77.

Perkins TL, Clements K, Baas JH, Jago CF, Jones DL, Malham SK, et al. Sediment composition influences spatial variation in the abundance of human pathogen indicator bacteria within an estuarine environment. PLoS ONE 2014;9:e112951.

Rincé A, Balière C, Hervio-Heath D, Cozien J, Lozach S, Parnaudeau S, et al. Occurrence of bacterial pathogens and human noroviruses in shellfish-harvesting areas and their catchments in France. Frontiers in Microbiology 2018; 9:Article No. 2443.

Rozen Y, Belkin S. Survival of enteric bacteria in seawater. FEMS Microbiology Reviews 2001;25:513-29.

Rodier J, Legube B, Merlet N, Brunet R. Water Analysis: Natural Waters, Wastewater, Seawater. Paris, France: Dunod; 2009.

Shah AH, Abdelzaher AM, Phillips M, Hernandez R, Solo-Gabriele HM, Kish J, et al. Indicator microbes correlate with pathogenic bacteria, yeasts and helminthes in sand at a subtropical recreational beach site. Journal of Applied Microbiology 2011;110:1571-83.

Soumastre M, Piccini J, Rodríguez-Gallego L, González L, Rodríguez-Graña L, Calliari D, et al. Spatial and temporal dynamics and potential pathogenicity of fecal coliforms in coastal shallow groundwater wells. Environmental Monitoring and Assessment 2022;194:1-17.

Valério E, Santos ML, Teixeira P, Matias R, Mendonça J, Ahmed W, et al. Microbial source tracking as a method of determination of beach sand contamination. International Journal of Environmental Research and Public Health 2022; 19:Article No. 7934.

Wang D, Wu J, Wang Y, Ji Y. Finding high-quality groundwater resources to reduce the hydatidosis incidence in the Shiqu County of Sichuan Province, China: Analysis, assessment, and management. Exposure and Health 2020;12:307-22.

Whitman RL, Harwood VJ, Edge TA, Nevers MB, Byappanahalli M, Vijayavel K, et al. Microbes in beach sands: Integrating environment, ecology and public health. Reviews in Environmental Science and Bio/Technology 2014;13:329-68.

Zhang Q, He X, Yan T. Differential decay of wastewater bacteria and change of microbial communities in beach sand and seawater microcosms. Environmental Science and Technology 2015;49:8531-40.

Zhang SY, Tsementzi D, Hatt JK, Bivins A, Khelurkar N, Brown J, et al. Intensive allochthonous inputs along the Ganges River and their effect on microbial community composition and dynamics. Environmental Microbiology 2019;21:182-96.

Zimmer-Faust AG, Thulsiraj V, Marambio-Jones C, Cao Y, Griffith JF, Holden PA, et al. Effect of freshwater sediment characteristics on the persistence of fecal indicator bacteria and genetic markers within a Southern California watershed. Water Research 2017;119:1-11.

Arsenic Levels in Soil and Rice and Health Risk Assessment via Rice Consumption in Industrial Areas of East Java, Indonesia

Nurul Laela[1], Satriani Aga Pasma[1*], and Muhayatun Santoso[2]

[1]Medical Intelligence Postgraduate Program, State Intelligence College, Bogor, Indonesia
[2]Research Center for Radiation Detection and Nuclear Analysis, Nuclear Energy Research Organization, National Research and Innovation Agency, Bandung, Indonesia

ARTICLE INFO

Received: 28 Feb 2023
Received in revised: 11 Jun 2023
Accepted: 14 Jun 2023
Published online: 10 Aug 2023
DOI: 10.32526/ennrj/21/20230049

Keywords:
Contamination/ Arsenic/ Soil/ Rice/ Risk assessment/ Human health

*** Corresponding author:**
E-mail:
satriani.aga.pasma@stin.ac.id

ABSTRACT

Industrial use of arsenic can potentially cause environmental problems in water, soil, and air. Arsenic is one of heavy metals that is highly toxic and carcinogenic. Arsenic contamination in the environment is harmful to human health because it can enter the body through the food chain. This study determined the concentration of arsenic in soil and rice and its impact on human health risks. Sampling was carried out in several East Java industrial cities or districts, for instance, Gresik, Mojokerto, Sidoarjo, Nganjuk, Ponorogo, and Surabaya. The measurement of arsenic in soil was done using Energy Dispersive X-Ray fluorescence (EDXRF), while the measurement of arsenic in rice was done by Total X-Ray Fluorescence (TXRF). The results showed that arsenic concentration in several areas of East Java has varying levels. The concentration of arsenic in soil was highest in Gresik (13,786 mg/kg). The highest arsenic concentration in rice was found in Mojokerto (0.154 mg/kg). The results of risk assessment in this study showed that the Hazard Quotient (HQ) value was >1 and the Excess Cancer Risk (ECR) was $>10^{-4}$ in all areas at the age of children <2 years. Health risk assessment of adults showed HQ>1 and ECR$>10^{-4}$ in several areas of East Java. This indicates that consumption of rice contaminated with arsenic has the potential to pose non-carcinogenic and carcinogenic health risks.

1. INTRODUCTION

Indonesia, as one of the developing countries, has experienced massive growth in the industrial sector. The Ministry of Industry (2017) stated that Indonesia is included in the top five countries with a fairly high industrial contribution. Nevertheless, industry also has negative impacts on the escalation of environmental pollution, whether in the water, soil, or air. This is due to the fact that high industrial activity has the potential to produce hazardous waste that can damage the environment and ecosystems. One of the hazardous industrial wastes that currently concerns the world is arsenic. Arsenic is a metal that is widely used in industrial activities; for instance, in the paint industry, ore processing and mining (Andhani and Husaini, 2017).

The contamination of the environment with arsenic becomes an important issue for global health because arsenic can be harmful to human health, especially for children. Arsenic is a non-essential heavy metal that is highly toxic and carcinogenic (Anetor et al., 2007). Arsenic exposure in children is more vulnerable than in adults, this is because children's weight is lower than adults, so their intake level is higher. In addition, children have organs that are still developing, so metabolism for elimination is still lacking compared to adults (Ferguson et al., 2018). Gardner et al. (2013) showed that arsenic exposure caused poor growth in children. In a study in Bangladesh, Wasserman et al. (2004) showed that there is a strong relationship of high concentrations of arsenic in the urine of children with low intellectual function.

In groundwater, arsenic exists in two forms, namely aerobic and anaerobic. Arsenic in the anaerobic form is reduced arsenic, also called arsenite (ASIII). Arsenite is fat-soluble and can be absorbed, by the body, through the digestive tract, respiratory tract, or skin. In contrast, arsenic, in its aerobic form,

Citation: Laela N, Pasma SA, Santoso M. Arsenic levels in soil and rice and health risk assessment via rice consumption in industrial areas of East Java, Indonesia. Environ. Nat. Resour. J. 2023;21(4):370-380. (https://doi.org/10.32526/ennrj/21/20230049)

is oxidized arsenic, also called arsenate (ASV) (Majmuder et al., 2019). Arsenic contamination in the soil is the primary source of contamination of water or food. The results of Hamzah and Hapsari (2017) research proved that arsenic content in Batu City paddy soil exceeded the threshold value, with a concentration of 0.89 ppm. The studies of Komarawidjaja (2017) showed that there was arsenic contamination that exceeded the threshold in the soil in the paddy fields of Jelegong Village, Rancaekek, Bandung (4.0 mg/L). Hazardous arsenic contamination in the soil can be harmful to human health because it can enter the body through the food chain. The nature of heavy metals makes them difficult to decompose, and deposits on the soil surface can be absorbed by organisms. This process is known as biomagnification, which is an increase in heavy metal contamination in the tissues of organisms through the food chain (Hidayah et al., 2014).

Arsenic can be easily accumulated in all types of cereals, especially rice, because of its high bioavailability in the soil (Huang et al., 2013). Rice is a major food in Asian countries and it's the main staple food source for Indonesian people. Several studies have shown high levels of arsenic in rice. It was reported that the levels of arsenic in several countries are 0.257 mg/kg (American rice), 0.188 mg/kg (Australian rice), 0.183 mg/kg (France rice) 0.147 mg/kg (Paksitani rice), and 0.103 mg/kg (Indian rice) (Shraim, 2017). Meanwhile, arsenic levels in several districts of Indonesia were reported to be 0.33 mg/kg in Medan (Ginting et al., 2018) and 1.76 mg/kg in Yogyakarta (Alfrianti, 2019). High concentrations of arsenic in rice can potentially be a major source of arsenic exposure, especially in countries that have rice diets.

It is crucial for East Java Indonesia to identify arsenic levels in soil and rice. Based on data from SI (2020), East Java is the province that has the largest contribution to rice production in Indonesia, producing around 9,944,538.26 tons of GKG or the equivalent of 5,712,597.01 tons of rice. On the other hand, East Java is also one of the industrial center provinces with 6,746 large and medium industries, and 92,031 micro industries (SI, 2019). The large rice production and high industrial activity in East Java can cause a potential hazard of arsenic contamination from industrial activities, which will spread into the environment and accumulate in the rice consumed by society. In addition, the existence of potential health hazards to children cannot be ignored, so it is necessary to analyze the potential risks of arsenic exposure to children's health.

The analysis of the arsenic content was carried out using the X-Ray Fluorescence (XRF) method. The method used for analysis of arsenic in soil was Energy Dispersive X-ray Fluorescence (EDXRF). This method is an analytical method that can measure elemental content from low atomic number to high atomic number, from the range of % to ppm, the method is fast, sensitive, and the equipment is easy to operate (Kurniawati et al., 2014). The method used for the analysis of arsenic in rice is Total X-Ray Fluorescence (TXRF). This method is a simple procedure, has good capability in measuring samples in very small concentrations in nanograms or micrograms, high sensitivity, and low detection limits in the order of ppb (Gruber et al., 2020).

2. METHODOLOGY

2.1 Materials

In this study, measurement of the arsenic in soil used the Energy Dispersive X-ray Fluorescence (EDXRF) spectrometer MiniPal 4 (PANalytical). Measurement of arsenic in rice used Total X-ray Fluorescence (TXRF) spectrometer S4 T-STAR (Bruker). Other equipment used in this study includes an analytical balance type 2842 (Sartorius), titan-eyed blender, hot plate (SI Analitycal), desiccator, Memmert oven, mortar, American standards testing stainless steel and material (ASTM) sieve with sizes of 100 mesh and 200 mesh, ultrasonic Elma 37 KHz, and other supporting equipment. The materials needed in this study included soil samples, rice samples, Standard Reference Material National Institute of Standards and Technology (SRM NIST) 2711a Montana Soil, SRM NIST 1568a Wheat Flour, demineralized water, standard Ga solution, triton X-100 solution, quartz glass, and other common materials.

2.2 Sampling of soil and rice

In this study, the sampling method was conducted by purposive sampling, in which the samples were obtained from agricultural areas around industrial activity. Soil and rice samples were collected from six cities/district in East Java, Indonesia. They were from several industrial area of Gresik (S07.174498°; E112.537473°), Mojokerto (S07.460749°; E112.469620°), Sidoarjo (S07.383-4359°; E112.6375614°), Nganjuk (S07.5857786; E112.5933989°), Ponorogo (S07.56177°; E112.26-463°), and Surabaya (S07.247968°; E112.651635°),

shown in Figure 1. Soil samples were obtained from paddy field by randomly taking soils of depths 0-10 cm (surface) and 10-30 cm (subsurface) from three spots and mixed to give representative samples. Soil samples taken at each sampling point were approximately 1 kg. Meanwhile, rice samples were taken by collecting rice yields in the soil sampling area. Rice samples were taken from direct agricultural products at each location point and about 1 kg samples were collected. The type of the tested rice was white rice (*Oryza sativa* L).

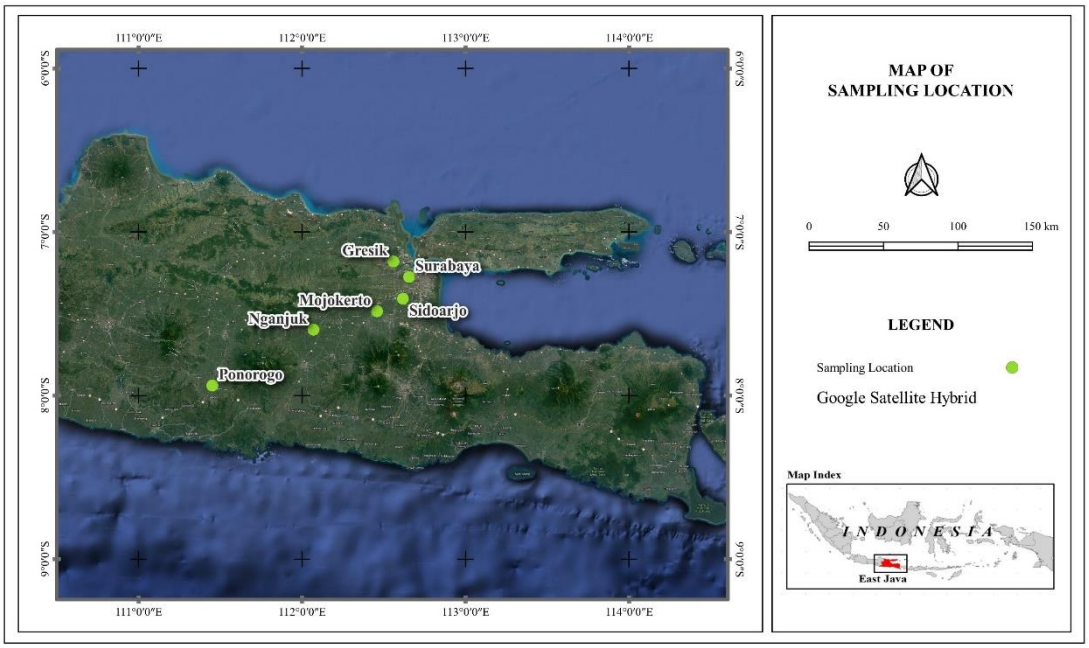

Figure 1. Sampling location map

2.3 Sample preparation and analysis

2.3.1 Preparation

Sample and standard preparation were carried out according to Adventini et al. (2016) and Syahfitri (2021) with several modifications. Paddy soil samples that had been obtained were sun-dried for 5-7 days. Then, the soil sample was homogenized with a mortar and filtered through a 200 mesh sieve. The soil sample was put into plastic and labeled according to the location point. The standard used for validating the EDXRF MiniPal 4 method for soil measurement was the SRM NIST 2711a Montana Soil.

Soil samples and standards were weighed at ±1 g, then placed into the sample holder cup, which was covered with mylar plastic. Soil samples and standards were measured using EDXRF spectrometer MiniPal 4. Meanwhile, the rice samples were mashed using a titan-eyed blender and dried in an oven at 105°C, and then the water content was calculated. Rice samples with a moisture content below 14% were homogenized using a 100-mesh sieve. About 200 mg of the rice sample was put into a corning tube, then 5 mL of triton X-100 solution and 10 µL of 1,000 ppm Ga standard were added. Then the sample was vortexed and incubated in an ultrasonic incubator for five minutes; then, 10 µL of the sample was pipetted onto quartz. Rice samples were analyzed using the TXRF spectrometer.

2.3.1 Measurement

Soil samples were placed in a sample holder cup and loaded into the EDXRF spectrometer MiniPal 4. Then, soil samples were irradiated with an X-Ray generated from the Rhodium (Rh) tube in the tool using soil sediment application software with optimum conditions: voltage 30 kV, current 150 uA, measurement time of 300 sec, Al filter, and air media. The rice samples were irradiated using a TXRF spectrometer device with TPPA Mo-K and TPPA W-Brem applications. The optimum measurement conditions of arsenic were as follows: voltage 50 kV, current 1,000 uA, and measurement time 1,000 sec. The measurement results were in the form of intensity, while the concentration elements were in the sample obtained by comparing the intensity of the sample with the standard based on formula (1) as follows:

$$C_{spl} = \frac{I_{spl}}{I_{std}} \times C_{std} \quad (1)$$

Where; C_{spl} is the concentration of the element in the sample, I_{spl} is the intensity of the sample, I_{std} is the intensity of the standard, and C_{std} is the concentration of the element in the standard.

2.4 Health risk assessment

In this study, the health risk assessment of arsenic focused only on the rice exposure assessment and risk characterization. This risk assessment aims to determine the average daily intake (ADI), hazard quotient (HQ), and excess cancer risk (ECR). The ADI value is used to determine the exposure dose received by the body through food so that arsenic intake from contaminated rice can be determined with the following equation:

$$ADI = \frac{C \times IR}{BM} \quad (2)$$

Where; ADI is the Average Daily Intake (mg/kg/day), C is the Concentration of heavy metals in rice, IR is the Ingestion Rate, and BM is Body Mass. The total rice consumption in East Java is 88 kg/capita/year or equal to 0.241 kg/capita/day (MCITI, 2016). The risk assessment in this study was conducted on children aged 6-8 months, 9-12 months, and 13-24 months. The average body weight is 7.6 kg for children aged 6-8 months, 8.4 kg for children aged 9-12 months, 11.9 kg for children aged 13-24 months, and 60 kg for adults (Suyanto et al., 2021; Adventini et al., 2016).

The Hazard Quotient (HQ) value is needed to determine the potential health risk of non-carcinogenic (non-cancerous) contaminants. If the value of HQ<1, then the potential health risk is low, and it can be said that the pollution which occurs is still within safe limits. If HQ>1, then the potential health risk is high. It needs to be controlled. The HQ value is obtained by the following equation:

$$HQ = \frac{ADI}{RfD} \quad (3)$$

Where; ADI is the daily intake of heavy metals, and the RfD is the estimated maximum daily dose intake allowed.

The level of risk of carcinogenic effects is expressed in Excess Cancer Risk (ECR). The ECR value determines an individual's lifetime estimate of cancer risk. If the ECR value is >10-4, it is at risk of causing cancer. The ECR value is obtained by payment as follows:

$$ECR = ADI \times SF \quad (4)$$

Where; ADI is the average daily intake of heavy metals and SF is the cancer slope factor.

3. RESULTS AND DISCUSSION

3.1 Validation result

In this study, method validation tests were used to confirm the test results quality by using Standard Reference Materials (SRM). Furthermore, soil sample testing was validated with EDXRF spectrometer MiniPal 4 using SRM NIST 2711a Montana Soil. Meanwhile, the rice samples testing was validated with TXRF spectrometer using SRM NIST 1568b Rice Flour. The results of the SRM NIST 2711a Montana Soil validation compared to the certificate value are shown in Table 1. The results of the SRM NIST 1568 b Rice Flour validation are shown in Table 2.

Table 1. The validation results on SRM NIST 2711a Montana Soil

Element	Certificate value (mg/kg)	Analysis value (average)	Recovery (%)
Arsenic	107±5	107	100

Table 2. The validation results on SRM NIST 1568b Rice Flour

Element	Certificate value (mg/kg)	Analysis value (average)	Recovery (%)
Arsenic	0.29±0.03	0.27	95

The validation results in Table 1 and Table 2 show that the percentage accuracy value (%) on SRM NIST 2711a Montana Soil is 100%, and the percentage accuracy value (%) on SRM NIST 1568b Rice Flour is 95%. This result follows the acceptability limit of the AOAC (2002), in the range of 85-110% for SRM NIST 2711a Montana Soil and 75-120% for SRM NIST 1568b Rice Flour. The validation results also show a good relationship between the measurement results and the certificate value. Thus, the test method is valid and reliable for testing soil and rice samples.

3.2 Arsenic concentration in soil

Arsenic concentration in the soil in several cities/districts of East Java, Indonesia, is shown in Figure 2. Arsenic concentration was analyzed in the soil at two depths, i.e., 0-10 cm and 10-30 cm depth.

The analysis showed no significant difference between arsenic levels in 0-10 cm and 10-30 cm depth, the concentration ratio between the two depths is 1. Arsenic in rice fields in six regencies of East Java was found at high levels, and variation ranged from 11,940-13,786 mg/kg.

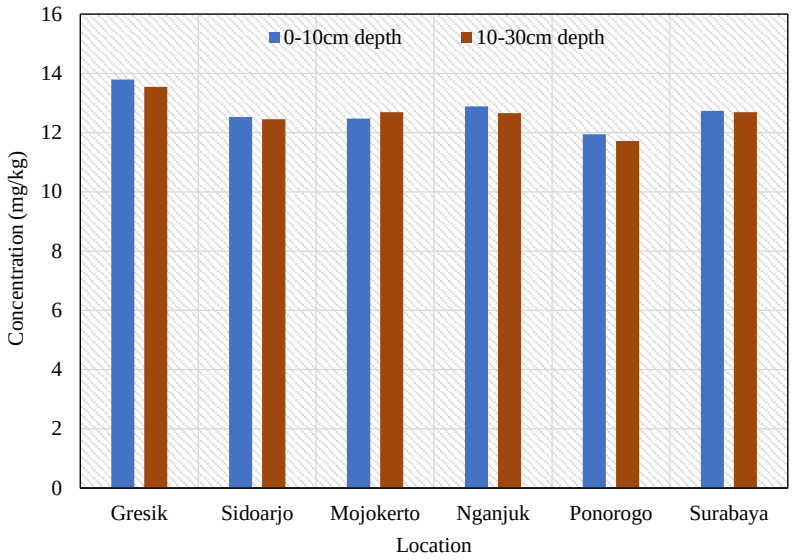

Figure 2. Arsenic concentration in soil

The variability of arsenic concentration in soil differs from region to region, as shown in Figure 3. Arsenic level was higher in industrial area of Gresik were 13,786 mg/kg, followed by Nganjuk (12.884 mg/kg), Surabaya (12.729 mg/kg), Sidoarjo (12.522 mg/kg), Mojokerto (12.474 mg/kg), and Ponorogo (11.940 mg/kg). The ranking order of arsenic level from soil was Gresik > Nganjuk > Surabaya > Sidoarjo > Mojokerto > Ponorogo. Furthermore, Figure 4 shows the comparison results between arsenic levels in this study and the threshold values allowed by World Health Organization (WHO), Food and Agriculture Organization (FAO), and European Union (EU). The results showed that the concentration of arsenic in the soil was above the maximum threshold value of 5 mg/kg (Toth et al., 2016).

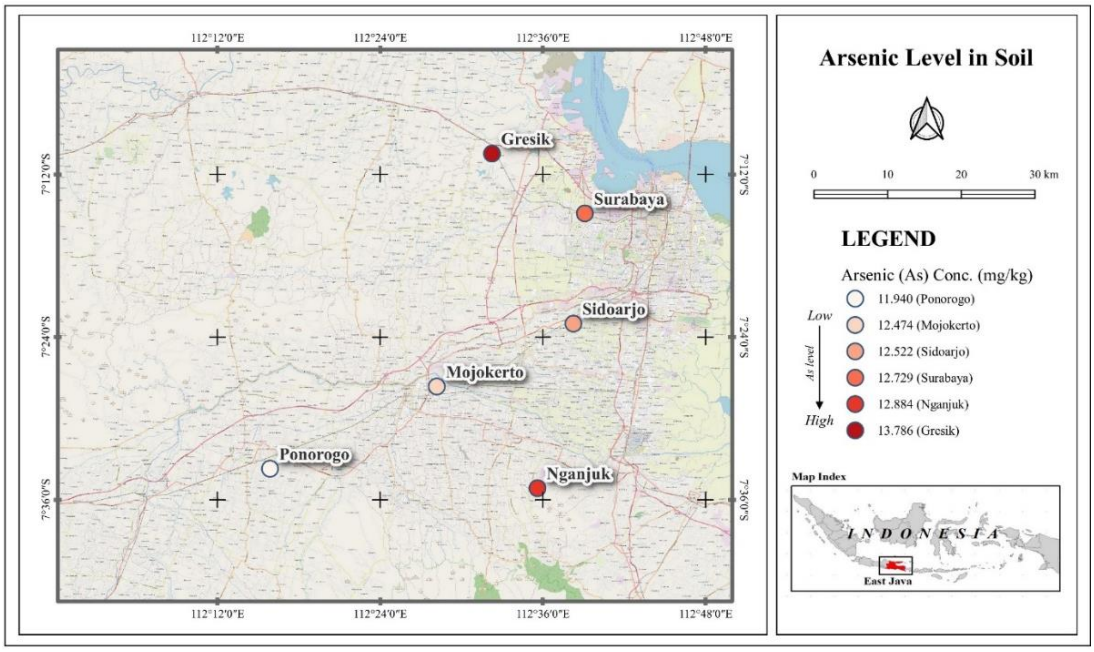

Figure 3. The spatial representation of arsenic levels in soil

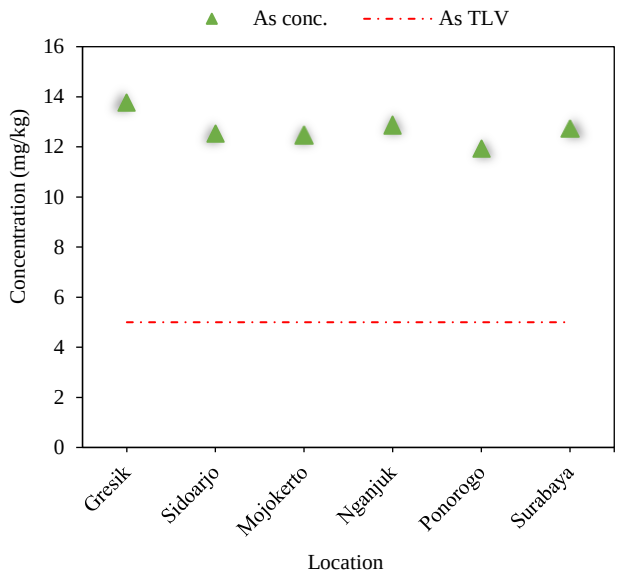

Figure 4. Arsenic concentration in soil with threshold value

Arsenic concentrations in the soil in some areas of East Java have varying levels from one region to another region. The variability of arsenic is not only diverse in the locations of this study but also gives different results from other studies, as shown in Table 3. Arsenic levels in this study were higher than arsenic levels in studies in Mainland China at 10.7 mg/kg (Huang et al., 2019), Thailand at 7.5 mg/kg (Zarcinas et al., 2004b), and Southern Europe at 10 mg/kg (Reimann and de Caritat, 2012). However, there are also research results showing that arsenic levels in this study are lower than those in Malaysia, which were 16.8 mg/kg (Zarcinas et al., 2004a), England and Wales, which were 20 mg/kg (Rawlins et al., 2012), and China's Xunyang, which were 72 mg/kg (Wang et al., 2019). The variability of arsenic levels can be influenced by various factors, such as geological factors and human activities, which are sources of anthropogenic contamination (Zeng et al., 2015).

3.3 Arsenic concentration in rice

Arsenic in the soil can be accumulated into the rice through a process called biomagnification. The biomagnification process is the occurrence of increased heavy metal contamination in organism tissues through the food chain (Hidayah et al., 2014). The result of this study showed that arsenic concentration in rice also varied from one region to another region. Figure 5 shows the analysis of arsenic concentrations in rice in six regions of East Java, ranged from 0.023-0.154 mg/kg.

Table 3. Variability of arsenic levels in soil

Location	Depth (cm)	As concentration (mg/kg)	Reference
Gresik	0-10	13.79	In this study
	10-30	13.55	In this study
Sidoarjo	0-10	12.52	In this study
	10-30	12.45	In this study
Mojokerto	0-10	12.47	In this study
	10-30	12.69	In this study
Jombang	0-10	11.58	In this study
	10-30	11.98	In this study
Nganjuk	0-10	12.88	In this study
	10-30	12.65	In this study
Ponorogo	0-10	11.94	In this study
	10-30	11.72	In this study
Surabaya	0-10	12.73	In this study
	10-30	12.69	In this study
Shandong, China	0-20	13.38	Jia et al. (2010)
Mainland, China	0-20	10.7	Huang et al. (2019)
Peninsular Malaysia	0-15	16.8	Zarcinas et al. (2004a)
Thailand	0-15	7.5	Zarcinas et al. (2004b)
England dan Wales	0-15	20	Rawlins et al. (2012)
Xunyang, China	0-20	72	Wang et al. (2019)
Southern Europe	0-20	10	Reimann and de Caritat (2012)

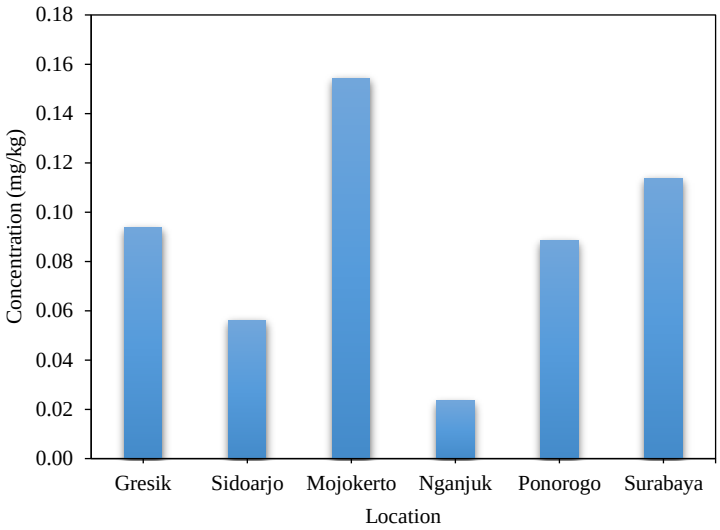

Figure 5. Arsenic concentration in rice

Figure 6 shows a representation of arsenic levels in each region. The highest levels of arsenic are found in the industrial area of Mojokerto, which were 0.154 mg/kg, and the lowest arsenic levels are in Nganjuk, which were 0.023 mg/kg. Arsenic levels in order from highest to lowest were Mojokerto > Gresik > Surabaya > Ponorogo > Sidoarjo > Nganjuk. While Figure 7 shows a comparison of the arsenic levels obtained in this study with the threshold value. The concentration of arsenic in this study was above the maximum value of the National Agency of Drug and Food Control Indonesia (0.1 mg/kg) in Mojokerto and Surabaya.

In comparison, the highest concentration arsenic in soil did not correlate with the highest concentration in rice. The results showed that the concentration of arsenic in several cities/districts was high, but less in rice. This could be due to the absorption or accumulation of arsenic in the rice plant. Abedin et al. (2002) observed a higher accumulation of arsenic in the roots than in any other parts of the plant. This has the effect of lowering the arsenic concentration in grain rice. In this study, the uptake of arsenic by rice plants might be different from one region to another.

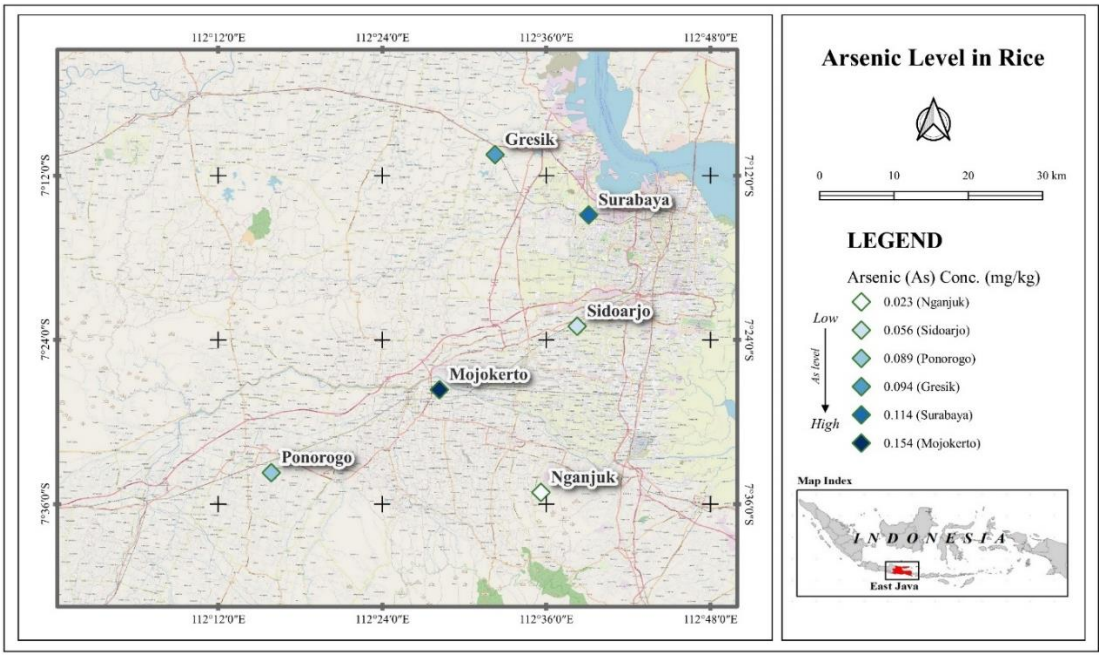

Figure 6. The spatial representation of arsenic levels in rice

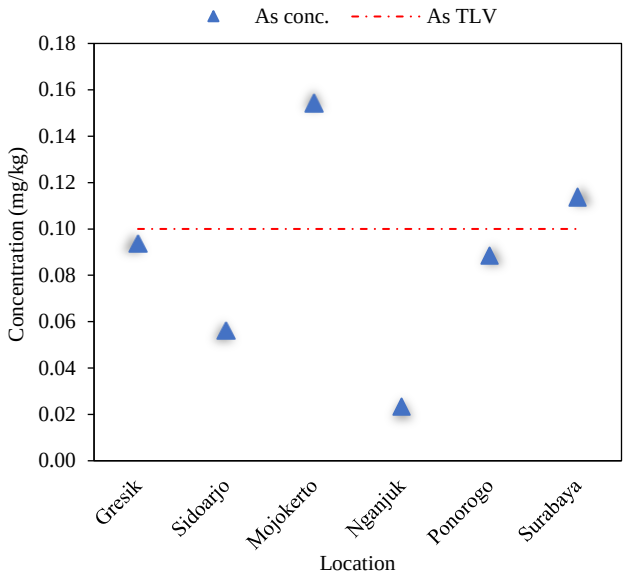

Figure 7. Arsenic concentration in rice with threshold value

The variability of arsenic concentration in rice in this study and other studies is shown in Table 4. Arsenic levels in this study were in the same order as the results of studies in Iran, at 0.12 mg/kg (Rastmanesh et al., 2022), and Savar Bangladesh, at 0.075 mg/kg (Hasan et al., 2022). However, the results of arsenic levels in this study were lower compared to 0.33 mg/kg in Medan (Ginting et al., 2018), 1.79 mg/kg in Yogyakarta (Alfrianti, 2019), 0.224 mg/kg in Matlab Bangladesh (Azmy, 2020), and 0.23 mg/kg in Jiangsu China (Li et al., 2018). Variations in arsenic levels from one region to another region can be caused by various factors, such as the mineral composition of soil, the use of fertilizers, chemical content in the soil, weather conditions during growth, soil pH, rice type, and soil interaction with plant root microbes, that play important roles in regulating movement from soil to plant (Damastuti et al., 2020).

Table 4. Variability of arsenic levels in rice

Location	As concentration (mg/kg)	Reference
Gresik	0.09	In this study
Sidoarjo	0.06	In this study
Mojokerto	0.15	In this study
Nganjuk	0.02	In this study
Ponorogo	0.09	In this study
Surabaya	0.11	In this study
Medan	0.33	Ginting et al. (2018)
Yogyakarta	1.79	Alfrianti (2019)
Iran	0.12	Rastmanesh et al. (2022)
Savar, Bangladesh	0.075	Hasan et al. (2022)
Matlab, Bangladesh	0.224	Azmy (2020)
Jiangsu, China	0.23	Li et al. (2018)

3.4 Human health assessment

The potential health risks caused by arsenic exposure can be determined from the average daily intake of arsenic in the body. The daily intake of arsenic was determined based on the average daily intake of rice per capita/day for the East Java population. The results of study in Figure 8 show that the daily intake of children aged 6-8 months ranged from 0.0007-0.049 mg/kg BW/day, children aged 9-12 months ranged from 0.0007-0.0044 mg/kg BW/day, children aged 13-24 months ranged from 0.0006-0.0049 mg/kg BW/day, and adults ranged from 0.0001-0.0006 mg/kg BW/day. The region with the highest average daily intake of arsenic for all age ranges for children and adults is the Mojokero Region.

Potential non-carcinogenic health risk can be identified from average daily intake value using the Hazard Quotient (HQ) and potential carcinogenic health risks using the Excess Cancer Risk (ECR). HQ results can be seen in Figure 9. These results show that the potential risk of non-carcinogenic exposure for children with HQ>1 ranged from 2.477-16.315 (age 6-8 months), 2.241-14.761 (age 9-12 months), and 1.901-12.525 (age 13-24 months). It shows that at the age of under two years, consuming rice contaminated with arsenic potentially causes non-carcinogenic health effects. While the HQ value in adulthood was found in four areas (Gresik, Mojokerto, Ponorogo, and Surabaya) with HQ>1 ranging from 1.214-2.115, and two areas (Sidoarjo and Nganjuk) with HQ value <1, the HQ value for children is much higher than for adults.

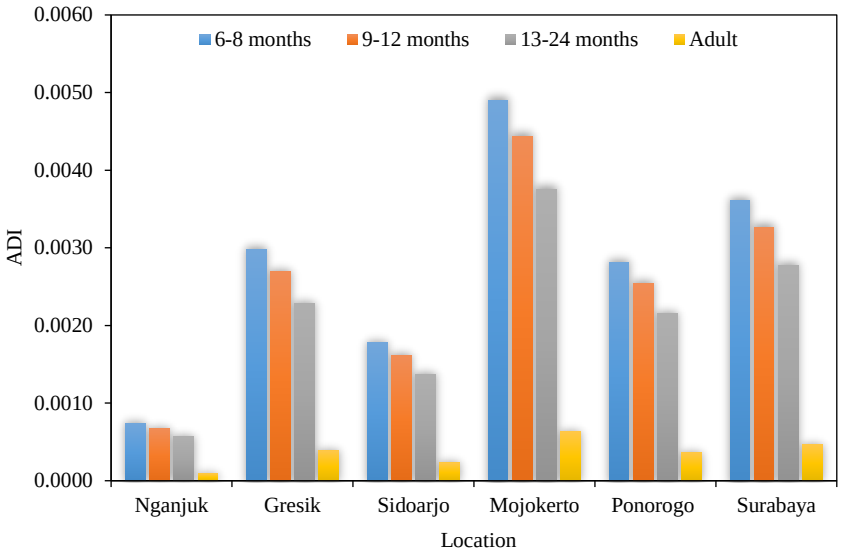

Figure 8. Average daily intake of arsenic

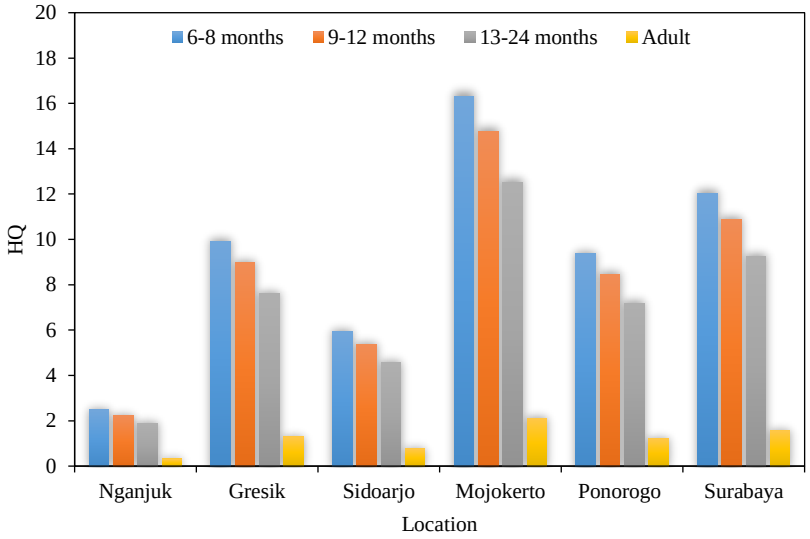

Figure 9. Hazard quotient value in each location

The potential risk of arsenic to carcinogenic health can be seen in Figure 10. The analysis results show that the average daily intake of arsenic from rice consumption in all age ranges of children in all regions has an ECR > 10^{-4}, ranging from 10^{-3}-7×10^{-3} (age 6-8 months), 10^{-3}-6×10^{-3} (age 9-12 months), and 10^{-3}-5×10^{-3} (age 13-24 months). This means that the consumption of rice contaminated with arsenic can pose a cancer risk. The ECR values in adults in some areas of East Java were ECR > 10^{-4}, except in Nganjuk, where they ranged from 2×10^{-4} to 4×10^{-4}. It shows that consuming contaminated rice in the Gresik, Sidoarjo, Mojokerto, Ponorogo, and Surabaya regions poses a cancer risk to adults.

When comparing the HQ and ECR values in adults and children, both values in children are much higher. This shows that the potential risk of arsenic to children's health is much higher than in adults. Children have a higher potential risk because they have smaller bodies with a large amount of rice consumption, while adults have large bodies. As a result, children are exposed to more arsenic than adults. In addition, children are also more sensitive to the harzardous effects of arsenic because their bodies are still developing, so they do not have the mature body system to get rid of harmful chemicals like adults. Arsenic exposure in children continuously and from time to time can cause growth problems, decreased IQ, impaired brain development, an unhealthy immune system, and the development of cancer as an adult (Murray, 2022).

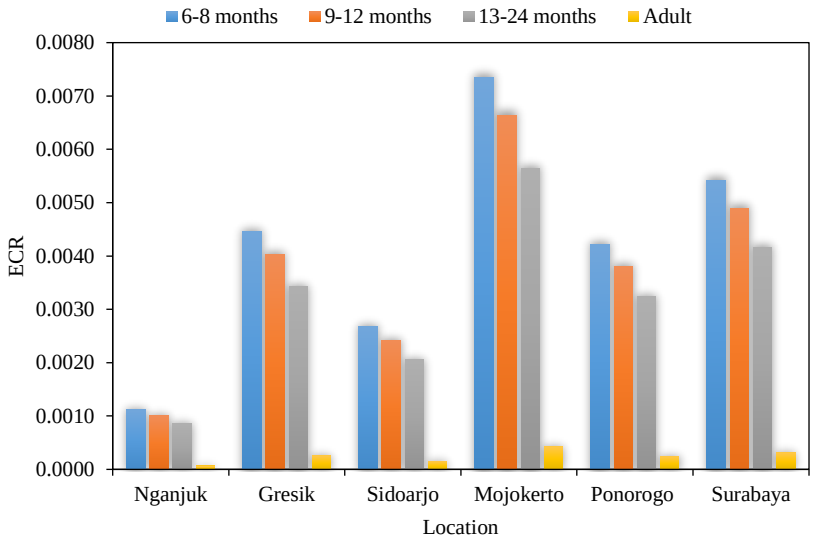

Figure 10. Excess cancer risk value in each location

4. CONCLUSION

In this study, the concentration of arsenic in several industrial areas of East Java had varying levels from one region to another. The highest arsenic level in soil was found in Gresik. The highest level in rice was found in Mojokerto. The concentration of arsenic in the soil exceeded the threshold value in all study areas. Meanwhile, the concentration of arsenic in rice exceeding the threshold value was only found in two regions, namely Mojokerto and Surabaya. Based on the results of this study, arsenic exposure from rice consumption has the potential to pose a health risk to children, both non-carcinogenic and carcinogenic health. Overall, this study provides information about the profile of arsenic concentration in several industrial areas of East Java. These results could be an early warning for local governments to take preventive measures and could also be applied to evaluate the surrounding industrial areas to minimize the hazardous potential of arsenic.

ACKNOWLEDGEMENTS

The Authors are grateful to Medical Intelligence Postgraduate Program, State Intelligence College for funding this study. And also authors thank to Research Center for Radiation Detection and Nuclear Analysis, Nuclear Energy Research Organization, National Research and Innovation Agency for facilities support.

REFERENCES

Abedin MD, Cresser MS, Meharg AA, Feldmann J, Howells JC. Arsenic accumulation and metabolism in rice (*Oryza sativa* L.). Environmental Science and Technology 2002;36(5):962-8.

Adventini N, Santoso M, Lestiani DD, Syahfitri WYN, Rixson L. Lead identification in soil surrounding a used lead acid battery smelter area in Banten, Indonesia. Proceedings of the International Nuclear Science and Technology Conference; 2016 Aug 4-6; Bangkok: Thailand; 2016.

Alfrianti D. Analysis of Arsenic in Rice Using Rhodamine-B Complexing by UV-VIS [dissertation]. Yogyakarta, Gadjah Mada University; 2019 (in Indonesian).

Andhani R, Husaini. Heavy Metals around Humans. Banjarmasin, Indonesia: Mangkurat University Press; 2017 (in Indonesian).

Anetor JI, Wanibuchi H, Fukushima S. Arsenic exposure and its health effects and risk of cancer in developing countries: Micronutrients as host defence. Asian Pasific Journal of Cancer Prevention 2007;8(1):13-23.

Association of Official Agricultural Chemist (AOAC). Guidelines for single laboratory validation of chemical methods for dietary supplements and botanicals [Internet]. 2002 [cited 2022 Dec 25]. Available from: https://s27415.pcdn.co/wp-content/uploads/2020/01/64ER20-7/Validation_Methods/d-AOAC_Guidelines_For_Single_Laboratory_Validation_Dietary_Supplements_and_Botanicals.pdf.

Azmy S. Detection of Metals and Trace Elements in Rice in Matlab, Bangladesh: A Descriptive Study [dissertation]. Sweden, UPPSALA Universitet; 2020.

Damastuti E, Kurniawati S, Syahfitri WYN. Geterminations of minerals composition of rices in Java Island, Indonesia. Journal of Nutritional Science and Vitaminology 2020;66:479-85.

Ferguson AC, Black JC, Sims IB, Welday JN, Elmir SM, Goff KF, et al. Risk assessment for children exposed to arsenic on baseball fields with contaminated fill material. International Journal of Environmental Research and Public Health 2018;15(67):2-23.

Gardner RM, Kippler M, Tofail F, Bottai M, Hamadani J, Grander M, et al. Environmental exposure to metals and children's growth to age 5 years: A prospective cohort study. American Journal of Epidemiology 2013;177(12):1356-67.

Ginting EE, Silalahi J, Putra ED. Analysis of arsenic in rice in Medan, North Sumatera Indonesia by atomic absorption spectrophotometer. Oriental Journal of Chemistry 2018; 34(5):2651-5.

Gruber A, Muller R, Wagner A, Colucci S, Spasic MV, Leopold K. Total reflection X-ray fluorescence spectrometry for trace determination of iron and some additional elements in biological samples. Analytical and Bioanalytical Chemistry 2020;412:6419-29.

Hamzah A, Hapsari I. Remediation of agricultural land polluted by heavy metals to produce healthy food products. Proceedings of the Kanjuruhan Livestock Food Research; 2017 Aug; Kanjuruhan University, Malang, Indonesia; 2017 (in Indonesian).

Hasan GMM, Das AK, Satter MA. Accumulation of heavy metals in rice (*Oryza sativa* L.) grains cultivated in three major industrial areas of Bangladesh. Journal of Environmental and Public Health 2022:2022;Article No. 1836597

Hidayah AM, Purwanto, Soeprobowati TR. Bioconcentration of heavy metal factors Pb, Cd, Cr, and Cu in tilapia (*Oreochromis niloticus* Linn.) in lake Rawa Pening Cages. Bioma 2014;16(1):1-9 (in Indonesian).

Huang Y, Wang L, Wang W, Li T, He Z, Yang X. Current status of agricultural soil pollution by heavy metals in China: A meta-analysis. Science of the Total Environment 2019;651: 3034-42.

Huang Z, Pan XD, Wu PG, Han JL, Chen Q. Health risk assessment of heavy metal in rice to the population in Zhejiang. Journal Pone 2013;8(9):1-6.

Jia L, Wang W, Li Y, Yang L. Heavy metal in soil and crops of an intensively farmed area: A case study in Yucheng City, Shandong Province, China. International Journal of Environmental Research and Public Health 2010;7:395-412.

Komarawidjaja W. Exposure to industrial wastewater containing heavy metals in paddy fields in Jelegong Village, Rancaekek District, Bandung Regency. Journal of Environmental Technology 2017;18(2):173-81 (in Indonesian).

Kurniawati S, Kusmartini I, Lestiani DD, Syahfitri WYN. Intercomparison test of AAN and XRF methods for analysis of IAEA sediment samples. Ganendra Nuclear Science and Technology Journal 2014;17(1):27-33 (in Indonesian).

Li T, Song Y, Yuan X, Li J, Ji J, Fu X, et al. Incorporating bioaccessibility into human health risk assessment of heavy metals in rice (*Oryza sativa* L.): A probabilistic-based analysis. Journal Agricultural and Food Chemistry 2018;66:5683-90.

Majmuder B, Das S, Mukhopadhyay S, Biswas AK. Identification of arsenic-tolerant and arsenic-sensitive rice (*Oryza sativa* L.) cultivars on the basis of arsenic accumulation assisted stress perception, morpho-biochemical responses, and alteration in genomic template stability. Protoplasma 2019;256(1):193-211.

Ministry of Communication and Information Technology, Indonesia (MCITI). Rice consumption of East Java people, 2016 [Internet]. 2016 [cited 2022 Jun 28]. Available from: http://kominfo.jatimprov.go.id/read/umum/konsumsi-beras-masyarakat-jatim-88-kg-per-kapita-per-tahun.

Ministry of Industry. Indonesia enters the category of industrial countries [Internet]. 2017 [cited 2022 Jun 30]. Available from: https://kemenperin.go.id/artikel/18473/indonesia-masuk-kategori-negara-industri.

Murray C. Arsenic and children [Internet]. 2022 [cited 2022 Jun 28]. Available from: https://sites.dartmouth.edu/arsenicandyou/arsenic-and-children/.

Rastmanesh F, Ghazalizadeh S, Shalbaf F, Zarasvandi A. Investigation of micronutrient and heavy metals in rice farms of Ahvaz and Bawie Counties, Khuzestan Province, Iran. Research Square 2022. DOI: https://doi.org/10.21203/rs.3.rs-1375747/v1.

Rawlins BG, McGrath, Scheib SP, Breward AJ, Cave N, Lister M, et al. The Advanced Soil Geochemical Atlas of England and Wales. England: British Geological Survey; 2012.

Reimann C, de Caritat P. New soil composition data for Europe and Australia: Demonstrating comparability, identifying continental-scale processes and learning lessons for global geochemical mapping. Science of the Total Environment 2012;416:239-52.

Shraim AM. Rice is potential dietary source of not only arsenic but also other toxic elements like lead and chromium. Arabian Journal of Chemistry 2017;10(2):3434-43.

Statistics Indonesia (SI). Central Bureau of Statistics Indonesia: Harvest Area and Rice Production in Indonesia at 2020. Jakarta, Indonesia: Central Bureau of Statistics; 2020 (in Indonesian).

Statistics Indonesia (SI). Directory of Large and Medium Industrial Companies in East Java Province. Surabaya, Indonesia: East Java Central Bureau of Statistics; 2019 (in Indonesian).

Suyanto, Lioe HM, Giriwono PE, Fardiaz D. Total arsenic in complementary food and its exposure assessment for children aged 6-24 months. Food Control 2021;122:1-11.

Syahfitri WYN. Determination of Arsenic Content in Rice and Its Processed Using X-Ray Fluorescence Method [dissertation]. Bandung, Bandung Institute of Technology; 2021 (in Indonesian).

Toth G, Hermann T, Da Silva MR, Montanarella L. Heavy metals in agricultural soils of the european union with implications for food safety. Environment International 2016;88:299-309.

Wang N, Han J, Wei Y, Li G, Sun Y. Potential ecological risk and health risk assessment of heavy metals and metalloid in soil around Xunyang Mining Areas. Sustainability 2019;11:2-16.

Wasserman GA, Liu X, Parvez F, Ahsan H, Factor-Litvak P, Geen A, et al. Water arsenic exposure and children's intellectual function in Araihazar, Bangladesh. Environmental Health Perspective 2004;112(13):1329-33.

Zarcinas BA, Pongsakul P, McLaughin MJ, Cozens G. Heavy metals in soils and crops in Southeast Asia 1. Peninsular Malaysia. Environmental Geochemistry and Health 2004a; 26:343-57.

Zarcinas BA, Pongsakul P, McLaughlin MJ, Cozens G. Heavy metals in soils and crops in Southeast Asia. 2. Thailand. Environmental Geochemistry and Health 2004b;26:359-71.

Zeng F, Wei W, Li M, Huang R, Yang F, Duan Y. Heavy metal contamination in rice-producing soils of Hunan Province, China and potential health risks. Environmental Research and Public Health 2015;12:15584-93.

INSTRUCTION FOR AUTHORS

Publication and Peer-reviewing processes of Environment and Natural Resources Journal

Environment and Natural Resources Journal is a peer reviewed and open access journal that is published in six issues per year. Manuscripts should be submitted online at https://ph02.tci-thaijo.org/index.php/ennrj/about/submissions by registering and logging into this website. Submitted manuscripts should not have been published previously, nor be under consideration for publication elsewhere (except conference proceedings papers). A guide for authors and relevant information for the submission of manuscripts are provided in this section and also online at: https://ph02.tci-thaijo.org/index.php/ennrj/author. All manuscripts are refereed through a **single-blind peer-review** process.

Submitted manuscripts are reviewed by outside experts or editorial board members of **Environment and Natural Resources Journal**. This journal uses double-blind review, which means that both the reviewer and author identities are concealed from the reviewers, and vice versa, throughout the review process. Steps in the process are as follows:

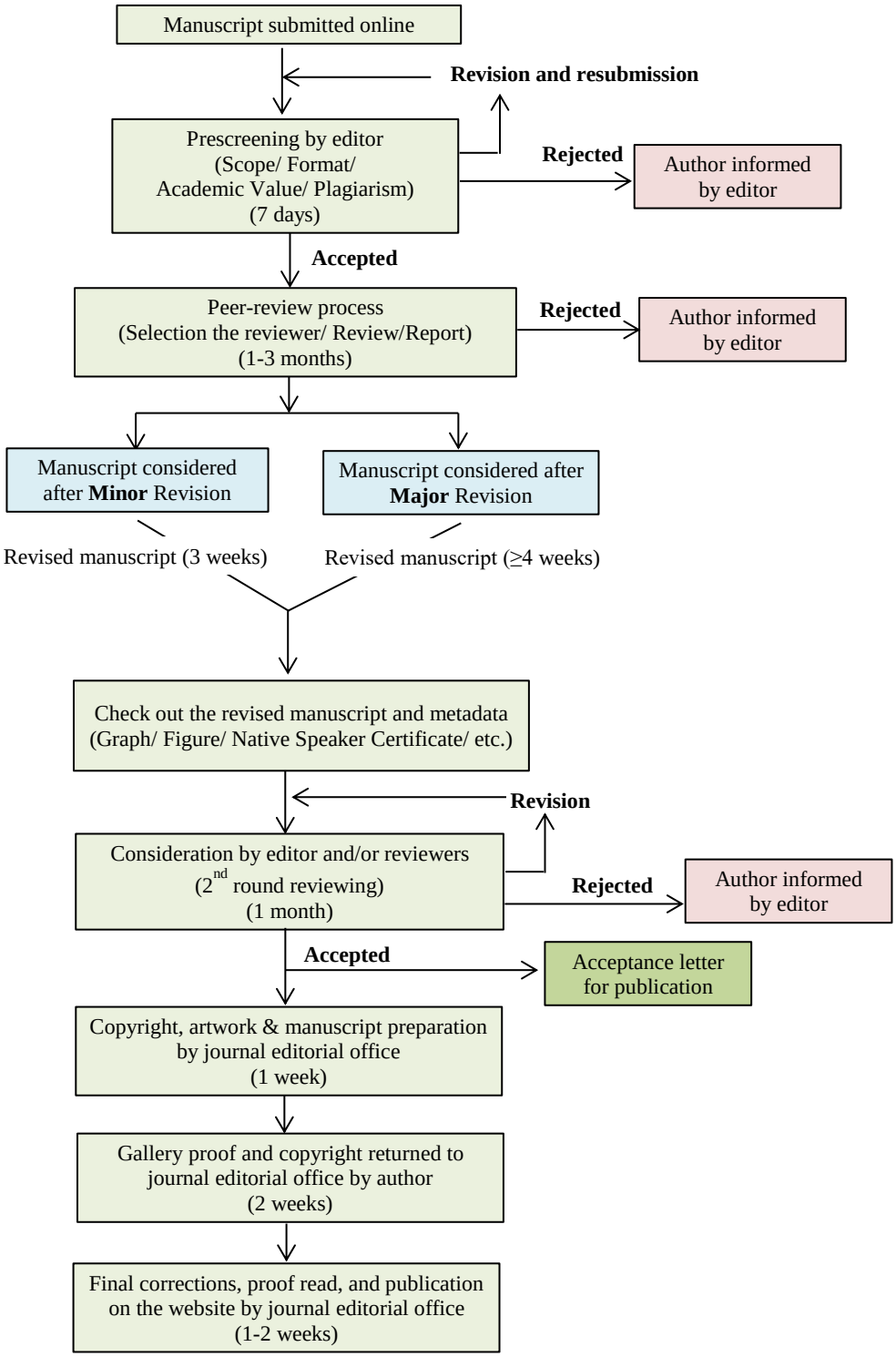

The Environment and Natural Resources Journal (EnNRJ) accepts 2 types of articles for consideration of publication as follows:

- *Original Research Article:* Manuscripts should not exceed 3,500 words (excluding references).
- *Review Article (by invitation):* This type of article focuses on the in-depth critical review of a special aspect in the environment and also provides a synthesis and critical evaluation of the state of the knowledge of the subject. Manuscripts should not exceed 6,000 words (excluding references).

Submission of Manuscript

Cover letter: Key points to include:

- Statement that your paper has not been previously published and is not currently under consideration by another journal
- Brief description of the research you are reporting in your paper, why it is important, and why you think the readers of the journal would be interested in it
- Contact information for you and any co-authors
- Confirmation that you have no competing interests to disclose

Manuscript-full: Manuscript (A4) must be submitted in Microsoft Word Files (.doc or .docx). Please make any identifying information of name(s) of the author(s), affiliation(s) of the author(s). Each affiliation should be indicated with superscripted Arabic numerals immediately after an author's name and before the appropriate address. Specify the Department/School/Faculty, University, Province/State, and Country of each affiliation.

Manuscript-anonymized: Manuscript (A4) must be submitted in Microsoft Word Files (.doc or .docx). Please remove any identifying information, such as authors' names or affiliations, from your manuscript before submission and give all information about authors at title page section.

Reviewers suggestion *(mandatory)*: Please provide the names of 3 potential reviewers with the information about their affiliations and email addresses. *The recommended reviewers should not have any conflict of interest with the authors. Each of the reviewers must come from a different affiliation and must not have the same nationality as the authors.* Please note that the editorial board retains the sole right to decide whether or not the recommended potential reviewers will be selected.

Preparation of Manuscript

Manuscript should be prepared strictly as per guidelines given below. The manuscript (A4 size page) must be submitted in Microsoft Word (.doc or .docx) with Times New Roman 12 point font and a line spacing of 1.5. *The manuscript that is not in the correct format will be returned and the corresponding author may have to resubmit*. The submitted manuscript must have the following parts:

Title should be concise and no longer than necessary. Capitalize first letters of all important words, in Times New Roman 12 point bold.

Author(s) name and affiliation must be given, especially the first and last names of all authors, in Times New Roman 11 point bold.

Affiliation of all author(s) must be given in Times New Roman 11 point italic.

Abstract should indicate the significant findings with data. A good abstract should have only one paragraph and be limited to 250 words. Do not include a table, figure or reference.

Keywords should adequately index the subject matter and up to six keywords are allowed.

Text body normally includes the following sections: 1. Introduction 2. Methodology 3. Results and Discussion 4. Conclusions 5. Acknowledgements 6. References

Reference style must be given in Vancouver style. Please follow the format of the sample references and citations as shown in this Guide below.

Unit: The use of abbreviation must be in accordance with the SI Unit.

Format and Style

Paper Margins must be 2.54 cm on the left and the right. The bottom and the top margin of each page must be 1.9 cm.

Introduction is critically important. It should include precisely the aims of the study. It should be as concise as possible with no sub headings. The significance of problem and the essential background should be given.

Methodology should be sufficiently detailed to enable the experiments to be reproduced. The techniques and methodology adopted should be supported with standard references.

Headings in Methodology section and Results and Discussion section, no more than three levels of headings should be used. Main headings should be typed (in bold letters) and secondary headings (in bold and italic letters). Third level headings should be typed in normal and no bold, for example;

2. Methodology
2.1 Sub-heading
2.1.1 Sub-sub-heading

Results and Discussion can be either combined or separated. This section is simply to present the key points of your findings in figures and tables, and explain additional findings in the text; no interpretation of findings is required. The results section is purely descriptive.
Tables Tables look best if all the cells are not bordered; place horizontal borders only under the legend, the column headings and the bottom.
Figures should be submitted in color; make sure that they are clear and understandable. Please adjust the font size to 9-10, no bold letters needed, and the border width of the graphs must be 0.75 pt. *(Do not directly cut and paste them from MS Excel.)* Regardless of the application used, when your electronic artwork is finalized, please 'save as' or convert the images to TIFF (or JPG) and separately send them to EnNRJ. The images require a resolution of at least 300 dpi (dots per inch). If a label needed in a figure, its font must be "Times New Roman" and its size needs to be adjusted to fit the figure without borderlines.

All Figure(s) and Table(s) should be embedded in the text file.

Conclusions should include the summary of the key findings, and key take-home message. This should not be too long or repetitive, but is worth having so that your argument is not left unfinished. Importantly, don't start any new thoughts in your conclusion.

Acknowledgements should include the names of those who contributed substantially to the work described in the manuscript but do not fulfill the requirements for authorship. It should also include any sponsor or funding agency that supported the work.

References should be cited in the text by the surname of the author(s), and the year. This journal uses the author-date method of citation: the last name of the author and date of publication are inserted in the text in the appropriate place. If there are more than two authors, "et al." after the first author' name must be added. Examples: (Frits, 1976; Pandey and Shukla, 2003; Kungsuwas et al., 1996). If the author's name is part of the sentence, only the date is placed in parentheses: "Frits (1976) argued that . . ."

Please be ensured that every reference cited in the text is also present in the reference list (and vice versa).

In the list of references at the end of the manuscript, full and complete references must be given in the following style and punctuation, arranged alphabetically by first author's surname. Examples of references as listed in the References section are given below.

Book
Tyree MT, Zimmermann MH. Xylem Structure and the Ascent of Sap. Heidelberg, Germany: Springer; 2002.

Chapter in a book
Kungsuwan A, Ittipong B, Chandrkrachang S. Preservative effect of chitosan on fish products. In: Steven WF, Rao MS, Chandrkachang S, editors. Chitin and Chitosan: Environmental and Friendly and Versatile Biomaterials. Bangkok: Asian Institute of Technology; 1996. p. 193-9.

Journal article
Muenmee S, Chiemchaisri W, Chiemchaisri C. Microbial consortium involving biological methane oxidation in relation to the biodegradation of waste plastics in a solid waste disposal open dump site. International Biodeterioration and Biodegradation 2015;102:172-81.

Published in conference proceedings
Wiwattanakantang P, To-im J. Tourist satisfaction on sustainable tourism development, amphawa floating marketSamut songkhram, Thailand. Proceedings of the 1st Environment and Natural Resources International Conference; 2014 Nov 6-7; The Sukosol hotel, Bangkok: Thailand; 2014.

Ph.D./Master thesis

Shrestha MK. Relative Ungulate Abundance in a Fragmented Landscape: Implications for Tiger Conservation [dissertation]. Saint Paul, University of Minnesota; 2004.

Website

Orzel C. Wind and temperature: why doesn't windy equal hot? [Internet]. 2010 [cited 2016 Jun 20]. Available from: http://scienceblogs.com/principles/2010/08/17/wind-and-temperature-why-doesn/.

Report organization:

Intergovernmental Panel on Climate Change (IPCC). IPCC Guidelines for National Greenhouse Gas Inventories: Volume 1-5. Hayama, Japan: Institute for Global Environmental Strategies; 2006.

Remark

** Please be note that manuscripts should usually contain at least 15 references and some of them must be up-to-date research articles.*

** Please strictly check all references cited in text, they should be added in the list of references. Our Journal does not publish papers with incomplete citations.*

Changes to Authorship

This policy of journal concerns the addition, removal, or rearrangement of author names in the authorship of accepted manuscripts:

Before the accepted manuscript

For all submissions, that request of authorship change during review process should be made to the form below and sent to the Editorial Office of EnNRJ. Approval of the change during revision is at the discretion of the Editor-in-Chief. The form that the corresponding author must fill out includes: (a) the reason for the change in author list and (b) written confirmation from all authors who have been added, removed, or reordered need to confirm that they agree to the change by signing the form. Requests form submitted must be consented by corresponding author only.

After the accepted manuscript

The journal does not accept the change request in all of the addition, removal, or rearrangement of author names in the authorship. Only in exceptional circumstances will the Editor consider the addition, deletion or rearrangement of authors after the manuscript has been accepted.

Copyright transfer

The copyright to the published article is transferred to Environment and Natural Resources Journal (EnNRJ) which is organized by Faculty of Environment and Resource Studies, Mahidol University. The accepted article cannot be published until the Journal Editorial Officer has received the appropriate signed copyright transfer.

Online First Articles

The article will be published online after receipt of the corrected proofs. This is the official first publication citable with the Digital Object Identifier (DOI). After release of the printed version, the paper can also be cited by issue and page numbers. DOI may be used to cite and link to electronic documents. The DOI consists of a unique alpha-numeric character string which is assigned to a document by the publisher upon the initial electronic publication. The assigned DOI never changes.

Mahidol University

Wisdom of the Land

Research and Academic Service Section, Faculty of Environment and Resource Studies, Mahidol University
999 Phutthamonthon 4 Rd, Salaya, Nakhon Pathom 73170, Phone +662 441-5000 ext. 2108 Fax. +662 441 9509-10
E-mail: ennrjournal@gmail.com Website: https://www.tci-thaijo.org/index.php/ennrj